Lehrstuhl für Hochfrequenztechnik
Technische Universität München

Singularity Cancellation Transformations and Hierarchical Higher Order Basis Functions for the Hybrid Finite Element Boundary Integral Technique

Li Li

Vollstndiger Abdruck der von der Fakultät für Elektrotechnik und Informationstechnik der Technischen Universität München zur Erlangung des akademischen Grades eines

Doktor-Ingenieurs

genehmigten Dissertation.

Vorsitzender:	Univ.-Prof. Dr.-Ing. Gerhard Rigoll
Prüfer der Dissertation:	1. Univ.-Prof. Dr.-Ing. Thomas Eibert
	2. Univ.-Prof. Dr. Romanus Dyczij-Edlinger, Universität des Saarlandes

Die Dissertation wurde am 29.01.2016 bei der Technischen Universität München eingereicht und durch die Fakultät für Elektrotechnik und Informationstechnik am 04.04.2016 angenommen.

Abstract

Accurate and efficient electromagnetic modeling and simulations are always required for modern high frequency component and wireless communication systems design, where large scale simulations, unique solutions as well as radiation and scattering patterns are required for complicated configurations. Electromagnetic analysis and large scale computations are challenging problems with respect to computer resources.

In this work, accurate and efficient electromagnetic simulations are accomplished by solving the numerically exact hybrid finite element boundary integral (FE-BI) equations for arbitrarily shaped perfect electrically conducting (PEC) objects and also PEC components enclosed by dielectric materials. The finite element method (FEM) is utilized to solve the fields inside the dielectric materials, surface integral equations (IEs) are solved through the method of moments (MoM). Highly accurate analytical solutions are proposed for the FEM and the system matrices in the FEM are evaluated efficiently. Numerical solutions are utilized for the MoM, where techniques of great significance are proposed, such as the adaptive singularity cancellation technique for near-coupling computations, higher order (HO) modeling of the surface currents and the $\hat{k}$-space solution of the spherical harmonics expansion for the multilevel fast multipole method (MLFMM). The HO basis functions are implemented into the algorithm for surface current and volume field evaluations.

The self-coupling and near mutual-coupling integrals need special treatments for their accurate computations in the MoM solution, where the integral kernels involve the Green's function and the gradient of the Green's function. The efficient and accurate evaluations of the self-coupling and of mutual couplings are obtained through the singularity cancellation technique with the adaptive selection of quadrature points in the planar testing and source domains. The fundamental shortcoming of the low order (LO) $Rao - Wilton - Glission$ (RWG) basis functions lies in its insufficient accuracy even for dense geometrical discretization, even though the LO basis functions have been widely utilized in the expansion of unknown surface current densities. Improved accuracy is achieved with the combination of hierarchical HO basis functions together with the LO for the surface current evaluations, where the same total number of unknowns are utilized for the mixed order modeling as for the pure LO simulations. Efficient and accurate solutions are provided by the fast multipole method (FMM) and the multilevel fast multipole method (MLFMM) in fast solvers for large scale simulations. However, traditional MLFMM methods turn out to be less efficient for the HO, as they require larger element dimensions. Then, the $\hat{k}$-space algorithm has been proposed in the SE-MLFMM, where the required memory has been considerably reduced due to the efficient storage of the individual basis functions with the spherical harmonics expansion. Thus, very efficient iterative solutions are obtained for the equation system.

The hierarchical HO basis functions are utilized in the FEM, where the compatibility is required between the basis functions in the FEM and the MoM, respectively. The efficient self-identification technique is proposed for the achievement of basis function compatibility, where the basis functions in the FEM automatically discern the constructions of the MoM basis functions and the basis functions from the ajacent elements. Then, the FEM basis functions organize themselves to obtain compatibility at the element boundaries. Analytical solutions are also obtained with the usage of the self-identification technique, where the

common local-global transformation process in the traditional FEM is avoided.

Various numerical simulation results are shown to demonstrate the applicability, the robustness and the efficiency of the realized hybrid finite element boundary integral algorithms.

Contents

1 Introduction **1**

1.1 The Surface Integral Equations 1

1.2 The Finite Element Method 3

1.3 The Hybrid Finite Element Boundary Integral Technique 3

1.4 The Outline of the Thesis 4

2 Electromagnetic Modeling by the Hybrid Finite Element Boundary Integral Technique **7**

2.1 Maxwell Equations 7

2.2 The Symmetric Maxwell Equations 8

2.3 The Modeling Approach 8

2.4 Equivalent Currents 11

2.5 Huygens' Principle 12

2.6 The Hybrid Finite Element Boundary Integral Technique 15

3 The Boundary Integral (BI) Equations **19**

3.1 The Spatial Electromagnetic Integral Equations 19

3.2 Electric Field Integral Equation 20

3.3 Magnetic Field Integral Equation 21

3.4 Combined Field Integral Equation 21

3.5 Method of Moments (MoM) 22

3.6 Multilevel Fast Multipole Method 26

3.6.1 Fast Multipole Method (FMM) 26

3.6.2 Maxtrix Elements with FMM 28

3.6.3 Spherical Harmonics Expansion of the $\hat{k}$-space Integrals 30

3.6.4 Multilevel Fast Multipole Method 31

4 Singularity Treatment Approaches **33**

4.1 Singular Integral Configurations 33

4.2 Singular Integral Kernels 33

4.3 Singularity Subtraction Method 34

4.4 Radial Angular Singularity Cancellation Transformations Derived by the Variable Separation Method 36

4.4.1 Introduction 36

4.4.2 The Variable Separation Method 39
4.4.3 General Solution to Radial-Angular Transformations 40
4.4.4 General Solution to Augmented Radial-Angular Transformations . . 40
4.5 The Family of Radial-Angular-R^1 Transformations 41
4.5.1 The Radial-Angular-R^1 Transformation 41
4.5.2 The Augmented Radial-Angular-R^1 Transformation 42
4.6 The Family of Radial-Angular-R^2 Transformations 43
4.6.1 The Radial-Angular-R^2 Transformation 43
4.6.2 The Radial-Angular-R^2-Cosh Transformation 43
4.6.3 The Augmented Radial-Angular-R^2 Transformation 44
4.7 The Family of Radial-Angular-R^3 Transformations 45
4.7.1 The Radial-Angular-R^3 Transformation 45
4.7.2 The Arcsinh-R^3 Transformation 45
4.7.3 The Augmented-Radial-Angular-R^3 Transformation 46
4.8 Numerical Results 46
4.8.1 Normalized Integration Domain 47
4.8.2 Accuracy of the 1st Order Transformation Schemes 48
4.8.3 Accuracy of the 2nd Order Transformation Schemes 51
4.8.4 Accuracy of the 3rd Order Transformation Schemes 54
4.8.5 Accuracy Analysis Dependent on the Exclusion Disk Radius 57
4.8.6 Accuracy for Deformed Triangles 59
4.8.7 Accuracy Analysis 64
4.9 Conclusion 65

5 Hierarchical Basis Functions in the Method of Moments for the Surface Integral Equations 67

5.1 Introduction 67
5.2 Definitions of the Hierarchical Vector Basis Functions 68
5.3 Numerical Results of MoM for Perfect Electric Conductor (PEC) Objects . 73
5.3.1 PEC Sphere 73
5.3.2 PEC Stealth Aircraft Model 76
5.3.3 PEC Flamme 81

6 The Finite Element Method **87**

6.1 Variational Formulation 87

6.2 Finite Element Discretization 89

6.2.1 The Mathematical Foundation for the Method of Finite Elements . . 89

6.2.2 The Discretization of the Field Vectors 90

6.2.3 The Discretization of the Integral Space 91

6.3 The Definition and Properties of the FE Parameters 93

6.4 The System Matrices of the Variational Formulation 95

7 The Hierarchical 3-D Vector Basis Functions within the Finite Element Method **97**

7.1 Introduction 97

7.2 The First Order Rotational Space 100

7.3 The First Order Gradient Space 100

7.4 The Second Order Rotational Space 101

7.5 The Second Order Gradient Space 102

7.6 The Third Order Rotational Space 103

7.7 Numerical Results of the FE-BI Method 110

7.7.1 Coated Sphere 110

7.7.2 Stealth Bomber Aircraft with Absorbing Materials 112

7.7.3 Flamme with Absorbing Materials 117

7.8 Conclusion 122

8 Accuracy Analysis of the Finite Element Boundary Integral Method **123**

8.1 The Definition of Root Mean Square (RMS) Error 123

8.2 Accuracy Analysis Against Analytical Models 124

8.3 The RMS Electric Field Error for the Air Block 124

8.4 The RMS Electric Field Error for Air Spheres 127

9 Summary and Conclusion **129**

Appendix A **131**

List of Abbreviation

BI	boundary integral
Bi-RCS	bistatic radar cross section
CEM	computational electromagnetics
CFIE	combined field integral equation
EFIE	electric field integral equation
EM	electromagnetics
FE	finite element
FE-BI	finite element boundary integral
FMM	fast multipole method
HO	higher order
IE	integral equation
LO	low order
MFIE	magnetic field integral equation
MLFMM	multilevel fast multipole method
MoM	method of moments
PEC	perfect electric conductor
RCS	radar cross section
SE	spherical harmonics expansion
SE-MLFMM	SE based MLFMM
SIE	surface integral equation

List of Symbols

$\boldsymbol{A}_i$	normal surface area with respect to node i
A_T	area of the triangle
$\boldsymbol{B}$	magnetic flux density
$\boldsymbol{D}$	electric flux density
$\boldsymbol{E}$	electric field
$\boldsymbol{E}_{ad}$	adjoint electric field
$\boldsymbol{E}^{inc}$	incident plane wave electric field
$\boldsymbol{f}_n$	the vector basis function for BI
$\boldsymbol{f}_{pq}^n$	expansion coefficient
G	scalar Green's function
$\bar{G}$	dyadic Green's function
$\boldsymbol{H}$	magnetic field
$\boldsymbol{H}^{inc}$	incident plane wave magnetic field
$\boldsymbol{J}$	impressed electric current density
$\boldsymbol{J}_s$	electric surface current
k_0	wave number in free space
$\boldsymbol{M}_s$	magnetic surface current
$\hat{n}$	surface normal unit vector
N	number of points

P_l	Legendre polynomial of order l
P_p^q	Lengendre polynomial of order p with degree q
R	distance between two points
RMS	root mean square
RWG	Rao-Wilton-Glisson
$\boldsymbol{t}_{ij}$	edge vector of triangle pointing from node i towards node j
T_L	translation operator in MLFMM
V_T	volume of a tetrahedron
Y_{pq}	spherical harmonics
$\|z\|$	projection height of the observation point
Z_0	intrinsic impedance of free space
$\boldsymbol{\alpha}_n$	vector basis function for FE
ϵ	permittivity
ϵ_0	permittivity in free space
ϵ_r	relative permittivity
μ	permeability
μ_0	permeability in free space
μ_r	relative permeability
ρ	charge density
ρ_e	electric charge density
ρ_m	magnetic charge density
λ_i	simplex coordinate with respect to node i

1 Introduction

The Maxwell equations [Maxwell, 1873] have been proposed in 19th century to describe the propagation of electromagnetic waves. However, only some simple solution domains can have analytical solutions for electromagnetic waves. So, the design of electromagnetic devices, such as antennas, relied much on experiments and measurements in the early days of electromagnetics.

The computer technology development allows for efficient numerical solutions to electromagnetic problems. The differential and integral equations that derived from Maxwell equations can be solved numerically with the growing power of computers. The numerical techniques in electromagnetic simulations are applicable to analyze complicated structures and also provide solutions to the design of electromagnetic devices. Simulations tremendously reduce the cost of electromagnetic component design, as the manufacturers of the devices are supported by simulation results. Moreover, the time-consuming measurements are also replaced by simulations, so that the efficiency of the component calibration is significantly improved. The exploitation periods of new products are reduced and the procedure from design to market is accelerated. Numerical algorithms are versatile for arbitrarily shaped configurations and able to utilize simultaneous simulations with different component parameters for system optimization. As it turns out, numerical algorithms for discretized modeling become independent solutions within electromagnetic component design. Numerical simulations are very efficient in the development of electromagnetic devices such as antennas, filters, couplers, radar systems as well as in the analysis of electromagnetic compatibility for radio frequency circuits.

Various techniques in numerical simulations have been exploited and they are improved continuously. However, each single solution contains its own advantages and disadvantages. So, hybrid techniques have been proposed to keep the advantages and overcome the shortages of different solution techniques. However, none of the single techniques nor the hybrid method are verified to meet all physical requirements. Suitable solutions have to be determined for specific electromagnetic models and the efficiency and accuracy of algorithms are still being improved.

1.1 The Surface Integral Equations

The surface integral equations (SIE) [Chakraborty and Jandhyala, 2006, Chew et al., 2008, Cloux et al., 1994, Jandhyala et al., 2002, Kapur and Long, 1998, Liu et al., 2009a, Nabors and White, 1991, Raziman et al., 2015, Shi et al., 2002, Srivastava et al., 2008, Wang et al., 2004, Zhu et al., 2003] are derived from the Maxwell equations and also from the Huygens' theory [Huygens, 1912, Lindell, 1996, Lu and Chew, 1995, Monzon, 1993]. They can be utilized to obtain equivalent electric and magnetic surface currents. The Huygens' principle illustrates that the space can be divided into outside and inside spaces by enclosed surfaces. The radiation in the outside and inside spaces can be computed through the equivalent electric surface current $\boldsymbol{J}_s$ and magnetic surface current $\boldsymbol{M}_s$ on the enclosed boundary surfaces.

To obtain $\boldsymbol{J}_s$ and $\boldsymbol{M}_s$, the SIEs can be solved by the method of moments (MoM) [Gibson, 2008, Harrington, 1990, 1993, Liu et al., 2009b, Varmazyar et al., 2008]. The MoM is applied to the electric field integral equation (EFIE) [Correia and Singer, 1999, Mautz and Harrington, 1984, Wilton and Glisson, 1981], the magnetic field integral equation (MFIE) [Ergül and Gürel, 2004, Hodges and Samii, 1997, Ingber and Ott, 1991, Zhang et al., 2003], or their combination, the combined field integral equation (CFIE) [Jung and Sarkar, 2004a,b, Mautz and Harrington, 1978a,b, 1979, Oijala, 2008, Rao and Wilton, 1990, Song and Chew, 1995, Yaghjian, 1981, YlÄ-Oijala and Taskinen, 2003, Ylä-Oijala and Taskinen, 2005]. It has been verified that the EFIE can obtain a very good accuracy, however, the pure EFIE has resonances on the resonant frequencies for objects with enclosed surfaces. Then, the CFIE is proposed to cure the resonances [Collins et al., 1992, Eibert and Hansen, 1996b, Jin, 2002, Mittra and Klein, 1975, Murphy et al., 1990, Peterson, 1990], where the CFIE combines the EFIE and also the MFIE.

The SIEs are often solved through the Galerkin process, where the testing functions are the same as the basis functions. The system matrix can be obtained through mutual couplings. The system matrix for MoM is very dense and it is necessary to cancel out the singularities for near couplings. Many techniques have been proposed for singularity treatments [Butler, 1975, Duffy, 1982, Eibert and Hansen, 1995b, 1996a, Fink et al., 2005, Huber et al., 1997a,b, Ismatullah and Eibert, 2008, Khayat et al., 2008, Wilton et al., 1984] and the singularity cancellation technique is one of the most effective solutions. Through variable transformations, the Jacobian can cancel out the singularities in the system matrices. Different variable transformation schemes may have different forms of Jacobians and various distributions of the sampling points in the source domain. The sampling points in the source domain can influence the efficiency of the transformation schemes, especially for the vector integral kernels in MoM.

To speed up MoM, the mutual couplings far away are computed through the multilevel fast multipole method (MLFMM) [Dembart and Yip, 1998, Donepudi et al., 2000, Eibert, 2005, Koc et al., 1999, Song et al., 1997]. The MLFMM tremendously saves computation time of the mutual couplings with very good accuracy, the required RAM is also much reduced. With spherical harmonics expansions of the basis function radiation patterns, better performance of the MLFMM has been obtained.

The nearly orthogonal hierarchical 2-D basis functions [Graglia et al., 1997, Jin, 2002, Jorgensen et al., 2005, Nedelec, 1980, Notaros, 2008, Sun et al., 2001, Webb, 1999, Zhu and Cangellaris, 2006] can also be implemented into MoM. The hierarchical basis functions are curl conforming, where the orthogonal components of the basis functions are continuous at the mesh boundaries. The hierarchical basis functions are composed of different orders of rotational and gradient spaces. The near orthogonality of the basis functions provides an improved condition number for the system matrix. Thus, better convergence of the iterative solvers can be obtained to solve the unknown coefficients. The low order basis functions require fine meshes. However, the higher order basis functions decrease the requirements for the mesh element size. Curved wave fronts within the mesh cells can also be represented accurately with higher order basis functions.

The SIEs can be applied to arbitrarily shaped components, including perfect electrically

conducting (PEC) objects or dielectric components with homogeneous materials. Dependent on frequency, reasonable mesh element size and mesh qualities are required to obtain good performance. The SIEs have been verified to be efficient for electromagnetic model simulations.

1.2 The Finite Element Method

The finite element method (FEM) is also derived from the Maxwell equations. It is utilized to solve for the electric field $\boldsymbol{E}$ or the magnetic field $\boldsymbol{H}$ inside dielectric materials and also on the boundaries. The FE method is a variational solver to compute the fields. The functionals proposed in the FE method are made stationary through the Ritz process [Jin, 2002], where the adjoint field is employed to test the Maxwell equations.

In numerical solutions, the unknown fields are expanded into 3-D vector basis functions [Sun et al., 2001] multiplied with the corresponding unknown coefficients. The 3-D nearly orthogonal hierarchical basis functions are employed in FEM, also including different orders of rotational and gradient spaces. The basis functions are defined based on geometrical meshes. Generally, the volumes of the dielectric materials are meshed into tetrahedra. The definitions of basis functions rely on the tetrahedral vertices, edges, faces and volumes. According to the tetrahedral mesh, the basis functions can be classified into the edge-related, face-associated and volume-associated basis functions. The edge-related basis functions are connected to the edges of the tetrahedron, where the two local node numbers of the edge are utilized. The face-associated basis functions are connected to the faces, where the three local node numbers are utilized. The volume-associated basis functions are connected to the volume of the tetrahedron defined by all nodes. All basis functions are curl-conforming, where the tangential components of the basis functions are continuous at the mesh element boundaries.

The system equations for unknown coefficients are obtained under the condition of minimizing the systematic error. The functional is differentiated with respect to the adjoint fields and the resulting equations are forced to be zero. The system matrices of FEM are sparse as the mutual couplings are only relevant to the local basis functions inside the tetrahedra and on the relevant triangles. However, the system matrices of FEM can be computed analytically through the integration properties of the simplex coordinates inside the tetrahedral volume. So the numerical solution based on FEM is very efficient and accurate to solve the fields inside the finite elements.

1.3 The Hybrid Finite Element Boundary Integral Technique

The hybrid finite element boundary integral (FE-BI) method [Eibert, 1997, Jin, 2002, Jin and Riley, 2008, Jin and Volakis, 1991, Volakis et al., 1998] is a combination of FEM and the method of boundary integral (BI) in terms of SIE. The 3-D vector basis functions for the FE method should be compatible with the 2-D basis functions for BI. This requires that the 3-D FE basis functions have the same node order as the 2-D BI basis functions. Moreover, on the boundary faces of the finite elements, the FE basis functions in different tetrahedra are also required to follow the same node order. As it is easy to fix the node

order of the triangular mesh for the BI method, the FE basis functions have to meet the requirements of the compatibility.

A traditional solution to solve the compatibility of the basis functions is a so called local-global transformation. First, the FE matrices are computed through the mutual couplings of the local basis functions, where the local basis functions are defined by the local node order of the tetrahedra. When linking to solvers, the local matrices need to be modified according to global node orders. As a result, more computation time for the system matrices is required. Moreover, this local-global transformation procedure is more complicated for the hierarchical basis functions.

A self-identification technique [Li et al., 2014c] is proposed to meet the compatibility requirement. The basis functions are defined directly by the global node orders. Then, the basis functions follow the same node order at the boundaries of the finite elements and satisfy the boundary continuity condition of the basis functions. The basis functions for the MoM on the boundary triangles follow the global node orders of the edges or faces and the basis functions for the FE method are self-identified with the node orders of the boundary triangles. Then, the compatibility between the FE and BI methods can be obtained. The self-identification technique avoids the procedure of the local-global transformations.

1.4 The Outline of the Thesis

The whole construction of this document is as follows. Chapter 2 describes the modeling for the FE-BI simulations. A short review of Maxwell equations is the start and the Huygens' principle, equivalence theory and the Galerkin process are also reviewed.

Chapter 3 discusses the boundary integral equations. The BI method is based on MoM, including the EFIE, MFIE and CFIE. The numerical expansions of the electric and magnetic currents are explained in detail. Through the Galerkin process, the system matrices for EFIE and MFIE are provided. The MLFMM is then introduced as BI method acceleration. The spherical harmonics expansion of the $\hat{k}$-space integrals is also shown in the MLFMM.

Chapter 4 talks about the singularity treatment technologies. The configurations for different projection points are illustrated for singularity treatments and a summary of singularity treatment solutions is provided. In the singularity cancellation technique, a new family of radial-angular-R^n transformations are proposed based on the variable separation method. General solutions are presented for the variable separation method and a family of transformation schemes are obtained for different orders of singularity cancellations. The performance for deformed triangles is in detail studied for the new transformation schemes. High efficiency and accuracy are achieved by the new transformation schemes.

Chapter 5 discusses the 2-D hierarchical basis functions for MoM. The $Rao-Wilton-Glission$ (RWG) [Rao et al., 1982] basis functions are utilized as the low order (LO) basis functions, higher order (HO) basis functions are also implemented into MoM and MoM simulations of PEC objects are shown. The efficacy and accuracy of MoM are proven by numerical results based on the nearly orthogonal basis functions.

Chapter 6 reviews the FEM. The variational formulation is derived from the Maxwell

equations tested by the ad-joint field through the Galerkin process. The variational formulation is effective for homogeneous or inhomogeneous, isotropic or anisotropic materials and can compute the fields inside of materials. The system matrices of FEM are sparse and the elements in the matrix are computed analytically. The simulations of FEM are accurate and efficient.

Chapter 7 displays the 3-D vector hierarchical basis functions for the FEM. The geometrical information of a tetrahedron is shown. The integration properties of the simplex coordinates are reviewed. Then, analytical solutions can be obtained for the system matrices by the mutual couplings of the hierarchical basis functions. Together with MoM, the hybrid FE-BI method is formulated incorporating the FEM. Then, coated objects can be simulated for both radiation fields and also the fields inside the dielectric materials. Numerical results of the FE-BI method are shown for different coated configurations.

Chapter 8 proposes an accuracy analysis of the FE-BI method for the nearly orthogonal hierarchical basis functions. The accuracy of the FE-BI method mainly depends on the ratio between the mesh size and the wavelength. Accuracy comparisons are provided for different orders of basis functions. The root mean square (RMS) error is defined to evaluate the accuracy. The RMS error is flexible for different variables and lower RMS error indicates higher accuracy. The accuracy of the FE-BI method is shown for various models and the performance is also discussed in detail for all orders of hierarchical basis functions.

Chapter 9 summarizes the most important numerical results proposed in the thesis, conclusions are also highlighted for the efficient algorithms.

2 Electromagnetic Modeling by the Hybrid Finite Element Boundary Integral Technique

The hybrid finite element boundary integral (FE-BI) method is well known for the solution of wave scattering and radiation problems. The hybrid FE-BI method combines the finite element method (FEM) and the boundary integral (BI) method and it also overcomes the negative effects of the pure FE or BI methods. The pure FEM can be inefficient for the electromagnetic simulation of non-convex shaped objects. The pure boundary integral method is not effective for the electromagnetic simulation of objects with inhomogeneous materials, even though the BI method has been proven to be efficient for the simulation of perfect electric conductor objects or objects with homogeneous materials. The hybrid FE-BI method contains the advantages of the BI method for simulations of arbitrarily shaped objects and also the efficiency of the FE method for simulations of objects with inhomogeneous and anisotropic materials. The hybrid FE-BI method also obtains good performance in accuracy and efficiency.

The FE-BI method is applied to the modeling of arbitrarily shaped objects enclosed by fictitious outside boundary surfaces. The objects can contain perfect electric conductors (PEC), semi-conductors or dielectric materials. The scattering fields outside the boundary surfaces are described through the BI based on equivalent surface electric and magnetic currents. The fields inside the boundary surfaces are modeled through the FEM. For PEC, the electric field vanishes at PEC boundaries and also inside the PEC objects. For semi-conductors, the problem can be equivalent to set a minus number to the imaginary part of the permittivity of the material. With a negative number in the imaginary part of the permittivity, the semiconductor is lossy compared with pure dielectric materials. Thus, the field analysis inside the boundaries can take advantage of the FEM. Inhomogeneous and anisotropic dielectrics are represented by various permittivities and permeabilities. The fields inside the materials can be accurately computed by the FE-BI method.

In this chapter, the modeling of electromagnetics by the FE-BI method is introduced. The Maxwell equations and the symmetric Maxwell equations are reviewed, a general description of the object model for simulations is provided, the equivalent currents for the BI and the Huygens' principle for scattering are also demonstrated, the general mathematical solutions for the FE-BI method are also discussed for the modeling of electromagnetic simulations.

2.1 Maxwell Equations

The essential foundations for electromagnetics are the Maxwell equations, where the specified time factor $e^{j\omega t}$ can be suppressed. The Maxwell equations [Chew et al., 2001,

Harman, 1995, Jin, 2002] can be given as

$$\nabla \times \boldsymbol{H}(\boldsymbol{r}) = j\omega\epsilon(\boldsymbol{r})\boldsymbol{E}(\boldsymbol{r}) + \boldsymbol{J}(\boldsymbol{r}), \tag{2.1.1}$$

$$\nabla \times \boldsymbol{E}(\boldsymbol{r}) = -j\omega\mu(\boldsymbol{r})\boldsymbol{H}(\boldsymbol{r}), \tag{2.1.2}$$

$$\nabla \cdot \big(\mu(\boldsymbol{r})\boldsymbol{H}(\boldsymbol{r})\big) = 0, \tag{2.1.3}$$

$$\nabla \cdot \big(\epsilon(\boldsymbol{r})\boldsymbol{E}(\boldsymbol{r})\big) = \rho(\boldsymbol{r}), \tag{2.1.4}$$

where $\boldsymbol{J}(\boldsymbol{r})$ is an impressed electric current density, $\rho(\boldsymbol{r})$ is the corresponding charge density in the model. $\boldsymbol{E}(\boldsymbol{r})$ and $\boldsymbol{H}(\boldsymbol{r})$ are the electric and magnetic fields, $\epsilon(\boldsymbol{r})$ and $\mu(\boldsymbol{r})$ are the relative permittivity and relative permeability of the materials, $\boldsymbol{r}$ is the position inside the medium.

The equations from (2.1.1) to (2.1.4) are the Maxwell equations in differential form. (2.1.1) is the differential form of the Ampere's law, (2.1.2) is the differential form of the Faraday's law, (2.1.3) demonstrates that there are no isolated magnetic charges and (2.1.4) is the differential form of the Gauss' law.

2.2 The Symmetric Maxwell Equations

It is well known that the electric current density $\boldsymbol{J}(\boldsymbol{r})$ exists and the radiating fields are generated by the electric current sources as considered in (2.1.1). While to achieve the symmetric Maxwell equations, an assumed magnetic current density $\boldsymbol{M}(\boldsymbol{r})$ is introduced. Thus, the Maxwell equations turn out to be

$$\nabla \times \boldsymbol{H}(\boldsymbol{r}) = j\omega\epsilon(\boldsymbol{r})\boldsymbol{E}(\boldsymbol{r}) + \boldsymbol{J}(\boldsymbol{r}), \tag{2.2.1}$$

$$\nabla \times \boldsymbol{E}(\boldsymbol{r}) = -j\omega\mu(\boldsymbol{r})\boldsymbol{H}(\boldsymbol{r}) - \boldsymbol{M}(\boldsymbol{r}), \tag{2.2.2}$$

$$\nabla \cdot \big(\mu(\boldsymbol{r})\boldsymbol{H}(\boldsymbol{r})\big) = \rho_m(\boldsymbol{r}), \tag{2.2.3}$$

$$\nabla \cdot \big(\epsilon(\boldsymbol{r})\boldsymbol{E}(\boldsymbol{r})\big) = \rho_e(\boldsymbol{r}), \tag{2.2.4}$$

where ρ_e is the electric charge density and ρ_m is the magnetic charge density. The radiating fields in the space can be visualized as final effects of both the electric and magnetic current density sources inside the object.

2.3 The Modeling Approach

An easy model to meet the general physical case of arbitrarily shaped objects is shown in Fig. 1 and it is called FE-BI object. The FE-BI object is combined with PEC and dielectric materials. In the PEC object, some of the surfaces are part of the outside boundary surfaces of the FE-BI object and they conform to the outside PEC boundaries. The other parts of the PEC surfaces are connected with the dielectric materials inside and they conform to the inside PEC boundaries. For the dielectric object, the surfaces outside the FE-BI object, together with the outside PEC boundaries, construct the enclosed surfaces of the FE-BI object. They are utilized as the outside equivalent fictitious surfaces for the FE-BI algorithm.

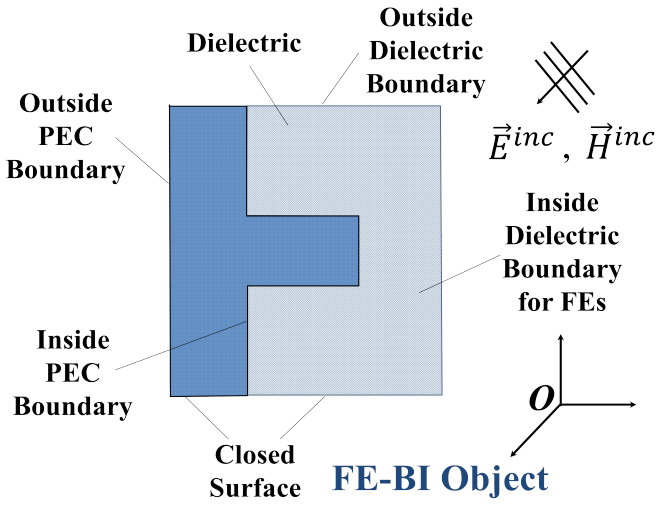

Figure 1: The general geometrical configuration for the finite element boundary integral method.

A model of equivalent surfaces from the FE-BI object is shown in Fig. 2. Compared with Fig. 1, the outside boundary surfaces of the FE-BI object are selected as the equivalent surfaces. In the model, A_d is the assembled enclosed envelope, V_a is a finite volume enclosed by A_d, $\hat{n}(\boldsymbol{r}')$ is a normal vector pointing out of V_a and $\hat{s}(\boldsymbol{r}')$ is a normal vector pointing inside V_a. The outside space is represented by V_o. The equivalent electric surface currents $\boldsymbol{J}_s(\boldsymbol{r}')$ and the magnetic surface currents $\boldsymbol{M}_s(\boldsymbol{r}')$ are distributed on the equivalent surfaces A_d. The equivalent currents on A_d are utilized in the BI method. In Fig. 2, the fields terminate inside the PEC object, the tangential electric field is zero at the PEC inside and outside boundaries in the FE-BI object model. As a result, only the possibly anisotropic and inhomogeneous materials inside the finite volume V_a contain electric and magnetic fields. The materials are characterized by the permittivity $\bar{\epsilon}(\boldsymbol{r}')$ and the permeability $\bar{\mu}(\boldsymbol{r}')$. The fields inside the materials need to be determined through the FEM. The hybrid FE-BI method is efficient for the electromagnetic simulations of the FE-BI object model and accurate results can be obtained.

Dependent on the properties of inhomogeneous and anisotropic dielectric materials, the electric flux density and the magnetic flux density are determined by the constitutive relations shown as

$$\boldsymbol{D}(\boldsymbol{r}) = \bar{\epsilon}(\boldsymbol{r}) \cdot \boldsymbol{E}(\boldsymbol{r}), \tag{2.3.1}$$

$$\boldsymbol{B}(\boldsymbol{r}) = \bar{\mu}(\boldsymbol{r}) \cdot \boldsymbol{H}(\boldsymbol{r}), \tag{2.3.2}$$

where the fields in the dielectric materials are modeled through the FEM, which is discussed in Chapter 3.

In the FEM, the objects are subdivided into sub-regions, the material properties within a single section are constant, even though the material properties may have a continuous variation with the changing positions inside the volumes. This represents that the sub-

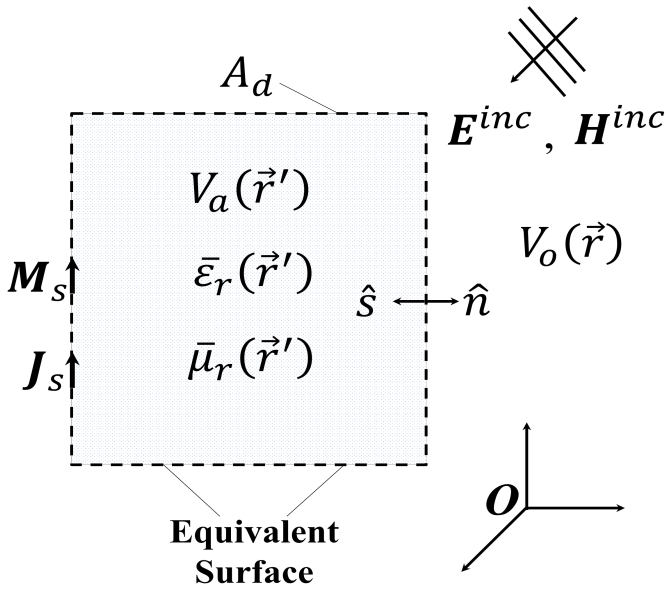

Figure 2: The general geometrical configuration for equivalent surfaces.

regions can be arbitrarily small and the FEM can increase the accuracy of the electromagnetic (EM) simulations by decreasing the mesh element sizes. With equations (2.1.1) to (2.1.4), combined with (2.3.1) and (2.3.2), the specified fields inside the dielectrics can be precisely described. Moreover, based on the structure of the divided sections, the fields in the sections are expanded as the product of the basis functions and the corresponding coefficients. The basis functions are defined based on the geometrical information of the divided sections, the coefficients are unknowns to be solved. Compared with the wavelength, a smaller size of the sections can increase the EM simulation accuracy. With larger mesh element size, higher order basis functions can be utilized to obtain good accuracy. The FE can also have effects on the surface electric and magnetic currents. As a result, the FE method can describe the effects of the dielectric materials on the radiating fields in the outside space.

As shown in Fig. 2, the radiating fields can be computed through the equivalent surface electric currents $\boldsymbol{J}_s(\boldsymbol{r'})$ and the magnetic currents $\boldsymbol{M}_s(\boldsymbol{r'})$. They are calculated in the BI. In the BI method, the fictitious enclosed envelope A_d is subdivided into sections. Similar to the FE method, a smaller size of the sections can also increase the accuracy. The currents $\boldsymbol{J}_s(\boldsymbol{r'})$ and $\boldsymbol{M}_s(\boldsymbol{r'})$ are also expanded into products of basis functions and the corresponding coefficients. The basis functions are defined based on the geometric information of the divided sections and the coefficients are the unknowns to be computed. With higher order basis functions, the accuracy of the BI can also be improved for larger mesh element size.

In the FE-BI method, it is advantageous to be compatible between the basis functions for the BI method and the basis functions for the FE method. The selected basis functions for the BI method are div conforming, meaning that the orthogonal components at the section boundaries are continuous. The selected basis functions for the FE method are curl

conforming, where the tangential components on the section boundaries are continuous. The curl-conforming and the divergence-conforming basis functions have to follow the same geometric information of the corresponding sections. Thus, the compatibility of the hybrid FE-BI method is obtained.

2.4 Equivalent Currents

The equivalent electric and magnetic currents are utilized to compute the scattering fields in the outer space. The model of the equivalent currents derived for the FE-BI object is shown in Fig. 2. Through the Huygens' principle, the equivalent electric currents and the magnetic currents are distributed on the enclosed envelopes. The same radiating fields to the outside free space can be achieved through the equivalent electric and magnetic currents. Then, the fields inside V_a can be neglected.

Based on the boundary conditions of the Huygens' principle, the surface electric currents $\boldsymbol{J}_s(\boldsymbol{r})$ and the magnetic currents $\boldsymbol{M}_s(\boldsymbol{r})$ are written as

$$\boldsymbol{J}_s(\boldsymbol{r}) = \hat{n}(\boldsymbol{r}) \times \boldsymbol{H}(\boldsymbol{r}) \,, \tag{2.4.1}$$

$$\boldsymbol{M}_s(\boldsymbol{r}) = -\hat{n}(\boldsymbol{r}) \times \boldsymbol{E}(\boldsymbol{r}) \tag{2.4.2}$$

on the outside surfaces A_d. In computational electromagnetics, the electric currents $\boldsymbol{J}_s$ and the magnetic currents $\boldsymbol{M}_s$ are essential for the field scattering. In most EM simulations, $\boldsymbol{J}_s$ and $\boldsymbol{M}_s$ are unknowns to be solved for.

In the FE method, the fields in the volume are discretized. However, the electric and the magnetic fields on the outside boundaries maintain the compatibility with the surface electric and magnetic currents, as shown in (2.4.1) and (2.4.2). Thus, the FE method is also connected to the surface currents.

The boundary integral equations are focused on the envelope A_d. Through the numerical expansions of the electric and magnetic currents, the unknowns need to be solved. A very efficient solution to the boundary integral equations is the method of moments (MoM), where the Galerkin process is applied to obtain the system matrices. To accurately evaluate the mutual couplings in MoM, the well known Gauss-Legendre quadrature is utilized for the integrals. The system matrices of the BI method are full-filled. The pure BI method is very effective to solve PEC problems. Both the electric and magnetic fields vanish inside the PEC objects and the electric fields are also zero on the PEC surfaces. Moreover, the pure BI method is also effective to compute the fields and currents for homogeneous materials. However, without cooperating with other techniques, it can not tackle inhomogeneous and anisotropic materials.

The hybrid FE-BI method is efficient for both $\boldsymbol{J}_s$ and $\boldsymbol{M}_s$ computations. It is applicable to objects with inhomogeneous and anisotropic materials. The reconstructed surface currents are utilized to compute the scattering fields outside the envelope without considering the sources inside. The currents derived from the boundary conditions (2.4.1) and (2.4.2) are visualized as the only sources for the outside space. The electric and magnetic fields inside the volumes are determined precisely through the FE method.

2.5 Huygens' Principle

The Huygens' principle develops from the equivalence theorem. The general FE-BI object is shown in Fig. 1. It consists of finite volumes filled with dielectric materials and also PEC components. The PEC components are connected with the dielectric components. The whole FE-BI object is enclosed by an envelope and the envelope is represented by the closed surfaces. To efficiently solve electromagnetic problems with the FE-BI object models, the equivalence theorem is utilized. A simplified model for the equivalence theorem is shown in Fig. 2. The outside enclosed surfaces are represented by A_d. A_d separates the space into the inside volume $V_a(\boldsymbol{r'})$ and the outside volume $V_o(\boldsymbol{r})$, where $\boldsymbol{r'}$ is the position inside A_d and $\boldsymbol{r}$ describes the position outside A_d. The equivalence theorem focuses on A_d and computes the equivalent electric currents $\boldsymbol{J}_s$ and magnetic currents $\boldsymbol{M}_s$, as shown in Fig. 2. The reconstructed electric and magnetic currents on the enclosed boundary surfaces generate the same scattering fields in the outside space as the sources inside V_a. As it turns out, the fields, sources and structures inside V_a can be neglected.

To prove the Huygens' principle [Kong, 1986], the model in Fig. 2 is utilized. An incident wave in an arbitrary direction is assumed as the excitation of the model. $\bar{\epsilon}(\boldsymbol{r'})$ is the permittivity and $\bar{\mu}(\boldsymbol{r'})$ is the permeability inside the volume V_a. However, the scattering fields are only dependent on the surface equivalent currents $\boldsymbol{J}_s$ and $\boldsymbol{M}_s$. $\hat{n}$ is the unit vector orthogonal to A_d pointing outside V_a and inside V_o. $\hat{s}$ is the unit vector also orthogonal to A_d pointing inside V_a and outside V_o. As shown in Fig. 2, at a position on the surface of A_d, $\hat{n}$ and $\hat{s}$ are parallel and pointing in the inverse directions, which means $\hat{n}(\boldsymbol{r}) = -\hat{s}(\boldsymbol{r})$.

Assume V_o is a source free homogeneous space, it gives $\boldsymbol{J}(\boldsymbol{r}) = \boldsymbol{M}(\boldsymbol{r}) = 0$ and $\rho_m(\boldsymbol{r}) = \rho_e(\boldsymbol{r}) = 0$. As it turns out, the symmetric Maxwell equations from (2.2.1) to (2.2.4) are the same as the Maxwell equations from (2.1.1) to (2.1.4). With (2.1.1) and (2.1.2) utilized in V_o, it is obtained that

$$\nabla \times \nabla \times \boldsymbol{E}(\boldsymbol{r}) - k^2 \boldsymbol{E}(\boldsymbol{r}) = 0, \tag{2.5.1}$$

where $k = \omega\sqrt{\epsilon_0 \mu_0}$ is the wave number in free space. To solve (2.5.1), the dyadic Green's function is introduced. The format of the dyadic Green's function is written as

$$\nabla \times \nabla \times \bar{G}(\boldsymbol{r}, \boldsymbol{r'}) - k^2 \bar{G}(\boldsymbol{r}, \boldsymbol{r'}) = \bar{I}\delta(\boldsymbol{r} - \boldsymbol{r'}), \tag{2.5.2}$$

where $\bar{G}(\boldsymbol{r'}, \boldsymbol{r})$ is the dyadic Green's function and $\bar{I} = \hat{x}\hat{x} + \hat{y}\hat{y} + \hat{z}\hat{z}$ is the unit dyad. A general solution to the dyadic Green's function in (2.5.2) is given by

$$\bar{G}(\boldsymbol{r}, \boldsymbol{r'}) = \left(\bar{I} + \frac{\nabla\nabla}{k^2}\right) G(\boldsymbol{r}, \boldsymbol{r'}) \tag{2.5.3}$$

and

$$G(\boldsymbol{r}, \boldsymbol{r'}) = \frac{e^{-jk\left|\boldsymbol{r}-\boldsymbol{r'}\right|}}{4\pi\left|\boldsymbol{r} - \boldsymbol{r'}\right|} \tag{2.5.4}$$

in (2.5.3) is the scalar Green's function [Jin, 2002] (Page 720, C.30 and Page 724, C.62). With the dyadic Green's function dot with (2.5.1) and the electric field $\boldsymbol{E}(\boldsymbol{r})$ dot with

(2.5.2) [Kong, 1986], it is found that

$$\boldsymbol{E}(\boldsymbol{r})\cdot\nabla\times\nabla\times\bar{G}(\boldsymbol{r'},\boldsymbol{r})-\nabla\times\nabla\times\boldsymbol{E}(\boldsymbol{r})\cdot\bar{G}(\boldsymbol{r'},\boldsymbol{r})=\boldsymbol{E}(\boldsymbol{r})\delta(\boldsymbol{r}-\boldsymbol{r'}). \tag{2.5.5}$$

Through the integral of (2.5.5) over V_o, where the boundary surfaces of V_o include A_d and the infinitely far away surface S_∞, it is obtained

$$\boldsymbol{E}(\boldsymbol{r'})=\iiint_{V_o}\boldsymbol{E}(\boldsymbol{r})\cdot\nabla\times\nabla\times\bar{G}(\boldsymbol{r'},\boldsymbol{r})-\nabla\times\nabla\times\boldsymbol{E}(\boldsymbol{r})\cdot\bar{G}(\boldsymbol{r'},\boldsymbol{r})\,dv. \tag{2.5.6}$$

(2.5.6) can be rewritten by the second vector-dyadic Green's theorem [Jin, 2002] (Page 712, A.29), shown as

$$\iiint_V \boldsymbol{a}\cdot\nabla\times\nabla\times\bar{b}-\nabla\times\nabla\times\boldsymbol{a}\cdot\bar{b}\,dv=-\oiint_S\hat{n}\cdot\left[\boldsymbol{a}\times\nabla\times\bar{b}+(\nabla\times\boldsymbol{a})\times\bar{b}\right]\,ds. \tag{2.5.7}$$

Let $\boldsymbol{a}=\boldsymbol{E}(\boldsymbol{r})$, $\bar{b}=\bar{G}(\boldsymbol{r},\boldsymbol{r'})$, $V=V_o$, $\hat{n}=\hat{s}$ and $S=A_d+S_\infty$. Under the Sommerfeld radiation condition [Sommerfeld, 1949], the integration over S_∞ vanishes, the integration over the outside boundary turns to be $S=A_d$. Then, it is found that

$$\begin{aligned}&\iiint_{V_o}\boldsymbol{E}(\boldsymbol{r})\cdot\nabla\times\nabla\times\bar{G}(\boldsymbol{r'},\boldsymbol{r})-\nabla\times\nabla\times\boldsymbol{E}(\boldsymbol{r})\cdot\bar{G}(\boldsymbol{r'},\boldsymbol{r})\,dv\\&=-\oiint_{A_d}\hat{s}\cdot\left[\boldsymbol{E}(\boldsymbol{r})\times\nabla\times\bar{G}(\boldsymbol{r'},\boldsymbol{r})+(\nabla\times\boldsymbol{E}(\boldsymbol{r}))\times\bar{G}(\boldsymbol{r'},\boldsymbol{r})\right]\,ds.\end{aligned} \tag{2.5.8}$$

Through the use of (2.5.5) in (2.5.8), it is found that

$$\boldsymbol{E}(\boldsymbol{r'})=-\oiint_{A_d}\left[(\hat{s}\times\boldsymbol{E}(\boldsymbol{r}))\cdot\left(\nabla\times\bar{G}(\boldsymbol{r'},\boldsymbol{r})\right)+(\hat{s}\times\nabla\times\boldsymbol{E}(\boldsymbol{r}))\cdot\bar{G}(\boldsymbol{r'},\boldsymbol{r})\right]\,ds. \tag{2.5.9}$$

To further expand (2.5.9), an arbitrary constant assisting vector $\boldsymbol{e}$ is utilized. The first term in (2.5.9) is written as

$$\begin{aligned}&(\hat{s}\times\boldsymbol{E}(\boldsymbol{r}))\cdot\nabla\times\bar{G}(\boldsymbol{r'},\boldsymbol{r})\cdot\boldsymbol{e}=(\hat{s}\times\boldsymbol{E}(\boldsymbol{r}))\cdot\nabla\times(G(\boldsymbol{r'},\boldsymbol{r})\boldsymbol{e}+\nabla\nabla\cdot G(\boldsymbol{r'},\boldsymbol{r})\boldsymbol{e})\\&=(\hat{s}\times\boldsymbol{E}(\boldsymbol{r}))\cdot(\nabla G(\boldsymbol{r'},\boldsymbol{r})\times\boldsymbol{e})=(\hat{s}\times\boldsymbol{E}(\boldsymbol{r}))\times\nabla G(\boldsymbol{r'},\boldsymbol{r})\cdot\boldsymbol{e}.\end{aligned} \tag{2.5.10}$$

As $\boldsymbol{e}$ is an arbitrary constant vector, (2.5.10) proves that

$$(\hat{s}\times\boldsymbol{E}(\boldsymbol{r}))\cdot\nabla\times\left(\bar{G}(\boldsymbol{r'},\boldsymbol{r})\right)=(\hat{s}\times\boldsymbol{E}(\boldsymbol{r}))\times\nabla G(\boldsymbol{r'},\boldsymbol{r}). \tag{2.5.11}$$

The second term with the constant vector $\boldsymbol{e}$ in (2.5.9) can be written as

$$\begin{aligned}&(\hat{s}\times\nabla\times\boldsymbol{E}(\boldsymbol{r}))\cdot\bar{G}(\boldsymbol{r'},\boldsymbol{r})\cdot\boldsymbol{e}\\&=(\hat{s}\times\nabla\times\boldsymbol{E}(\boldsymbol{r}))\cdot\left(G(\boldsymbol{r'},\boldsymbol{r})\boldsymbol{e}+\frac{1}{k^2}\nabla\nabla\cdot G(\boldsymbol{r'},\boldsymbol{r})\boldsymbol{e}\right) &\text{(2.5.12a)}\\&=(\hat{s}\times\nabla\times\boldsymbol{E}(\boldsymbol{r}))\cdot G(\boldsymbol{r'},\boldsymbol{r})\boldsymbol{e}+\frac{1}{k^2}\hat{s}\cdot(\nabla\times\boldsymbol{E}(\boldsymbol{r})\times\nabla\nabla\cdot G(\boldsymbol{r'},\boldsymbol{r})\boldsymbol{e})\,. &\text{(2.5.12b)}\end{aligned}$$

As a vector identity is known as $(\nabla \times \boldsymbol{A}) \times \nabla\phi = \phi(\nabla \times \nabla \times \boldsymbol{A}) - \nabla \times (\phi \nabla \times \boldsymbol{A})$, and when $\boldsymbol{A} = \boldsymbol{E}(\boldsymbol{r})$, $\phi = \nabla \cdot G(\boldsymbol{r'}, \boldsymbol{r})\boldsymbol{e}$, the second term in (2.5.12b) turns to be

$$\begin{aligned}
&\frac{1}{k^2}\hat{s} \cdot (\nabla \times \boldsymbol{E}(\boldsymbol{r}) \times \nabla\nabla \cdot G(\boldsymbol{r'}, \boldsymbol{r})\boldsymbol{e}) \\
=&\frac{1}{k^2}\hat{s} \cdot \Big\{ (\nabla \times \nabla \times \boldsymbol{E}(\boldsymbol{r}))\, \nabla \cdot G(\boldsymbol{r'}, \boldsymbol{r})\boldsymbol{e} - \nabla \times [(\nabla \cdot G(\boldsymbol{r'}, \boldsymbol{r})\boldsymbol{e})\, (\nabla \times \boldsymbol{E}(\boldsymbol{r}))] \Big\} \qquad (2.5.13)
\end{aligned}$$

and

$$\begin{aligned}
&\oiint_{A_d} \hat{s} \cdot (\nabla \times [(\nabla \cdot G(\boldsymbol{r'}, \boldsymbol{r})\boldsymbol{e})\, (\nabla \times \boldsymbol{E}(\boldsymbol{r}))])\, ds \\
=&\iiint_{V_o} \nabla \cdot (\nabla \times [(\nabla \cdot G(\boldsymbol{r'}, \boldsymbol{r})\boldsymbol{e})\, (\nabla \times \boldsymbol{E}(\boldsymbol{r}))])\, dv = 0. \qquad (2.5.14)
\end{aligned}$$

Then, it is found

$$\begin{aligned}
&\oiint_{A_d} \frac{1}{k^2}\hat{s} \cdot (\nabla \times \boldsymbol{E}(\boldsymbol{r}) \times \nabla\nabla \cdot G(\boldsymbol{r'}, \boldsymbol{r})\boldsymbol{e})\, ds \\
=&\oiint_{A_d} \frac{1}{k^2}\hat{s} \cdot (\nabla \times \nabla \times \boldsymbol{E}(\boldsymbol{r}))\, (\nabla G(\boldsymbol{r'}, \boldsymbol{r}) \cdot \boldsymbol{e})\, ds. \qquad (2.5.15)
\end{aligned}$$

By substituting (2.5.11), (2.5.12b) and (2.5.15) into (2.5.9), it follows

$$\begin{aligned}
\boldsymbol{E}(\boldsymbol{r'}) = -&\oiint_{A_d} \Big[(\hat{s} \times \boldsymbol{E}(\boldsymbol{r})) \times \nabla G(\boldsymbol{r'}, \boldsymbol{r}) \\
&+ (\hat{s} \times \nabla \times \boldsymbol{E}(\boldsymbol{r}))\, G(\boldsymbol{r'}, \boldsymbol{r}) + \frac{1}{k^2}\, (\hat{s} \cdot (\nabla \times \nabla \times \boldsymbol{E}(\boldsymbol{r})))\, \nabla G(\boldsymbol{r'}, \boldsymbol{r}) \Big]\, ds. \qquad (2.5.16)
\end{aligned}$$

Together with (2.1.2), (2.5.1) and $\hat{n} = -\hat{s}$, (2.5.16) turns to be

$$\begin{aligned}
\boldsymbol{E}(\boldsymbol{r'}) =&\oiint_{A_d} \Big[(\hat{n}(\boldsymbol{r}) \times \boldsymbol{E}(\boldsymbol{r})) \times \nabla G(\boldsymbol{r'}, \boldsymbol{r}) \\
&- j\omega\mu(\boldsymbol{r})\, (\hat{n}(\boldsymbol{r}) \times \boldsymbol{H}(\boldsymbol{r}))\, G(\boldsymbol{r'}, \boldsymbol{r}) + (\hat{n}(\boldsymbol{r}) \cdot \boldsymbol{E}(\boldsymbol{r}))\, \nabla G(\boldsymbol{r'}, \boldsymbol{r}) \Big]\, ds. \qquad (2.5.17)
\end{aligned}$$

Moreover, the positions of the variables $\boldsymbol{r'}$ and $\boldsymbol{r}$ in (2.5.17) can be exchanged, as they are equivalent in the scalar Green's functions. So (2.5.17) can also be written as

$$\begin{aligned}
\boldsymbol{E}(\boldsymbol{r}) =&\oiint_{A_d} \Big[(\hat{n}(\boldsymbol{r'}) \times \boldsymbol{E}(\boldsymbol{r'})) \times \nabla' G(\boldsymbol{r}, \boldsymbol{r'}) \\
&- j\omega\mu(\boldsymbol{r'})\, (\hat{n}(\boldsymbol{r'}) \times \boldsymbol{H}(\boldsymbol{r'}))\, G(\boldsymbol{r}, \boldsymbol{r'}) + (\hat{n}(\boldsymbol{r'}) \cdot \boldsymbol{E}(\boldsymbol{r'}))\, \nabla' G(\boldsymbol{r}, \boldsymbol{r'}) \Big]\, ds'. \qquad (2.5.18)
\end{aligned}$$

In a similar process, the magnetic field $\boldsymbol{H}(\boldsymbol{r})$ can be written as

$$\begin{aligned}
\boldsymbol{H}(\boldsymbol{r}) =&\oiint_{A_d} \Big[(\hat{n}(\boldsymbol{r'}) \times \boldsymbol{H}(\boldsymbol{r'})) \times \nabla' G(\boldsymbol{r}, \boldsymbol{r'}) \\
&+ j\omega\epsilon(\boldsymbol{r'})\, (\hat{n}(\boldsymbol{r'}) \times \boldsymbol{E}(\boldsymbol{r'}))\, G(\boldsymbol{r}, \boldsymbol{r'}) + (\hat{n}(\boldsymbol{r'}) \cdot \boldsymbol{H}(\boldsymbol{r'}))\, \nabla' G(\boldsymbol{r}, \boldsymbol{r'}) \Big]\, ds'. \qquad (2.5.19)
\end{aligned}$$

With the definitions of the surface electric and magnetic currents (2.4.1) and (2.4.2) into (2.5.19), it is obtained that

$$\boldsymbol{E}(\boldsymbol{r}) = \oiint_{A_d} \left[-j\omega\mu \boldsymbol{J}_s(\boldsymbol{r'}) G(\boldsymbol{r}, \boldsymbol{r'}) - \boldsymbol{M}_s(\boldsymbol{r'}) \times \nabla' G(\boldsymbol{r}, \boldsymbol{r'}) + \frac{1}{\epsilon} \rho_e(\boldsymbol{r'}) \nabla' G(\boldsymbol{r}, \boldsymbol{r'}) \right] ds', \quad (2.5.20)$$

$$\boldsymbol{H}(\boldsymbol{r}) = \oiint_{A_d} \left[\boldsymbol{J}_s(\boldsymbol{r'}) \times \nabla' G(\boldsymbol{r}, \boldsymbol{r'}) - j\omega\epsilon \boldsymbol{M}_s(\boldsymbol{r'}) G(\boldsymbol{r}, \boldsymbol{r'}) + \frac{1}{\mu} \rho_m(\boldsymbol{r'}) \nabla' G(\boldsymbol{r}, \boldsymbol{r'}) \right] ds', \quad (2.5.21)$$

where $\rho_e(\boldsymbol{r'}) = \hat{n}(\boldsymbol{r'}) \cdot (\epsilon(\boldsymbol{r'}) \cdot \boldsymbol{E}(\boldsymbol{r'}))$ is the equivalent electric charge density, $\rho_m(\boldsymbol{r'}) = \hat{n}(\boldsymbol{r'}) \cdot (\mu(\boldsymbol{r'}) \cdot \boldsymbol{H}(\boldsymbol{r'}))$ is the equivalent magnetic charge density. $G(\boldsymbol{r}, \boldsymbol{r'})$ is the Green's function in free space. The equivalent currents and charges are distributed outside A_d. In computational electromagnetics, it is necessary to compute the electromagnetic fields outside the objects based on the equivalent currents. The radiating electric field $\boldsymbol{E}(\boldsymbol{r})$ and the radiating magnetic field $\boldsymbol{H}(\boldsymbol{r})$ are determined by the surface electric currents $\boldsymbol{J}_s(\boldsymbol{r'})$ and the magnetic currents $\boldsymbol{M}_s(\boldsymbol{r'})$, where the radiating fields are given by (2.5.20) and (2.5.21).

2.6 The Hybrid Finite Element Boundary Integral Technique

The hybrid method in this work means a combination of a local computation method and a global computation method. The local computation method is represented by the FEM and the boundary integral (BI) method is the global method. The FE method is utilized in the hybrid method, this is due to its high flexibility and adaptive properties for arbitrarily shaped penetrable objects. The BI method is also required in the hybrid method, this lies in its accuracy and efficiency for the EM simulations. When the FE method is combined with the BI method, the hybrid finite element boundary integral (FE-BI) method is obtained. The hybrid FE-BI method is effective for EM simulations of objects with inhomogeneous and anisotropic materials. Moreover, it is also effective for models with dielectrics combined with PEC components. However, the hybrid FE-BI method requires the compatibility between FE and BI. The basis functions in the FE and BI methods need to follow the same node orders. The compatibility in FE-BI provides an effective and accurate solution to different kinds of complicated geometrical models. As a result, the formulations of the hybrid FE-BI method are advantageous with inheriting the efficiency of the FEM and also the accuracy of the BI method.

The FEM is a numerical procedure to obtain approximate values of the fields on the boundaries of the objects and also inside the dielectric volumes. In this work, the FEM is computed through the Ritz method [Jin, 2002]. The Ritz method produces system matrices and the matrices are also applicable to specified values on the boundaries. Through minimizing the error, a solution to the variable coefficients is obtained for the fields. The general formulation is written as

$$L\phi = f, \quad (2.6.1)$$

where L is a linear operator, f is a function based on the excitations, ϕ is the unknown function which needs to be computed. The Ritz procedure is utilized to find ϕ and the

problem is written as a functional

$$F(\phi) =< L\phi, \phi > - < f, \phi >, \tag{2.6.2}$$

where the inner product is defined as

$$< \phi, \tilde{\phi} >= \int_{\Omega} (\phi\, \tilde{\phi}) d\Omega \tag{2.6.3}$$

and

$$< \phi, \tilde{\phi} >=< \tilde{\phi}, \phi >, \tag{2.6.4}$$

where $\tilde{\phi}$ is a trial function. The variable ϕ can be expanded as

$$\phi = \sum_{i=1}^{N} c_i v_i, \tag{2.6.5}$$

where v_i are defined basis functions, c_i are unknown coefficients to be determined and N is the total number of unknowns. Under the condition of minimizing the error, the formulation is computed as

$$\begin{aligned} \frac{\partial F(\phi)}{\partial c_i} &= \frac{\partial}{\partial c_i}(< L \sum_{i=1}^{N} c_i v_i, \sum_{j=1}^{N} c_j v_j > - < \sum_{i=1}^{N} c_i v_i, f >) \\ &= \sum_{j=1}^{N} < L v_i, v_j > c_j - < v_i, f >= 0, \qquad i = 1, 2, 3, ..., N. \end{aligned} \tag{2.6.6}$$

Then, the matrix equation can be obtained as

$$[A]\,[c] = [b]\,, \tag{2.6.7}$$

with the system matrix elements written as

$$A_{ij} =< L v_i, v_j >= \int_{\Omega} (v_j\, L v_i) d\Omega, \qquad i, j = 1, 2, 3, ..., N \tag{2.6.8}$$

and the elements in the vector $[b]$ are given as

$$b_i =< v_i, f >= \int_{\Omega} (v_i\, f) d\Omega, \qquad i = 1, 2, 3, ..., N. \tag{2.6.9}$$

The Ritz process can be applied for the FE method. ϕ can be the field to be computed, $\tilde{\phi}$ can be selected as the ad-joint field, f can be the excitation. With application of basis functions, the system equations can be determined through (2.6.6) to (2.6.9). Then, the unknowns can be determined through iterative solvers. Iterative solvers, such as GMRES [Aiello et al., 2013, Eibert, 2003, Saad and Schultz, 1986], LSQR [Ergül and Gürel, 2008, Paige and Saunders, 1982a,b], BiCG_Stab [Sleijpen and Fokkema, 1993] and so on, can be

employed to solve the system equations. With the thresholds set for the solvers, an accurate approximation of $[c]$ can be obtained.

The BI method utilizes the method of moments (MoM) [Harrington, 1993] to solve the boundary equivalent electric and magnetic currents. MoM takes advantage of the Galerkin process [Peterson et al., 1996]. A group of functions are utilized as the testing functions. The system matrix equations are derived from (2.6.1) and they are written as

$$< w_i, L\phi >=< w_i, f >, \qquad i = 1, 2, 3, ..., N \tag{2.6.10}$$

and the system formulation is obtained as

$$[V]\,[c] = [K]\,, \tag{2.6.11}$$

where

$$V_{ij} =< w_i, Lv_j >= \int_{\Omega} (w_j\, Lv_j) d\Omega, \qquad i, j = 1, 2, 3, ..., N \tag{2.6.12}$$

and

$$K_i =< w_i, f >= \int_{\Omega} (w_i\, f) d\Omega, \qquad i = 1, 2, 3, ..., N. \tag{2.6.13}$$

In the Galerkin process, the testing functions are generally selected as the basis functions. Thus, the testing functions are written as

$$w_i = v_i, \qquad i = 1, 2, 3, ..., N. \tag{2.6.14}$$

As a result, the BI formulation can be solved through (2.6.11) for the unknown coefficients c_i.

It can be noticed that, compared with the pure FE and BI methods, the hybrid FE-BI method has often better performance. The simulations for the fields in free space can be determined through the BI method, while the fields in the penetrable materials can be computed through the FE method. The boundary integral equations derived from the Galerkin process are implemented for the model simulations, so the hybrid FE-BI method is very effective and efficient. When many independent objects are separated with possibly inhomogeneous and anisotropic materials far away, the hybrid FE-BI method can also provide an efficient and accurate solution to the EM simulations. The fields inside the dielectric materials can be computed, the currents on the boundary surfaces can be reconstructed and the scattering fields in the outside space can also be obtained. Moreover, the hybrid FE-BI method also contains the compatibility between the FE and BI methods. The analytical solution can be utilized for the system matrices in FE, while specified algorithms, such as MLFMM, can also be utilized for the BI method. Then, the simulations with sufficient accuracy can be obtained and the efficiency is improved since the amount of computations is tremendously reduced.

3 The Boundary Integral (BI) Equations

The boundary integral (BI) equations are well applied to the simulation of arbitrarily shaped components such as antennas, aircrafts, vehicles and so on. Generally, the enclosed boundary surfaces of the objects for the boundary integral separate the space into the inside and outside parts. The solutions of the boundary integral equations emphasize on radiations in the outside space based on the reconstructed equivalent surface electric and magnetic currents. As it turns out, the BI method is efficient for the radiation computations in the outside space, especially for PEC objects. Some simulations of the BI method also generate the radiation to the inside space for the inner space field computations. However, this is only applicable to homogeneous materials.

Compared with other integral techniques, such as the volume integral equations, the BI method is more efficient with fewer discretizations as the meshes are only located on the surfaces. Moreover, combined with FE, it can also compute the field distributions for inhomogeneous and anisotropic materials. Thus, the BI method provides a flexible and versatile solution to electromagnetic simulations.

A successful numerical solution to the boundary integral is the method of moments (MoM). MoM is often realized through the Galerkin process, including the electric field integral equation (EFIE) and the magnetic field integral equation (MFIE). The pure EFIE contains a problem of the interior resonances for the objects with enclosed surfaces. Thus, the CFIE is innovated, where the CFIE is a linear combination of the EFIE and the MFIE. The CFIE provides stable and unique solutions for all closed objects, so it is very efficient to resolve the interior resonances. The CFIE can also achieve a similarly good accuracy as the EFIE, when both of them are working at a non-resonant frequency.

As the boundary integral is combined with the method of finite elements, the basis functions in the BI method should be compliant with the basis functions in the FEM. Then, the boundary continuity conditions are satisfied. The radiation in the outside space is only dependent on the reconstructed electric and magnetic currents on the surfaces, the fields in the inner space can be computed by the FE method. Thus, the fields in both inside and outside spaces are solved precisely.

3.1 The Spatial Electromagnetic Integral Equations

The general objective of the boundary integral equations is the computation of the electromagnetic fields in the outside free space. The total fields in free space combine the fields generated from the sources and also the scattering fields by arbitrarily shaped objects. The fields derived from the sources can be visualized as the inputs for the simulation models. Enclosed by the envelope, the scattering of arbitrarily shaped objects depends on the equivalent surface electric and magnetic currents. The radiation fields are computed under the Sommerfeld condition.

The sources of the models can be input plane waves, or voltage sources of impressed currents. The input plane waves and voltage sources will be considered in the integral equations based on the current sources from the outside space. The total fields are dependent

on the input waves and the scattering fields. The impressed currents will be integrated into the method of finite elements for computations of the fields and the equivalent currents.

With (2.5.20), the integral representation in the outside source free space for fields can be written as

$$\boldsymbol{E}(\boldsymbol{r}) + \oiint_{A_d} [(\hat{n}' \cdot \boldsymbol{E}(\boldsymbol{r'}))\nabla G_0 + (\hat{n}' \times \boldsymbol{E}(\boldsymbol{r'})) \times \nabla G_0 + j\omega\mu_0(\hat{n}' \times \boldsymbol{H}(\boldsymbol{r'}))G_0]da' = \boldsymbol{E}^{inc}(\boldsymbol{r}), \tag{3.1.1}$$

where $\boldsymbol{r}$ belongs to the source free space outside A_d and S_J. Following (2.5.21), it is found that

$$\boldsymbol{H}(\boldsymbol{r}) + \oiint_{A_d} [(\hat{n}' \cdot \boldsymbol{H}(\boldsymbol{r'}))\nabla G_0 + (\hat{n}' \times \boldsymbol{H}(\boldsymbol{r'})) \times \nabla G_0 - j\omega\epsilon_0(\hat{n}' \times \boldsymbol{E}(\boldsymbol{r'}))G_0]da' = \boldsymbol{H}^{inc}(\boldsymbol{r}). \tag{3.1.2}$$

By substituting (2.4.1) and (2.4.2) into (3.1.1) and (3.1.2), it gives

$$\boldsymbol{E}(\boldsymbol{r}) + jk_0Z_0 \left[\frac{1}{k_0^2} \nabla \oiint_{A_d} G_0 \nabla' \cdot \boldsymbol{J}_s da' + \oiint_{A_d} \boldsymbol{J}_s G_0 da' \right] + \oiint_{A_d} \nabla G_0 \times \boldsymbol{M}_s da' = \boldsymbol{E}^{inc}(\boldsymbol{r}), \tag{3.1.3}$$

$$\boldsymbol{H}(\boldsymbol{r}) + \frac{jk_0}{Z_0} \left[\frac{1}{k_0^2} \nabla \oiint_{A_d} G_0 \nabla' \cdot \boldsymbol{M}_s da' + \oiint_{A_d} \boldsymbol{M}_s G_0 da' \right] - \oiint_{A_d} \nabla G_0 \times \boldsymbol{J}_s da' = \boldsymbol{H}^{inc}(\boldsymbol{r}), \tag{3.1.4}$$

where $k_0 = \omega\sqrt{\mu_0\epsilon_0}$ is the wave number in free space, $Z_0 = \sqrt{\mu_0/\epsilon_0}$ is the intrinsic impedance of free space. $\boldsymbol{E}^{inc}(\boldsymbol{r})$ and $\boldsymbol{H}^{inc}(\boldsymbol{r})$ are the input plane waves for the FE-BI object models. $\boldsymbol{E}(\boldsymbol{r})$ and $\boldsymbol{H}(\boldsymbol{r})$ are the total electric and magnetic fields in the source free space. $\boldsymbol{J}_s$ and $\boldsymbol{M}_s$ are the equivalent electric and magnetic surface currents.

3.2 Electric Field Integral Equation

To solve for the equivalent electric and magnetic currents, $\boldsymbol{J}_s$ and $\boldsymbol{M}_s$, on the boundary surfaces, (3.1.3) is utilized. When the position $\boldsymbol{r}$ in the source free space approaches A_d, the unit vector $\hat{n}$ is pointing outside A_d, the cross product of $\hat{n}$ for both sides of the equation is applied, together with (2.4.1) and (2.4.2), it turns out to be [Jin, 2002]

$$\begin{aligned} -\frac{1}{2}\boldsymbol{M}_s(\boldsymbol{r}) + jk_0Z_0\hat{n} \times \left[\frac{1}{k_0^2} \nabla \oiint_{A_d} G_0 \nabla' \cdot \boldsymbol{J}_s da' + \oiint_{A_d} \boldsymbol{J}_s G_0 da' \right] \\ + \hat{n} \times \oiint_{A_d} \nabla G_0 \times \boldsymbol{M}_s da' = \hat{n} \times \boldsymbol{E}^{inc}(\boldsymbol{r}) \end{aligned} \tag{3.2.1}$$

and (3.2.1) is called the electric field integral equation (EFIE). The clear formulation of the EFIE demonstrates that the 2-D integrals over the surfaces contain the kernels to determine the electric current $\boldsymbol{J}_s$ and the magnetic current $\boldsymbol{M}_s$. Once the currents are obtained, the scattering fields can be determined through (2.5.14) and (2.5.15). Moreover, from (3.2.1), it illustrates that the EFIE is focused on the radiations in free space. The EFIE can also be utilized for homogeneous scattering problems with modifications of the wave number and the intrinsic impedance of the materials. However, when combining with the method of finite elements, the EFIE only concentrates on the radiation problems in free space.

It is shown that the electric and magnetic currents are distributed on A_d and they are responsible for the exterior scatterings. It is well known that the EFIE is well applied to solve the scattering fields in the outside space. However, for the enclosed surface objects, there are resonances for the EFIE, where the equation system becomes ill-posed. An effective solution to the drawback of the resonance problem is to utilize the method of finite elements combined with the complexification of the wave number [Collins et al., 1992, Eibert and Hansen, 1996b, Jin, 2002, Monzon and Damaskos, 1994, Peterson, 1990], another technique called the dual-surface technique [Shore and Yaghjian, 2005, 2002] can also be used to cope with the resonances of EFIE. In this work, to solve this problem, the magnetic field integral equation (MFIE) is employed in conjunction with the EFIE. It is well known as the combined field integral equation (CFIE) [Chew et al., 2001, Mautz and Harrington, 1978a, Yaghjian, 1981, YlÄ-Oijala and Taskinen, 2003].

3.3 Magnetic Field Integral Equation

Through a similar process based on the scalar Green's theorem [Stratton, 1941] for $\boldsymbol{H}$, the integral equation (3.1.4) on the envelope surfaces A_d turns out to be

$$\frac{1}{2}\boldsymbol{J}_s(\boldsymbol{r}) + \frac{jk_0}{Z_0}\hat{n} \times \left[\frac{1}{k_0^2} \nabla \oiint_{A_d} G_0 \nabla' \cdot \boldsymbol{M}_s da' + \oiint_{A_d} \boldsymbol{M}_s G_0 da' \right] - \hat{n} \times \oiint_{A_d} \nabla G_0 \times \boldsymbol{J}_s da' = \hat{n} \times \boldsymbol{H}^{inc}(\boldsymbol{r}) \tag{3.3.1}$$

and it is called the magnetic field integral equation (MFIE). Even though the MFIE converges fast for the enclosed object models, it also contains the resonant frequencies for the enclosed surface objects.

3.4 Combined Field Integral Equation

The linear combination of EFIE and MFIE is called the combined field integral equation (CFIE) and it is given by

$$\alpha EFIE + (1-\alpha) Z_0 \hat{n} \times MFIE, \tag{3.4.1}$$

where α is the CFIE coefficient between 0 and 1. To obtain a better condition of the system matrices, $\hat{n}$ is utilized to cross MFIE. Thus, the bases for the EFIE and the pure MFIE

are orthogonalized. The benefits of the CFIE are that it deletes the drawbacks of the pure EFIE or MFIE, where the CFIE avoids the resonant frequencies and it can be applied to both enclosed and open objects. Moreover, the CFIE also inherits the advantages from both EFIE and MFIE, such that the CFIE converges fast with iterative solvers and maintains a good accuracy.

The CFIE is effective as BI within the FE-BI method, where the CFIE in (3.4.1) is usually computed in free space. However, the CFIE can also be utilized independently. For enclosed or open PEC objects, (3.4.1) provides an effective and accurate solution for scattering. Moreover, within homogeneous materials, the CFIE can also compute the radiation in both outside and inside spaces according to the corresponding material parameters.

3.5 Method of Moments (MoM)

To solve the electric and magnetic currents on enclosed surfaces with MoM, the currents $\boldsymbol{J}_s$ and $\boldsymbol{M}_s$ on each cell are separated with the vector basis functions, which are dependent on the configurations of the 2-D surfaces, and also the unknown coefficients, which rely on the inputs of the models. Based on meshes, general descriptions of $\boldsymbol{J}_s$ and $\boldsymbol{M}_s$ of the models are expanded into a series of vector basis functions and the corresponding coefficients. They are given by

$$\boldsymbol{J}_s = \sum_{n=1}^{N_I} I_n \boldsymbol{f}_n, \quad \boldsymbol{M}_s = \sum_{n=1}^{N_M} V_n \boldsymbol{f}_n, \tag{3.5.1}$$

where I_n and V_n are the unknown coefficients for the corresponding electric and magnetic currents. N_I and N_M are the numbers of unknowns for the electric and magnetic currents, $N = N_I + N_M$ is the total number of unknowns. The $\boldsymbol{f}_n$ are vector basis functions, which are defined by the structural information of the mesh cells. One famous choice of the basis functions on a triangular mesh are called the $Rao{-}Wilton{-}Glisson$ (RWG) basis functions [Rao et al., 1982]. They are defined as

$$\boldsymbol{f}_n(\boldsymbol{r}) = \begin{cases} \frac{1}{2A}(\boldsymbol{r} - \boldsymbol{r}_v) & \boldsymbol{r} \in \Omega \\ 0 & \boldsymbol{r} \notin \Omega \end{cases}, \tag{3.5.2}$$

where Ω represents the domain of the corresponding cell, A is the area of the domain, $\boldsymbol{r}_v$ is a vertex of the triangle and $\boldsymbol{r}$ is a position inside the domain for the non-zero value of $\boldsymbol{f}_n$. It is also clear that the basis function is a linear function of the distance between the position in the source domain and the vertex. As well known, the RWG basis functions are accurate and efficient when the mesh element size is below $\lambda/8$, where λ is the wavelength based on the working frequency within the corresponding material. However, the format of the RWG basis functions can also be expressed through the simplex coordinates and the gradient of the simplex coordinates. The orders of the basis functions are represented by the order of the simplex coordinate polynomials in other formats apart from the RWG basis functions. Moreover, to maintain the compatibility between BI and FE, the definitions of $\boldsymbol{f}_n$ must be compliant with the definitions of the basis functions for FE within the connecting

tetrahedron. Meanwhile, the boundary continuity conditions of the basis functions have to be guaranteed within the FE-BI method.

In the process of MoM, testing functions are selected to produce an inner product with the original equations. Different kinds of testing functions may contain various testing domains, thus, the system matrices are different. One type of testing functions is called *point matching* or *point collocation* [Ascher and Petzold, 1998, Hairer et al., 1993, Iserles, 1996] and defined as

$$\boldsymbol{g}_m(\boldsymbol{r}) = \hat{f}(\boldsymbol{r}_m)\delta(\boldsymbol{r} - \boldsymbol{r}_m)\,, \tag{3.5.3}$$

where $\boldsymbol{g}_m$ is the testing function, $\hat{f}$ is a general unit vector and $\boldsymbol{r}_m$ is the position on the source domain. The matrices based on the *point matching* solution are simple. However, the singularity of the matrices have to be considered. The positions of the sampling points are fixed through the δ function. Another type of testing functions is called *sub-domain collocation* function [Chen et al., 2009] and defined as

$$\boldsymbol{g}_m(\boldsymbol{r}) = \begin{cases} 1 & \boldsymbol{r} \in \Omega_m \\ 0 & \boldsymbol{r} \notin \Omega_m \end{cases}, \tag{3.5.4}$$

where Ω_m is the mth sub-domain. The matrices based on the *sub-domain collocation* are also simple.

A third kind of testing functions are selected the same as the basis functions in the source domain. This is well known as the Galerkin prcess for MoM, where

$$\boldsymbol{g}_m(\boldsymbol{r}) = \boldsymbol{f}_m(\boldsymbol{r})\,. \tag{3.5.5}$$

Compared with the other techniques, the Galerkin process requires heavier computations of the matrix entries, however, the matrices are more robust and more general for complicated meshes. The system matrix turns out to be symmetric when the integral operators are symmetric. Thus, the Galerkin process is widely applied to MoM for the BI.

The Galerkin process takes advantage of the inner product between the testing functions and the equations. When applied to the CFIE with numerical expansions [Eastwood and Morgan, 2008, Fink et al., 2005], the system matrices are written as

$$\begin{aligned} EFIE: \quad & \sum_{n=1}^{N_M} \left[\frac{1}{2}A_{mn} + D_{mn}\right] V_n \\ & + jZ_0k_0 \sum_{n=1}^{N_I} \left[B_{mn} + \frac{C_{mn}}{k_0^2}\right] I_n = G_m^E, \quad m = 1, ..., N_I, \end{aligned} \tag{3.5.6}$$

$$\begin{aligned} MFIE: \quad & \sum_{n=1}^{N_I} \left[-\frac{1}{2}A'_{mn} - D'_{mn}\right] I_n \\ & + j\frac{k_0}{Z_0} \sum_{n=1}^{N_M} \left[B'_{mn} + \frac{C'_{mn}}{k_0^2}\right] V_n = G_m^H, \quad m = 1, ..., N_I. \end{aligned} \tag{3.5.7}$$

The CFIE can be obtained through a linear combination of EFIE and MFIE according to (3.4.1). The corresponding system matrices in (3.5.6) and (3.5.7) are given by

$$A_{mn} = \iint\limits_{S_m} \boldsymbol{g}_m(\boldsymbol{r}) \cdot \hat{n} \times \boldsymbol{f}_n(\boldsymbol{r}) ds, \tag{3.5.8}$$

$$B_{mn} = \iint\limits_{S_m} \boldsymbol{g}_m(\boldsymbol{r}) \cdot \iint\limits_{S_n} G_0(\boldsymbol{r}, \boldsymbol{r'}) \boldsymbol{f}_n(\boldsymbol{r'}) ds' ds, \tag{3.5.9}$$

$$C_{mn} = \iint\limits_{S_m} \boldsymbol{g}_m(\boldsymbol{r}) \cdot \nabla \iint\limits_{S_n} G_0(\boldsymbol{r}, \boldsymbol{r'}) \nabla'_s \cdot \boldsymbol{f}_n(\boldsymbol{r'}) ds' ds, \tag{3.5.10}$$

$$= C^M_{mn} - C^E_{mn}, \tag{3.5.10a}$$

$$C^E_{mn} = \iint\limits_{S_m} \nabla_s \cdot \boldsymbol{g}_m(\boldsymbol{r}) \iint\limits_{S_n} G_0(\boldsymbol{r}, \boldsymbol{r'}) \nabla'_s \cdot \boldsymbol{f}_n(\boldsymbol{r'}) ds' ds, \tag{3.5.11}$$

$$C^M_{mn} = \oint\limits_{C_m} \boldsymbol{g}_m(\boldsymbol{r}) \cdot \hat{u}_m \iint\limits_{S_n} G_0(\boldsymbol{r}, \boldsymbol{r'}) \nabla'_s \cdot \boldsymbol{f}_n(\boldsymbol{r'}) ds' dl, \tag{3.5.12}$$

$$D_{mn} = \iint\limits_{S_m} \boldsymbol{g}_m(\boldsymbol{r}) \cdot \iint\limits_{S_n} \nabla G_0(\boldsymbol{r}, \boldsymbol{r'}) \times \boldsymbol{f}_n(\boldsymbol{r'}) ds' ds, \tag{3.5.13}$$

$$G^E_m = \iint\limits_{S_m} \boldsymbol{f}_m(\boldsymbol{r}) \cdot \boldsymbol{E}^{inc}(\boldsymbol{r}) ds, \tag{3.5.14}$$

$$G^H_m = \iint\limits_{S_m} \hat{n} \times \boldsymbol{f}_m(\boldsymbol{r}) \cdot \boldsymbol{H}^{inc}(\boldsymbol{r}) ds. \tag{3.5.15}$$

In the computations of the system matrices, $\boldsymbol{g}_m = \boldsymbol{f}_m$ is utilized in the $A, .., D$ matrices for the EFIE, while $\boldsymbol{g}_m = \hat{n} \times \boldsymbol{f}_m$ in the $A', ..., D'$ for the MFIE. Through the application of the Gauss' divergence theorem [Bladel, 2007, Rao et al., 1982], the system matrix C_{mn} for the EFIE can be split into C^E_{mn} and C^M_{mn} and the same results can also be obtained for the MFIE. (3.5.10) denotes that in the CFIE, the divergence of the testing functions have to be computed to evaluate the mutual couplings. (3.5.12) illustrates that a line integral also needs to be computed in the testing domain. C_m is the line boundary of the testing domain. $\hat{u}_m$ represents the unit vector in the testing domain plane, on the line boundary, perpendicular to the curve and pointing outside the area. S_m and S_n represent

the corresponding testing domain and source domain. The RWG basis functions are the first order div conforming space, where the curl of the RWG functions vanishes inside the triangles. For higher order (HO) basis functions, the curl and the divergence of the spaces are also utilized for mutual couplings. With the application of HO basis functions in MoM, higher accuracy can be achieved especially for higher frequencies.

In the mutual couplings, C_{mn}^{E} and C_{mn}^{M} contain the Green's function inside the kernels and they become singular for near couplings, where S_m is near to S_n. They are also singular for self-couplings where $S_m = S_n$. Moreover, the D_{mn} matrix contains the gradient of the Green's function. It introduces a hyper singularity into the integrals. To cancel out the singularities, new singularity cancellation techniques are innovated with different orders. In the singularity cancellation techniques, the adaptive approaches are also applied [Ismatullah and Eibert, 2008] to the numerical integral solutions. The Jacobian determinants of the new coordinate transformation schemes are efficient to cancel out the singularities in singular and hyper-singular kernels. Obviously, the higher order singularity cancellation techniques are also effective to the lower order singular kernels. As it turns out, the versatile techniques are well performed for arbitrarily positioned singular and hyper singular mutual couplings, even for the kernels multiplied with scalar and vector functions inside.

3.6 Multilevel Fast Multipole Method

The fast multipole method (FMM) [Coifman et al., 1993, Engheta et al., 1992] and the multilevel fast multipole method (MLFMM) [Chew et al., 2001, Dembart and Yip, 1998, Donepudi et al., 2000, Eibert, 2005, Kalbasi and Demarest, 1993, Koc et al., 1999, Velamparambil et al., 2003] are always very efficient for arbitrary three-dimensional geometries. Compared with the direct MoM, the memory requirement of MLFMM for fast solvers is reduced from $O(N^2)$ to $O(N\log N)$, where N is the number of BI unknowns. Then, MLFMM is efficient and effective for large scale EM simulations. The FMM group size can determine the number of levels for MLFMM, the minimum size of FMM is limited by the largest edge length of the geometrical mesh. With higher order basis functions, the mesh size with respect to the wavelength can be extended, so the FMM group size increases and fewer MLFMM levels are required. As it turns out, more near couplings are computed within the near FMM groups. The SE-MLFMM [Eibert, 2005] is introduced, in which, the $\hat{k}$-space integral over the Ewald sphere is computed. With the orthonormalized spherical harmonics and the basis functions, the expansion coefficients can be obtained through the $\hat{k}$-space integral. Then, the far mutual couplings are computed through the translation operator. With SE-MLFMM, the memory requirements and the computational time are much reduced and more efficient performance is obtained.

3.6.1 Fast Multipole Method (FMM)

A general model of the fast multipole method (FMM) is shown in Fig. 3. $\boldsymbol{r}_n$ is a point in the source domain and $\boldsymbol{r}_m$ is a point in the testing domain. The direct coupling path is $\boldsymbol{r}_{mn} = \boldsymbol{r}_m - \boldsymbol{r}_n$. $\boldsymbol{r}_{n'}$ is the center of the FMM group of the source domain, $\boldsymbol{r}_{m'}$ is the center of the FMM group of the testing domain. The vectors utilized in FMM are defined as $\boldsymbol{r}_{mm'} = \boldsymbol{r}_m - \boldsymbol{r}_{m'}$, $\boldsymbol{r}_{nn'} = \boldsymbol{r}_n - \boldsymbol{r}_{n'}$ and $\boldsymbol{r}_{m'n'} = \boldsymbol{r}_{m'} - \boldsymbol{r}_{n'}$. It can be seen that $\boldsymbol{r}_{mn} = \boldsymbol{r}_{mm'} + \boldsymbol{r}_{m'n'} - \boldsymbol{r}_{nn'}$.

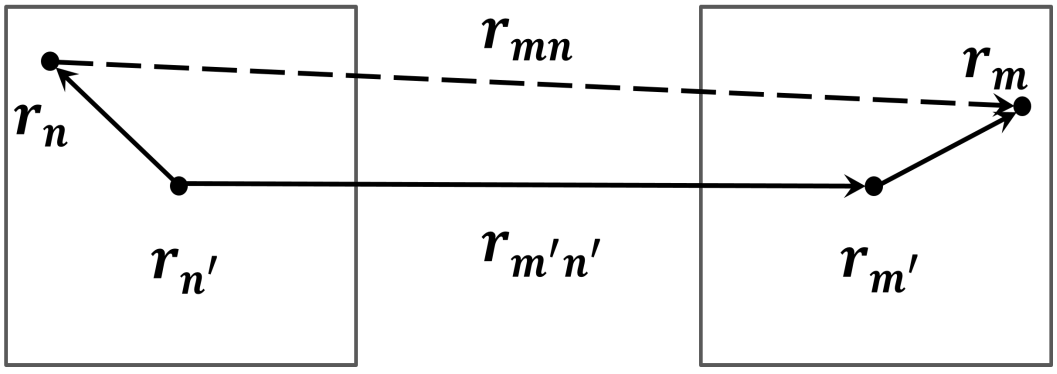

Figure 3: FMM expansion of Green's function.

The FMM takes advantage of the spherical multipole expansion of the free space Green's function. Dependent on the Gegenbauer's addition theorem [Abramowitz and Stegun, 1972],

the free space Green's function can be expanded as

$$\frac{e^{-jk|\boldsymbol{D}+\boldsymbol{d}|}}{|\boldsymbol{D}+\boldsymbol{d}|} = -jk\sum_{l=0}^{\infty}(-1)^l(2l+1)j_l(kd)h_l^{(2)}(kD)P_l(\hat{d}\cdot\hat{D}), \tag{3.6.1.1}$$

where

$$\boldsymbol{D} = \boldsymbol{r}_{m'n'}, \tag{3.6.1.2a}$$

$$\boldsymbol{d} = \boldsymbol{r}_{mm'} - \boldsymbol{r}_{nn'} \tag{3.6.1.2b}$$

and $D > d$ must be guaranteed, j_l is the l order spherical Bessel function, $h_l^{(2)}$ is the l order spherical Hankel function of the second kind, P_l is the l order Legendre polynomial.

The spherical wave functions in (3.6.1.1) can be rewritten in terms of a spectral integral with application of the identity [Stratton, 1941]

$$4\pi(-j)^l j_l(kd)P_l(\hat{d}\cdot\hat{D}) = \oiint_{\hat{k}} e^{-j\boldsymbol{k}\cdot\boldsymbol{d}}P_l(\hat{d}\cdot\hat{D})d\hat{k}^2, \tag{3.6.1.3}$$

where the right hand side of (3.6.1.3) is an integral over the unit sphere and $\hat{k}$ represents the direction of the normal unit vector on the spherical surface. By replacing (3.6.1.3) into (3.6.1.1), it gives that

$$\frac{e^{-jk|\boldsymbol{D}+\boldsymbol{d}|}}{|\boldsymbol{D}+\boldsymbol{d}|} \approx \frac{-jk}{4\pi}\oiint_{\hat{k}} e^{-j\boldsymbol{k}\cdot\boldsymbol{d}}T_L(\hat{d}\cdot\hat{D})d\hat{k}^2, \tag{3.6.1.4}$$

where T_L is the translation operator defined as

$$T_L(\hat{d}\cdot\hat{D}) = \sum_{l=0}^{L_m}(-j)^l(2l+1)h_l^{(2)}(kD)P_l(\hat{k}\cdot\hat{D}). \tag{3.6.1.5}$$

As shown in Fig. 3, it can be seen in (3.6.1.5) that the translator T_L translates the waves from the center of the source group directly to the center of the testing group. The multipole series expansion of the spherical wave functions is truncated by L_m. The error introduced by the truncation of L_m is controllable in FMM as shown in [Chew et al., 2001]

$$L_m \approx kd + 1.8d_0^{2/3}(kd)^{1/3}, \tag{3.6.1.6}$$

where d_0 is the digital number of the accuracy and the relative error is given by $\epsilon = 10^{-d_0}$. Through the approximation of the multipole order, the error magnitude of the translator can meet the accuracy requirements. However, the accuracy estimation can only be obtained under the condition of far FMM groups. For near groups, the direct MoM needs to be utilized. The $\hat{k}$-space integral over the Ewald sphere in (3.6.1.4) is computed with numerical solutions. The Gauss-Legendre quadrature with (L_m+1) sampling points is utilized for integration over θ, the trapezoidal quadrature rule with $2(L_m+1)$ points is used for integration over ϕ. Then, the total integration points over the Ewald sphere are $2(L_m+1)^2$ with the multipoles order from 0 up to L_m.

3.6.2 Maxtrix Elements with FMM

From (3.2.1) and (3.3.1), the MoM system matrix for the CFIE derived from the mutual couplings can be written as

$$\begin{aligned} Z_{mn,J}^{CFIE} =& + c_1 \iint_{S_m} \boldsymbol{f}_m(\boldsymbol{r}_m) \cdot \iint_{S_n} \left(\bar{I} + \frac{1}{k_0^2} \nabla\nabla' \right) G_0(\boldsymbol{r}_m, \boldsymbol{r}_n) \cdot \boldsymbol{f}_n(\boldsymbol{r}_n) dS_m dS_n \\ & + c_2 \iint_{S_m} [\nabla \times \boldsymbol{\alpha}_m(\boldsymbol{r}_m)] \cdot \iint_{S_n} G_0(\boldsymbol{r}_m, \boldsymbol{r}_n) \boldsymbol{f}_n(\boldsymbol{r}_n) dS_m dS_n \,, \qquad (3.6.2.1) \\ Z_{mn,M}^{CFIE} =& + c_3 \iint_{S_m} \boldsymbol{\alpha}_m(\boldsymbol{r}_m) \cdot \iint_{S_n} \left(\bar{I} + \frac{1}{k_0^2} \nabla\nabla' \right) G_0(\boldsymbol{r}_m, \boldsymbol{r}_n) \cdot \boldsymbol{f}_n(\boldsymbol{r}_n) dS_m dS_n \\ & + c_4 \iint_{S_m} [\nabla \times \boldsymbol{f}_m(\boldsymbol{r}_m)] \cdot \iint_{S_n} G_0(\boldsymbol{r}_m, \boldsymbol{r}_n) \boldsymbol{f}_n(\boldsymbol{r}_n) dS_m dS_n \,, \qquad (3.6.2.2) \end{aligned}$$

where $\boldsymbol{\alpha}_m(\boldsymbol{r}) = \hat{n}(\boldsymbol{r}) \times \boldsymbol{f}_m(\boldsymbol{r})$ are edge related basis functions and equal to the tangential counterpart of the RWG basis functions $\boldsymbol{f}_m$. $Z_{mn,J}^{CFIE}$ and $Z_{mn,M}^{CFIE}$ are the system coupling matrices of the CFIE for the surface electric and magnetic current unknowns respectively. The coefficients c_1 to c_4 are computed as

$$c_1 = -jZ_0 \frac{k_0}{4\pi} \alpha, \qquad (3.6.2.3a)$$

$$c_2 = Z_0 \frac{1}{4\pi} (1 - \alpha), \qquad (3.6.2.3b)$$

$$c_3 = jZ_0 \frac{\omega \epsilon_0}{4\pi} (1 - \alpha), \qquad (3.6.2.3c)$$

$$c_4 = \frac{1}{4\pi} \alpha. \qquad (3.6.2.3d)$$

By using (3.6.1.1)-(3.6.1.5), the scalar Green's function (2.5.4) in free space can be rewritten as

$$G_0(\boldsymbol{r}_m, \boldsymbol{r}_n) = \frac{e^{-jk_0|\boldsymbol{r}_m - \boldsymbol{r}_n|}}{4\pi|\boldsymbol{r}_m - \boldsymbol{r}_n|} \approx \oiint_{\hat{k}_0} e^{-j\boldsymbol{k}_0 \cdot \boldsymbol{r}_{mm'}} T_L(\hat{k}_0 \cdot \hat{r}_{m'n'}) e^{j\boldsymbol{k}_0 \cdot \boldsymbol{r}_{nn'}} d\hat{k}_0^2 \,. \qquad (3.6.2.4)$$

Through substituting (3.6.2.4) into (3.6.2.1) and (3.6.2.2), the MoM matrices for CFIE are obtained as

$$\begin{aligned} Z_{mn,J}^{far} =& - j\frac{k_0 Z_0}{4\pi} \alpha \oiint_{\hat{k}_0} \tilde{\boldsymbol{f}}_m^*(\hat{k}_0) \cdot T_L(\hat{k}_0 \cdot \hat{r}_{m'n'}) (\bar{I} - \hat{k}_0 \hat{k}_0) \cdot \tilde{\boldsymbol{f}}_n(\hat{k}_0) d\hat{k}_0^2 \\ & + j\frac{k_0 Z_0}{4\pi} (1 - \alpha) \oiint_{\hat{k}_0} \left[\hat{k}_0 \times \tilde{\boldsymbol{\alpha}}_m^*(\hat{k}_0) \right] \cdot T_L(\hat{k}_0 \cdot \hat{r}_{m'n'}) \tilde{\boldsymbol{f}}_n(\hat{k}_0) d\hat{k}_0^2, \qquad (3.6.2.5) \\ Z_{mn,M}^{far} =& + j\frac{k_0}{4\pi} \alpha \oiint_{\hat{k}_0} \left[\hat{k}_0 \times \tilde{\boldsymbol{f}}_m^*(\hat{k}_0) \right] \cdot T_L(\hat{k}_0 \cdot \hat{r}_{m'n'}) \tilde{\boldsymbol{f}}_n(\hat{k}_0) d\hat{k}_0^2 \\ & + j\frac{k_0}{4\pi} (1 - \alpha) \oiint_{\hat{k}_0} \tilde{\boldsymbol{\alpha}}_m^*(\hat{k}_0) \cdot T_L(\hat{k}_0 \cdot \hat{r}_{m'n'}) (\bar{I} - \hat{k}_0 \hat{k}_0) \cdot \tilde{\boldsymbol{f}}_n(\hat{k}_0) d\hat{k}_0^2, \qquad (3.6.2.6) \end{aligned}$$

where

$$\tilde{\boldsymbol{f}}_n(\hat{k}_0) = \iint_{S_n} \boldsymbol{f}_n(\boldsymbol{r}_n) e^{j\boldsymbol{k}_0 \cdot \boldsymbol{r}_{nn'}} dS_n \,, \tag{3.6.2.7}$$

$$\tilde{\boldsymbol{\alpha}}_n(\hat{k}_0) = \iint_{S_n} \boldsymbol{\alpha}_n(\boldsymbol{r}_n) e^{j\boldsymbol{k}_0 \cdot \boldsymbol{r}_{nn'}} dS_n \,, \tag{3.6.2.8}$$

where $\boldsymbol{\alpha}_n(\boldsymbol{r}) = \hat{n}(\boldsymbol{r}) \times \boldsymbol{f}_n(\boldsymbol{r}_n)$. The functions $\tilde{\boldsymbol{f}}_n$ and $\tilde{\boldsymbol{\alpha}}_n$ are the $\hat{k}$-space basis functions and * denotes the complex conjugation. $T_L(\hat{k}_0 \cdot \hat{r}_{m'n'})$ is the translation operator given by (3.6.1.5). As FMM is utilized in free space for the BI, the wave number in free space k_0 is used in the matrix elements with FMM.

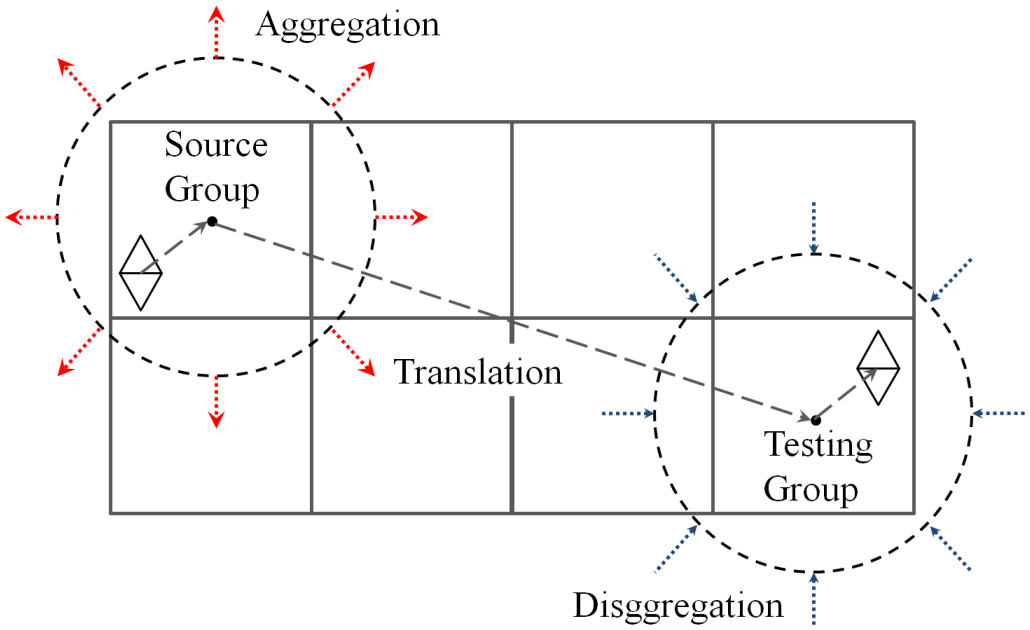

Figure 4: Aggregation, translation and disaggregation processes in FMM.

The acceleration of the mutual coupling computation for the MoM matrix with FMM relies on the aggregation process of the nearby basis functions within the independent FMM groups. In the aggregation process, the basis functions are collected to the center of the corresponding FMM group through (3.6.2.7) and (3.6.2.8), where the basis functions for the $\hat{k}$-space integral are obtained in terms of their far field radiation patterns. After the aggregation process of the independent FMM groups, the source FMM groups can be translated to the far testing groups through the translation operator. When the distance between the centers of the source and testing groups is far enough, where the distance D between the group centers is larger than the distance d with respect to the threshold of FMM, the collective evaluation of the source group can be translated to the testing group center. Within the testing group, the received wave field is finally transferred to the testing functions by multiplying the far field radiation patterns with respect to the center of the testing group. The procedure of indirect computation of the MoM matrix with FMM groups is constructed by aggregation, translation and disaggregation processes as shown in Fig. 4.

3.6.3 Spherical Harmonics Expansion of the $\hat{k}$-space Integrals

In computations of the mutual couplings with FMM, the number of sampling points on the Ewald sphere is associated with the translation operator and the factor derived from the dyadic Green's function. The numerical integration of the source and testing basis functions over the corresponding domains, as shown in (3.6.2.7) and (3.6.2.8), requires large numbers of sampling points and a large amount of memory is utilized. The $\hat{k}$-space representation of the basis functions in spherical harmonics [Eibert, 2005] is introduced. The far-field pattern of the basis functions in the $\hat{k}$-space representation (3.6.2.7) is expanded with spherical harmonics Y_{pq} [Harrington, 1961]. The basis function radiation pattern is rewritten as

$$\tilde{\boldsymbol{f}}_n(\vartheta,\varphi) = \sum_{p=0}^{P}\sum_{q=-p}^{p} \boldsymbol{f}_{pq}^n Y_{pq}(\vartheta,\varphi) \tag{3.6.3.1}$$

and the orthonormalized spherical harmonics $Y_{pq}(\vartheta,\varphi)$ are given by

$$Y_{pq}(\vartheta,\varphi) = \sqrt{\frac{(2p+1)(p-q)!}{4\pi(p+q)!}} P_p^q(\cos\vartheta) e^{jq\varphi}, \tag{3.6.3.2}$$

where P_p^q is the Lengendre polynomial of degree p with order q. The expansion coefficients $\boldsymbol{f}_{pq}^n$ in (3.6.3.1) are computed as

$$\boldsymbol{f}_{pq}^n = \oiint_{\hat{k}_0} \tilde{\boldsymbol{f}}_n(\vartheta,\varphi) Y_{pq}^*(\vartheta,\varphi) d\hat{k}_0^2 \tag{3.6.3.3}$$

for all the corresponding basis functions in the initialization step. This can be finished through the application of the Gauss Legendre quadrature rules [Koc et al., 1999]. The increasing computational time for the expansion coefficients is typically negligible compared to the traditional initialization steps. Moreover, to avoid the Gibb's phenomenon [Harmuth and Hussain, 1994], where the spherical vector components are not continuous, the vector basis functions $\tilde{\boldsymbol{f}}_n$ are considered as Cartesian vector components for the integral evaluations.

In a similar procedure, the received wave can be expanded with the orthonormality of the spherical harmonics as

$$T_L(\hat{k}_0 \cdot \boldsymbol{r}_{m'n'})(\bar{\boldsymbol{I}} - \hat{k}_0\hat{k}_0) \cdot \tilde{\boldsymbol{f}}_n(\hat{k}_0) = \sum_{p=0}^{P}\sum_{q=-p}^{p} \boldsymbol{g}_{pq}^n Y_{pq}(\vartheta,\varphi) \tag{3.6.3.4}$$

and the expansion coefficients $\boldsymbol{g}_{pq}^n$ can be computed analogously with (3.6.3.3). Therefore, the integral over the closed Ewald sphere yields the simplified series as

$$Z_{mn} = -j\frac{\omega\mu}{4\pi}\sum_{p=0}^{P}\sum_{q=-p}^{p} (\boldsymbol{f}_{pq}^m)^* \cdot \boldsymbol{g}_{pq}^n. \tag{3.6.3.5}$$

With (3.6.3.5), the testing step is accelerated significantly and better performance can be obtained.

3.6.4 Multilevel Fast Multipole Method

For large scale simulations, the pure FMM can meet limitation of efficiency. The basis functions in a single FMM group have to utilize the direct MoM, the large number of unknowns in the FMM group requires much memory and the computations of mutual couplings are also heavy. To increase the efficiency of the system matrix computation, the FMM algorithm can be further improved into hierarchical schemes by extending the FMM levels. Then, the multilevel fast multipole method (MLFMM) algorithm is obtained. The multilevel FMM groups start from a single box containing all basis functions, each block from the FMM is subdivided by half the edge length and the sub-blocks in the corresponding FMM block are obtained. Then, the basis functions in the FMM group are indexed into the corresponding sub-divided blocks. Through repeating the subdivision process for each subdivided block until a minimum box size is reached, the total number of levels of the groups is obtained. With the half-dividing procedure of obtaining the multilevel groups, each above level box is subdivided into eight below level boxes, the construction of the MLFMM groups can be referred to an octree.

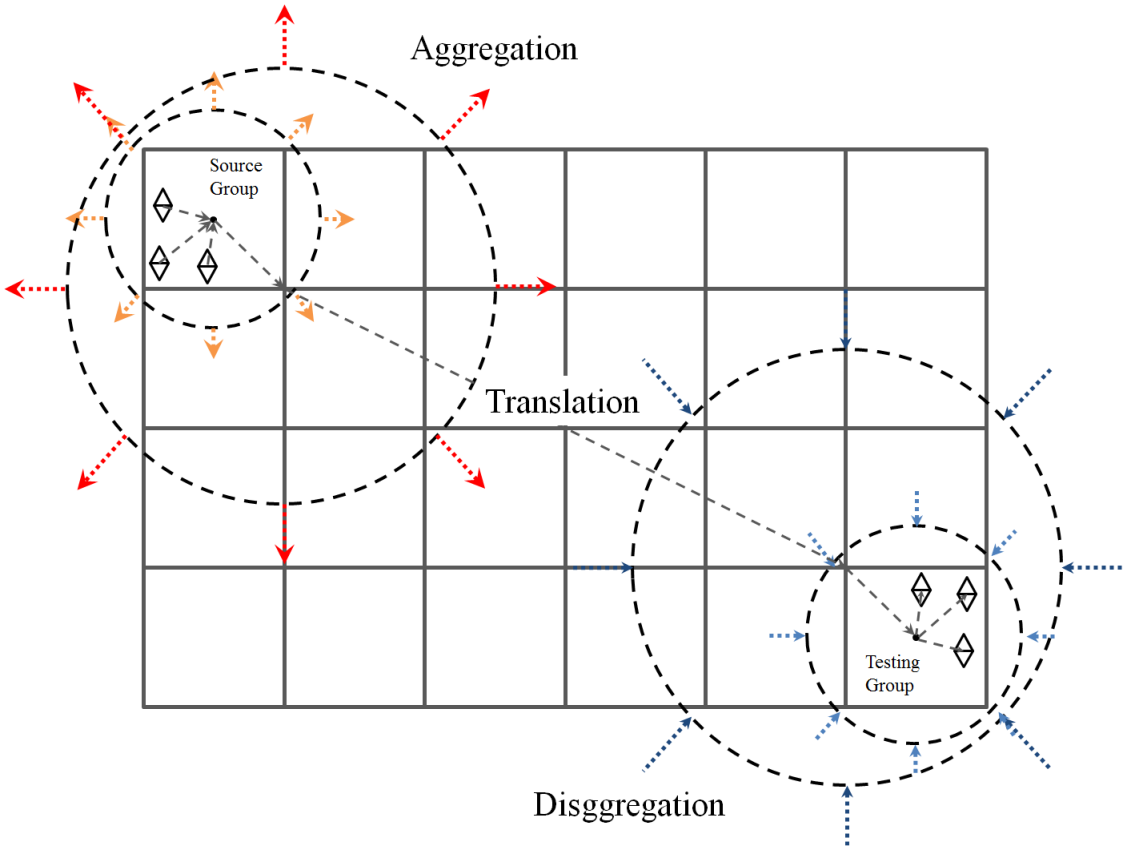

Figure 5: Aggregation, translation and disaggregation processes in MLFMM.

The MLFMM can increase the efficiency of the system matrix computations as the boxes in the lowest level are clustered and the mutual couplings are evaluated collectively up to a higher level. The number of the multipoles in the lowest level depends on the minimum group size. In an optimized solution, the multipole number for each level is kept as low as possible.

The computation procedure of the mutual couplings in MLFMM starts from the aggregation process to the centers of the boxes in the lowest level. This process is the same as in the FMM shown in Fig. 4. All the non-empty lowest level boxes perform the aggregation procedure. Then, the radiating wave patterns in the lowest groups are transformed to the center of the next higher level, this is finished through a phase shift. The aggregation process of the wave patterns to the higher level box requires a larger number of multipoles according to the higher level box size. The aggregation process performs up to the higher level of FMM groups until the current level of source and testing groups are well separated. Then, the aggregated wave patterns of the source group is transformed to the center of the testing group through the translation operator in the current level. In the testing group in the corresponding level of translation, the disaggregation process begins. The wave patterns are disaggregated level by level until the lowest level box, then transformed to the individual testing functions. The disaggregation process is also fulfilled through phase shifts. In each disaggregation process from the higher to the lower level, the number of multipoles is well selected according to the lowest level for an accurate evaluation. The aggregation, translation and disaggregation processes in MLFMM are shown in Fig. 5.

MLFMM can increase the efficiency of far zone mutual coupling evaluations with computation effort proportional to $O(N \log N)$, where N is the number of total BI unknowns. In the optimized efficient solutions, the size of the lowest level box is set as small as possible. However, the minimum box size should be larger than about the maximum edge length and also greater than about $\lambda/5$. To obtain optimal accuracy, when MLFMM is applied to hierarchical basis functions, the number of multipoles for the lowest level is determined by the box size. The spherical harmonics degree in the basis function expansion can be set as half the multipole number.

4 Singularity Treatment Approaches

Computations of mutual coupling integrals, especially the couplings of singular kernels, determine the accuracy of MoM for the surface integral equations. When testing and source domains are near, singularities are introduced into the coupling integrals due to the Green's function and the gradient of the Green's function. Then, direct couplings can not be evaluated with the numerical quadrature. Under this case, special numerical treatments for such singularities are required for near couplings. The adaptive singularity cancellation technique is detailed discussed and a new family of radial-angular-R^n coordinate transformation schemes are proposed. The coupling integrals are evaluated efficiently and accurately with singularity cancellation techniques.

4.1 Singular Integral Configurations

Three integration configurations are considered dependent on the relative position of the projection point O with respect to the source domain. The three configurations together with the relevant geometric parameters are depicted in Figs. 6 to 8. The distance between the observation point and the projection point O is $|z|$, the distance between the observation point and the sampling point inside the source domain is R, the distance between the projection point and the sampling point is r, the angle between R and $|z|$ is denoted as ϑ. Also, the angular integration range is from Φ_l to Φ_u and the radial integration range in the source plane is from r_l to r_u. For $|z| = 0$, $r_l = \delta_a$ must be chosen in order to avoid the common singularity in transformations, if the projection point is located inside the source domain.

4.2 Singular Integral Kernels

Under consideration of the mutual couplings from (3.5.9) to (3.5.13), the integrals contain singular kernels in the MoM solution. The singular integrals can be written as

$$B = \iint_A \eta(\boldsymbol{r'})\boldsymbol{\beta}(\boldsymbol{r'})\frac{e^{-jk_0R}}{R}da', \tag{4.2.1}$$

$$D = \iint_A \eta(\boldsymbol{r'})\boldsymbol{\beta}(\boldsymbol{r'}) \times \nabla\frac{e^{-jk_0R}}{R}da', \tag{4.2.2}$$

where A is the integral source domain, η is a scalar function, $\boldsymbol{\beta}$ is a vector function, $\boldsymbol{r}$ is the observation point in the testing domain, $\boldsymbol{r'}$ is the position in the source domain, $R = |\boldsymbol{r} - \boldsymbol{r'}|$ is the distance between the observation point and the sampling point in the source domain. The $1/R$-type kernel B contains a weak singularity, the $\boldsymbol{R}/R^3$-type kernel D contains a hyper singularity. In the configurations of Fig. 7 and Fig. 8, where the projection of the observation point is outside the source domain, the corresponding kernels turn to be near singular and near hyper singular.

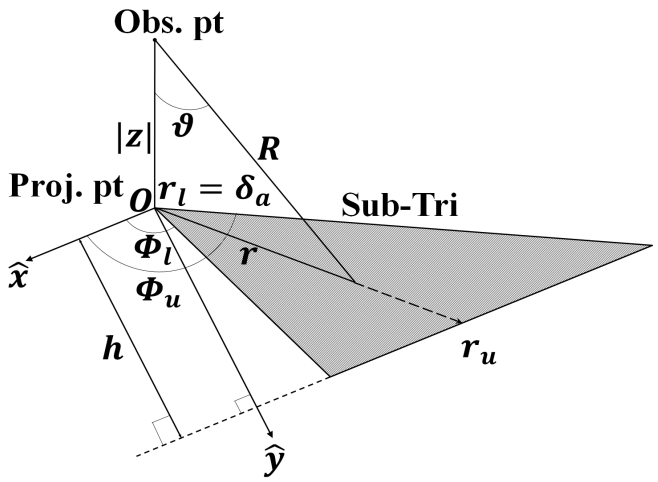

Figure 6: Geometric confiugration for projection point inside.

4.3 Singularity Subtraction Method

The singularity subtraction method splits the singular kernel into two terms. One term can be approximated under the condition of the neighboring testing and source domains. The second term can be computed through analytical solutions. Take the scalar Green's function for the singularity subtraction method as an example

$$\iint_A \frac{e^{-jk_0R}}{R} da' = \iint_A \frac{e^{-jk_0R} - 1}{R} da' + \iint_A \frac{1}{R} da', \tag{4.3.1}$$

where the first term on the right hand side can be computed numerically and the second term can be computed analytically [Eibert and Hansen, 1995a, 1996a].

The singularity subtraction method can be applied to the constant, first order and also higher order polynomial basis functions [Butler, 1975, Eibert and Hansen, 1995a, 1996a, Järvenpää et al., 2006a,b, Wilton et al., 1984]. It is also applicable to both linear and non-linear geometrical configurations [Eastwood and Morgan, 2008, Järvenpää et al., 2003, Knockaert, 1991]. Different orders of basis functions can be integrated over planar triangles and also over curved triangles. The curved triangles can be extended into tangent planar elements, where the same integration on the planar elements can be utilized. However, in the singularity subtraction method, the integrands of the polynomials are not easily approximated in the vicinity of the singularity. So, the accuracy of the quadrature rule is limited. When it comes to higher order basis functions, curved elements, or complex Green's functions, the Taylor expansions of the variables turn to be more complicated. So the improved radial-angular-R^n singularity cancellation techniques are introduced next.

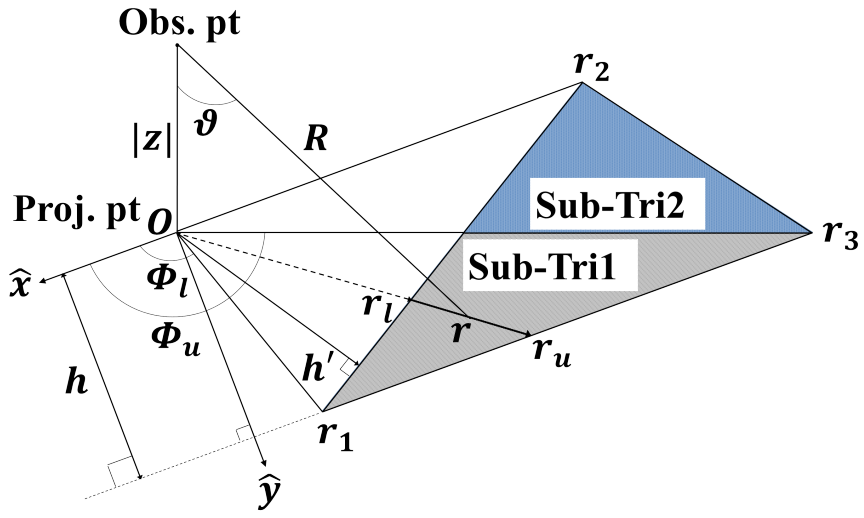

Figure 7: Geometric configuration for 1st type of projection point outside.

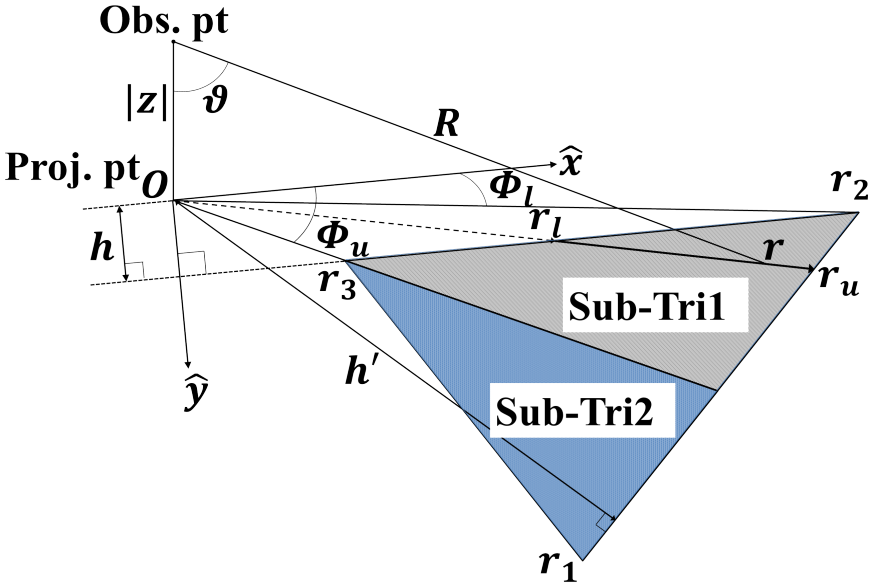

Figure 8: Geometric configuration for 2nd type of projection point outside.

4.4 Radial Angular Singularity Cancellation Transformations Derived by the Variable Separation Method

The variable separation method [Stone and Goldbart, 2009] is employed to formulate new radial-angular-R^n coordinate transformation schemes for the singularity cancellation technique. Derived from the concept of obtaining an ideal Jacobian of the transformations and with different parameter settings in the variable separation method, a new augmented radial-angular-R^1 transformation, new radial-angular-R^2 and radial-angular-R^2-cosh transformations, together with a new radial-angular-R^3, an augmented radial-angular-R^3 and an arcsinh-R^3 transformation are introduced. The proposed R^2 and R^3 transformations are efficient and applicable to different types of singular kernels in the Method of Moments (MoM) solution of electromagnetic surface integral equations, whereas the R^1 transformation is only suitable for the first order singular integrals. The newly proposed transformation schemes are verified and they are also utilized for deformed triangles, where good performance is still obtained. Detailed discussions of the new family of radial-angular-R^n transformation schemes have already been proposed in [Li and Eibert, 2016].

4.4.1 Introduction

Singularity and hyper singularity treatments are essential for the computation of the mutual coupling integrals in the method of moments (MoM) [Chew et al., 2001, Ismatullah and Eibert, 2009]. The singularity cancellation techniques are regarded as very effective solutions to the singularity problems. Derived from the Helmholtz equation, the boundary integral (BI) equations involve the scalar Green's function [Chew et al., 2001, Ismatullah and Eibert, 2009, Rao et al., 1982] and its gradient in the integral kernels. In the procedure of the Gauss Legendre evaluation of mutual couplings and when the observation points in the testing domain approaching the source domain, the $1/R$-type of kernels from the Green's function and the $\boldsymbol{R}/R^3$-type kernels from the gradient of the Green's function import the singularity into the integrals. Thus, the $1/R$-type and $\boldsymbol{R}/R^3$-type kernels require the corresponding order of singularity cancellation treatments. Moreover, the lower order singular coupling integral kernels can also be effectively solved by the higher order singularity treatment solutions.

A lot of singularity subtraction and cancellation techniques for the $1/R$-type and $\boldsymbol{R}/R^3$-type of kernels have been proposed [Botha, 2013, 2014, Duffy, 1982, Eibert and Hansen, 1995b, Fink et al., 2005, 2008, Graglia, 1993, Ismatullah and Eibert, 2008, Järvenpää et al., 2006a, Khayat and Wilton, 2005, Khayat et al., 2008, Li et al., 2014a, Polimeridis et al., 2013, Vipiana et al., 2008, Vipiana and Wilton, 2011] A number of effective schemes are proposed in [Fink et al., 2005], including the Arcsinh scheme for the 1st order singular kernels and radial-angular schemes for 1st, 2nd and 3rd order near-singularity cancellation. In [Vipiana and Wilton, 2011], an optimized solution to the evaluation of singular and near-singular potential integrals has been provided. In [Polimeridis et al., 2013], an efficient singularity treatment algorithm is presented for mutual couplings, where the testing and the source domains contain one common edge or one common vertex. Partly analytical solutions are introduced to some of the integrations and the integral dimensions are re-

duced. In [Botha, 2013, 2014], a family of augmented Duffy transformation schemes have been provided for near-singularity cancellations, where augmentation means that further, successive smoothing transformations are utilized to achieve cancellations of various orders of near-singularities. However, the radial angular transformations are related and sensitive to the projection height of the observation points above the source plane. An augmented radial-angular-R^2 transformation has been proposed in [Li et al., 2014a], where the negative effects of the observation points in the testing domain are removed effectively. In this chapter, a new family of radial-angular-R^n transformation schemes are proposed for the 1st, 2nd and 3rd order singular coupling integral kernels. The new schemes are innovated from the variable separation method. Improvements in accuracy and efficiency for the corresponding types of kernels are obtained for the singularity and the near-singularity cancellation techniques.

The geometrical configurations [Ismatullah and Eibert, 2008, Li et al., 2014a] are classified dependent on the observation points and their projection points on the source domain plane. As displayed from Figs. 6 to 8, three kinds of configurations are considered: Fig. 6, the projection of the observation point into the source plane is inside the source domain, Fig. 7, the projection point is outside the source domain and the projection point can directly see only one edge of the source triangle and it is called the 1st type of outside projection, Fig. 8, the projection point is outside the source domain and the projection point can directly see two edges of the source triangle and it is called the 2nd type of outside projection. $\boldsymbol{r}_3$ can also be located between the triangle edge from $\boldsymbol{r}_1$ to $\boldsymbol{r}_2$ and the projection point. In this case, r_l and r_u should, however, be flipped in order to obtain the correct integration results. In Fig. 6, the source triangle has been separated into three sub-triangles and only one sub-triangle is shown. In Fig. 7 and Fig. 8, the source triangle is divided into two sub-triangles and the sub-triangles are integrated independently. In the singularity cancellation techniques, the coordinates (x, y) are transformed into (u, v). So, a Jacobian is required to be multiplied inside the integral kernels. R is the distance between the sampling point in the source domain and the observation point, J is the Jacobian of the coordinate transformation from (x, y) to (u, v). The 1st, 2nd and 3rd order transformation schemes are all effective for singularity cancellation in the B type of integrals, where the Jacobian J contains an R, R^2 or an R^3 factor correspondingly. Moreover, the 2nd and 3rd order transformation schemes are effective for singularity cancellations in the D-type integrals. To obtain an R^n factor within J $(n = 1, 2, 3)$, the variable separation method is utilized in this work.

The variable separation method, set up with the parameters in the transformed coordinates, is utilized for the radial and the angular functional dependencies. The radial variable is defined as a product of two separated functions and the angular variable is assumed as a sum of two independent separated functions. With a desired Jacobian, differential equations are obtained for the separated functions. The differential equations are almost symmetric in the transformed coordinates. Dependent on the properties of the separated functions, certain limit conditions are required to be satisfied, which are applied to solve the separated functions. General solutions are provided for the transformation schemes with 1st, 2nd and 3rd order.

To increase the efficiency of the numerical solutions, the adaptive technique [Ismatullah

and Eibert, 2008, Li et al., 2014a] is utilized for the singularity cancellation transformation schemes. The advantages of the adaptive solutions are that the sampling points are located only inside the source domain. For Figs. 7 and 8, the numbers of the sub-triangles are reduced as compared to the traditional non-adaptive techniques. As it turns out, fewer sampling points are required and faster accuracy convergence is obtained. The adaptive technique is used for all the transformation schemes mentioned in this work. For Fig. 6, a fixed threshold is always set to obtain a well-performed integral.

To obtain good performance for deformed triangles, the transformation schemes should have well-performed integration limits in the (u, v) coordinates, ideally the (u, v) integration domain should be the full unit square block or a rectangular triangle for the adaptive schemes in the cases of projection point outside.

A series of transformation schemes are proposed in this chapter, which effectively satisfy the requirements of regular and deformed triangles. Within the variable separation method, general solutions to the radial-angular-R^n transformation schemes are proposed and also augmented radial-angular-R^n transformation schemes are given. In general solutions, several constant parameters can be freely selected. These parameters together with the augmentation function, in case of the augmented transformations, are set to optimize the normalized integration domain in the (u, v) coordinates. For different orders of the transformation schemes, numerical results are provided and the accuracy for the corresponding types of integral kernels is discussed. It is found that excellent performance of the radial-angular-R^n and the augmented radial-angular-R^n transformation schemes is obtained for regular and deformed triangles.

4.4.2 The Variable Separation Method

The variable separation method is utilized within the singularity cancellation technique. The parameters to be separated are R and Φ, where R is the distance between the observation point and the sampling point in the source domain and Φ is the angle between the x-axis and the line connecting the origin (the projection point on the source domain plane) and the sampling point in the source domain. R and Φ are given by

$$\begin{cases} R(u,v) = f(u)g(v) \\ \Phi(u,v) = \phi(u) + \theta(v) \end{cases}, \tag{4.4.2.1}$$

where (u, v) are the transformed coordinates and (x, y) are the original coordinates in Figs. 6-8. $f(u)$ and $\phi(u)$ are functions of coordinate u only, $g(v)$ and $\theta(v)$ are functiona of coordinate v only.

Through the geometric relationships between (x, y) and (R, Φ), the distance r between the origin O and the sampling point in the source domain is given by

$$r = \sqrt{R^2 - |z|^2} = \sqrt{f^2 g^2 - |z|^2}, \tag{4.4.2.2}$$

where $|z|$ is the height of the observation point above the source domain plane. Thus, (x, y) can be written as

$$\begin{cases} x = r\cos(\Phi) \\ y = r\sin(\Phi) \end{cases} \tag{4.4.2.3}$$

and it is obtained that

$$\begin{cases} \frac{\partial x}{\partial u} = \frac{fg^2}{\sqrt{f^2g^2-|z|^2}}\cos(\phi+\theta)\frac{df}{du} - \sqrt{f^2g^2-|z|^2}\sin(\phi+\theta)\frac{d\phi}{du} \\ \frac{\partial x}{\partial v} = \frac{f^2g}{\sqrt{f^2g^2-|z|^2}}\cos(\phi+\theta)\frac{dg}{dv} - \sqrt{f^2g^2-|z|^2}\sin(\phi+\theta)\frac{d\theta}{dv} \\ \frac{\partial y}{\partial u} = \frac{fg^2}{\sqrt{f^2g^2-|z|^2}}\sin(\phi+\theta)\frac{df}{du} + \sqrt{f^2g^2-|z|^2}\cos(\phi+\theta)\frac{d\phi}{du} \\ \frac{\partial y}{\partial v} = \frac{f^2g}{\sqrt{f^2g^2-|z|^2}}\sin(\phi+\theta)\frac{dg}{dv} + \sqrt{f^2g^2-|z|^2}\cos(\phi+\theta)\frac{d\theta}{dv} \end{cases}. \tag{4.4.2.4}$$

By combining (4.4.2.1), (4.4.2.2) and (4.4.2.3), the Jacobian of the transformation from (x, y) to (u, v) is given by

$$J = \begin{vmatrix} \frac{\partial x}{\partial u} & \frac{\partial x}{\partial v} \\ \frac{\partial y}{\partial u} & \frac{\partial y}{\partial v} \end{vmatrix} = \frac{\partial x}{\partial u}\frac{\partial y}{\partial v} - \frac{\partial x}{\partial v}\frac{\partial y}{\partial u} = fg\left(g\frac{df}{du}\frac{d\theta}{dv} - f\frac{d\phi}{du}\frac{dg}{dv}\right). \tag{4.4.2.5}$$

Equation (4.4.2.5) is a general solution for the Jacobian based on the variable separation according to (4.4.2.1). It is utilized as an equation to achieve general solutions for $f(u)$, $\phi(u)$, $g(v)$ and $\theta(v)$. Then, with (4.4.2.1) and (4.4.2.3), the transformations from (u, v) to (x, y) are obtained.

4.4.3 General Solution to Radial-Angular Transformations

The essence of the Radial-Angular transformation schemes is to cancel out the singularities in the coupling integrals. To achieve this, the Jacobian is required to be

$$J = R^n = f^n(u)g^n(v), \quad n = 1, 2, 3... , \tag{4.4.3.1}$$

where n is the order of the singular coupling integral kernels. With (4.4.2.5), it is found that

$$g\frac{df}{du}\frac{d\theta}{dv} - f\frac{d\phi}{du}\frac{dg}{dv} = f^{n-1}g^{n-1}. \tag{4.4.3.2}$$

Therefore,

$$\frac{d\phi}{du} = \left(g\frac{d\theta}{dv}\Big/\frac{dg}{dv}\right)\frac{1}{f}\frac{df}{du} - \left(g^{n-1}\Big/\frac{dg}{dv}\right)f^{n-2} \tag{4.4.3.3}$$

and its integration gives

$$\phi = \left(g\frac{d\theta}{dv}\Big/\frac{dg}{dv}\right)\ln f - \left(g^{n-1}\Big/\frac{dg}{dv}\right)\int f^{n-2}du. \tag{4.4.3.4}$$

Since ϕ is a function of u only and g as well as θ are functions of v only, it is found that

$$\left(g^{n-1}\Big/\frac{dg}{dv}\right) = c_1 \Rightarrow g = \left[-\frac{(v+c_2)(n-2)}{c_1}\right]^{\frac{1}{2-n}}, \tag{4.4.3.5}$$

$$\left(g\frac{d\theta}{dv}\Big/\frac{dg}{dv}\right) = c_3 \Rightarrow \theta = c_3 \ln g + c_4\,, \tag{4.4.3.6}$$

where c_1, c_2, c_3 and c_4 are constants and $c_1 \neq 0$.

From equations (4.4.3.3)-(4.4.3.6), it is clear that for any function $f(u) \neq 0$, the Jacobian $J = R^n$ can be found. The different constants c_1, c_2, c_3 and c_4 can determine the different transformation equations. However, in the singularity cancellation techniques, it is necessary to compute the upper and lower integral limits of (u, v) for the Gauss Legendre quadrature. A very complicated $f(u)$ or strange constant settings may make the integral limits difficult to be computed. A family of radial-angular-R^n transformation schemes are proposed with $n = 1, 2, 3$ and a certain number of $f(u)$ are also selected as examples.

4.4.4 General Solution to Augmented Radial-Angular Transformations

With well-behaved functions multiplied into the Jacobian, a better behaved integration domain in (u, v) and a more powerful distribution of the sampling points in the source domain can be obtained. Thus, a general solution is proposed for the variable separation method combined with well-behaved functions multiplied inside the Jacobian.

A simple case of (4.4.2.1) is obtained with $f(u) = 1$ and $\theta(v) = 0$. In this case, $R(u, v) = R(v)$, $r(u, v) = r(v)$ and $\Phi(u, v) = \Phi(u) = \phi(u)$. With (4.4.2.2), the Jacobian can be written as

$$J = -R\frac{dR}{dv}\frac{d\phi}{du} = -r\frac{dr}{dv}\frac{d\phi}{du}. \tag{4.4.4.1}$$

The Jacobian proposed in (4.4.3.1) achieves an exact singularity cancellation in the transformation schemes. However, the Jacobian is still effective if it multiplies with a non-zero and non-singular factor. Thus, the Jacobian employed to define augmented transformation schemes can be written as

$$J = R^n h(u, v), \tag{4.4.4.2}$$

where $h(u, v) \not\equiv 0$. To construct a group of augmented radial-angular transformation schemes, the function $h(u, v)$ is chosen as $h(u, v) = h(\vartheta)$, where ϑ is the angle between R and $|z|$ and $r = R\sin(\vartheta)$. In the family of radial-angular-R^n transformation schemes, the function $h(\vartheta)$ is effective to modify the normalized integration domain in the transformed coordinates and it can also modify the strength of the Jacobian relevant to ϑ. A good selection of $h(\vartheta)$ can result in improved integration efficiency and accuracy. From (4.4.4.1) and (4.4.4.2), it gives that

$$R\frac{dR}{dv}\frac{d\phi}{du} = r\frac{dr}{dv}\frac{d\phi}{du} = -R^n h(\vartheta). \tag{4.4.4.3}$$

For different orders of transformation schemes, a family of augmented radial-angular-R^n transformation schemes are proposed with the function $h(\vartheta)$ chosen in various formats.

4.5 The Family of Radial-Angular-R^1 Transformations

To obtain singularity cancellation techniques for the $1/R$-type of singular coupling integral kernels, the power of the Jacobian can be set as $n = 1$. Then, the solution in (4.4.3.5) can be written as

$$\left(1 \Big/ \frac{dg}{dv}\right) = c_1 \Rightarrow g = \frac{v + c_2}{c_1}\,, \tag{4.5.1}$$

where c_1 and c_2 are constants and $c_1 \neq 0$. For simplicity of the solutions, the constants are set as $c_1 = -1$, $c_2 = c_3 = c_4 = 0$ as an example. Different functions $f(u)$ will then determine the different formats of the transformation schemes.

4.5.1 The Radial-Angular-R^1 Transformation

With the constant settings and the function $f(u)$ set as $f(u) = 1$, the radial-angular-R^1 (R-A-R1) transformation is achieved as

$$\begin{cases} u = \arctan(\frac{y}{x}) \\ v = -R \end{cases}, \quad J = -R\,. \tag{4.5.1.1}$$

(4.5.1.1) is equivalent to the radial (extended polar) transformation scheme in [Fink et al., 2005, Khayat et al., 2008]. The influence of the projection height of the observation point $|z|$ is deleted. The transformation scheme and the Jacobian are independent from the projection height $|z|$. The corresponding integration limits are found to be

$$u_{l,u} = \Phi_{l,u}\,, \quad v_{l,u} = \sqrt{r_{l,u}^2 + |z|^2}\,. \tag{4.5.1.2}$$

From (4.5.1.1) and (4.5.1.2), it is seen that u is a monotonically increasing function of Φ and v is a monotonically decreasing function of r. Thus, (4.5.1.1) is flexible in transforming from (x, y) to (u, v) and vice versa. When $|z| \to 0$, the Jacobian is not zero. Thus, (4.5.1.1) is effective for singular kernels.

4.5.2 The Augmented Radial-Angular-R^1 Transformation

The power of the Jacobian can be set as $n = 1$ for the $1/R$-type kernels. The solutions derived from (4.4.3.2) illustrate that the Jacobians are exactly R for $n = 1$. With $n = 1$ and also with

$$h(\vartheta) = \frac{\sin\vartheta}{(1+\sin\vartheta)}\,, \tag{4.5.2.1}$$

an augmented $1/R$-type transformation is found with Jacobian

$$J = R\frac{\sin\vartheta}{1+\sin\vartheta} = -r\frac{dr}{dv}\frac{d\phi}{du}, \quad 0 \le \vartheta \le \frac{\pi}{2}\,, \tag{4.5.2.2}$$

according to (4.4.4.1) $h(\vartheta)$ is here a general testing function to prove the efficacy of (4.4.4.3). To obtain an easy solution, $d\phi/du = -1$ is selected. It provides the solution for $\Phi(u)$ as $\Phi(u) = -u$. From (4.4.4.3), (4.5.2.2) and with $\sin\vartheta = r/R$, it gives

$$\frac{dR}{dv} = -\frac{dr}{dv} + 1 \Rightarrow r = \frac{(v+c_1)^2 - |z|^2}{2(v+c_1)}, \tag{4.5.2.3}$$

where c_1 is an arbitrary constant. With $c_1 = 0$, a solution to the transformed coordinate v is given by $v = R + r$. Thus, the resulting augmented radial-angular-R^1 (A-R-A-R1) transformation turns out to be

$$\begin{cases} u = -\arctan(\frac{y}{x}) \\ v = R + r \end{cases}, \quad J = R\frac{\sin\vartheta}{1+\sin\vartheta}, \quad 0 \le \vartheta \le \frac{\pi}{2}. \tag{4.5.2.4}$$

In Fig. 6, if $|z| \neq 0$, $\vartheta = 0$ only when the sampling point in the source domain is exactly positioned at the origin O . For the case of $|z| \neq 0$, $\vartheta < \pi/2$ is always satisfied. For $|z| = 0$, it is shown that $\vartheta = \pi/2$ and the Jacobian turns to be $J = r/2$.

For different geometric configurations in Figs. 6-8, the adaptive integration limits of (4.5.2.4) are given by

$$u_{l,u} = -\Phi_{u,l}, \quad v_{l,u} = \sqrt{r_{l,u}^2 + |z|^2} + r_{l,u}, \tag{4.5.2.5}$$

where for the determination of $\Phi_{l,u}$ and $r_{l,u}$, the reader is referred to [Li et al., 2014a]. From (4.5.2.4), it is clear that the Jacobian is relevant to the angle ϑ, which depends on the height of the observation point $|z|$. When $|z| \to 0$, the Jacobian turns out to be stable.

4.6 The Family of Radial-Angular-R^2 Transformations

To obtain singularity cancellation techniques for the $\boldsymbol{R}/R^3$-type of singular coupling integral kernels, the power of the Jacobian can be set as $n = 2$. However, the solution of (4.4.3.5) has to be modified into

$$\left(g \Big/ \frac{dg}{dv}\right) = c_1 \Rightarrow g = \exp\left(\frac{v + c_2}{c_1}\right), \tag{4.6.1}$$

where c_1 and c_2 are constants and $c_1 \neq 0$. To simplify the solutions, the constants are set as $c_1 = 1$, $c_2 = c_3 = c_4 = 0$ as an example. Different functions $f(u)$ will then determine the different transformation schemes.

4.6.1 The Radial-Angular-R^2 Transformation

With the same constant settings as above and the function $f(u)$ set as $f(u) = 1$, the radial-angular-R^2 (R-A-R2) transformation is found to be

$$\begin{cases} u = -\arctan(\frac{y}{x}) \\ v = \ln R \end{cases}, \quad J = R^2. \tag{4.6.1.1}$$

The transformation scheme (4.6.1.1) is similar to the radial-angular-R^2 transformation in [Fink et al., 2005, Ismatullah and Eibert, 2008]. However, the influence of the projection height of the observation point $|z|$ is removed. The transformation equations and the Jacobian are irrelevant to the projection height $|z|$. When $|z| \to 0$ in Fig. 6, a threshold is required to determine the integration limits for R. The corresponding integration limits are achieved as

$$u_{l,u} = -\Phi_{u,l}\,, \quad v_{l,u} = \frac{1}{2}\ln(r_{l,u}^2 + |z|^2)\,. \tag{4.6.1.2}$$

From (4.6.1.1) and (4.6.1.2), it is found that u is a monotonically decreasing function of Φ and v is a monotonically increasing function of r. Thus, (4.6.1.1) is useful to transform from (x, y) to (u, v) and vice versa. When $|z| \to 0$, the Jacobian is not zero. Thus, (4.6.1.1) is effective for both singular and hyper singular integral kernels.

4.6.2 The Radial-Angular-R^2-Cosh Transformation

With the same constant settings as before, the function $f(u) = \cosh(u)$ is used to achieve an improved normalized integration domain in the transformed coordinates. Then, the radial-angular-R^2-Cosh (R-A-R2-C) transformation is found as

$$\begin{cases} u = -\arctan(\frac{y}{x}) \\ v = \ln R - \cosh(u) \end{cases}, \quad J = R^2. \tag{4.6.2.1}$$

In (4.6.2.1), the influence of the projection height of the observation point $|z|$ is also removed. As in Figs. 7 and 8, the transformation scheme and the Jacobian are independent from $|z|$.

When $|z| \to 0$, in Fig. 6, a threshold is required to determine the integration limits for R. The corresponding integration limits for all types of the geometric configurations are found to be

$$u_{l,u} = -\Phi_{u,l}, \quad v_{l,u} = \frac{1}{2}\ln(r_{l,u}^2 + |z|^2) - \cosh(u). \tag{4.6.2.2}$$

u is also a monotonically decreasing function of Φ. With a fixed value of u, the function value $\cosh(u)$ is also fixed. So the upper boundary limit r_l and the lower boundary limit r_u are determined. Thus, v is a monotonically increasing function of r. So, the scheme in (4.6.2.1) is effective for both singular and hyper singular integral kernels.

4.6.3 The Augmented Radial-Angular-R^2 Transformation

When $n = 2$ and $d\phi/du = 1$, $\Phi(u) = u$ is obtained. To obtain a well performed numerical integration, $h(\vartheta) = -\frac{1}{2}\sin\vartheta$ is utilized to improve the effect of the Jacobian dependent on theta. The Jacobian can be written as

$$J = -\frac{1}{2}R^2\sin\vartheta = -r\frac{dr}{dv}\,. \tag{4.6.3.1}$$

From (4.6.3.1), it is found that

$$\frac{d^2r}{dv^2} - \frac{1}{4}r = 0 \Rightarrow r = c_1 e^{\frac{1}{2}v} + c_2 e^{-\frac{1}{2}v}\,, \tag{4.6.3.2}$$

where c_1 and c_2 are arbitrary constant values. Let $c_1 = -\frac{|z|^2}{2}$ and $c_2 = \frac{1}{2}$, then

$$r = \frac{e^{-\frac{1}{2}v} - |z|^2 e^{\frac{1}{2}v}}{2}. \tag{4.6.3.3}$$

Thus, an augmented radial-angular-R^2 (R-A-R2-Z2) transformation based on (4.6.3.3) and $\Phi(u)$ is written as

$$\begin{cases} u = \arctan(\frac{y}{x}) \\ v = -2\ln(R + r) \end{cases}, \quad J = -\frac{1}{2}R^2\sin\vartheta, \tag{4.6.3.4}$$

where ϑ is the angle between R and $|z|$. The corresponding integration limits turn out to be

$$u_{l,u} = \Phi_{l,u}, \quad v_{l,u} = -\ln(\sqrt{r_{u,l}^2 + |z|^2} + r_{u,l}). \tag{4.6.3.5}$$

u is once more a monotonically increasing function of Φ and v is again a monotonically decreasing function of r. The Jacobian in (4.6.3.4) is not always zero when $|z| \to 0$. So, it is effective for both singular and hyper singular integral kernels. As a member of the radial-angular-R^2 family, the R-A-R2-Z2 transformation is equivalent to the transformation proposed in [Li et al., 2014a].

4.7 The Family of Radial-Angular-R^3 Transformations

To obtain singularity cancellation for $\boldsymbol{R}/R^3$-type singular coupling integral kernels, the power of the Jacobian can also be set as $n = 3$, where the third order singularity is canceled out directly. With the constant parameters set as $c_1 = -1$, $c_2 = c_3 = c_4 = 0$, it is obtained that

$$g(v) = \frac{1}{v}, \quad \phi(u) = \int f du \,. \tag{4.7.1}$$

With different formats of $f(u)$, several radial-angular-R^3 transformation schemes are constructed.

4.7.1 The Radial-Angular-R^3 Transformation

With $f(u) = 1$, the corresponding radial-angular-R^3 (R-A-R3) transformation scheme is proposed as

$$\begin{cases} u = \arctan(\frac{y}{x}) \\ v = \frac{1}{R} \end{cases}, \quad J = R^3. \tag{4.7.1.1}$$

This transformation is similar to the radial-angular-R^3 scheme in [Fink et al., 2005]. However, the influence of the projection height of the observation point $|z|$ is removed. The transformation equations and the Jacobian are irrelevant to $|z|$. When $|z| \to 0$ in Fig. 6, a threshold is required to determine the integration limits for R. The corresponding integration limits for all types of the geometric configurations are written as

$$u_{l,u} = \Phi_{l,u} \,, \quad v_{l,u} = \frac{1}{\sqrt{r_{u,l}^2 + |z|^2}} \,. \tag{4.7.1.2}$$

With the Jacobian in (4.7.1.1) for different configurations in Figs. 6-8, the scheme in (4.7.1.1) is effective for near singular and also near-hyper singular integral kernels.

4.7.2 The Arcsinh-R^3 Transformation

Another selection of the function $f(u)$ is written as $f(u) = \cosh(u)$. Based on $\phi(u)$ in (4.7.1), the integration of $f(u)$ turns out to be $\phi(u) = \sinh(u)$. The corresponding Arcsinh-R^3 (Asinh-R3) transformation equations turn to be

$$\begin{cases} u = \sinh^{-1}\left(\arctan\left(\frac{y}{x}\right)\right) \\ v = \frac{1}{R}\sqrt{1 + \arctan^2(\frac{y}{x})} \end{cases}, \quad J = R^3 \,. \tag{4.7.2.1}$$

These equations also avoid the influence of the projection height $|z|$. As before, a threshold is required for R to determine the integration limits for $|z| \to 0$ in Fig. 6. The corresponding integration limits for all types of the geometric configurations are

$$u_{l,u} = \sinh^{-1} \Phi_{l,u} \,, \quad v_{l,u} = \frac{1}{\sqrt{r_{u,l}^2 + |z|^2}} \sqrt{1 + \Phi^2} \,. \tag{4.7.2.2}$$

Similar to (4.7.1.1), the scheme in (4.7.2.1) is also effective for both near singular and near-hyper singular integral kernels.

4.7.3 The Augmented-Radial-Angular-R^3 Transformation

When $n = 3$ and $d\phi/du = 1$, it is achieved that $\Phi(u) = u$. With $h(\vartheta) = \sin\vartheta(1+\sin\vartheta)$, the kernel turns out to be dependent on the projection height and an improved integration performance is obtained. The Jacobian for the third order transformation can be proposed as

$$J = R^3\sin\vartheta(1+\sin\vartheta) = -R\frac{dR}{dv} = -r\frac{dr}{dv} \tag{4.7.3.1}$$

and it is found that

$$\begin{cases} dr/dv &= -R(R+r) \\ dR/dv &= -r(R+r) \end{cases} \Rightarrow \frac{d(R+r)}{dv} = -(R+r)^2. \tag{4.7.3.2}$$

Thus,

$$\frac{d(R+r)}{(R+r)^2} = -dv \Rightarrow v = \frac{1}{R+r} + c, \tag{4.7.3.3}$$

where c is an arbitrary constant value. Then, with $c = 0$, an augmented radial-angular-R^3 (A-R-A-R3) transformation is obtained as

$$\begin{cases} u = \arctan(\frac{y}{x}) \\ v = \frac{1}{R+r} \end{cases}, \quad J = R^3\sin\vartheta\,(1+\sin\vartheta)\,, \tag{4.7.3.4}$$

where ϑ is the angle between R and $|z|$. The corresponding integration limits are found as

$$u_{l,u} = \Phi_{l,u}, \quad v_{l,u} = \frac{1}{\left(\sqrt{r_{u,l}^2 + |z|^2} + r_{u,l}\right)}. \tag{4.7.3.5}$$

Similar to (4.7.1.1) and (4.7.2.1), the scheme in (4.7.3.4) is effective for both near singular and near-hyper singular integral kernels.

4.8 Numerical Results

The numerical results from all the new transformation schemes are compared with some traditional transformation equations. The unit source domains displayed in Fig. 8 are utilized dependent on the locations of the projection points. The adaptive integration techniques according to [Ismatullah and Eibert, 2008] are applied to all of the transformation schemes together with the corresponding integral limits. The accuracy convergence of the different types of the coupling integral kernels with the increasing number of sampling points are studied for all of the geometric configurations in Figs. 6-8. The performance of the accuracy with changing height is also analyzed. The results are compared according to the corresponding orders of the the singularity cancellation techniques. Moreover, the performance of the different transformation techniques is also studied for deformed triangles.

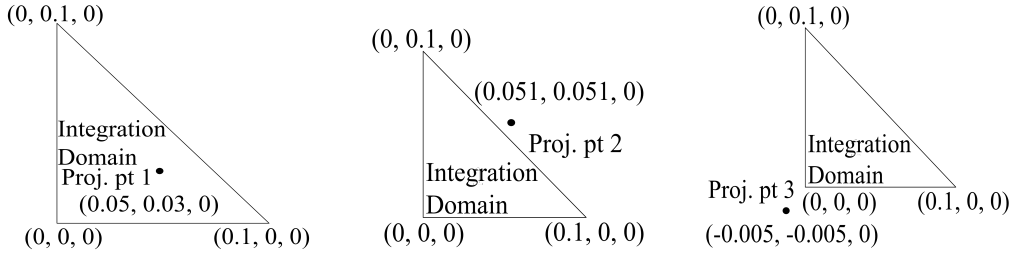

Figure 9: Unit source domain with different locations of the observation point: (a) Projection point inside the source domain. (b) The 1st type of outside projection point. (c) The 2nd type of outside projection point.

4.8.1 Normalized Integration Domain

An important property of all the transformation schemes is the transformed integration domain for singularity cancellation. The normalized integration domains of the proposed transformation formulas are proven to be very well performed when the height of the observation point $|z|$ tends to be zero. The normalized integration domains of the following transformation schemes are evaluated:

a) Augmented Radial-Angular-R^1 (4.5.2.4) (A-R-A-R1);
b) Radial-Angular-R^2 (4.6.1.1) (R-A-R2);
c) Radial-Angular-R^2-Cosh (4.6.2.1) (R-A-R2-C);
d) Augmented Radial-Angular-R^3 (4.7.3.4) (A-R-A-R3);
e) Radial-Angular-R^3 (4.7.1.1) (R-A-R3);
f) Arcsinh-R^3 (4.7.2.1) (Asinh-R3).

The normalized integration domains are shown in Fig. 10 for the radial-angular-R^n transformation schemes with zero height $|z| = 0$. The normalized transformed integration domains are shown in Fig. 10(a) for a projection point located inside the integration domain with a symmetric triangle. As shown in Fig. 9(a), the considered sub-triangle is always a full triangle, the projection point is located on a vertex of it. It is found that the normalized integration domains of the A-R-A-R1, R-A-R2-C and Asinh-R3 deviate from the full square unit block with $|z| = 0$. However, the normalized integration domains of the R-A-R2, A-R-A-R3 and R-A-R3 are very near to the full square unit block. The normalized integration domains for a projection point outside the integration domain with $|z| = 0$ are shown in Fig. 10(b). The projection point is always on an extension of one of the edges, as the integration domains are always sub-triangles according to the configurations in Figs. 9(b) and (c). For convenience, a symmetric triangle is again utilized as source sub-domain. Due to the adaptive integration technique, the ideal transformed integration domains are now near to rectangular triangles and some of the shown transformations approach this ideal domain.

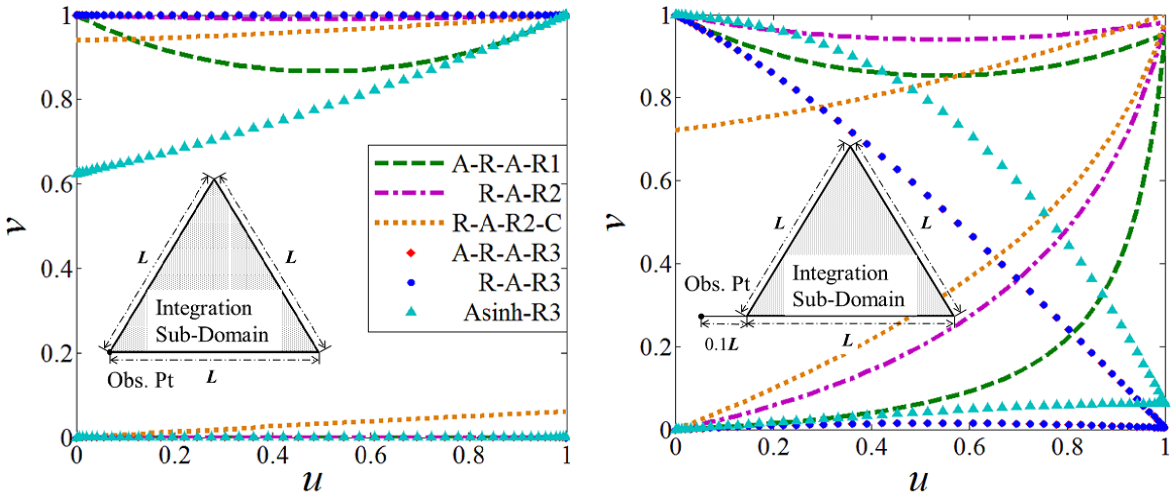

Figure 10: Normalized integration sub-domain with $|z| = 0$. (a) Inside projection point, (b) Outside projection point with the same legend as in (a).

4.8.2 Accuracy of the 1st Order Transformation Schemes

The considered evaluated integral in the source domain and the corresponding error are defined as

$$I = \iint_s \frac{g(\lambda_1, \lambda_2)}{\sqrt{x^2 + y^2 + z^2}} ds, \quad \delta = \left| \frac{I_{quad} - I_{ref}}{I_{ref}} \right|, \tag{4.8.2.1}$$

where $(\lambda_1, \lambda_2, \lambda_3)$ are the simplex coordinates defined in the source domain, $g(\lambda_1, \lambda_2)$ is a scalar function of the simplex coordinates multiplied inside the kernel. The 1-D order N is the Gauss-Legendre sampling point number in both (u, v). The following transformation schemes are evaluated:

a) Augmented Radial-Angular-R^1 (4.5.2.4) (A-R-A-R1);
b) Arcsinh [Fink et al., 2005, Khayat et al., 2008] (Archsinh-R1);
c) Extended Duffy scheme [Fink et al., 2005, Khayat et al., 2008] (Duffy-R1);
d) Radial (Extended Polar) [Fink et al., 2005, Khayat et al., 2008] (Radial-R1-P);
e) Radial-Angular [Fink et al., 2005, Khayat et al., 2008] (Radial-R1-S);
f) Augmented-Duffy-R^1-Constant [Botha, 2013] (A-D-R1-C);
g) Augmented-Duffy-R^1-Linear [Botha, 2013] (A-D-R1-L);
h) Augmented-Duffy-R^1-Linear-2014 [Botha, 2014] (A-D-R1-S).

Figs. 11 and 12 display the relative integral errors for the inside projection point. Fig. 13 illustrates the integration error for the outside projection points. Figure 11(a) compares the different $1/R$ schemes for increasing N. Figure 11(b), Fig. 13(a), Fig. 13(b) compare the different $1/R$-type transformation schemes multiplied with a scalar function inside the kernels. Figure 12 compares the different $1/R$-type transformation schemes for inside

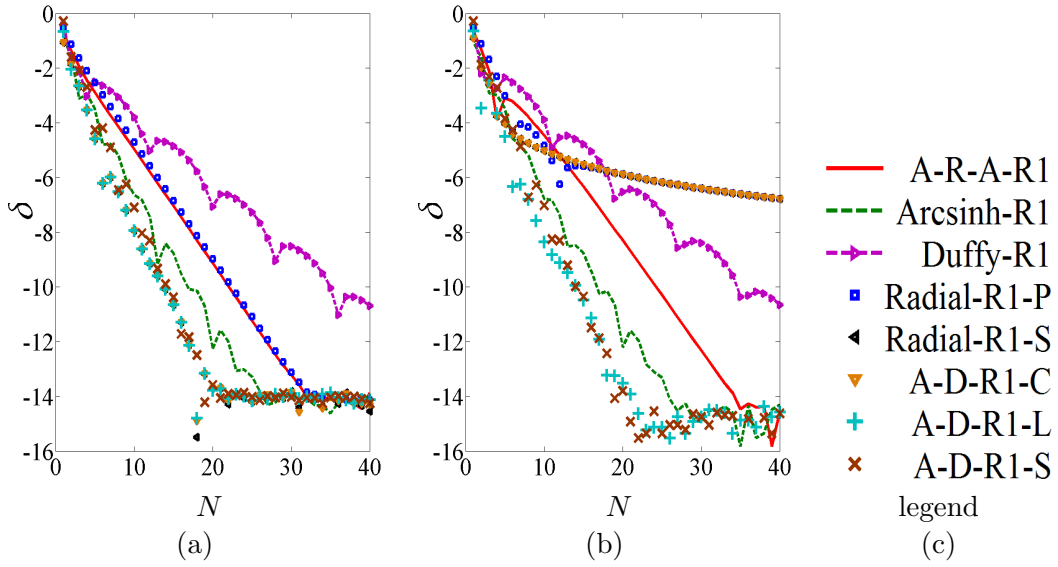

Figure 11: Comparison for $1/R$-type kernel ($n = 1$) and the configuration in Fig. 9(a). Logarithmic relative integration error δ versus sampling order N, with $|z| = 10^{-2}$. (a) $g = 1.0$, (b) $g = \lambda_1^2 + \lambda_2$, (c) The legend of Figs. (a) and (b).

projection point in Fig. 9(a) for changing $|z|$. With $|z| \to 0$, the new transformation scheme of (4.5.2.4) (A-R-A-R1) obtains in particular good accuracy. For the cases of outside projection points, all schemes achieve stable results independent from $|z|$. From the numerical results, it can be found that the A-D-R1-L in [Botha, 2013] and the A-D-R1-S in [Botha, 2014] show also excellent performance.

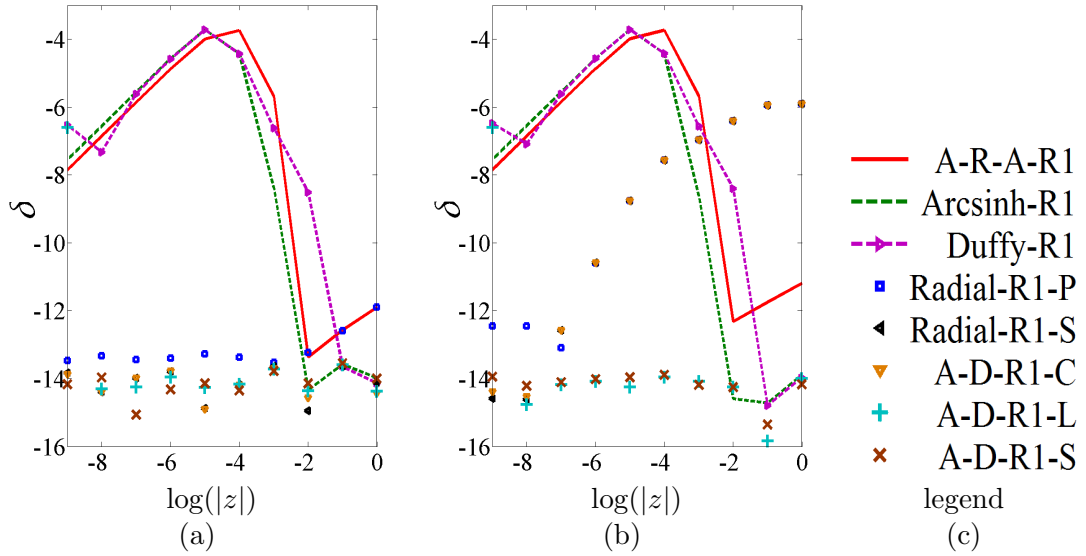

Figure 12: Comparison for $1/R$-type kernel ($n = 1$) and the configuration in Fig. 9(a). Logarithmic relative integration error δ versus $\log(|z|)$, with sampling order $N = 30$. (a) $g = 1.0$, (b) $g = \lambda_1^2 + \lambda_2$, (c) The legend for Figs. (a) and (b).

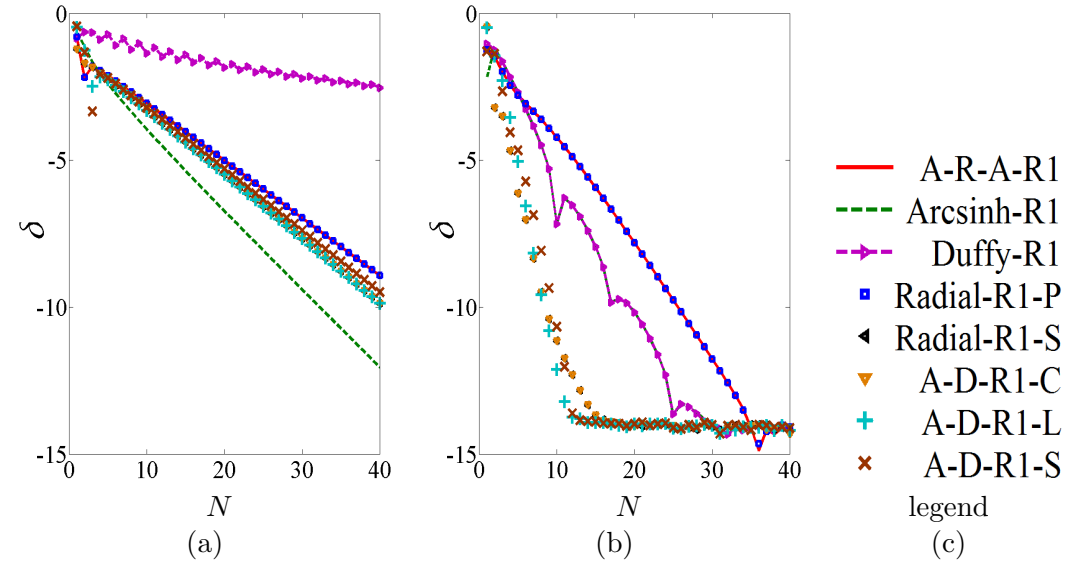

Figure 13: Comparison for $1/R$-type kernel ($n = 1$). Logarithmic relative integration error δ versus sampling order N, with $|z| = 10^{-4}$, $g = \lambda_1^2 + \lambda_2$. (a) Projection point 2 in Fig. 9(b), (b) Projection point 3 in Fig. 9(c), (c) The legend for Figs. (a) and (b).

4.8.3 Accuracy of the 2nd Order Transformation Schemes

The evaluated integrals in the source domain and the corresponding error are defined as

$$\boldsymbol{I}=\iint_s \frac{g(\lambda_1,\lambda_2)\boldsymbol{f}(\lambda_1,\lambda_2)}{x^2+y^2+z^2}ds, \quad \delta=\frac{|\boldsymbol{I}_{quad}-\boldsymbol{I}_{ref}|}{|\boldsymbol{I}_{ref}|} \tag{4.8.3.1}$$

and the following transformation schemes are evaluated:

a) Radial-Angular-R^2 (4.6.1.1) (R-A-R2);
b) Radial-Angular-R^2-Cosh (4.6.2.1) (R-A-R2-C);
c) Augmented Radial-Angular-R^2 [Li et al., 2014a] (R-A-R2-Z2);
d) Radial Angular-R^2 [Fink et al., 2005, Ismatullah and Eibert, 2008] (R-A-R2-Z1);
e) Augmented-Duffy-R^2-Constant [Botha, 2013] (A-D-R2-C);
f) Augmented-Duffy-R^2-Linear [Botha, 2013] (A-D-R2-L);
g) Augmented-Duffy-R^1-Linear-2014 [Botha, 2014] (A-D-R1-S).

Figs. 14-16 exhibit the numerical relative vector integration error for the radial-angular-R^2 transformation schemes. The unit vector $\hat{R}$ is pointing from the sampling point in the source domain toward the observation point. Figs. 14 and 15 exhibit the relative vector integration error for the inside projection point. Fig. 16 shows the vector integration error for the projection point 2 in Fig. 9(b). Figure 14(a) shows the vector integration error with increasing sampling order N, where a pure vector cross product is multiplied inside the kernel. Figure 14(b) displays the similar type of error as in Fig. 14(a), but it contains another scalar function multiplied with a vector cross product inside the kernel. Figure 15(a) displays the relative vector integration error changing with the projection height, where the unit vector $\hat{R}$ is multiplied inside the kernel. Figure 15(b) demonstrates the same type of performance as in Fig. 15(a), but with a vector cross product multiplied inside the kernel. Figure 16(a) displays the relative vector integration error versus N for the projection point 2 in Fig. 9(b). Figure 16(b) exhibits the vector integration error changing with the projection height with the unit vector $\hat{R}$ multiplied inside the kernel for the projection point 2 in Fig. 9(b).

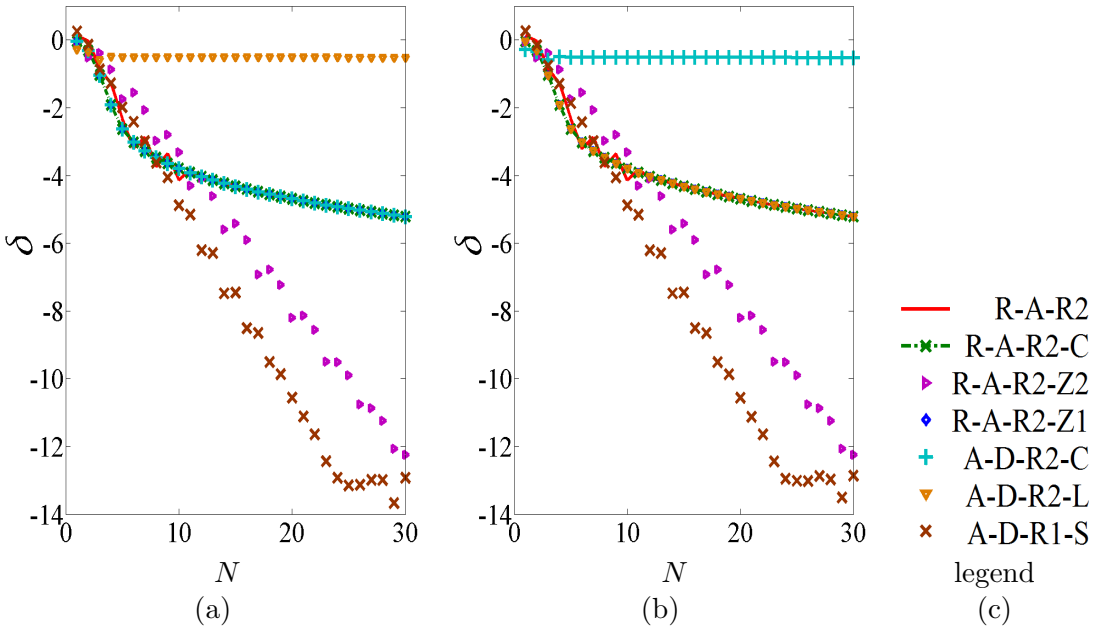

Figure 14: Comparison for $\boldsymbol{R}/R^3$-type kernel ($n = 2$) and the configuration in Fig. 9(a). Logarithmic relative vector integration error δ versus sampling order N, with $|z| = 10^{-6}$, $\boldsymbol{f} = (\lambda_1\boldsymbol{t}_1 + \lambda_2\boldsymbol{t}_2 + \lambda_3\boldsymbol{t}_3) \times \hat{R}(\lambda_1, \lambda_2)$. (a) $g = 1$, (b) $g = \lambda_1^2 + \lambda_2$, (c) The legend for Figs. (a) and (b).

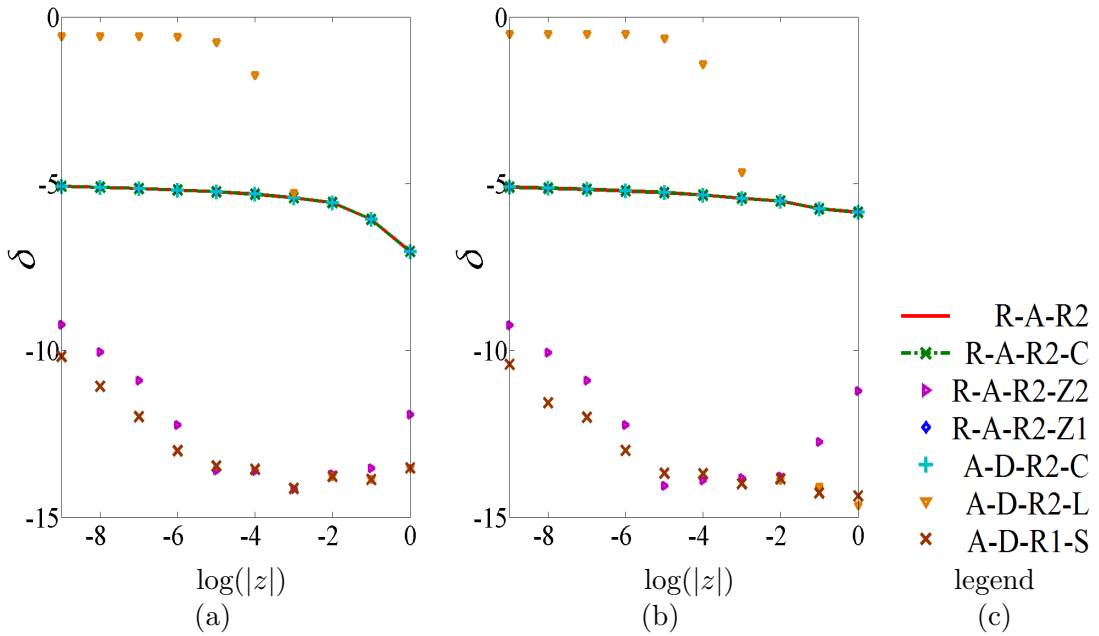

Figure 15: Comparison for $\boldsymbol{R}/R^3$-type kernel ($n = 2$) and the configuration in Fig. 9(a). Logarithmic relative vector integration error δ versus $\log(|z|)$, with sampling order $N = 30$ and $g = 1.0$. (a) $\boldsymbol{f} = \hat{R}(\lambda_1, \lambda_2)$, (b) $\boldsymbol{f} = (\lambda_1\boldsymbol{t}_1 + \lambda_2\boldsymbol{t}_2 + \lambda_3\boldsymbol{t}_3) \times \hat{R}(\lambda_1, \lambda_2)$, (c) The legend for Figs. (a) and (b).

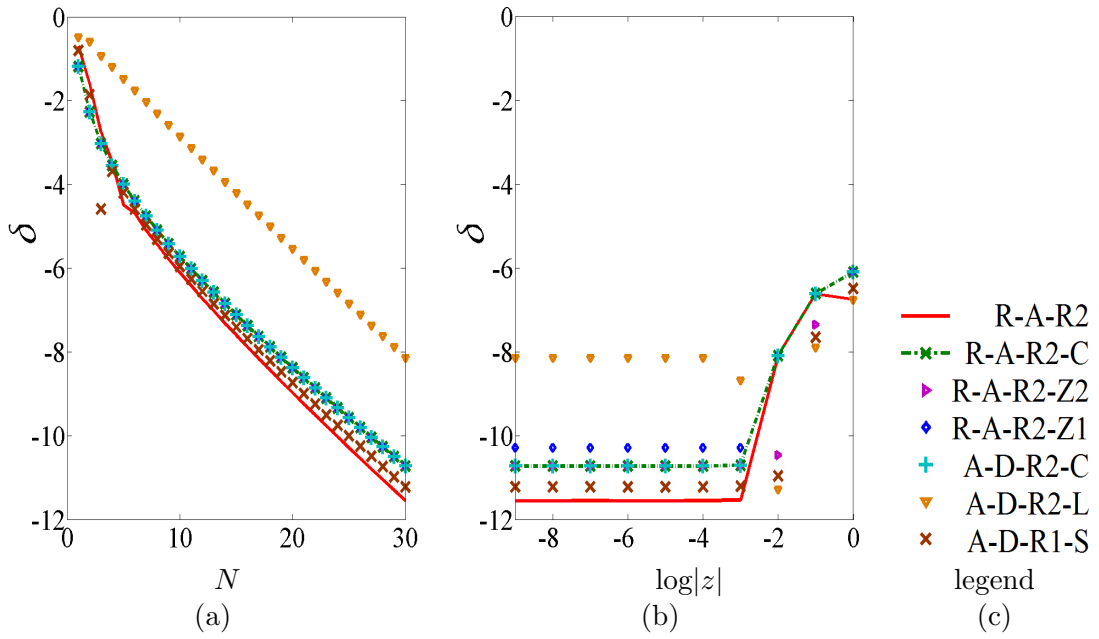

Figure 16: Comparison for $\boldsymbol{R}/R^3$-type kernel ($n = 2$). $g = 1.0$, $\boldsymbol{f} = \hat{R}(\lambda_1, \lambda_2)$. (a) Logarithmic relative vector integration error δ versus sampling order N, with $|z| = 10^{-6}$ for the projection point 2 in Fig. 9(b), (b) Logarithmic relative vector integration error δ versus $\log(|z|)$, with sampling order $N = 30$ for the projection point 2 in Fig. 9(b), (c) The legend for Figs. (a) and (b).

4.8.4 Accuracy of the 3rd Order Transformation Schemes

The discussed integrals in the source domain and the corresponding error are defined as

$$\boldsymbol{I}=\iint_s \frac{g(\lambda_1,\lambda_2)\boldsymbol{f}(\lambda_1,\lambda_2)}{(x^2+y^2+z^2)^{\frac{3}{2}}}ds, \quad \delta=\frac{|\boldsymbol{I}_{quad}-\boldsymbol{I}_{ref}|}{|\boldsymbol{I}_{ref}|} \tag{4.8.4.1}$$

and the following transformation schemes are evaluated:

a) Augmented Radial-Angular-R^3 (4.7.3.4) (A-R-A-R3);
b) Radial-Angular-R^3 (4.7.1.1) (R-A-R3);
c) Arcsinh-R^3 (4.7.2.1) (Asinh-R3);
d) Augmented-Duffy-R^3-Constant [Botha, 2013] (A-D-R3-C);
e) Augmented-Duffy-R^3-Linear [Botha, 2013] (A-D-R3-L);
f) Radial-Angular-R^3 [Fink et al., 2005] (R-A-R3-Z);
g) Augmented-Duffy-R^1-Linear-2014 [Botha, 2014] (A-D-R1-S).
h) Augmented Radial-Angular-R^2 [Li et al., 2014a] (R-A-R2-Z2);

Figs. 17 to 19 exhibit the numerical relative vector integration error for the radial-angular-R^3 transformation schemes. Figs. 17 and 18 display the relative vector integration error for the inside projection point. Fig. 19 displays the integration error for projection point 2 in Fig. 9(b). Figure 17(a) shows the vector integration error with increasing sampling order N, where the unit vector is multiplied inside the kernel. Figure 17(b) displays the similar type of error as in Fig. 17(a), but with another scalar function together with a vector cross product multiplied inside the kernel. Figure 18(a) displays the relative vector integration error changing with the projection height, where the unit vector $\hat{R}$ is multiplied inside the kernel. Figure 18(b) displays the same result as in Fig. 18(a) with a scalar function together with a vector cross product multiplied inside the kernel. Figure 19(a) displays the relative vector integration error versus N for the projection point 2 in Fig. 9(b). Figure 19(b) displays the vector integration error changing with the projection height, where a scalar function and the unit vector $\hat{R}$ are multiplied inside the kernels for the projection point 2 in Fig. 9(b).

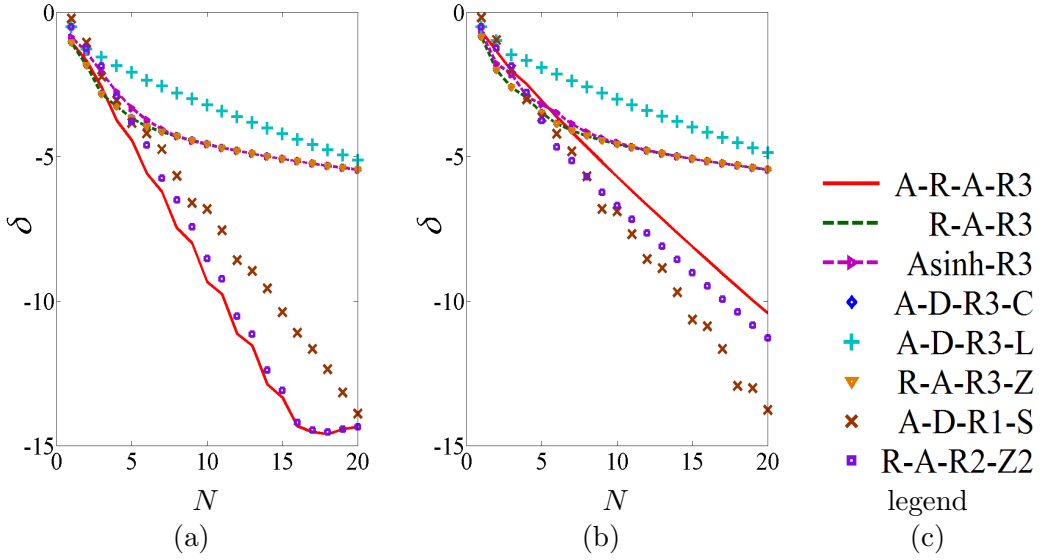

Figure 17: Comparison for $\boldsymbol{R}/R^3$-type kernel ($n = 3$) in Fig. 9(a). Logarithmic relative vector integration error δ versus sampling order N, with $|z| = 10^{-2}$. (a) $g = 1.0$ and $\boldsymbol{f} = \boldsymbol{R}(\lambda_1, \lambda_2)$, (b) $g = \lambda_1^2 + \lambda_2$ and $\boldsymbol{f} = (\lambda_1 \boldsymbol{t}_1 + \lambda_2 \boldsymbol{t}_2 + \lambda_3 \boldsymbol{t}_3) \times \boldsymbol{R}(\lambda_1, \lambda_2)$, (c) The legend for Figs. (a) and (b).

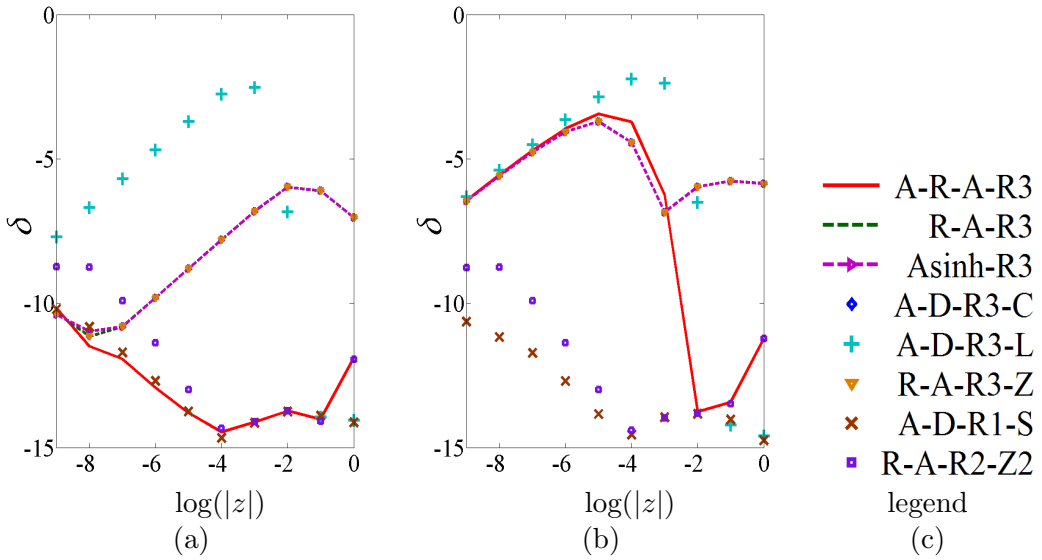

Figure 18: Comparison for $\boldsymbol{R}/R^3$-type kernel ($n = 3$) in Fig. 9(a). Logarithmic relative vector integration error δ versus $\log(|z|)$, with sampling order $N = 30$. (a) $g = 1.0$ and $\boldsymbol{f} = \boldsymbol{R}(\lambda_1, \lambda_2)$, (b) $g = \lambda_1^2 + \lambda_2$ and $\boldsymbol{f} = (\lambda_1 \boldsymbol{t}_1 + \lambda_2 \boldsymbol{t}_2 + \lambda_3 \boldsymbol{t}_3) \times \boldsymbol{R}(\lambda_1, \lambda_2)$, (c) The legend for Figs. (a) and (b).

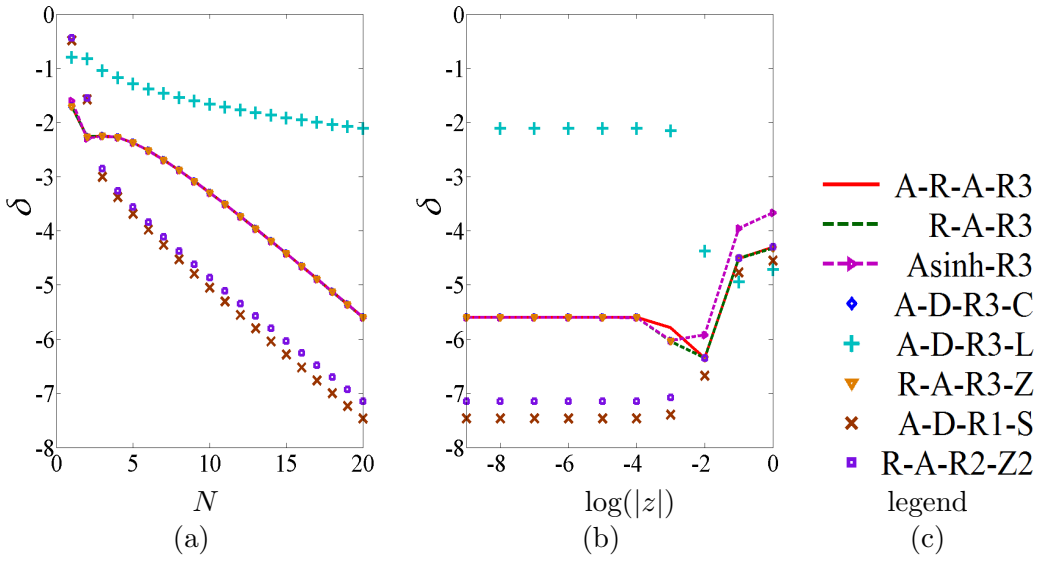

Figure 19: Comparison for $\boldsymbol{R}/R^3$-type kernel ($n = 3$), $g = \lambda_1^2 + \lambda_2$, $\boldsymbol{f} = \boldsymbol{R}(\lambda_1, \lambda_2)$. (a) Logarithmic relative vector integration error δ versus sampling order N, with $|z| = 10^{-6}$ for the projection point 2 in Fig. 9(b), (b) Logarithmic relative vector integration error δ versus $\log(|z|)$, with sampling order $N = 20$ for the projection point 2 in Fig. 9(b), (c) The legend for Figs. (a) and (b).

4.8.5 Accuracy Analysis Dependent on the Exclusion Disk Radius

This analysis of the integration accuracy is important for the radial-angular-R^n transformation schemes with $n > 1$ with changing radius threshold r_δ of the required exclusion disk for the case of inside projection point. When the corresponding singular kernels are treated by radial angular transformations, surface integrals over strong or hyper-singular kernels ($n = 2$ and $n = 3$) do in general not exist (the integration results are infinite) and this results in infinite integration domains. However, the relevant MoM integrals still exist, even though there may be a $1/R^2$ term in these integrals. In particular, the D-type integral in (4.2.2) exists, since it is a vector type integral with a cross product inside, it causes an additional cancellation effect. Thus, all integrals of interest exist and they can be computed by $1/R^2$ and $1/R^3$ cancellation transformations. An exclusion disk with a very small radius r_δ is utilized to avoid the infinite integration domains, it is proven that the integration results converge by reducing r_δ.

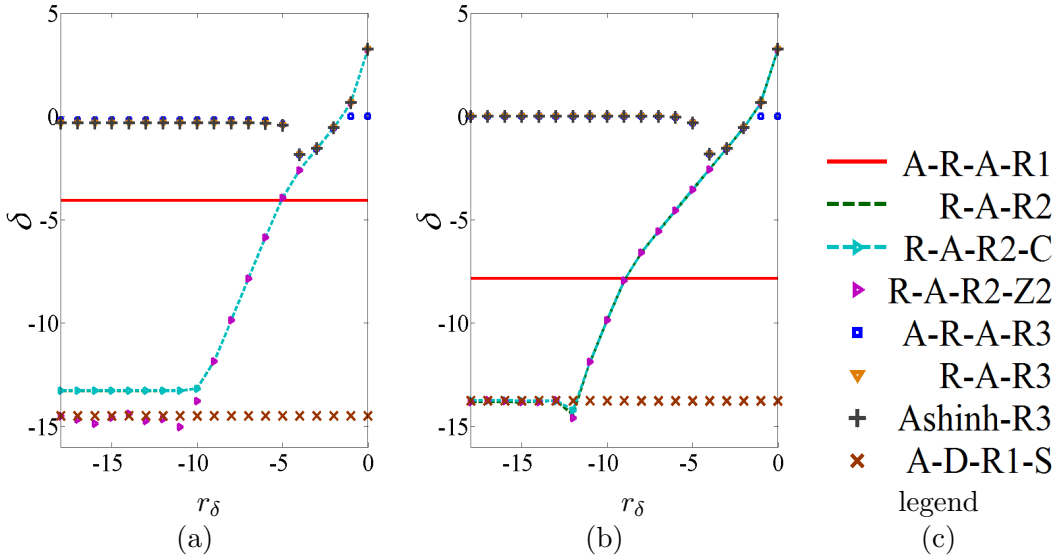

Figure 20: Comparison of the integration accuracy for projection point 1 in Fig. 9(a) versus the exclusion disk radius threshold r_δ, with $1/R$-type kernel ($n = 1$), sampling order $N = 40$, $g = \lambda_1^2 + \lambda_2$. (a) Logarithmic relative scalar integration error δ versus logarithmic r_δ with $|z| = 10^{-5}$, (b) Logarithmic relative scalar integration error δ versus logarithmic r_δ with $|z| = 10^{-9}$, (c) The legend for Figs. (a) and (b).

Figs. 20 and 21 exhibit the logarithmic integration accuracy changing with the disk radius threshold. The projection point is the point 1 in Fig. 9(a), the sampling order is $N = 40$ and a scalar function is multiplied inside the kernel. Figure 20 exhibits the relative scalar accuracy with decreasing r_δ for the $1/R$-type kernel ($n = 1$). In Fig. 20(a), the projection height is set as $|z| = 10^{-5}$. In Fig. 20(b), the projection height is set as $|z| = 10^{-9}$. Figure 21 exhibits the relative vector accuracy with decreasing r_δ for the $\boldsymbol{R}/R^3$-type kernel ($n = 2$), where a vector cross product is multiplied inside the kernel. In Fig. 21(a), the projection height is set as $|z| = 10^{-5}$. In Fig. 21(b), the projection height is set as $|z| = 10^{-7}$.

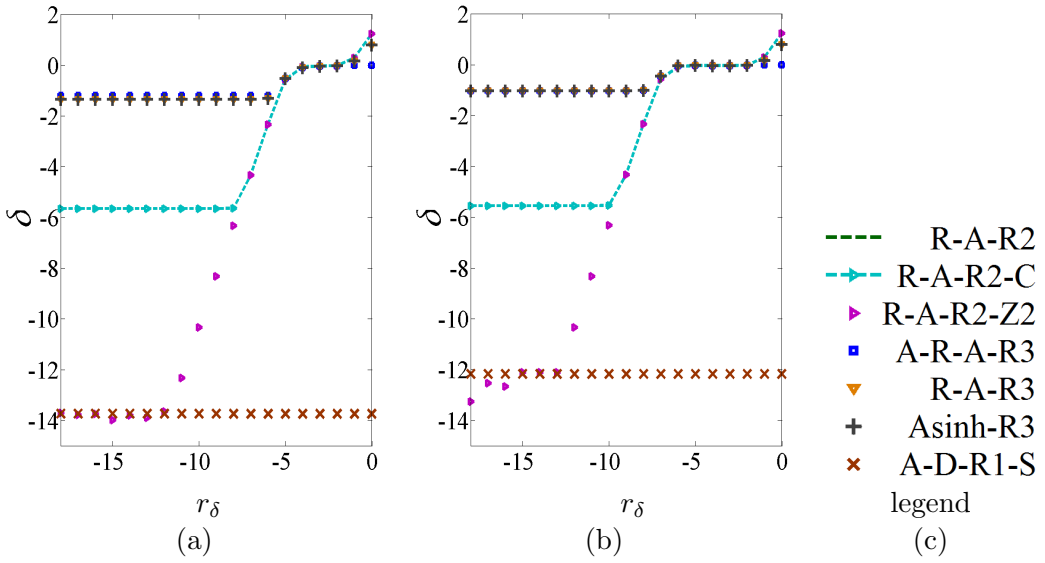

Figure 21: Comparison of the integration accuracy for projection point 1 in Fig. 9(a) versus the exclusion disk radius threshold r_δ, with $\boldsymbol{R}/R^3$-type kernel ($n = 2$), $\boldsymbol{f} = (\lambda_1 \boldsymbol{t}_1 + \lambda_2 \boldsymbol{t}_2 + \lambda_3 \boldsymbol{t}_3) \times \boldsymbol{R}(\lambda_1, \lambda_2)$, sampling order $N = 40$, $g = \lambda_1^2 + \lambda_2$. (a) Logarithmic relative vector integration error δ versus logarithmic r_δ with $|z| = 10^{-5}$, (b) Logarithmic relative vector integration error δ versus logarithmic r_δ with $|z| = 10^{-7}$, (c) The legend for Figs. (a) and (b).

From Figs. 20 and 21, it is shown that, when r_δ is sufficiently smaller than the projection height, the new family of radial-angular-R^n ($n > 1$) transformation schemes converges. For some of the exhibited transformations, the number of integration points was not large enough to approach machine accuracy.

4.8.6 Accuracy for Deformed Triangles

In MoM, it is recommended to study the performance of different transformation schemes for deformed triangles. In near couplings, deformed triangles require more sampling points to obtain good accuracy. The deformed triangle displayed in Fig. 22 is utilized for studying the efficiency of the transformation schemes. One edge of the triangle is set as ten percent of another edge. The accuracy of the transformation schemes proposed in this work are exhibited for the projection points 1, 2 and 3 as seen in Fig. 22.

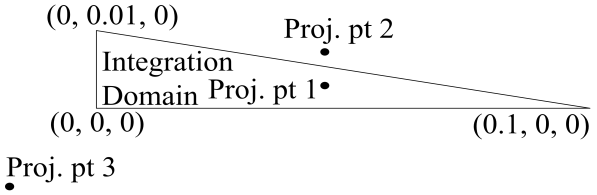

Figure 22: A deformed triangle with different projection points. Projection point 1: (0.05, 0.003, 0), Projection point 2: (0.05, 0.006, 0), Projection point 3: (-0.01, -0.01, 0)

Figs. 23 and 24 exhibit the accuracy performance of different transformation schemes for the $1/R$-type kernel ($n = 1$). For the radial-angular-R^n schemes, N_u is the sampling point number in u and N_v is the sampling number in v. For the other transformation schemes, the sampling point number is N in both u and v. With employing a real number η, the performance of radial-angular-R^n transformation schemes can be improved efficiently. The normalized integration domains in both (u, v) are utilized for the definition of η as shown in Fig. 10, where η is determined by the integration area in the normalized integration domain, given by

$$\eta = \int_0^1 \int_{v_l(u)}^{v_u(u)} dvdu\,. \tag{4.8.6.1}$$

It is noticed that the integration limits of u are from 0 to 1 and the integration limits of v are from $v_l(u)$ to $v_u(u)$, where $0 \le v_l(u) \le v_u(u) \le 1$, as shown in (4.8.6.1) and Fig. 10. To obtain better performance with a given number of sampling points in the source domain, u domain integration requires more sampling points and v domain integration requires fewer sampling points. Thus, the real number η between 0 and 1 is utilized to construct N_u and N_v for the radial-angular schemes, and they are written as

$$N_u = (1/\eta)N, \tag{4.8.6.2}$$

$$N_v = \eta N. \tag{4.8.6.3}$$

In numerical solutions, the nearest integer value is utilized. With increasing N, one obtains

$$\sqrt{N_u N_v} \approx N. \tag{4.8.6.4}$$

Fig. 23 is dependent on the projection point 1 in Fig. 22. A scalar function is multiplied inside the kernel. Figure 23(a) exhibits the relative accuracy dependent on $\sqrt{N_u N_v}$, where

$\eta = 0.4$ and $|z| = 10^{-2}$ have been selected. Figure 23(b) exhibits the relative integration error with changing height, where the sampling order $N = 40$, $\eta = 0.4$ and $\sqrt{N_u N_v} \approx 40$. Fig. 24 shows the accuracy of the transformation schemes for the $1/R$-type kernels dependent on the height. Figure 24(a) provides the performance for projection point 2 in Fig. 22 and Fig. 24(b) gives the performance for projection point 3 in Fig. 22.

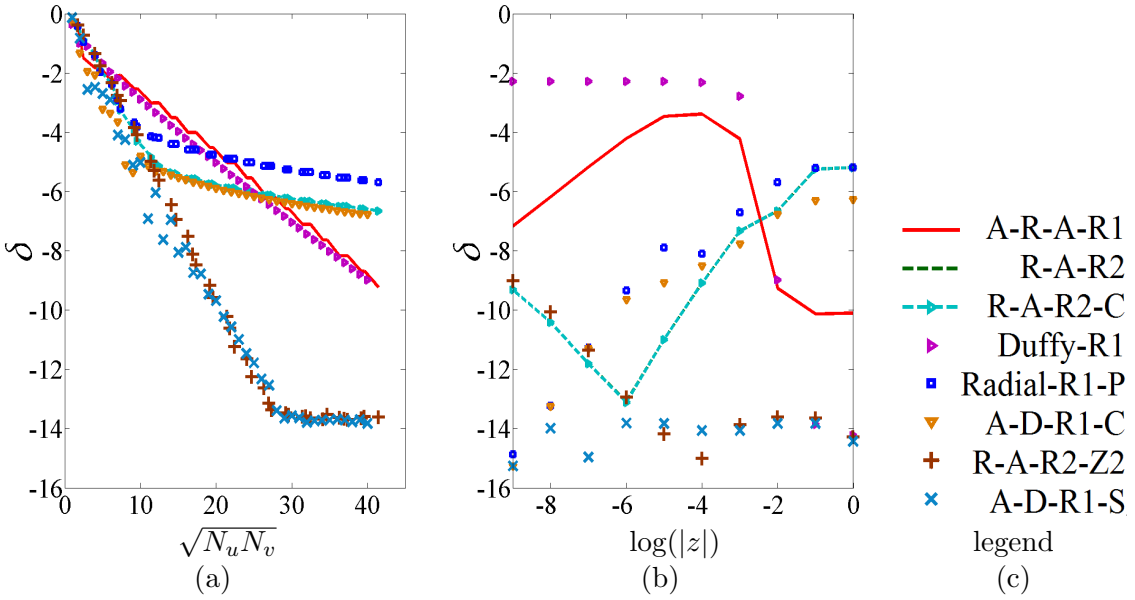

Figure 23: Comparison for $1/R$-type kernel ($n = 1$) of logarithmic relative integration error δ for Fig. 22 projection point 1, $g = \lambda_1^2 + \lambda_2$, $\eta = 0.4$. (a) Logarithmic relative integration error δ versus sampling order $\sqrt{N_u N_v}$, with $|z| = 10^{-2}$, (b) Logarithmic relative integration error δ versus $\log(|z|)$, with sampling order $\sqrt{N_u N_v} \approx N = 40$, (c) The legend for Figs. (a) and (b).

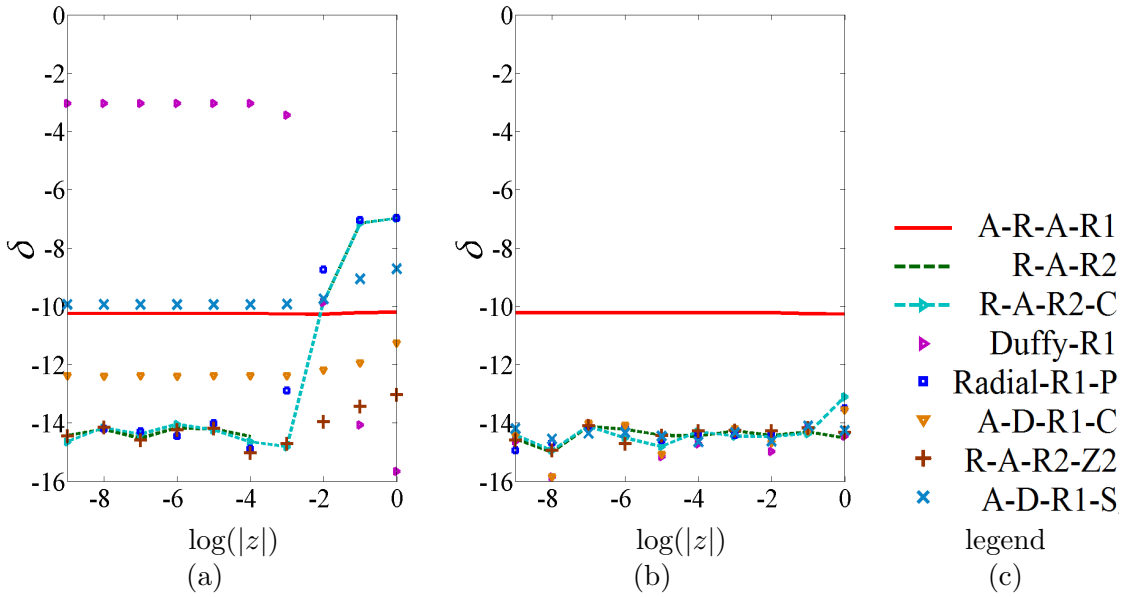

Figure 24: Comparison for $1/R$-type kernel ($n = 1$) of logarithmic relative integration error δ versus $\log(|z|)$, with square root of sampling order product $\sqrt{N_u N_v} \approx N = 40$, $\eta = 0.4$, $g = \lambda_1^2 + \lambda_2$. (a) Fig. 22, projection point 2, (b) Fig. 22, projection point 3, (c) The legend for Figs. (a) and (b).

Figs. 25 and 26 show the accuracy performance of the 2nd order transformation schemes for the $\boldsymbol{R}/R^3$-type kernel ($n = 2$). Fig. 25 is related to projection point 1 in Fig. 22, a scalar function and a vector cross product are multiplied inside the kernel. Figure 25(a) shows the relative vector accuracy dependent on $\sqrt{N_u N_v}$, where $\eta = 0.7$ and the height was set as $|z| = 10^{-4}$. Figure 25(b) shows the relative vector integration error with changing height, where $\eta = 0.7$ and the sampling orders are $\sqrt{N_u N_v} \approx N = 40$. Fig. 26 shows the accuracy of the 2nd order schemes for $\boldsymbol{R}/R^3$-type kernels according to changing height. Figure 26(a) is the performance for projection point 2 in Fig. 22 and Fig. 26(b) is the performance for projection point 3 in Fig. 22.

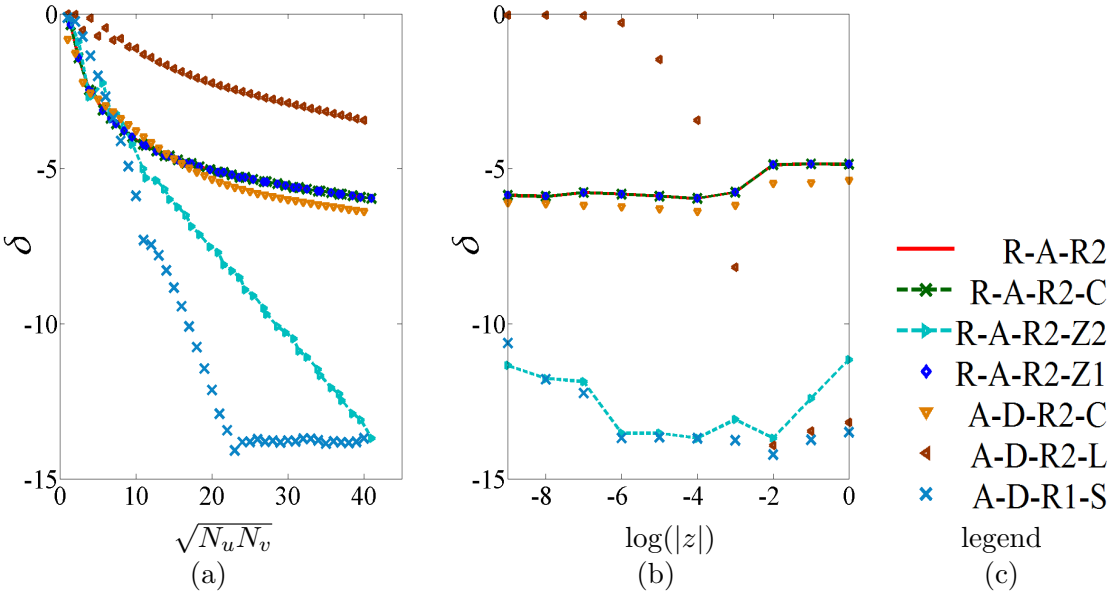

Figure 25: Comparison for $\boldsymbol{R}/R^3$-type kernel ($n = 2$) of logarithmic relative vector integration error δ for Fig. 22 projection point 1, with $\eta = 0.7$, $g = \lambda_1^2 + \lambda_2$, $\boldsymbol{f} = (\lambda_1 \boldsymbol{t}_1 + \lambda_2 \boldsymbol{t}_2 + \lambda_3 \boldsymbol{t}_3) \times \hat{R}(\lambda_1, \lambda_2)$. (a) Logarithmic relative vector integration error δ versus square root of sampling order product $\sqrt{N_u N_v}$, with $|z| = 10^{-4}$, (b) Logarithmic relative vector integration error δ versus $\log(|z|)$, with sampling order $\sqrt{N_u N_v} \approx N = 40$, (c) The legend for Figs. (a) and (b).

Figs. 27 and 28 exhibit the accuracy performance of the 3rd order transformation schemes for $\boldsymbol{R}/R^3$-type kernel ($n = 3$). Fig. 27 is related to projection point 1 in Fig. 22, a scalar function and a vector cross product are multiplied inside the kernels. Figure 27(a) exhibits the relative vector accuracy dependent on $\sqrt{N_u N_v}$, where $\eta = 0.6$ and the height is set as $|z| = 10^{-2}$. Figure 27(b) exhibits the relative vector integration error with changing height, where the sampling orders are $\sqrt{N_u N_v} \approx N = 40$ and $\eta = 0.6$. Fig. 28 shows the accuracy of the 3rd order schemes for the $\boldsymbol{R}/R^3$-type kernels according to changing height. Figure 28(a) is the performance for projection point 2 in Fig. 22. Figure. 28(b) is the performance for projection point 3 in Fig. 22.

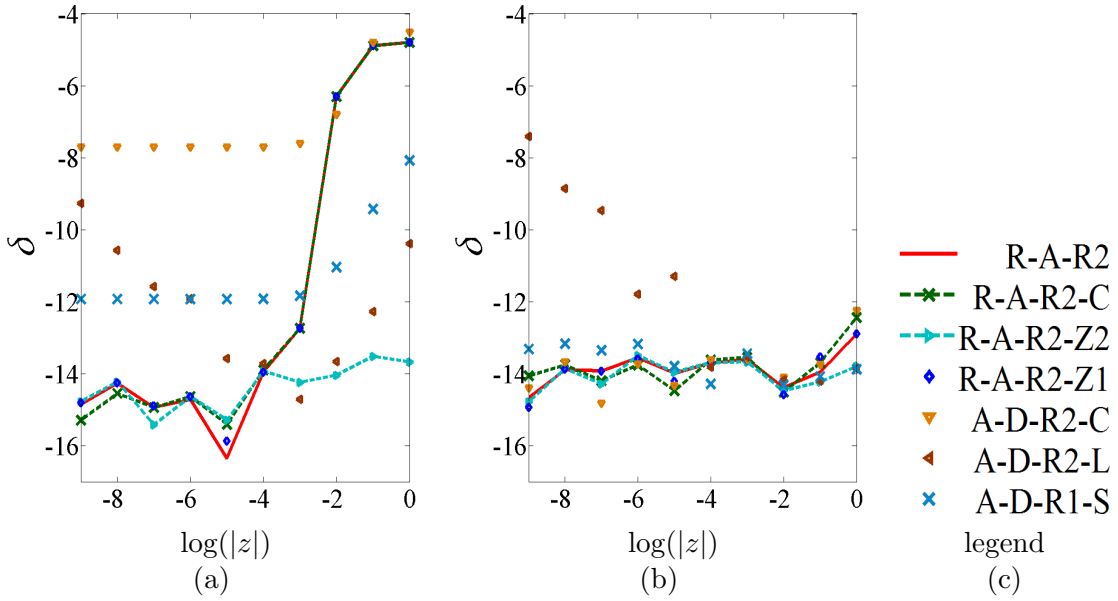

Figure 26: Comparison for $\boldsymbol{R}/R^3$-type kernel ($n = 2$) of logarithmic relative vector integration error δ versus $\log(|z|)$, with sampling order $\sqrt{N_u N_v} \approx N = 40$, $\eta = 0.3$, $g = \lambda_1^2 + \lambda_2$, $\boldsymbol{f} = (\lambda_1 \boldsymbol{t}_1 + \lambda_2 \boldsymbol{t}_2 + \lambda_3 \boldsymbol{t}_3) \times \hat{R}(\lambda_1, \lambda_2)$. (a) Fig. 22, projection point 2, (b) Fig. 22, projection point 3, (c) The legend for Figs. (a) and (b).

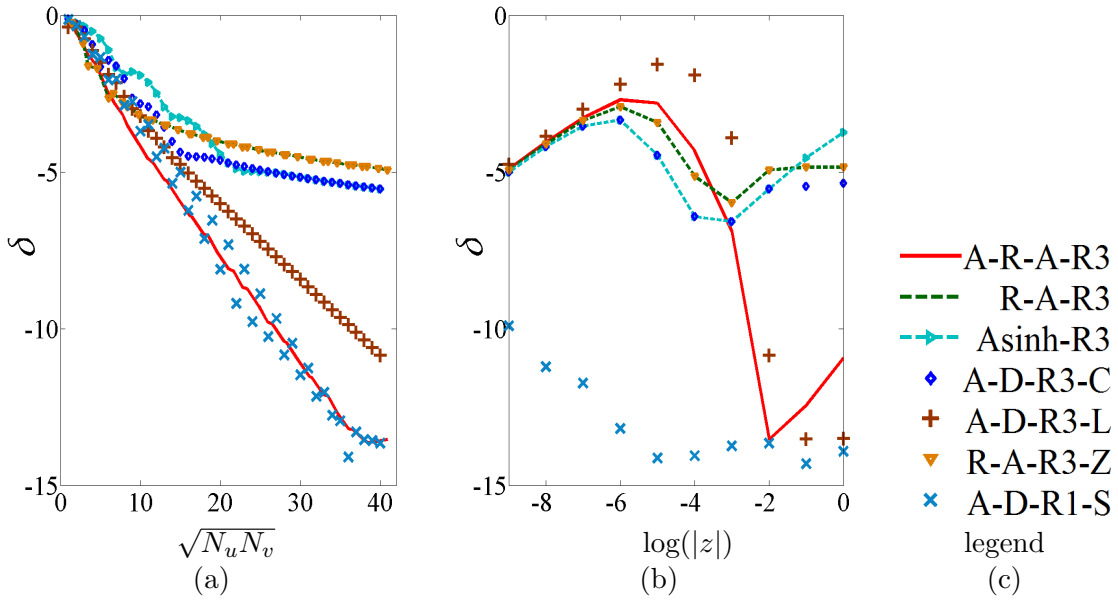

Figure 27: Comparison for $\boldsymbol{R}/R^3$-type kernel ($n = 3$) of logarithmic relative vector integration error δ for Fig. 22 projection point 1, with $\eta = 0.6$, $g = \lambda_1^2 + \lambda_2$, $\boldsymbol{f} = (\lambda_1 \boldsymbol{t}_1 + \lambda_2 \boldsymbol{t}_2 + \lambda_3 \boldsymbol{t}_3) \times \boldsymbol{R}(\lambda_1, \lambda_2)$. (a) Logarithmic relative vector integration error δ versus the square root of sampling order product $\sqrt{N_u N_v}$ and $|z| = 10^{-2}$, (b) Logarithmic relative vector integration error δ versus $\log(|z|)$, with sampling orders $\sqrt{N_u N_v} \approx N = 40$, (c) The legend for Figs. (a) and (b).

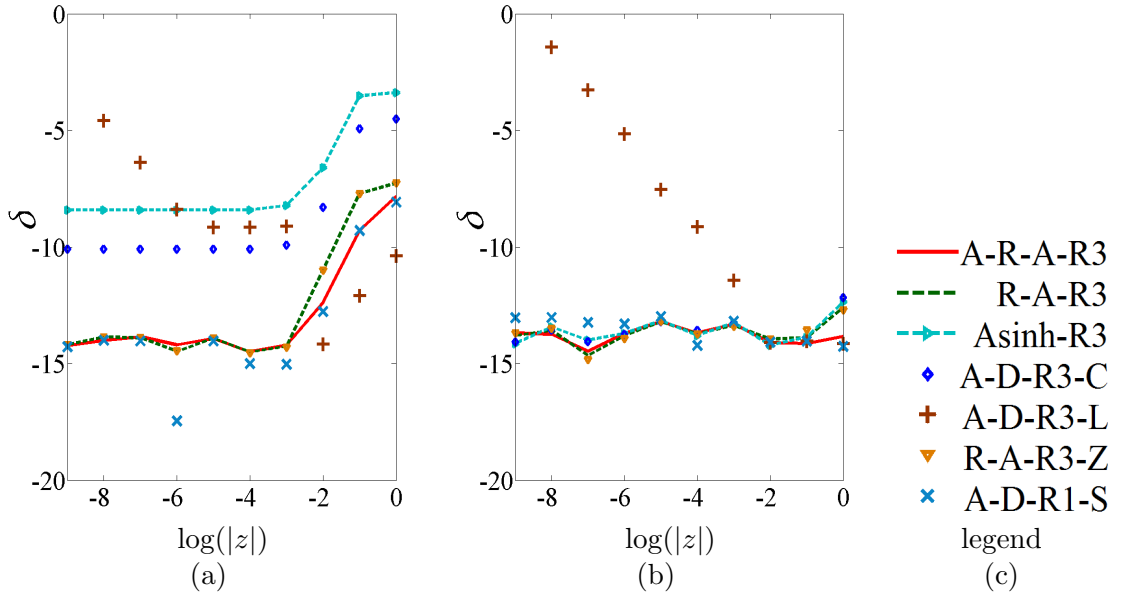

Figure 28: Comparison for $\boldsymbol{R}/R^3$-type kernel ($n = 3$) of logarithmic relative vector integration error δ versus $\log(|z|)$, with $\eta = 0.6$, sampling orders $\sqrt{N_u N_v} \approx N = 40$, $g = \lambda_1^2 + \lambda_2$, $\boldsymbol{f} = (\lambda_1 \boldsymbol{t}_1 + \lambda_2 \boldsymbol{t}_2 + \lambda_3 \boldsymbol{t}_3) \times \boldsymbol{R}(\lambda_1, \lambda_2)$. (a) Fig. 22, projection point 2, (b) Fig. 22, projection point 3, (c) The legend for Figs. (a) and (b).

4.8.7 Accuracy Analysis

The accuracy is stable for all the proposed transformation schemes in all orders ($n = 1, 2, 3$) for the outside projection points and regular source triangles, as seen in Figs. 9(b) and (c). When $n = 1$, the new A-R-A-R1 transformation scheme achieves a better accuracy for the $1/R$-type kernel with decreasing projection height for Fig. 9(a). The proposed R-A-R2 and R-A-R2-C transformation schemes achieve the same good accuracy in the case of a vector cross product multiplied inside the kernels for the $\boldsymbol{R}/R^3$-type kernel. The new A-R-A-R3, R-A-R3 and the Asinh-R3 transformation schemes obtain better accuracy performance with decreasing projection height compared with the traditional R^3 transformation schemes. However, it can be proven that with decreasing projection height, the 2nd order transformation schemes turn out to be more accurate, while on the other hand, with increasing height, the 3rd order transformation schemes are more accurate. Consequently, a strategy to obtain a good accuracy with changing height is that for the near couplings, the 2nd order ($n = 2$) transformation schemes can be utilized when the projection height is below a certain threshold, while, the 3rd order ($n = 3$) transformation schemes should be applied when the projection height is above the threshold.

For deformed source triangles and outside projection points, as shown in Fig. 22, the accuracy performance of almost all transformation schemes for R^1 kernels is stable for changing height. However, for the inside projection point, some schemes turn out to be unstable with decreasing height. In particular, the new cancellation schemes of

this work exhibit still good performance. All of the 2nd order transformation schemes are stable for the outside projection points for the $\boldsymbol{R}/R^3$-type kernels. However, for the inside projection point, the R-A-R2, R-A-R2-C, R-A-R2-Z2 and R-A-R2-Z1 obtain good performance with decreasing projection height, while, the A-D-R2-L transformation turns out to be more accurate for increasing projection height. For $\boldsymbol{R}/R^3$-type kernels and also outside projection points, the A-R-A-R3, R-A-R3, Asinh-R3 and A-D-R3-C schemes are stable and accurate with decreasing height. For the inside projection point, the A-R-A-R3, R-A-R3 and Asinh-R3 transformation schemes can obtain a better accuracy with decreasing height compared with the other 3rd order transformation schemes. With increasing height, they also exhibit good performance. The proposed transformation schemes can be optimally selected for good accuracy performance dependent on the projection height and different situations of the projection points. In many cases, it was shown that the A-D-R1-L from [Botha, 2013] and the A-D-R1-S from [Botha, 2014] exhibit also very good performance.

4.9 Conclusion

Through the application of the variable separation method to the singularity cancellation technique, a general solution was provided for the singularity cancellation transformation equations. Dependent on the settings of the constant parameters and the selection of all the $f(u)$ function, a new family of radial-angular-R^n transformation schemes were proposed. For the 1st order transformation schemes, a new A-R-A-R1 transformation equation was proposed and a better convergence for the $1/R$-type kernel was achieved compared with the other 1st order transformation schemes. For the 2nd order transformation schemes, the new R-A-R2 and R-A-R2-C transformation schemes were proposed and the same good accuracy as the R-A-R2-Z2 for the $\boldsymbol{R}/R^3$-type kernel was achieved. For the 3rd order transformation schemes, the new A-R-A-R3, R-A-R3 and Asinh-R3 transformation schemes were proposed, the better performance was achieved for the $\boldsymbol{R}/R^3$-type kernel compared with the traditional 3rd order transformation schemes. Moreover, when applied to deformed triangles, the new proposed transformation schemes still keep good performance for the corresponding types of kernels. Depending on the different projection situations and the projection height, certain singularity cancellation techniques can be selected to achieve good performance.

5 Hierarchical Basis Functions in the Method of Moments for the Surface Integral Equations

The hierarchical basis functions are utilized to discretize the surface electric and magnetic currents. The hierarchical spaces combine the low order (LO) [Ismatullah and Eibert, 2009, Rao et al., 1982] and the higher order (HO) [Eibert, 2005] vector basis functions. The LO basis functions can accurately simulate the surface currents with relatively dense mesh with respect to the wavelength. For geometrical edges and corners, LO is efficient and accurate with dense meshes. The HO basis functions are adapted to coarse meshes and they are able to obtain efficient and accurate performance for smooth geometrical surfaces. Moreover, compared to LO, HO produces more unknowns for each single mesh element. However, with coarse mesh size, the number of the mesh elements is reduced. Then, fewer total unknowns are achieved by HO to obtain the same accuracy as LO for surface integral equations (SIE) [Chiang and Chew, 2006a,b, Eibert, 2007, Ewe et al., 2004, Liu and Chew, 1990, Menshov and Okhmatovski, 2014, Nie et al., 2005, Ramahi and Mittra, 1991, Tong and Chew, 2012, Usner et al., 2006, Ylä-Oijala et al., 2005]. The LO basis functions are constructed by the 1st-order div conforming space, where the *Rao-Wilton-Glisson* (*RWG*) [Rao et al., 1982] basis functions are utilized. The HO basis functions are constructed by the 1st-order rotational space, the 2nd-order div conforming space, the 2nd-order rotational space and also the 3rd-order div conforming space in this work. The hierarchical basis functions are implemented for MoM [Harrington, 1993, Klopf et al., 2012], where the self-coupling and mutual couplings are computed with adaptive singularity cancellation techniques [Ismatullah and Eibert, 2008].

5.1 Introduction

The method of moments (MoM) takes advantage of the Galerkin process to obtain system matrices. Based on the Huygens' principle, the outside scatterings can be calculated from the surface currents. So an accurate computation of the surface currents is important to obtain accurate fields in the outside space [Martini et al., 2008]. To obtain the surface electric and magnetic currents, the boundary surfaces of arbitrarily shaped objects are descritized into meshes. The surface currents are expanded into the product of the basis functions and the unknown coefficients, where the unknown coefficients can be computed through iterative solvers and the basis functions are constructed by the geometrical information of the meshes.

The hierarchical vector basis functions [Sun et al., 2001] are utilized in this work. LO contains the *RWG* basis functions and it is widely applied to the simulation of electromagnetic fields and surface currents. However, LO requires the mesh element size below $\lambda/8$ to obtain accurate results, where λ is wavelength of the electromagnetic waves in the corresponding material. This results in a large number of unknowns. With denser mesh and increased number of unknowns, more RAM and computational time are required to obtain accurate results. However, the accuracy of LO simulations improves slowly with the increasing number of unknowns.

The HO basis functions are introduced to reduce the total number of unknowns and the desired good accuracy is also obtained. With HO together with LO, the average mesh size of the object can be extended up to $\lambda/2$. As a result, fewer mesh elements are required and the total number of unknowns is tremendously reduced, even though each single mesh cell produces more coefficients. Through the combination of LO and HO, the hierarchical basis functions are fully implemented for MoM. The performance of hierarchical basis functions is discussed in detail for the surface currents and the outside scatterings in this chapter.

5.2 Definitions of the Hierarchical Vector Basis Functions

The hierarchical vector basis functions are defined based on the geometrical information of the mesh elements. The construction of the hierarchical basis functions is node indexed and the node orders represent the directions of the vector basis functions. To obtain accurate simulation results, the fields and currents can be expanded with the hierarchical basis functions, in both the div conforming and also the rotational spaces.

The div conforming and the rotational spaces are 2-D hierarchical basis functions for MoM, as both spaces are defined on the surface mesh. The first order div conforming space and the first order rotational space are edge-related, where the edge-related basis functions are defined with two nodes. The second order div conforming space is face-associated, where the face-associated basis functions are defined with three nodes. The second order rotational space contains both edge-related and face-associated basis functions. The third order div conforming space is face-associated.

A good condition of the system matrix is required to obtain a faster convergence of the iterative solvers. The nearly orthogonal hierarchical basis functions [Sun et al., 2001] defined on the triangular mesh can improve the condition of the system matrix. The nearly orthogonal hierarchical basis functions $\boldsymbol{\alpha}_n$ are initialized for the field simulations [Chew et al., 2001, Jin, 2002, Sun et al., 2001], then the nearly orthogonal basis functions $\boldsymbol{f}_n$ [Chew et al., 2001, Eibert and Hansen, 1995b, Ismatullah and Eibert, 2009, Rao et al., 1982] for MoM are defined based on the tangential counterpart of $\boldsymbol{\alpha}_n$ and written as

$$\boldsymbol{f}_n = \hat{n} \times \boldsymbol{\alpha}_n \,, \tag{5.2.1}$$

where $\hat{n}$ is the surface unit normal vector pointing outward the boundary surfaces. The nearly orthogonal hierarchical basis functions are constructed by all of the sub-spaces.

The definitions of hierarchical basis functions are shown in Table 1, the general format of the basis functions can be presented as [Ismatullah and Eibert, 2009]

$$\boldsymbol{f}_n = \frac{u(\lambda_1, \lambda_2)\boldsymbol{t}_{12} + v(\lambda_1, \lambda_2)\boldsymbol{t}_{23} + w(\lambda_1, \lambda_2)\boldsymbol{t}_{13}}{2A} \,, \tag{5.2.2}$$

where λ_1, λ_2 and λ_3 are the simplex coordinates and $\lambda_1 + \lambda_2 + \lambda_3 = 1$. u, v and w are polynomials of λ_1 and λ_2. The orders of the simplex coordinates in u, v and w determine the orders of the hierarchical basis functions. A is the area of the element. The vector $\boldsymbol{t}_{ij}\,(i, j = 1, 2, 3;\, i < j)$ is the constant edge vector of the element. The divergence and the curl properties of the basis functions are also computed, they are constructed by the simplex

coordinates and the gradients of the simplex coordinates. The detailed definitions of the constant edge vectors, the gradients of the simplex coordinates and their corresponding relationships are shown in Fig. 29. The definitions of the edge vectors in Fig. 29 are based on the local node orders. However, when the basis functions, their divergence and curl properties are implemented into mutual couplings, the edge-related basis functions have to follow the global node orders of the edges, the face-associated basis functions also have to follow the global node orders of the face. The face unit vector in Fig. 29 is the local unit vector based on the local node orders. In MoM, the surface unit vector points outside the envelope. When the local unit vector is in the same direction as the global surface unit vector, it can be directly applied. Otherwise, the direction of the local unit vector has to be inverted for the mutual couplings in MoM.

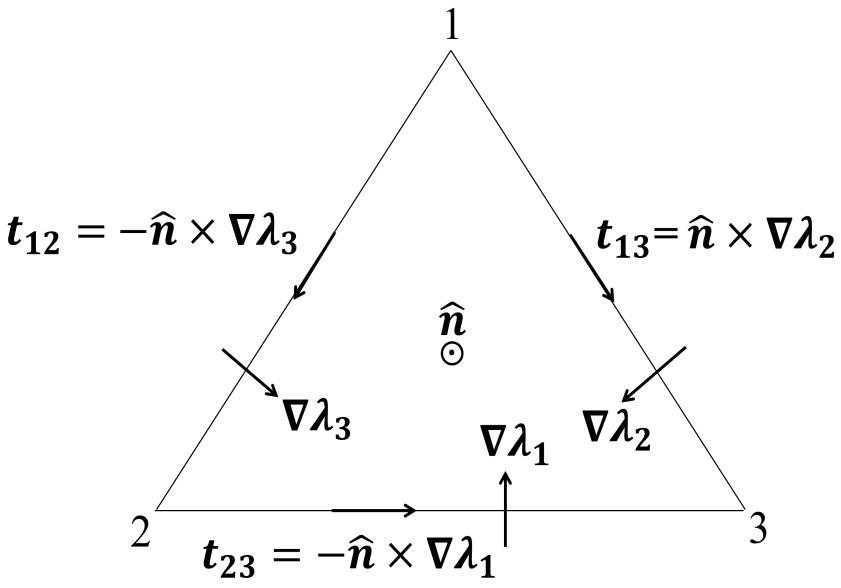

Figure 29: Triangular element construction of the local simplex coordinates for the definition of the vectorial representation of the basis functions.

The distributions of the first order div conforming space, the first order rotational space and the second order div conforming space can be referred to [Ismatullah and Eibert, 2009]. The distributions of the second order rotational space and the third order div conforming space inside the mesh elements are shown in Fig. 30 and Fig. 31 correspondingly. Figure 30(a) shows the edge-related basis functions in the second order rotational space with respect to the edge 23. It is clear that at the common edge of the adjacent elements, the orthogonal components of the basis functions are continuous, while the tangential components are not. Figure 30(b) shows the face-associated basis function in the second order rotational space. It shows that the orthogonal component of the basis functions disappear, only the tangential components are distributed along the edges of the element. All of the basis functions in the third order div conforming space are face-associated and they are shown in Fig. 31. Figure. 31(a) shows the distribution of $\boldsymbol{f}_{12}$, Fig.31(b) shows

Table 1: Hierarchical Basis Functions and Properties Within the Triangle

MoM Vector Basis Functions $\boldsymbol{f}_n$				$\nabla \cdot \boldsymbol{f}_n$	$\nabla \times \boldsymbol{f}_n = -[\nabla \cdot (\hat{n} \times \boldsymbol{f}_n)]\hat{n}$
G^1	$\boldsymbol{f}_0$	$\hat{n}\times(\lambda_1\nabla\lambda_2 - \lambda_2\nabla\lambda_1)$	$\frac{\lambda_1 \boldsymbol{t}_{13} + \lambda_2 \boldsymbol{t}_{23}}{2A}$	$-\frac{1}{A}$	$\mathbf{0}$
	$\boldsymbol{f}_1$	$\hat{n}\times(\lambda_1\nabla\lambda_3 - \lambda_3\nabla\lambda_1)$	$\frac{-\lambda_1 \boldsymbol{t}_{12} + \lambda_3 \boldsymbol{t}_{23}}{2A}$	$\frac{1}{A}$	$\mathbf{0}$
	$\boldsymbol{f}_2$	$\hat{n}\times(\lambda_2\nabla\lambda_3 - \lambda_3\nabla\lambda_2)$	$\frac{-\lambda_2 \boldsymbol{t}_{12} - \lambda_3 \boldsymbol{t}_{13}}{2A}$	$-\frac{1}{A}$	$\mathbf{0}$
R^1	$\boldsymbol{f}_3$	$\hat{n}\times(\lambda_1\nabla\lambda_2 + \lambda_2\nabla\lambda_1)$	$\frac{\lambda_1 \boldsymbol{t}_{13} - \lambda_2 \boldsymbol{t}_{23}}{2A}$	0	$2(\nabla\lambda_1 \cdot \nabla\lambda_2)\hat{n}$
	$\boldsymbol{f}_4$	$\hat{n}\times(\lambda_1\nabla\lambda_3 + \lambda_3\nabla\lambda_1)$	$\frac{-\lambda_1 \boldsymbol{t}_{12} - \lambda_3 \boldsymbol{t}_{23}}{2A}$	0	$2(\nabla\lambda_1 \cdot \nabla\lambda_3)\hat{n}$
	$\boldsymbol{f}_5$	$\hat{n}\times(\lambda_2\nabla\lambda_3 + \lambda_3\nabla\lambda_2)$	$\frac{-\lambda_2 \boldsymbol{t}_{12} + \lambda_3 \boldsymbol{t}_{13}}{2A}$	0	$2(\nabla\lambda_2 \cdot \nabla\lambda_3)\hat{n}$
G^2	$\boldsymbol{f}_6$	$\hat{n} \times (\lambda_1\lambda_2\nabla\lambda_3 + \lambda_2\lambda_3\nabla\lambda_1 - 2\lambda_1\lambda_3\nabla\lambda_2)$	$\frac{-\lambda_1\lambda_2 \boldsymbol{t}_{12} - \lambda_2\lambda_3 \boldsymbol{t}_{23} - 2\lambda_1\lambda_3 \boldsymbol{t}_{13}}{2A}$	$\frac{3(-\lambda_1 + \lambda_3)}{2A}$	$(-\lambda_1\nabla\lambda_2 \cdot \nabla\lambda_3 + 2\lambda_2\nabla\lambda_1 \cdot \nabla\lambda_3 - \lambda_3\nabla\lambda_1 \cdot \nabla\lambda_2)\hat{n}$
	$\boldsymbol{f}_7$	$\hat{n} \times (\lambda_1\lambda_2\nabla\lambda_3 - \lambda_2\lambda_3\nabla\lambda_1)$	$\frac{-\lambda_1\lambda_2 \boldsymbol{t}_{12} + \lambda_2\lambda_3 \boldsymbol{t}_{23}}{2A}$	$\frac{-\lambda_1 + 2\lambda_2 - \lambda_3}{2A}$	$(\lambda_1\nabla\lambda_2 \cdot \nabla\lambda_3 - \lambda_3\nabla\lambda_1 \cdot \nabla\lambda_2)\hat{n}$
R^2	$\boldsymbol{f}_8$	$\hat{n}\times[(2\lambda_2 - \lambda_1)\lambda_1\nabla\lambda_2 - (2\lambda_1 - \lambda_2)\lambda_2\nabla\lambda_1]$	$\frac{(2\lambda_2 - \lambda_1)\lambda_1 \boldsymbol{t}_{13} + (2\lambda_1 - \lambda_2)\lambda_2 \boldsymbol{t}_{23}}{2A}$	0	$2[\lambda_1\nabla\lambda_2 \cdot \nabla\lambda_2 - \lambda_2\nabla\lambda_1 \cdot \nabla\lambda_1 + 2(\lambda_2 - \lambda_1)\nabla\lambda_1 \cdot \nabla\lambda_2]\hat{n}$
	$\boldsymbol{f}_9$	$\hat{n}\times[(2\lambda_3 - \lambda_1)\lambda_1\nabla\lambda_3 - (2\lambda_1 - \lambda_3)\lambda_3\nabla\lambda_1]$	$\frac{-(2\lambda_3 - \lambda_1)\lambda_1 \boldsymbol{t}_{12} + (2\lambda_1 - \lambda_3)\lambda_3 \boldsymbol{t}_{23}}{2A}$	0	$2[\lambda_1\nabla\lambda_3 \cdot \nabla\lambda_3 - \lambda_3\nabla\lambda_1 \cdot \nabla\lambda_1 + 2(\lambda_3 - \lambda_1)\nabla\lambda_1 \cdot \nabla\lambda_3]\hat{n}$
	$\boldsymbol{f}_{10}$	$\hat{n}\times[(2\lambda_3 - \lambda_2)\lambda_2\nabla\lambda_3 - (2\lambda_2 - \lambda_3)\lambda_3\nabla\lambda_2]$	$\frac{-(2\lambda_3 - \lambda_2)\lambda_2 \boldsymbol{t}_{12} - (2\lambda_2 - \lambda_3)\lambda_3 \boldsymbol{t}_{13}}{2A}$	0	$2[\lambda_2\nabla\lambda_3 \cdot \nabla\lambda_3 - \lambda_3\nabla\lambda_2 \cdot \nabla\lambda_2 + 2(\lambda_3 - \lambda_2)\nabla\lambda_2 \cdot \nabla\lambda_3]\hat{n}$
	$\boldsymbol{f}_{11}$	$\hat{n} \times (\lambda_1\lambda_2\nabla\lambda_3 + \lambda_2\lambda_3\nabla\lambda_1 + \lambda_1\lambda_3\nabla\lambda_2)$	$\frac{-\lambda_1\lambda_2 \boldsymbol{t}_{12} - \lambda_2\lambda_3 \boldsymbol{t}_{23} + \lambda_1\lambda_3 \boldsymbol{t}_{13}}{2A}$	0	$2[\lambda_1\nabla\lambda_2 \cdot \nabla\lambda_3 + \lambda_2\nabla\lambda_1 \cdot \nabla\lambda_3 + \lambda_3\nabla\lambda_1 \cdot \nabla\lambda_2]\hat{n}$
G^3	$\boldsymbol{f}_{12}$	$\hat{n}\times[(\lambda_1 - \lambda_2)\lambda_1\lambda_2\nabla\lambda_3 - (\lambda_3 - \lambda_2)\lambda_2\lambda_3\nabla\lambda_1 + (\lambda_3 - \lambda_1)\lambda_1\lambda_3\nabla\lambda_2]$	$\frac{1}{2A}[-(\lambda_1 - \lambda_2)\lambda_1\lambda_2 \boldsymbol{t}_{12} + (\lambda_3 - \lambda_2)\lambda_2\lambda_3 \boldsymbol{t}_{23} + (\lambda_3 - \lambda_1)\lambda_1\lambda_3 \boldsymbol{t}_{13}]$	$\frac{1}{A}[-\lambda_1^2 - \lambda_2^2 - \lambda_3^2 + 2(\lambda_1\lambda_2 + \lambda_1\lambda_3 + \lambda_2\lambda_3)]$	$2[(\lambda_2 - \lambda_1)\lambda_3\nabla\lambda_1 \cdot \nabla\lambda_2 + (\lambda_1 - \lambda_3)\lambda_2\nabla\lambda_1 \cdot \nabla\lambda_3 + (\lambda_3 - \lambda_2)\lambda_1\nabla\lambda_2 \cdot \nabla\lambda_3]\hat{n}$
	$\boldsymbol{f}_{13}$	$\hat{n} \times [(393\lambda_3 + 80\lambda_1 - 212\lambda_2)\lambda_1\lambda_2\nabla\lambda_3 - (393\lambda_1 + 80\lambda_3 - 212\lambda_2)\lambda_2\lambda_3\nabla\lambda_1 + (-292\lambda_3 + 292\lambda_1)\lambda_1\lambda_3\nabla\lambda_2]$	$\frac{1}{2A}[-(393\lambda_3 + 80\lambda_1 - 212\lambda_2)\lambda_1\lambda_2 \boldsymbol{t}_{12} + (393\lambda_1 + 80\lambda_3 - 212\lambda_2)\lambda_2\lambda_3 \boldsymbol{t}_{23} + (-292\lambda_3 + 292\lambda_1)\lambda_1\lambda_3 \boldsymbol{t}_{13}]$	$\frac{1}{2A}[212(\lambda_1^2 - 2\lambda_2^2 + \lambda_3^2) + 977(\lambda_1\lambda_2 + 2\lambda_1\lambda_3 + \lambda_2\lambda_3)]$	$[(393\lambda_1\lambda_2\nabla\lambda_3 \cdot \nabla\lambda_3 - 393\lambda_2\lambda_3\nabla\lambda_1 \cdot \nabla\lambda_1 - 233\lambda_2(\lambda_3 - \lambda_1)\nabla\lambda_1 \cdot \nabla\lambda_3 + \lambda_1(372\lambda_1 - 424\lambda_2 - 191\lambda_3)\nabla\lambda_2 \cdot \nabla\lambda_3 + \lambda_3(-372\lambda_3 + 424\lambda_2 + 191\lambda_1)\nabla\lambda_1 \cdot \nabla\lambda_2]\hat{n}$
	$\boldsymbol{f}_{14}$	$\hat{n}\times[(-131\lambda_3 + 168\lambda_1 - 124\lambda_2)\lambda_1\lambda_2\nabla\lambda_3 + (-131\lambda_1 + 168\lambda_3 - 124\lambda_2)\lambda_2\lambda_3\nabla\lambda_1 + (-44\lambda_3 - 44\lambda_1 + 262\lambda_2)\lambda_1\lambda_3\nabla\lambda_2]$	$\frac{1}{2A}[(131\lambda_3 - 168\lambda_1 + 124\lambda_2)\lambda_1\lambda_2 \boldsymbol{t}_{12} - (-131\lambda_1 + 168\lambda_3 - 124\lambda_2)\lambda_2\lambda_3 \boldsymbol{t}_{23} + (-44\lambda_3 - 44\lambda_1 + 262\lambda_2)\lambda_1\lambda_3 \boldsymbol{t}_{13}]$	$\frac{1}{2A}[212(-\lambda_1^2 + \lambda_3^2) + 977(\lambda_1\lambda_2 - \lambda_2\lambda_3)]$	$[-131\lambda_1\lambda_2\nabla\lambda_3 \cdot \nabla\lambda_3 - 131\lambda_2\lambda_3\nabla\lambda_1 \cdot \nabla\lambda_1 + 262\lambda_1\lambda_3\nabla\lambda_2 \cdot \nabla\lambda_2 + \lambda_2(205\lambda_1 + 205\lambda_3 - 248\lambda_2)\nabla\lambda_1 \cdot \nabla\lambda_3 + \lambda_1(14\lambda_2 - 219\lambda_3 + 124\lambda_1)\nabla\lambda_2 \cdot \nabla\lambda_3 + \lambda_3(14\lambda_2 - 219\lambda_1 + 124\lambda_3)\nabla\lambda_1 \cdot \nabla\lambda_2]\hat{n}$

the distribution of $\boldsymbol{f}_{13}$ and Fig.31(c) shows the distribution of $\boldsymbol{f}_{14}$. It can be seen that the orthogonal components of the basis functions in the third order div conforming space vanish at the boundary edges of the elements, only the tangential components are distributed along the edges.

The unknown coefficients for the basis functions determine the total number of the unknowns for MoM. The products of the basis functions and the corresponding coefficients can determine the distribution of the surface currents inside the element. For each point in the element, the summary of all the hierarchical basis functions multiplied with the corresponding coefficients can determine the vector electric and magnetic currents. For the basis functions shown in Fig. 30(a), the coefficients are dependent on the corresponding edge. For the basis functions in Fig. 30(b) and in Figs. 31(a), (b) and (c), the coefficients are dependent on faces. With increasing frequencies, more accurate simulations can be obtained for electric and magnetic currents inside elements.

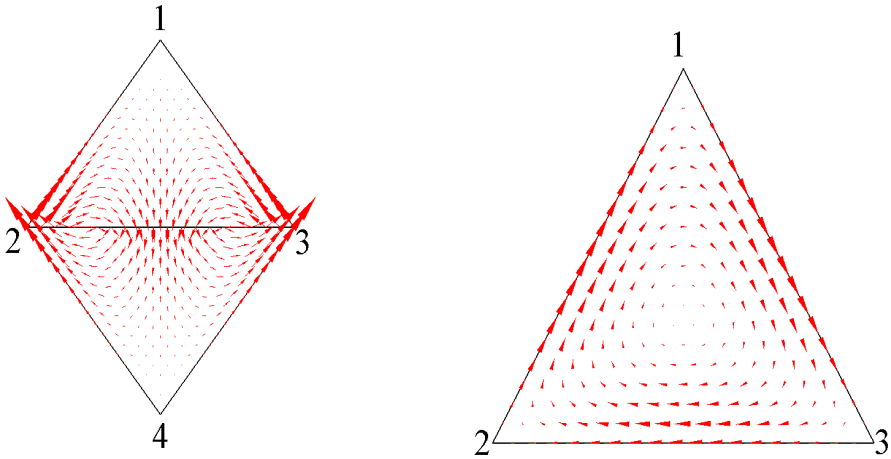

(a) (b)

Figure 30: Graphical representation of basis functions in the the 2^{nd} order rotational space: (a) 2^{nd} order, edge-related, rotational space, (b) 2^{nd} order, face-associated, rotational space. The basis function in (a) are related to the node order 12 of the two adjacent triangles. The basis function in (b) are face-associated with the node order 123. The 2^{nd} order of rotational space together with the 2^{nd} order of div conforming space construct the complete 2^{nd} order spaces.

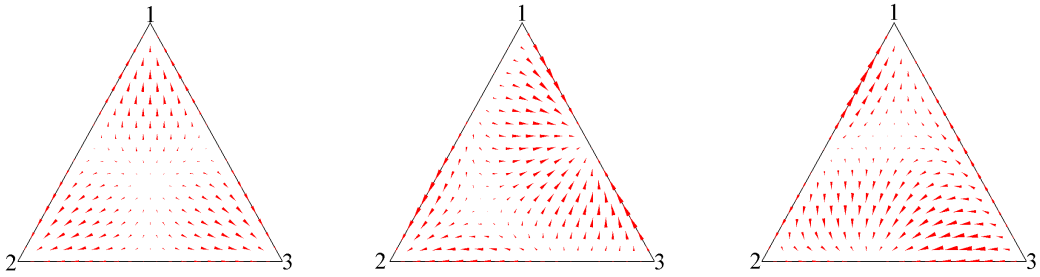

(a) (b) (c)

Figure 31: Graphical representations of basis functions in the the 3^{rd} order div conforming space: (a) $\boldsymbol{f}_{12}$ in the 3^{rd} order, face-associated, div conforming space, (b) $\boldsymbol{f}_{13}$ in the 3^{rd} order, face-associated, div conforming space, (c) $\boldsymbol{f}_{14}$ in the 3^{rd} order, face-associated, div conforming space. The basis functions are all face-associated with the node order 123.

5.3 Numerical Results of MoM for Perfect Electric Conductor (PEC) Objects

To testify the accuracy of different orders of hierarchical basis functions and mutual coupling matrices assembly in BI, several numerical simulation results are shown in this section. A convincing illustration is to utilize a PEC sphere as a testing case, where the scattering of an input plane wave is shown. The well known analytical RCS is the MIE scattering [Balanis, 1989], where the RCS is computed analytically. Good matching of RCS between the analytical solution and the numerical method verifies the efficacy of hierarchical basis functions for BI. For higher frequencies and finer meshes, more unknowns have to be solved. Moreover, BI applications are shown based on hierarchical basis functions for very large scale simulations through the RCS of PEC bomber and the PEC Flamme aircraft models. As 0th order of BI has been verified in many published articles [Eibert, 2007, Eibert and Hansen, 1997, Tzoulis and Eibert, 2005b], it can be utilized as a reference for BI with HO. The efficiency of BI is presented based on different orders of hierarchical basis functions. The 0th order is the first order div conforming space, 1st order adds the first order rotational space, 2nd order adds the second order div conforming space, 3rd order adds the second order rotational space, 4th order adds the 3rd order div conforming space. The sphere simulations were performed on a PC with Intel(R) Core(TM)2 Quad CPU Q9550 @ 2.83 GHz processor, installed memory (RAM) 16.0 GB and 64-bit operating system. The simulations of the B2 and the Flamme aircrafts were operated on a workstation with Intel(R) Xeon(R) CPU E5630 @ 2.53 GHz (2 processors), installed memory (RAM) 96.0 GB and 64-bit operating system. All simulations were computed on one core.

5.3.1 PEC Sphere

The PEC sphere is a good example to testify the efficiency and efficacy of numerical solutions to the surface integral equations based on the hierarchical vector basis functions. The symmetrical property of the sphere provides a privilege. The input plane waves are equivalent from any directions. So the input plane wave in the PEC spherical model propagates along the $+z$ axis, the polarization of the electric field is along the x axis, the amplitude of the electric field is 100 V/m. The efficiency of the hierarchical basis functions for MoM is represented by the performance of the results, including the run time, the required peak RAM for the PC, the surface current distributions and also the accuracy of the radiation power in space. The efficacy of MoM is represented by the accuracy of the simulation results. For studying the accuracy of the vector hierarchical basis functions, the MIE scattering [Balanis, 1989] of the PEC sphere is utilized. It is an analytical solution to the Bi-RCS of the spherical PEC object with plane input electromagnetic waves. For different frequencies, the root mean square (RMS) can show the accuracy of the final simulation results for the corresponding input waves.

The simulations of the PEC sphere are computed by a 64 bit workstation with processor X 5690 @ 3.47 GHz and RAM 192 GB. The same modeling mesh was used for all orders of hierarchical basis functions. The mesh size was set to 0.03 m, the mean edge length is 3.422 cm, with minimum edge length 2.304 cm and maximum edge length 5.406 cm. For

0th order, the total number of unknowns is 75 012. The run time was 19 685.5 s. For 1st order, the total number of unknowns is 150 024. The run time was 25 483.9 s. For 2nd order, the total number of unknowns is 250 040. The run time was 30 192.1 s. For 3rd order, the total number of unknowns is 375 060. The run time was 39 416.7 s. For 4th order, the total number of unknowns is 525 084. The run time was 47 955.7 s.

The numerical RCS results are compared with the MIE scattering of the PEC sphere. The mesh size of the PEC sphere is roughly from $\lambda/7$ to $\lambda/3$ in free space. The mean edge length is about $\lambda/5$. Compared with LO, the number of unknowns is much larger for HO. However, more accurate scattering results can be obtained by HO as shown in Fig. 33. The detailed accuracy analysis is studied for different orders of basis functions in the later chapters.

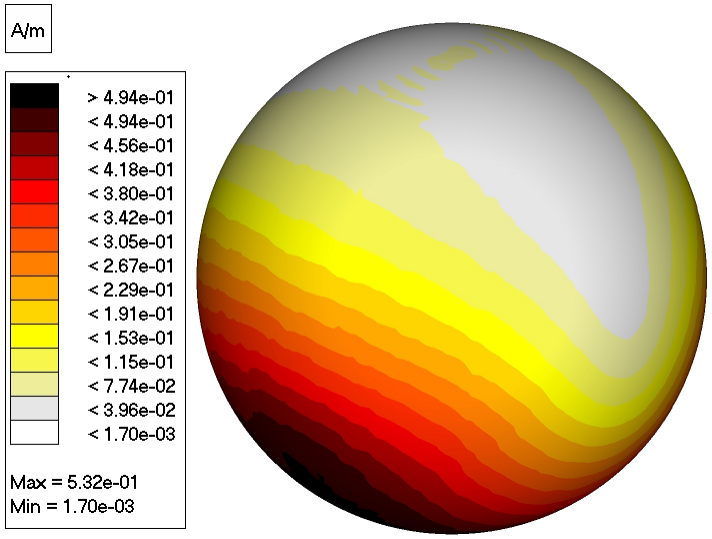

Figure 32: Surface electric current distribution of the PEC sphere @ 2 GHz.

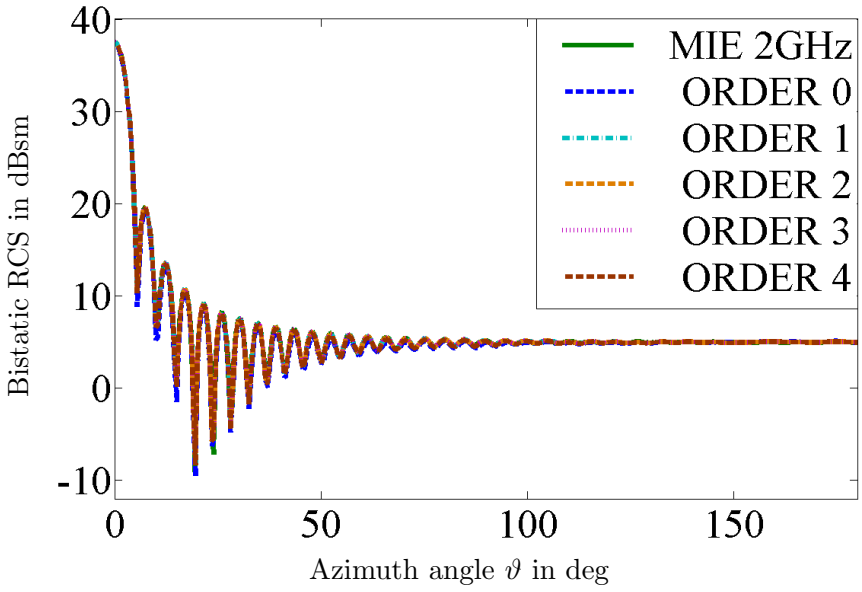

Figure 33: Bistatic RCS of PEC sphere @ 2 GHz on xz cut half plane ($\varphi = 0°$).

5.3.2 PEC Stealth Aircraft Model

The PEC stealth B2 aircraft model simulation is an application of MoM for a large scale computation. Simulations of the PEC stealth B2 are computed by a 64 bit workstation with processor X 5690 @ 3.47 GHz and RAM 192 GB. The PEC stealth B2 aircraft is located in the xz plane, with nose heading along the $+z$ axis, as shown in Fig. 34. The PEC stealth B2 aircraft is positioned in free space, where the permittivity is $\epsilon_r = 1.0$ and the permeability is $\mu_r = 1.0$. The simulation frequency is 1.5 GHz. The incident plane wave propagates towards $-z$ direction, with electric field $E_x = 100$ V/m. To visualize invisibility effects of the PEC stealth B2 Aircraft, the reflected power towards back to the incoming plane wave direction can be seen from the numerical results.

Figure 34 shows the real components of the equivalent surface electric current of the PEC stealth B2 aircraft. The RCS of the PEC stealth B2 in different cut planes are shown in Figs. 35 - 37. The normalized polar RCS of the PEC stealth B2 in different cut planes are shown in Figs. 38 - 40. The PEC stealth B2 aircraft is simulated through BI with 0th, 1st, 2nd, 3rd and 4th order of hierarchical basis functions. As the efficacy of 0th order has been verified with fine mesh with respect to the wavelength, here it is used as a reference. The RCS comparison shows that most of the input power goes over the PEC stealth B2. The reflected power in the inverse direction of the input wave is very low.

The simulation data summary for the PEC B2 is shown in Table 2. TB is the type of bases, D is the mesh size set for the model, $\bar{\mathrm{D}}$ is the mean mesh edge length, D_{min} is the minimum mesh edge length, D_{max} is the maximum mesh edge length, N is the total number of unknowns, N_J is the number of BI electric current unknowns, N_M is the number of BI magnetic current unknowns, L is the number of levels for MLFMM, PM is the peak memory consumption and T is the run time of the simulation.

Table 2: The Simulation Results for the PEC B2

TB	D (m)	$\bar{\mathrm{D}}$ (cm)	D_{min} (cm)	D_{max} (cm)	N	N_J	N_M	L	PM (MB)	T (s)
R^1	0.01	1.009	0.253	2.172	17 700	17 700	0	4	305.215	39 846.6
$R^1 + G^1$	0.01	1.009	0.253	2.172	35 400	35 400	0	4	975.574	45 093.3
$R^1 + G^1 + R^2$	0.01	1.009	0.253	2.172	59 000	59 000	0	4	2 464.742	51 057.8
$R^1 + G^1$ $+R^2 + G^2$	0.01	1.009	0.253	2.172	88 500	88 500	0	4	5 313.852	63 784.1
$R^1 + G^1$ $+R^2 + G^2 + R^3$	0.01	1.009	0.253	2.172	123 900	123 900	0	4	10 107.25	75 945.1

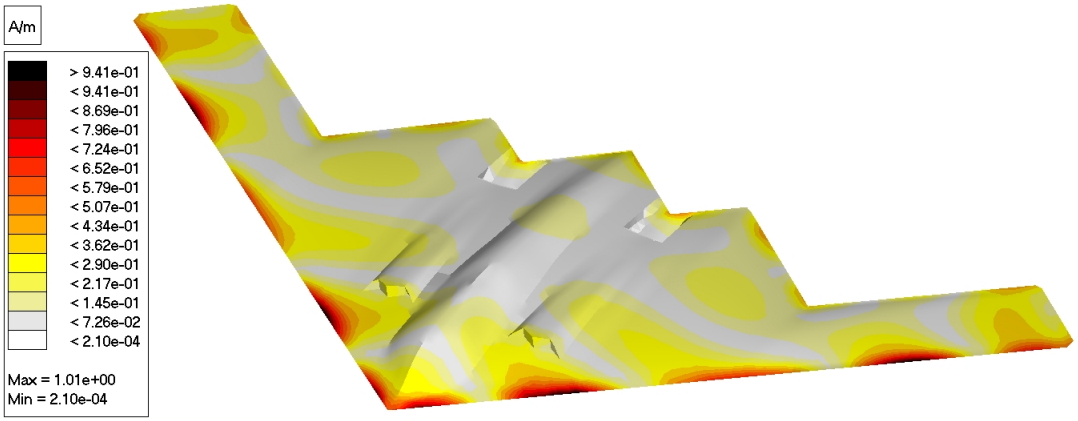

Figure 34: PEC stealth B2 real components of the surface current distribution @ 1.5 GHz.

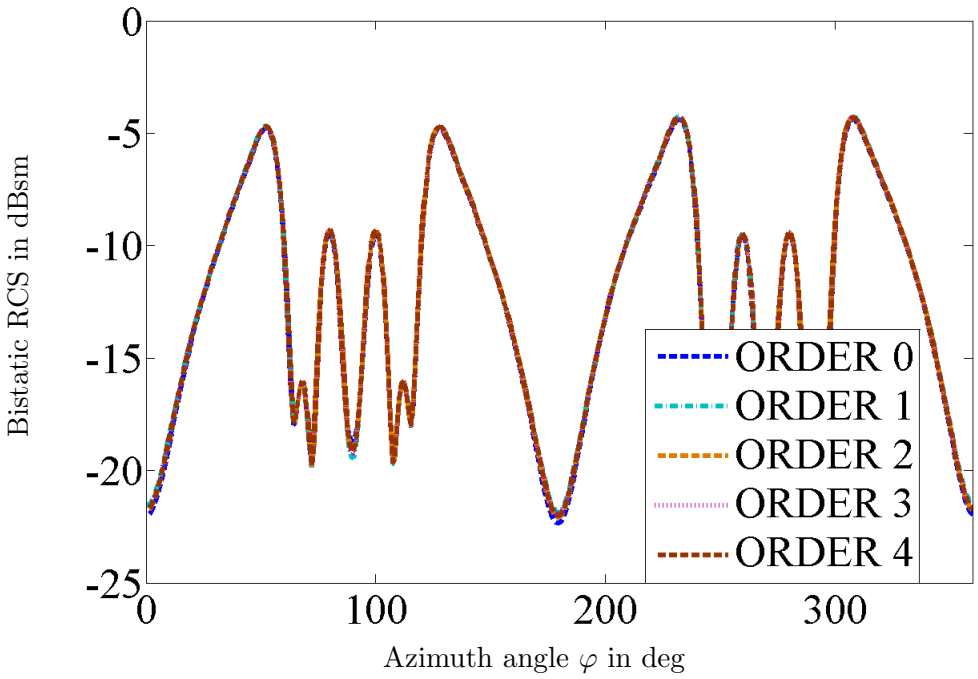

Figure 35: Bistatic RCS of PEC stealth B2 @ 1.5 GHz on xy cut plane ($\vartheta = 90°$).

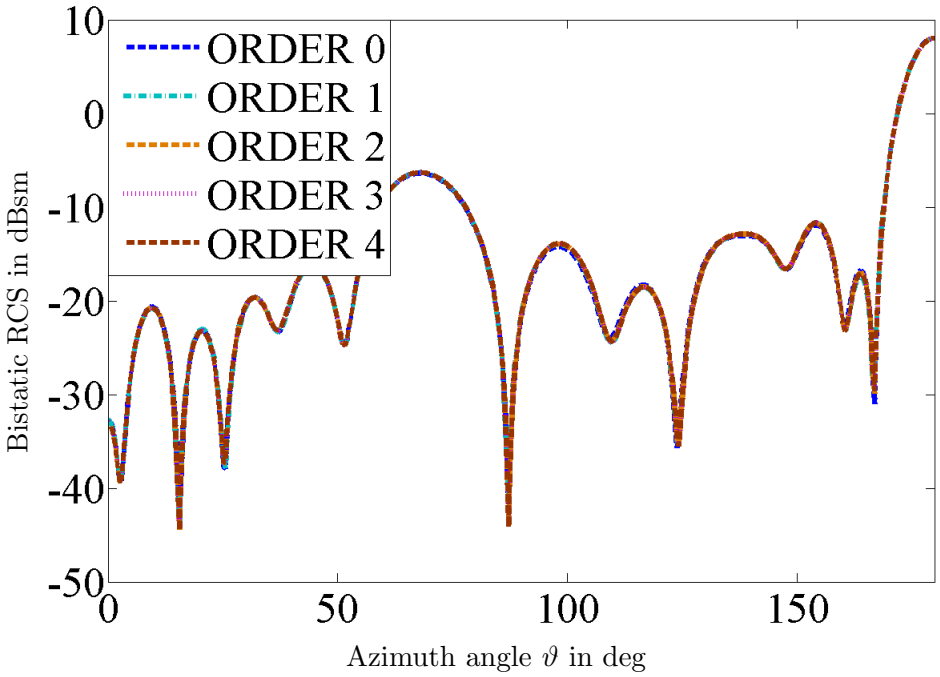

Figure 36: Bistatic RCS of PEC stealth B2 @ 1.5 GHz on xz cut half plane ($\varphi = 0°$).

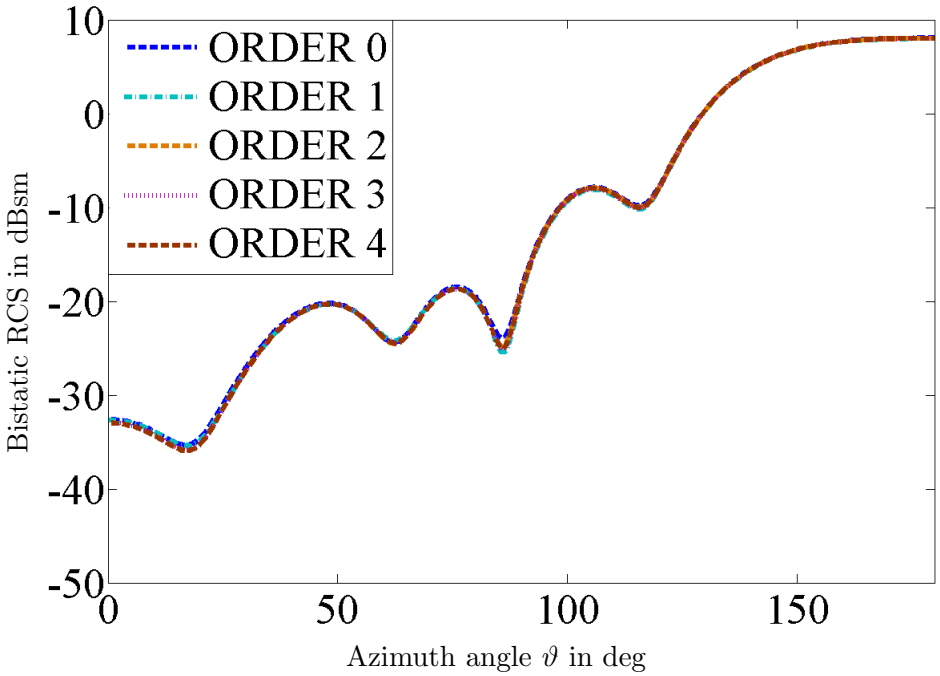

Figure 37: Bistatic RCS of PEC stealth B2 @ 1.5 GHz on yz cut half plane ($\varphi = 90°$).

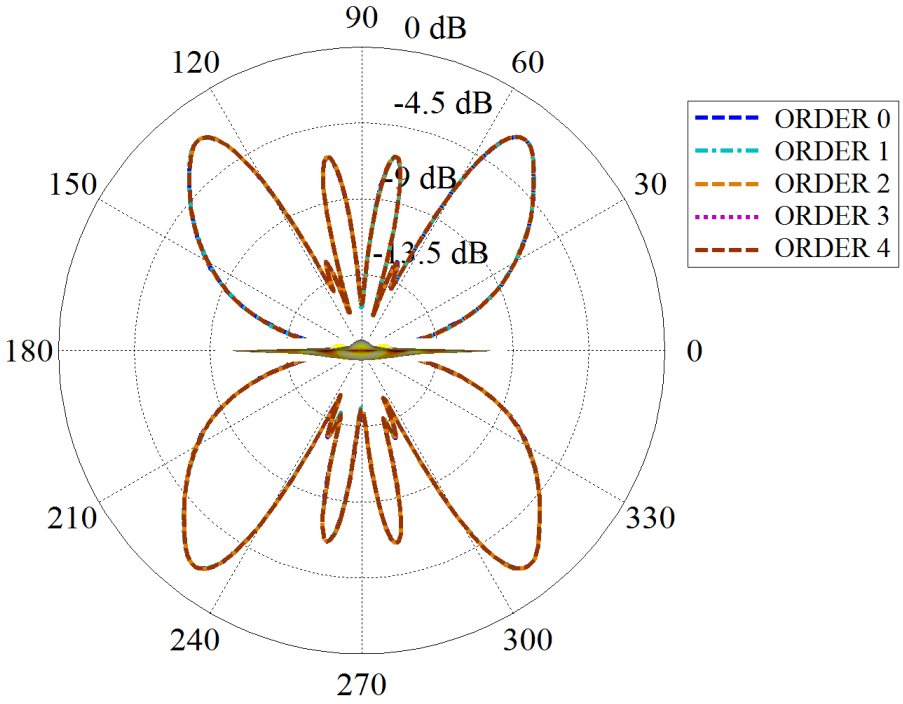

Figure 38: Normalized polar bistatic RCS of PEC stealth B2 @ 1.5 GHz on xy cut plane.

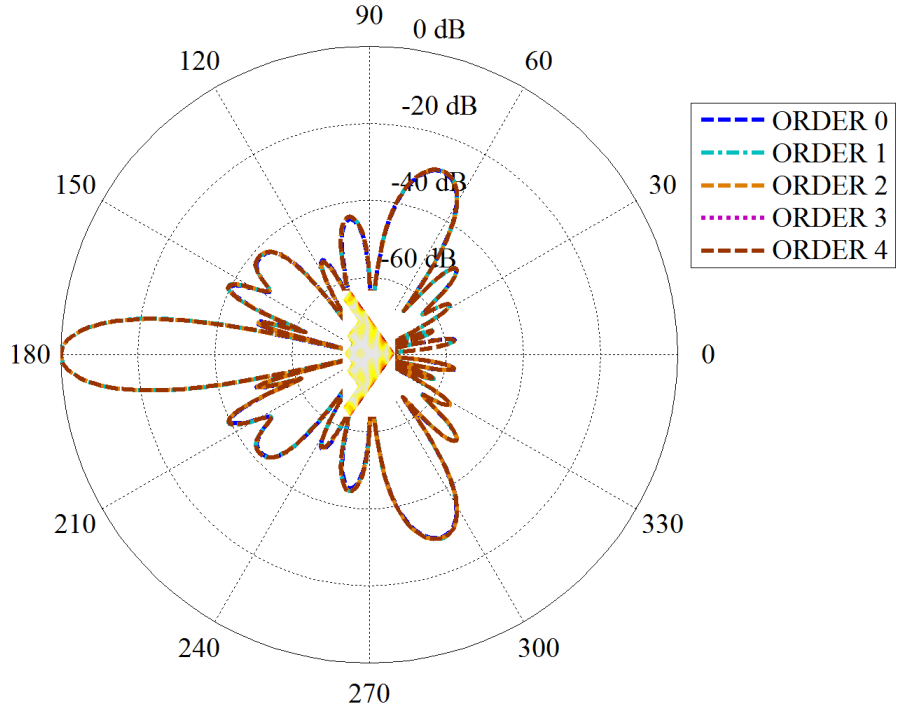

Figure 39: Normalized polar bistatic RCS of PEC stealth B2 @ 1.5 GHz on xz cut plane.

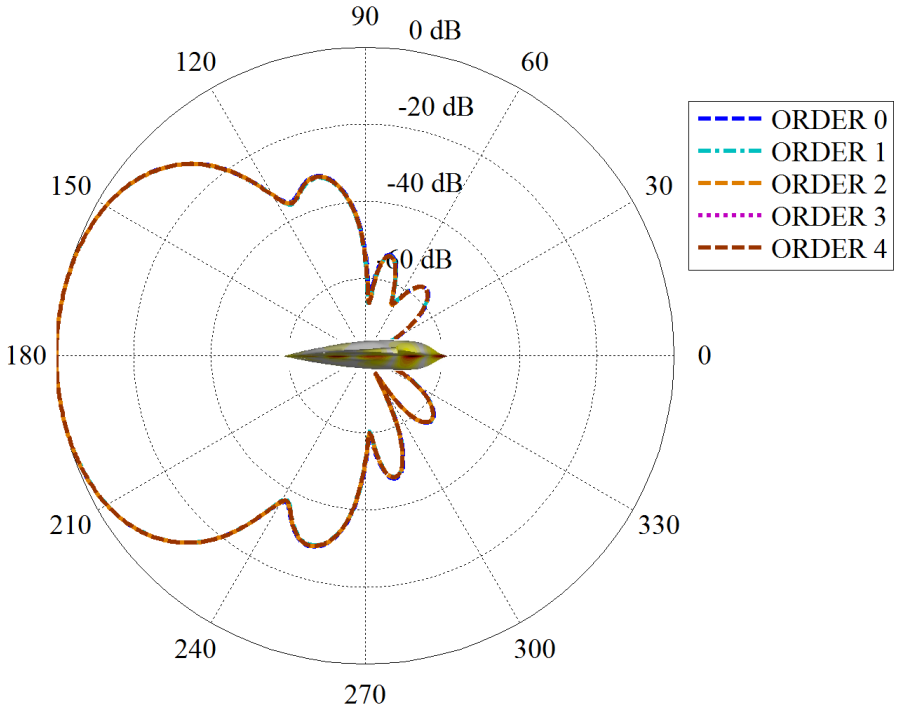

Figure 40: Normalized polar bistatic RCS of PEC stealth B2 @ 1.5 GHz on yz cut plane.

5.3.3 PEC Flamme

The PEC Flamme simulation is an application of BI for very large scale computation. The PEC Flamme is located in the xy plane, with nose heading along the $+x$ axis, as shown in Fig. 41. The Flamme is positioned in free space. The permittivity is $\epsilon_r = 1.0$ and the permeability is $\mu_r = 1$. The simulation frequency is 1.0 GHz. The incident plane wave propagates towards $-x$ direction with polarized electric field $E_z = 100$ V/m. The PEC Flamme is simulated through BI with different orders of hierarchical basis functions for comparisons.

The real components of equivalent surface electric currents on the PEC Flamme are shown in Fig. 41. The RCS of PEC Flamme in different cut planes are shown in Figs. 42 - 45. The normalized polar RCS of the PEC Flamme in different cut planes are shown in Figs. 46 - 48. The PEC Flamme is simulated through BI with 0th, 1st, 2nd, 3rd and 4th order of hierarchical basis functions. As the efficacy of LO with finer meshes has been verified, here it is used as a reference. The RCS comparison shows that most of the input power goes over the PEC Flamme.

The simulation data summary for the PEC Flamme is shown in Table 3. TB is the type of bases, D is the mesh size set for the model, $\bar{\mathrm{D}}$ is the mean mesh edge length, D_{min} is the minimum mesh edge length, D_{max} is the maximum mesh edge length, N is the total number of unknowns, N_J is the number of BI electric current unknowns, N_M is the number of BI magnetic current unknowns, L is the number of levels for MLFMM, PM is the peak memory consumption and T is the run time of the simulation.

Table 3: The Simulation Results for the PEC Flamme

TB	D (m)	$\bar{\mathrm{D}}$ (cm)	D_{min} (cm)	D_{max} (cm)	N	N_J	N_M	L	PM (MB)	T (s)
R^1	0.02	1.860	0.405	3.766	203 619	203 619	0	6	3 413.055	393 879.1
$R^1 + G^1$	0.07	5.924	0.405	15.216	33 744	33 744	0	4	1 006.406	35 102.7
$R^1 + G^1 + R^2$	0.07	5.924	0.405	15.216	56 240	56 240	0	4	2 504.887	43 477.0
$R^1 + G^1$ $+R^2 + G^2$	0.07	5.924	0.405	15.216	84 360	84 360	0	4	5 343.914	49 153.6
$R^1 + G^1$ $+R^2 + G^2 + R^3$	0.07	5.924	0.405	15.216	118 104	118 104	0	4	10 140.52	57 656.8

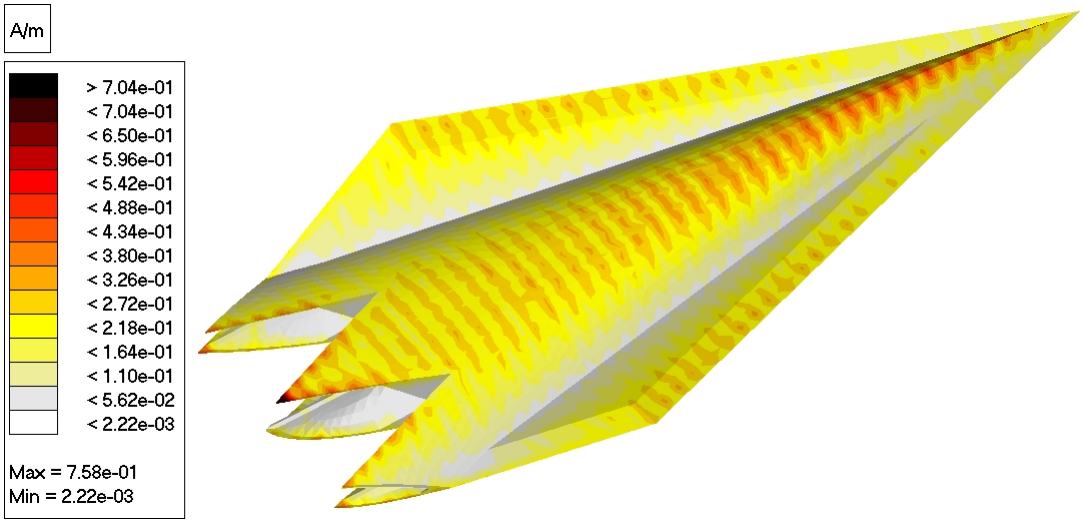

Figure 41: PEC flamme real components of the surface current distributions @ 1.0 GHz. The simulation is based on 0th order with dense mesh element size.

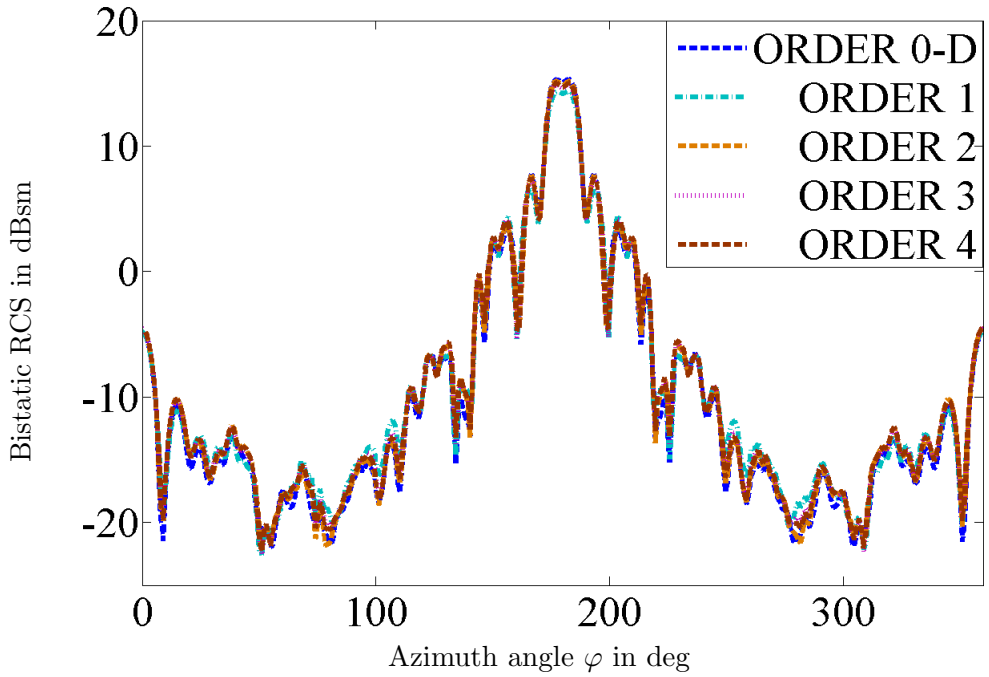

Figure 42: Bistatic RCS of PEC flamme @ 1 GHz on xy cut plane ($\vartheta = 90°$).

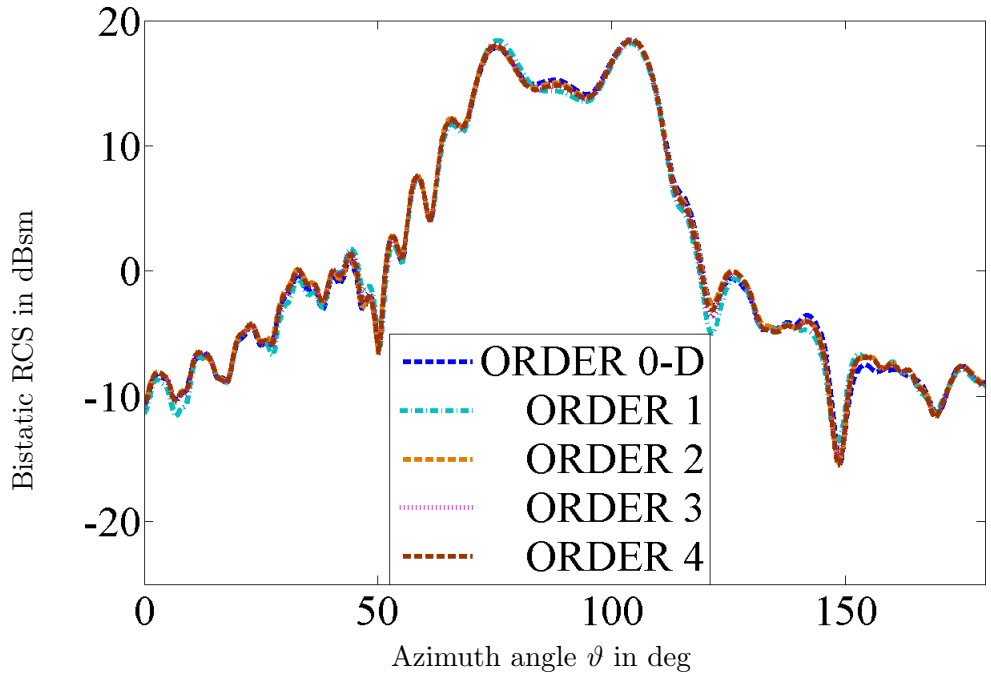

Figure 43: Bistatic RCS of PEC flamme @ 1 GHz on xz cut half plane ($\varphi = 180°$).

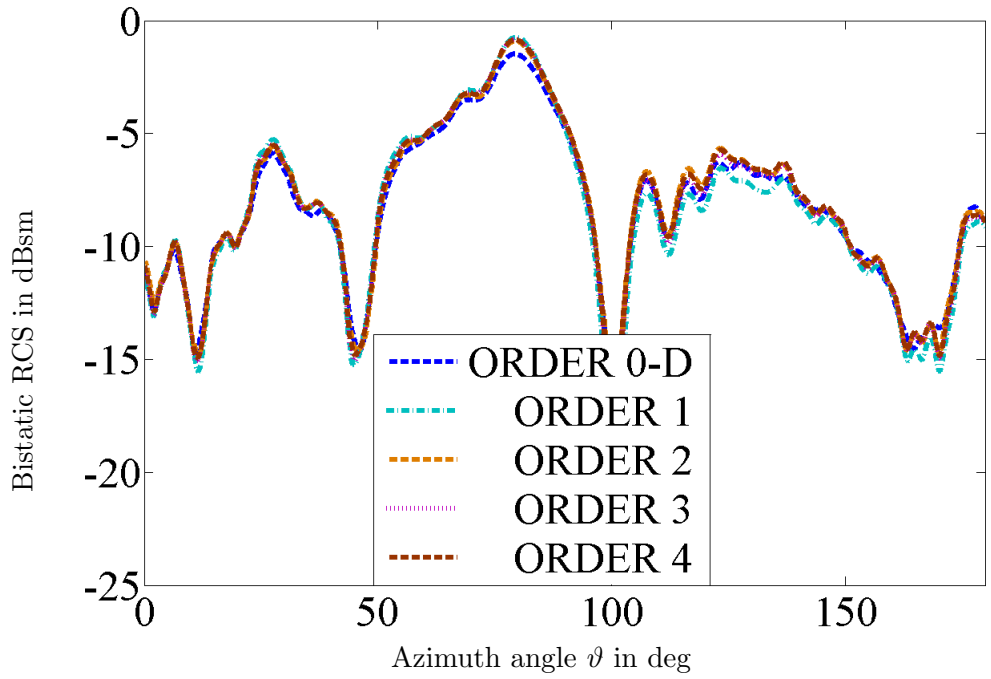

Figure 44: Bistatic RCS of PEC flamme @ 1 GHz on xz cut half plane ($\varphi = 0°$).

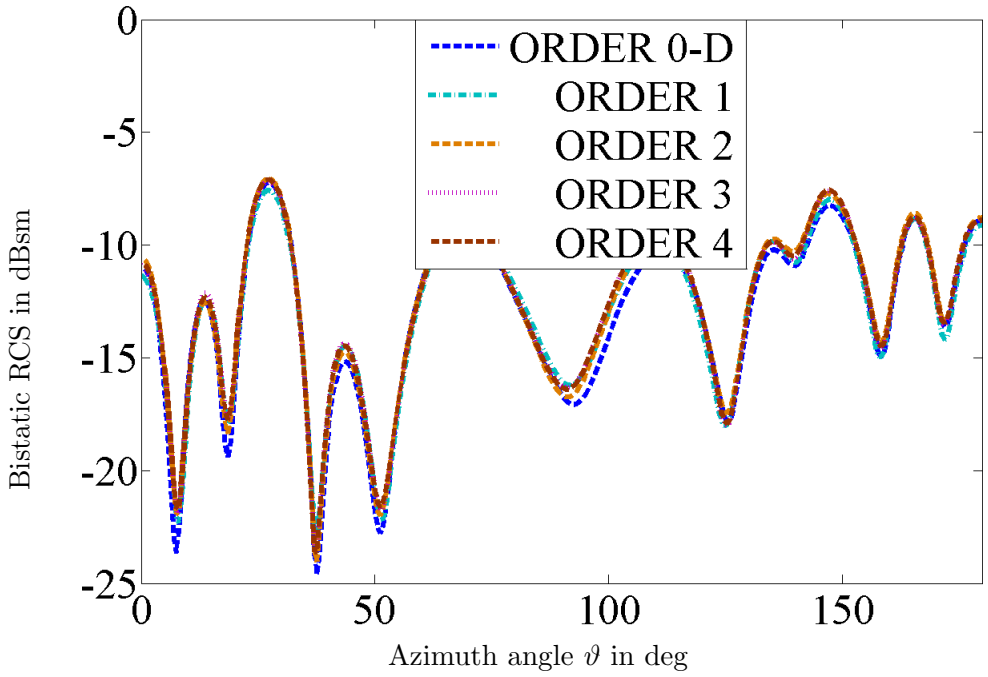

Figure 45: Bistatic RCS of PEC flamme @ 1 GHz on yz cut half plane ($\varphi = 90°$).

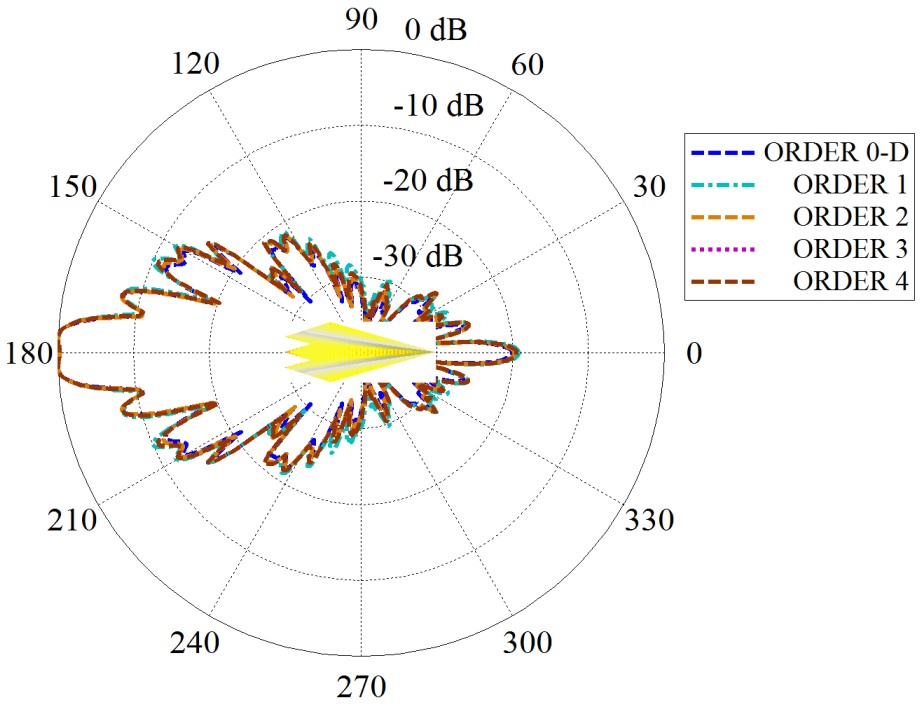

Figure 46: Normalized polar bistatic RCS of PEC stealth Bomber @ 1 GHz on xy cut plane.

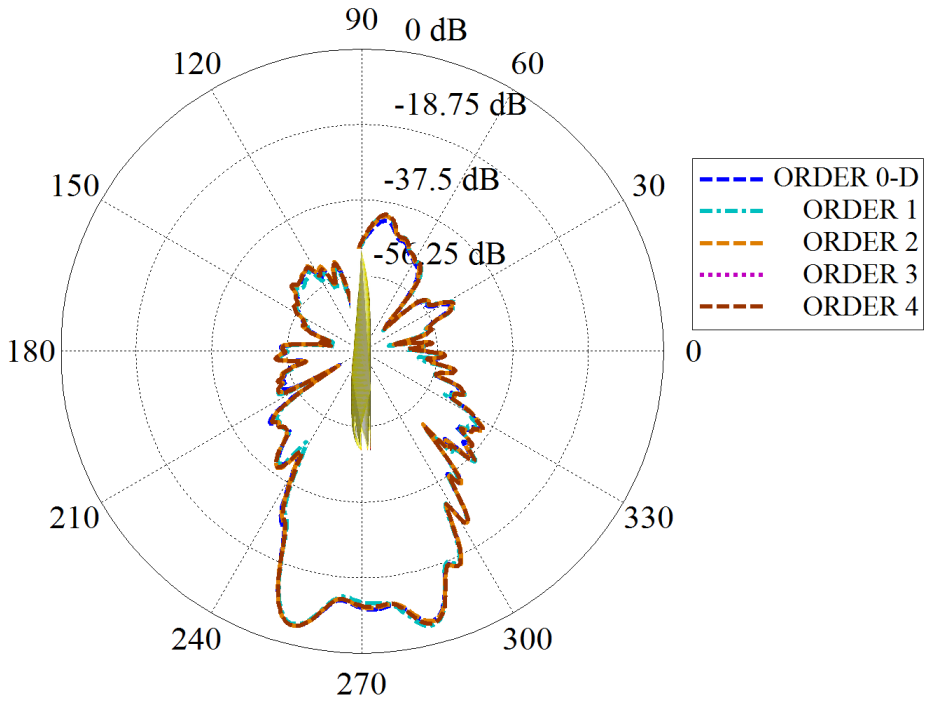

Figure 47: Normalized polar bistatic RCS of PEC stealth Bomber @ 1 GHz on xz cut plane.

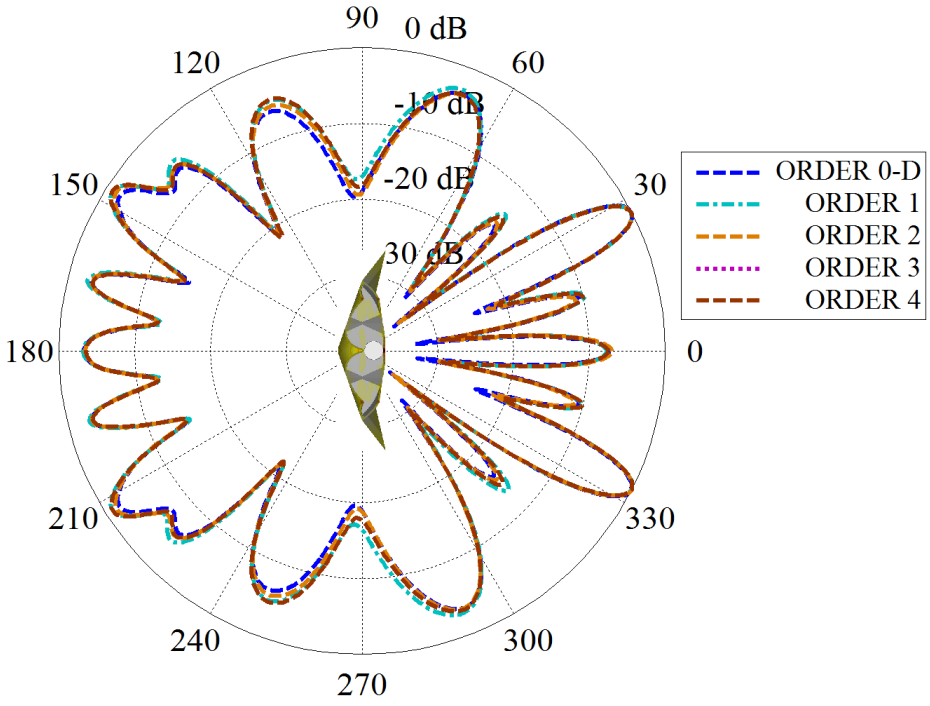

Figure 48: Normalized polar bistatic RCS of PEC stealth Bomber @ 1 GHz on yz cut plane.

6 The Finite Element Method

The finite element method (FEM) [Eibert and Hansen, 1996a, Jin, 2002] is a numerical technique to obtain an approximation of the electromagnetic field values in objects with enclosed boundary surfaces. As mentioned in Chapter 2 and shown in Fig. 1, FEM focuses on field computations on the enclosed envelope of the FE-BI object A_d and inside the dielectric volume V_a. V_a is the volume of the dielectric materials inside A_d. Since the electric field vanishes inside PEC volumes. FEM performs the field simulations in the PEC volume with dielectric materials in V_a only. On the outside boundary surfaces, the FEM has to be compatible with the BI. The basis functions for the FEM have to follow the same node order as in the BI. Moreover, the model simulated by FEM may consist of different disconnected components. In this chapter, the total volumes and the enclosed envelopes of the components are represented correspondingly by V_a and A_d.

6.1 Variational Formulation

To obtain the formulation of FEM in the homogeneous and isotropic dielectric materials, the variational method derives from the Maxwell equations for the time-harmonic fields. With the time factor $e^{j\omega t}$ suppressed, the Maxwell equations are written as

$$\nabla \times \boldsymbol{H}(\boldsymbol{r}) = j\omega\epsilon_0\bar{\epsilon}_r(\boldsymbol{r}) \cdot \boldsymbol{E}(\boldsymbol{r}) + \boldsymbol{J}_d(\boldsymbol{r}), \tag{6.1.1.1}$$

$$\nabla \times \boldsymbol{E}(\boldsymbol{r}) = -j\omega\mu_0\bar{\mu}_r(\boldsymbol{r}) \cdot \boldsymbol{H}(\boldsymbol{r}), \tag{6.1.1.2}$$

where the corresponding material properties are considered. ϵ_0 and μ_0 are the material properties in free space, $\boldsymbol{J_d}$ is the impressed electric current density inside V_a. The $\bar{\epsilon}_r$ and $\bar{\mu}_r$ inside V_a are the permittivity and the permeability of the material, they are assumed as constant complex values in a possibly lossy, inhomogeneous and anisotropic material. They are defined as

$$\bar{\epsilon}_r(\boldsymbol{r}) = \begin{bmatrix} \bar{\epsilon}_{xx} & \bar{\epsilon}_{xy} & \bar{\epsilon}_{xz} \\ \bar{\epsilon}_{yx} & \bar{\epsilon}_{yy} & \bar{\epsilon}_{yz} \\ \bar{\epsilon}_{zx} & \bar{\epsilon}_{zy} & \bar{\epsilon}_{zz} \end{bmatrix}, \quad \bar{\mu}_r(\boldsymbol{r}) = \begin{bmatrix} \bar{\mu}_{xx} & \bar{\mu}_{xy} & \bar{\mu}_{xz} \\ \bar{\mu}_{yx} & \bar{\mu}_{yy} & \bar{\mu}_{yz} \\ \bar{\mu}_{zx} & \bar{\mu}_{zy} & \bar{\mu}_{zz} \end{bmatrix}. \tag{6.1.3.3}$$

The permittivity and permeability of the inhomogeneous and anisotropic material have to be considered when achieving the variational formulation from the vector Maxwell equations. From (6.1.1.2), it leads to

$$\nabla \times (\bar{\mu}_r^{-1}(\boldsymbol{r}) \cdot \nabla \times \boldsymbol{E}(\boldsymbol{r})) = -j\omega\mu_0 \nabla \times \boldsymbol{H}(\boldsymbol{r}). \tag{6.1.1.4}$$

By substituting (6.1.1.1) into (6.1.1.4), the wave equation for the electric field $\boldsymbol{E}$ turns to be

$$\nabla \times (\bar{\mu}_r^{-1}(\boldsymbol{r}) \cdot \nabla \times \boldsymbol{E}(\boldsymbol{r})) - k_0^2\bar{\epsilon}_r(\boldsymbol{r}) \cdot \boldsymbol{E}(\boldsymbol{r}) = -jk_0 Z_0 \boldsymbol{J}_d(\boldsymbol{r}), \tag{6.1.1.5}$$

where $k_0 = \omega\sqrt{\mu_0\epsilon_0}$ is the wave number in free space and $Z_0 = \sqrt{\frac{\mu_0}{\epsilon_0}}$ is the wave impedance of free space.

Within the variational method, the ad-joint electric field $\boldsymbol{E_{ad}}$ is utilized. A complex-valued scalar product functional based on (6.1.1.5) is formed as

$$F(\boldsymbol{E}_{ad},\boldsymbol{E})=\iiint_{V_a}\Big[\boldsymbol{E}_{ad}(\boldsymbol{r})\cdot(\nabla\times(\bar{\mu}_r^{-1}(\boldsymbol{r})\cdot\nabla\times\boldsymbol{E}(\boldsymbol{r})))$$
$$-k_0^2\boldsymbol{E}_{ad}(\boldsymbol{r})\cdot\bar{\epsilon}_r(\boldsymbol{r})\cdot\boldsymbol{E}(\boldsymbol{r})+jk_0Z_0\boldsymbol{E}_{ad}(\boldsymbol{r})\cdot\boldsymbol{J}_d(\boldsymbol{r})\Big]dv \qquad (6.1.1.6)$$

and the real field $\boldsymbol{E}$ as well as the ad-joint filed $\boldsymbol{E}_{ad}$ are stationary in the solution. Based on the first vector Green's theorem [Jin, 2002]

$$\iiint_{V_a}\boldsymbol{a}\cdot(\nabla\times u\nabla\times\boldsymbol{b})dv=\iiint_{V_a}[u(\nabla\times\boldsymbol{a})\cdot(\nabla\times\boldsymbol{b})]\,dv-\oiint_{A_d}u(\boldsymbol{a}\times\nabla\times\boldsymbol{b})\cdot\hat{n}\,ds, \quad (6.1.1.7)$$

when setting $\boldsymbol{a}=\boldsymbol{E_{ad}}$, $u=1$, $\boldsymbol{b}=\boldsymbol{E}$ and substitute (6.1.1.7) into (6.1.1.6), the equation turns to be

$$F(\boldsymbol{E}_{ad},\boldsymbol{E})=\iiint_{V_a}[(\nabla\times\boldsymbol{E}_{ad}(\boldsymbol{r}))\cdot\bar{\mu}_r^{-1}(\boldsymbol{r})\cdot(\nabla\times\boldsymbol{E}(\boldsymbol{r}))-k_0^2\boldsymbol{E}_{ad}(\boldsymbol{r})\cdot\bar{\epsilon}_r(\boldsymbol{r})\cdot\boldsymbol{E}(\boldsymbol{r})$$
$$+jk_0Z_0\boldsymbol{E}_{ad}(\boldsymbol{r})\cdot\boldsymbol{J}_d(\boldsymbol{r})]dv+jk_0Z_0\oiint_{A_d}\boldsymbol{E}_{ad}(\boldsymbol{r})\cdot(\boldsymbol{H}(\boldsymbol{r})\times\hat{n}(\boldsymbol{r}))ds, \quad (6.1.1.8)$$

where $\hat{n}$ is the surface normal unit vector pointing out of V_a. The surface integral on A_d replaces the electric field $\boldsymbol{E}$ with the magnetic field $\boldsymbol{H}$. Here the boundary continuity conditions are utilized for $\boldsymbol{E}$ and $\boldsymbol{H}$ on A_d.

Compared with the real-valued functional formulation based on the Hermitian inner product, the generalized complex-valued functional formulation is achieved without claiming the uniqueness of the solution. However, there is no problem for this case since a clear formulation of the field problem is presumed. It is noticed that the complex scalar product (6.1.1.8) is applicable to the lossy materials, where the real-valued scalar product can not arrive.

In (6.1.1.8), the functional demonstrates that the fields described in the formulation only focus on the inside volume V_a without considering the fields in the outside space. However, it guarantees that the fields linking to the outside space on A_d satisfy the boundary continuity conditions through the surface integral. The magnetic field $\boldsymbol{H}$ utilized in the surface integral promotes (6.1.1.8) into a dual variational formulation. However, inside V_a, only the $\boldsymbol{E}$ field is taken into account. In most cases, the electric field is the main interest in most field problems. Moreover, the $\boldsymbol{E}$ field is zero in the ideally electrically conductive structures, as displayed in Fig. 1, the object contains PEC inside the volume. It leads to a smaller number of unknowns in the FE-discretizations.

The variational formulation can also utilize the electro-dynamic potentials to obtain the system matrices. Both the magnetic vector potential and the electric scalar potential are utilized. Compared with the analytical solutions, the variational formulation is more complicated than the direct field solution. The main difficulty arises from the non-uniqueness of the potential variables. That means that additional calibration methods are required for

the variable determinations and an unnecessarily increasing number of unknowns have to be computed in FEM. The calibration formulation for the electro-dynamic potentials contains an advantage that there are no jumps at the boundaries between different materials. Thus, it does not require treatments for cracks along with the materials. However, to calculate the electric and magnetic fields, the differentiation of the potentials must be carried out.

6.2 Finite Element Discretization

The concept of finite elements relies on the decomposition of the corresponding volume V_a into a series of finite spatial sections. Appropriate basis functions are utilized to represent the unknown fields inside the volumes.

6.2.1 The Mathematical Foundation for the Method of Finite Elements

To compute the re-constructed fields accurately and efficiently, the selection of the mathematical variables is important for the method of finite elements, where the variables are generally dependent on the geometrical configurations of the mesh cells. The solution of the fields can be referred to the mathematical concepts described by [Nedelec, 1980] as

K	the mesh section (tegrahedron, hexahedron, ...)
∂K	the boundary of K
$\bar{K}$	$K \cup \partial K$
P	a space of polynomials defined on K with dimension N
Q	Linear functionals on P with degree of freedom N
$L^2(K)$	Hilbert space of square integrable functions defined on K
$H(\text{curl})$	$\{\boldsymbol{u} \in (L^2(K))^3 \vert \nabla \times \boldsymbol{u} \in (L^2(K))^3\}$

where $\boldsymbol{u}$ is an arbitrary vector function. For the complex-valued scalar variational formulation, vector variables $\boldsymbol{E}$, $\boldsymbol{H}$ and $\nabla \times \boldsymbol{E}$ are utilized. Then the $H(\text{curl})$ space is considered for the solution of finite elements.

The FEM is able to obtain an accurate and unique solution for the system equations, where the system equations derive from the variational formulation. The orthogonality or near orthogonality of the vector basis functions can further improve the efficiency of FEM with obtaining faster convergence for iterative solvers. The achieved better performance of FEM mainly relies on the linear independence of the vector basis functions, where the orthogonality or near-orthogonality tremendously reduces the linear dependence of the basis functions. For each finite element in the variational formulation, the interpolation, defined as $\prod \boldsymbol{u} \in P$, is represented by

$$\zeta_i(\boldsymbol{u} - \prod \boldsymbol{u}) = 0, \quad \forall \zeta_i \in Q \tag{6.2.1.1}$$

to demonstrate the uniqueness. That means for any linear relationships on $\prod \boldsymbol{u} \in P$, there is a solution $\boldsymbol{u} \in (L^2(K))^3$ satisfying (6.2.1.1), where the solution is unique in this case.

The FEM with vector basis functions is more accurate and more efficient than the traditional methods with scalar basis functions for vector components. The scalar approach requires the interpolation of the scalar node values. When aiming at simulations for Cartesian vector components, the approach turns out to be ineffective. The electric field and magnetic field utilized in the variational formulation are field vectors belonging to the Hilbert space $H(\text{curl})$. They are also compliant with the Hilbert space $L^2(K)$. To satisfy this condition, the tangential component of the vector $\prod_1 \boldsymbol{u}$ defined on K_1 and the vector $\prod_2 \boldsymbol{u}$ defined on K_2 must be the same at the common area, which means $\partial K_1 = \partial K_2$. Thus, the basis functions defined in the FE method satisfy the continuity condition on the boundaries. It results in the establishment of the Maxwell equations integrated in the volume for electric field computations. The tangential continuity condition is required firmly. However, the FEM does not require the normal components of the basis functions to be continuous at the boundary ∂K, even if there is no material change. It avoids spurious modes in the FE solution.

A suitable operator ζ_i can determine the degrees of freedom for the basis functions in FEM. It can be selected precisely to avoid the spurious modes. The definitions of basis functions are generally referred to the tangential components of the vector elements. The basis functions are always classified as edge-related, face-associated and volume-associated forms with the corresponding degrees of the interpolations.

6.2.2 The Discretization of the Field Vectors

To solve the fields through the variational formulation in the FEM, the general starting step is the discretizations of the electric field $\boldsymbol{E}$, the magnetic field $\boldsymbol{H}$ and also the ad-joint electric field $\boldsymbol{E}_{ad}$. All fields are expanded into a series of polynomials constructed by real vector basis functions $\boldsymbol{\alpha}_n$ defined in the FE cells multiplied with the corresponding unknown coefficients. In FEM, the material is considered homogeneous in each single cell. So the fields are expanded as

$$\boldsymbol{E}(\boldsymbol{r}) = \sum_{n=1}^{N} u_n \boldsymbol{\alpha}_n(\boldsymbol{r}), \tag{6.2.2.1}$$

$$\boldsymbol{H}(\boldsymbol{r}) = \sum_{n=1}^{N} i_n \boldsymbol{\alpha}_n(\boldsymbol{r}), \tag{6.2.2.2}$$

$$\boldsymbol{E}_{ad}(\boldsymbol{r}) = \sum_{n=1}^{N} u_n^{ad} \boldsymbol{\alpha}_n(\boldsymbol{r}). \tag{6.2.2.3}$$

As the time factor $e^{j\omega t}$ is suppressed in the variational formulation, the expansion of the fields describe the field amplitudes in the corresponding cells.

In the field expansions from (6.2.2.1) to (6.2.2.3), the vector basis functions $\boldsymbol{\alpha}_n$ are the same for the electric field $\boldsymbol{E}$ and the magnetic field $\boldsymbol{H}$. The basis functions are defined through the dimensional parameters of the cells. N_E is the number of the unknowns for the electric field and N_H is the number of the unknowns for the magnetic field. In FE, N_E and N_H are not required to be the same. The electric field and the ad-joint field are

utilized in both terms of the volume and the surface integrals, however, the magnetic field is only utilized in the term of the surface integral. To obtain high efficiency, the electric and the magnetic fields are expanded independently. As a result, independent coefficients are utilized. u_n and i_n are independent coefficients for the electric field and the magnetic field correspondingly. Coefficients u_n^{ad} for the ad-joint electric field can be deleted through the differential process under the condition of minimizing the error of the variational formulation to obtain the unknowns.

6.2.3 The Discretization of the Integral Space

In EM simulations, the method of finite elements is required to be effective and efficient for arbitrarily shaped components. The arbitrarily shaped components can be constructed by different materials. To detailed describe the arbitrary geometrical configurations, different types of meshes can be utilized. In this work, the tetrahedral mesh is utilized for the volume discretizations and the triangular mesh is utilized for the boundary surface discretizations. The tetrahedral and triangular meshes are flexible and effective to match the arbitrarily shaped components. For complicated structures, the mesh size of the tetrahedra and triangles have to be reduced for more accurately discretized objects. However, with the decreasing mesh size, larger numbers of tetrahedra and triangles are required. So the total number of unknowns is increased, more computational time and more RAM are also required for EM simulations. Moreover, compared with the wavelength λ, the mesh size of tetrahedra and triangles is required to be less than $\lambda/8$ for the low order (LO) basis functions. With higher order (HO) basis functions, the mesh size can be extended up to $\lambda/3$ with the same good accuracy achieved as in LO.

The vector basis functions, including LO and HO, are defined based on the geometrical information of tetrahedra and triangles. The tetrahedron and the triangle mesh cells are shown in Fig. 49. Figure 49(a) shows the construction of a single tetrahedron. The numbers 0, 1, 2 and 3 are the local node numbers. Based on the local node numbers, the edge vectors $\boldsymbol{t}_{pq}$ $(p, q = 0, 1, 2, 3;\ p < q)$ are defined. The direction of the edge vectors are always from the lower node number p pointing towards the higher node number q. $\boldsymbol{A}_p$ $(p = 0, 1, 2, 3)$ is the face vector with respect to the corresponding node number, pointing inside the tetrahedron. The norm $|\boldsymbol{A}_p|$ is the area of the p-th face of the tetrahedron. $\boldsymbol{r}$ is the position inside the tetrahedron, h_p $(p = 0, 1, 2, 3)$ is the projection height of $\boldsymbol{r}$ to the corresponding p-th face. Figure 49(b) shows the construction of a single triangle. The numbers 1, 2 and 3 are the local node numbers. The edge vectors $\boldsymbol{t}_{pq}$ $(p, q = 1, 2, 3;\ p < q)$ are defined by the local node numbers, the directions are from the lower node number p pointing towards the higher node number q. $\boldsymbol{r}_s$ is the position inside the triangle, h_p $(p = 1, 2, 3)$ is the height of $\boldsymbol{r}_s$ to the corresponding p-th edge.

Tetrahedra are utilized for the volume integral terms in FE. The triangles are utilized for the surface integral term in FEM and also for the BI. Assuming that the triangle in Fig. 49(b) is a boundary surface triangle and it is one of the faces of the tetrahedron in Fig. 49(a), when $\boldsymbol{r}$ tends to be $\boldsymbol{r}_s$, the FE basis functions defined in the tetrahedron have to be compatible with the BI basis functions defined by the triangle. To obtain the compatibility between FE and BI, the basis functions of FE have to maintain the same global

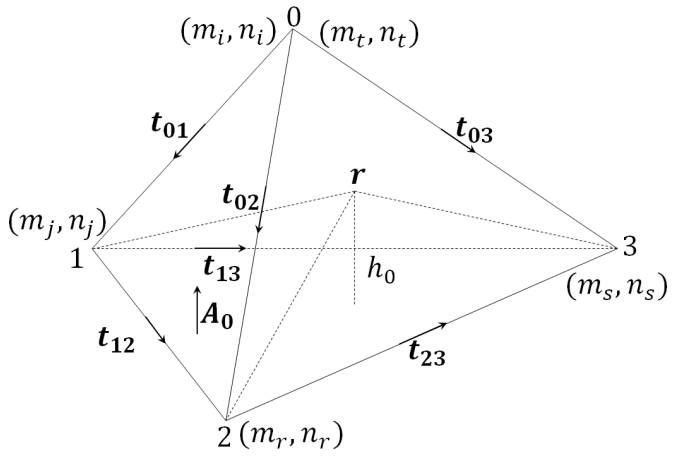

(a)

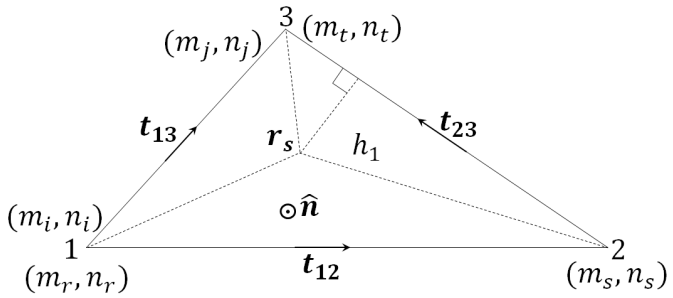

(b)

Figure 49: The definition of subscripts based on a single tetrahedron (a) and the surface boundary triangle (b). Every vertex index can be used as a row index m or as a column index n.

node order as the basis functions of BI. So the tetrahedral FE basis functions have a format represented by subscripts $k = (i, j)$ and $l = (r, s, t)$ as illustrated in Fig. 49. As elements of matrices need row and column positions, the subscripts (m_i, m_j) and (m_r, m_s, m_t) are introduced for row basis functions and subscripts (n_i, n_j) and (n_r, n_s, n_t) are assigned to column basis functions. In this work, (m_i, m_j) and (n_i, n_j) contain the global order of local node numbers for edge-related basis functions, whereas (m_r, m_s, m_t) and (n_r, n_s, n_t) represent the global order of nodes for face-associated basis functions, where $k = (i, j)$ and $l = (r, s, t)$ store the local node number of finite elements. As shown in Fig. 49, (m_i, n_i) always represent the starting point of the edge, (m_j, n_j) represent the ending point of the edge. (m_r, n_r), (m_s, n_s), (m_t, n_t) represent the node order of the triangles. Practically, the local node numbers are arrayed in the unique global order with respect to the BI and assigned to the corresponding subscripts for the FEM.

6.3 The Definition and Properties of the FE Parameters

The vector basis functions utilized in the FEM are defined by scalar and vector parameters of the tetrahedron in terms of volume integrals and also defined by parameters of the triangle in the term of the boundary surface integral. In the variational formulation of FE, the system matrices contain the integral of the volume inner product of the field curls and also the inner product of the fields in both volume and boundary surface integrals. In this work, the simplex coordinates of tetrahedra and triangles are utilized. The basis functions for field expansions are defined by simplex coordinates and also their gradients. The curls of the fields require the curls of the basis functions. The curl properties of the basis functions can be achieved through the cross product of the gradients of the simplex coordinates. In the variational formulation, the integral properties of the simplex coordinates, the edge vectors and also the face vectors are studied based on Fig. 49 for the FEM.

- The Fundamental Parameter Definitions of the Tetrahedron and Triangle.

i	local node index i
h_i	the height of the inside point relative to node i
V_T	volume of the tetrahedron
A_T	area of the triangle
$\boldsymbol{t}_{ij}$	local edge vector from node i to node j
$\boldsymbol{r}_i$	the vector position of node i
$\boldsymbol{A}_i$	normal surface area relative to node i pointing inward the tetrahedron
$\boldsymbol{r}$	the vector postion inside the tetrahedron
$\boldsymbol{r}_s$	the vector position inside the triangle

- Definitions of the Simplex Coordinates for Tetrahedron and Triangle Finite Elements

  The definitions of the simplex coordinates for the tetrahedron are utilized to locate the positions inside the tetrahedral volume. All of the simplex coordinates provide a real value between 0 and 1 inside the tetrahedron. As the inside point $\boldsymbol{r}$ can subdivide the tetrahedron into four sub-tetrahedra, the volume of the sub-tetrahedron is represented by V_i with respect to the corresponding node i. Then the simplex coordinate λ_i is defined as

$$\lambda_i = V_i(\boldsymbol{r})/V_T, \quad (i = 0, 1, 2, 3) \tag{6.3.1}$$

  and

$$\lambda_0 + \lambda_1 + \lambda_2 + \lambda_3 = 1, \tag{6.3.2}$$

$$\boldsymbol{r} = \lambda_0\boldsymbol{r}_0 + \lambda_1\boldsymbol{r}_1 + \lambda_2\boldsymbol{r}_2 + \lambda_3\boldsymbol{r}_3. \tag{6.3.3}$$

  The properties of the simplex coordinates (6.3.2) and (6.3.3) demonstrate a linear interpolation based on the vertices of the tetrahedron.

The definitions of the simplex coordinates for the triangle are similar to the tetrahedron. The inside point $\boldsymbol{r}_s$ subdivides the triangle into three sub-triangles. The area of a sub-triangle is represented by A_i and it is relative to the corresponding node i. The simplex coordinate λ_i is defined as

$$\lambda_i = A_i(\boldsymbol{r})/A_T, \quad (i = 0, 1, 2, 3), \tag{6.3.4}$$

where

$$\lambda_1 + \lambda_2 + \lambda_3 = 1, \tag{6.3.5}$$

$$\boldsymbol{r}_s = \lambda_1 \boldsymbol{r}_1 + \lambda_2 \boldsymbol{r}_2 + \lambda_3 \boldsymbol{r}_3. \tag{6.3.6}$$

From the definitions of the simplex coordinates, it is seen that the degrees of freedom for the triangle are fewer than for the tetrahedron. As a result, the basis functions and unknowns are more in a single tetrahedron than in a surface triangle. However, the basis functions have to be compliant based on the boundary continuity conditions.

- The Integration Properties of the Simplex Coordinates for the Tetrahedron and the Triangle

  The simplex coordinates are utilized to determine the point positions inside the finite elements. The integration properties of the simplex coordinates within the finite elements are important. The system matrices determined in the variational formulation require the volume and surface integrals of the simplex coordinates. The integration property of the simplex coordinates for the tetrahedron [Lapidus and Pinder, 1982] is shown as

$$\iiint_{V_T} \lambda_0^{m_0} \lambda_1^{m_1} \lambda_2^{m_2} \lambda_3^{m_3} dv = 6V \frac{m_0! m_1! m_2! m_3!}{(m_0 + m_1 + m_2 + m_3 + 3)!}, \tag{6.3.7}$$

  where m_0, m_1, m_2, m_3 are integer numbers representing the power orders of the simplex coordinates in the tetrahedron. The integration property of the simplex coordinates for the triangle [Lapidus and Pinder, 1982] is written as

$$\iint_{A_T} \lambda_1^{m_1} \lambda_2^{m_2} \lambda_3^{m_3} da = 2A_T \frac{m_1! m_2! m_3!}{(m_1 + m_2 + m_3 + 2)!}, \tag{6.3.8}$$

  where m_1, m_2, m_3 are integer numbers representing the power orders of the simplex coordinates in the triangle.

- The Definition of the Gradient of the Simplex Coordinates

  The computations of the simplex coordinate gradients in the tetrahedron derive from the definitions of the coordinates in (6.3.1). $V_i(\boldsymbol{r}) = h_i A_i/3$ is the volume with respect to the i-th node, h_i is the height of the point over the corresponding face. When the point $\boldsymbol{r}$ is moving inside the tetrahedron, the only changing value is h_i. So the gradient of λ_i is defined as

$$\nabla \lambda_i = \frac{\partial (V_i(\boldsymbol{r})/V_T)}{\partial h_i} \hat{h_i} = \frac{\boldsymbol{A}_i}{3V_T}, \tag{6.3.9}$$

where $\hat{h_i}$ is the unit vector pointing towards the changing trend of h_i. For the tetrahedron, $\hat{h_i}$ is in the same direction as $\boldsymbol{A}_i$, pointing inside the tetrahedron.

In a similar process, let $\boldsymbol{t}_{kl}$ represent the corresponding vector with respect to node i, where $(k, l \neq i)$ and $k < l$. Then the gradient of λ_i in the triangle turns into

$$\nabla\lambda_i = \frac{\partial(A_i(\boldsymbol{r})/A_T)}{\partial h_i}\hat{h_i} = \frac{\hat{n} \times \boldsymbol{t}_{kl}}{2A_T}(-1)^{l-k+1}, \tag{6.3.10}$$

where $\hat{n}$ is the local unit vector of the triangle, $\hat{h_i}$ is the unit vector with respect to the corresponding node pointing inside the triangle and $\nabla\lambda_i$ is also in the same direction as $\hat{h_i}$.

- The Computation of $\nabla\lambda_i \times \nabla\lambda_j$ for the Tetrahedron and Triangle

  Based on the configuration of the tetrahedron, the cross product of different simplex coordinate gradients is computed as

$$\nabla\lambda_i \times \nabla\lambda_i = \frac{\boldsymbol{A}_i \times \boldsymbol{A}_j}{9V_T^2} = \frac{s(-1)^{j-i}}{6V_T}\boldsymbol{t}_{kl}, \tag{6.3.11}$$

  where $s = \text{sgn}((\boldsymbol{t}_{12} \times \boldsymbol{t}_{13}) \cdot \boldsymbol{t}_{01})$. $\text{sgn}(x)$ is a function judging the sign of the variable x, its value is $+1$ or -1. The subscripts i, j, k, l are the node indices of the tetrahedron, where $i < j$ and $k < l$. (6.3.11) means the computation is applicable to any locally defined tetrahedral finite element.

  Based on the configuration of the triangle, the cross product of two different simplex coordinate gradients is calculated as

$$\nabla\lambda_i \times \nabla\lambda_i = -2\boldsymbol{A}_T(-1)^{j-i}, \tag{6.3.12}$$

  where i, j are node indices and $i < j$.

6.4 The System Matrices of the Variational Formulation

The system matrices for the FE unknowns derive from the variational formulation by utilizing the ad-joint electric field $\boldsymbol{E}_{ad}$. Under the condition of finding the stationary point of the variational formulation, it is required that

$$\frac{\partial F(\boldsymbol{E}_{ad}, \boldsymbol{E})}{\partial u_i^{ad}} = 0, \tag{6.4.1}$$

where $i = 1, 2, 3, ..., N$ indicates the unknowns. Then, the linear system matrices can be determined.

Through substituting (6.1.1.8) into (6.4.1), a linear system of equations is obtained as

$$[R_{mn}][u_n] - k_0^2[S_{mn}] + jk_0Z_0[T_{mn}] = -jk_0Z_0[w_m], \quad (m, n) = 1, ..., N\,, \tag{6.4.2}$$

with

$$[R_{mn}] = \iiint_{V_a} (\nabla \times \boldsymbol{\alpha}_m(\boldsymbol{r})) \cdot \bar{\mu}_r^{-1}(\boldsymbol{r}) \cdot (\nabla \times \boldsymbol{\alpha}_n(\boldsymbol{r}))dv, \tag{6.4.3}$$

$$[S_{mn}] = \iiint_{V_a} \boldsymbol{\alpha}_m(\boldsymbol{r}) \cdot \bar{\epsilon}_r(\boldsymbol{r}) \cdot \boldsymbol{\alpha}_n(\boldsymbol{r})dv, \tag{6.4.4}$$

$$[T_{mn}] = \oiint_{A_d} \boldsymbol{\alpha}_m(\boldsymbol{r}) \cdot (\boldsymbol{\alpha}_n(\boldsymbol{r}) \times \hat{n})da, \tag{6.4.5}$$

$$[w_m] = \iiint_{V_a} \boldsymbol{\alpha}_m(\boldsymbol{r}) \cdot \boldsymbol{J}_d(\boldsymbol{r})dv, \tag{6.4.6}$$

where k_0 and Z_0 are the wave number and the wave impedance of free space. V_a is the volume of the dielectric materials, A_d is the enclosed envelope of the object. The basis functions $\boldsymbol{\alpha}_m$ and $\boldsymbol{\alpha}_n$ are defined inside the finite elements. The mutual couplings $[R_{mn}]$, $[S_{mn}]$, $[T_{mn}]$ and the vector $[w_m]$ are also integrated inside the tetrahedron and the single surface triangle. Thus, it is found that $V_a = V_T$ and $A_d = A_T$ in each finite element for the system matrices from (6.4.3) to (6.4.6). The calculations of the system matrices $[R_{mn}]$ and $[S_{mn}]$ are shown in appendix A and B based on hierarchical 3-D vector basis functions, where the hierarchical 3-D vector basis functions are detailed discussed in the next chapter.

7 The Hierarchical 3-D Vector Basis Functions within the Finite Element Method

A hybrid higher-order finite element boundary integral (FE-BI) technique is discussed. The FE matrix elements are computed by a fully analytical procedure and the gobal matrix assembly is organized by a self-identifying procedure of the local to global transformation. This assembly procedure is applied to both FE and BI. The geometry is meshed into three-dimensional tetrahedra as finite elements and nearly orthogonal hierarchical basis functions are employed. The boundary conditions are implemented in a strong sense, such that the boundary values of the volume basis functions are directly utilized within the BI. The basis functions can be utilized for the tangential electric and magnetic fields and also for the associated equivalent surface current densities, where a cross product of the unit surface normal and the basis functions is applied. The self-identified method for the global matrix assembly automatically discerns the global order of the basis functions for generating the matrix elements. Higher order basis functions do need more unknowns for each single FE. However, fewer FEs are needed to achieve the same satisfiable accuracy. This improvement provides a lot more flexibility for meshing and allows the mesh size to raise up to $\lambda/3$. The performance of the implemented system is evaluated in terms of computation time, accuracy and memory occupation, where excellent results with respect to precision and computation time of large scale simulations are found.

7.1 Introduction

The finite element boundary integral (FE-BI) method [Eibert and Hansen, 1997, Jin, 2002, Tzoulis and Eibert, 2005b] is an efficient numerical technique for solving electromagnetic field problems. Traditional finite element methods rely on utilizing the local information of the FEs. The fixed local node order forces the local matrix elements to be transformed into global ones. Facing low order (LO) basis functions, the local-global transformation is easy as edge-related elements only follow the edge directions. When it comes to higher order (HO) basis functions [Djordjevic and Notaros, 2004, Fink et al., 2005, Ilic and Notaros, 2003, Ismatullah and Eibert, 2009, Jin, 2002, Klopf et al., 2012, Nedelec, 1980, Razi and Kasper, 2008], the basis functions are also related to faces or volumes. The local-global transformation procedure introduces then considerably more difficulties. In this work, a self-identified hierarchical basis function method is illustrated. This method effectively overcomes the problem mentioned above and provides more feasibility within FE-BI. Without fixing the node order or the sequence order of the basis functions for the local FEs, the self-identified hierarchical basis function organization allows a simple assembly of the global equation system. Simultaneously, this method guarantees the compatibility between FE and BI [Ismatullah and Eibert, 2009] fluently. All arbitrarily shaped components are meshed into tetrahedra [Jin, 2002] apart from perfect electric conductors (PEC) or perfect magnetic conductors (PMC), where $\boldsymbol{E}$ and $\boldsymbol{H}$ are forced to vanish inside the volume. As the FE-BI method solves for the field distribution inside the volume together with the corresponding equivalent surface currents (Ismatullah and Eibert [2009], Rao et al. [1982]), the self-identified hierarchical basis functions describe the distribution of fields within the

tetrahedra. When observation points tend to the enclosed boundary surface, the boundary condition determines the continuity of the $\boldsymbol{E}$ and $\boldsymbol{H}$ fields [Balanis, 1989, Bladel, 2007, Harrington, 2001, Kong, 1986]. So it is useful to guarantee that the basis functions for FEM are the same as the basis functions for BI.

Derived from the equivalence theorem, basis functions for BI are used to compose equivalent 2-D surface currents [Chew et al., 2001, Ismatullah and Eibert, 2009, Rao et al., 1982]. The currents are relevant to the surface unit normal vector and the polarization of the fields, thus, the tangential component of FE basis functions on the surface is perpendicular to the current basis functions. With respect to the corresponding sources (electric current $\boldsymbol{J}_s$ or magnetic current $\boldsymbol{M}_s$) and the surface normal unit vector, the corresponding subspaces ensure the compatibility between FEM and BI.

The LO basis functions have shortcomings when the simulation accuracy and the large number of unknowns are considered. Precision and efficiency of LO are difficult to improve with an increasing number of unknowns. The solution with LO basis functions demands the mesh size to be around $\lambda/20$ to $\lambda/8$. With coarser meshes, the elements may introduce inaccurate waveforms for field reconstruction.

The well-known mixed order basis functions are successful for electromagnetic field distributions and surface current reconstructions. $Rao - Wilton - Glisson$ (RWG) [Rao et al., 1982] basis functions are inherited as LO. As RWG is very effective for the BI, its corresponding first order Rotational Subspace (0th order) is utilized in FE tetrahedra. The Nedelec HO basis functions also form the first order Gradient Subspace (1st order), the second order Rotational Subspace (2nd order), the second order Gradient Subspace (3rd order), the third order Rotational Subspace (4th order) and so on. In this work, the hierarchical basis functions are extended up to the third order rotational subspace. Apart from BI, LO and HO basis functions are also utilized within FE and they improve the accuracy for field computations. In the FE-BI method, 0th and 1st order basis functions for the FE and BI methods are easy to match. Both of them are edge-related and follow the same direction of the edge vector. The situations for 2nd, 3rd and 4th order basis functions are more complicated. 2nd order basis functions are face-associated, 3rd order basis functions contain both edge-related and face-associated sub-spaces, 4th order basis functions contain both face-associated and volume-associated sub-spaces. To achieve compatibility between FE and BI, the edge-related and face-associated basis functions for FE and BI have to maintain the same global node order. The tetrahedral FE basis functions defined in Table 4 have a format represented by subscripts $k = (i, j)$ and $l = (r, s, t)$ as illustrated in Figs. 50 - 55. As elements of matrices need row and column positions, the subscripts (m_i, m_j) and (m_r, m_s, m_t) are introduced for row basis functions and subscripts (n_i, n_j) and (n_r, n_s, n_t) are assigned to column basis functions. In this work, (m_i, m_j) and (n_i, n_j) contain the global order of local node numbers for edge-related basis functions, whereas (m_r, m_s, m_t) and (n_r, n_s, n_t) represent the global order of nodes for face-associated basis functions, where $k = (i, j)$ and $l = (r, s, t)$ store the local node number of finite elements. The local node numbers are assigned to the volume-associated basis functions, where the tangential components of the basis functions vanish on the tetrahedral boundaries.

In FE analysis, the self-identified hierarchical basis functions are derived from the

geometrical information of the tetrahedra. In the mesh file, the data structure for each tetrahedron contains six edge identities and four face identities. Each edge is constructed with two node numbers and the order of the two nodes determines the edge global direction. Every face has the identity of the corresponding outside boundary triangles, inside volume triangles or inside boundary triangles. The outside boundary triangles are described by three edges in certain directions. The first edge gives out the first two nodes of the outside boundary triangle, the last node can be found through another two edges. The order of these three nodes are inherited as global node order. The inside volume triangles and inside boundary triangles are constructed by three nodes directly and the node order is viewed as the global node order. Through the index of edge and face identities, the tetrahedral FEs can easily consult the corresponding edges and triangles. Thus, the determined global node order can be set for the LO and HO basis functions. As shown in Fig. 49, (m_i, n_i) always represent the starting point of the edge, (m_j, n_j) represent the ending point and (m_r, n_r), (m_s, n_s), (m_t, n_t) represent the node order of the triangle. Practically, the local node numbers are arrayed in the unique global order and assigned to the corresponding subscripts. When generating the system matrices, the assigned subscripts are set to the corresponding positions into the list of basis functions. Then, elements of system matrices are automatically assigned to global edges and faces. If HO basis functions are implemented into FE, the matrix elements can be calculated analytically and precisely. Since these results are commonly not available in FE literature, it is a major contribution of this work to present these analytical matrix elements up to 4th order. As the order of basis functions is enlarged, the accuracy of the boundary integral (BI) should also be improved. As it turns out, the integration order for the testing surface integrals should be increased, the adaptive numbers of quadrature points in the singularity cancellation technique have to grow and larger maximum numbers for spherical harmonic expansion terms are needed within the Multilevel Fast Multipole Method [Chew et al., 2001, Eibert, 2005, Tzoulis and Eibert, 2005a]. HO achieves satisfactory accuracy with larger mesh size and it provides a better solution for non uniform finite elements. Good radar cross section (RCS) results of PEC structures coated by dielectric materials are acquired. Since LO is inherited by the hierarchical bases, orthogonality or near-orthogonality of basis functions is usefull for HO. Based on the structure of tetrahedra, system matrices built from nearly orthogonal basis functions converge faster and the solution is more accurate, so that the flexibility of mesh size provided by HO gives a more feasible solution. Meanwhile, HO improves the accuracy and also reduces the number of finite elements.

FE-BI solutions for coated spheres, the stealth bomber aircraft and the Flamme aircraft referring to the self-identified hierarchical nearly orthogonal basis functions are explicitly illustrated. The material of the layered sphere is homogeneous, isotropic and lossy. A variety of FE-BI simulations up to 3 million unknowns based on self-identified hierarchical basis functions are presented. The accuracy of HO testing cases is good, the simulation results based on HO basis functions are also compared with LO situations.

7.2 The First Order Rotational Space

The first order rotational space (0th order) is a subspace of $\boldsymbol{\alpha}_n$, constructed by edge-related basis functions in the FEs and represented by $\boldsymbol{a}$. The curls of the basis functions in the rotational space are not zero, however, the divergences vanish. As a result, the system matrices $[S_{mn}]$ and $[w_m]$ are dependent on the basis functions, the system matrices $[R_{mn}]$ are fulfilled by the mutual couplings of the curls of the basis functions within the FEs. Moreover, on the boundary surfaces, the tangential components of the edge-related basis functions are utilized to compute the $[T_{mn}]$ system matrices. At the face and edge boundaries of the FEs, the tangential components of the edge-related basis functions are continuous. However, the orthogonal components of the basis functions are not required to be continuous. As it turns out, the system matrices $[T_{mn}]$ are compliant with BI, where the current basis functions are the cross products of the surface unit normal vector and the field basis functions on the boundary surfaces.

The definitions of the edge-related basis functions take advantage of the nodes of edges in the first order rotational space. The node order determines the direction of the edge, while, the directions of the basis functions follow the corresponding directions of the global edges. Then, the system matrices derived from the local FEs have to be transformed into the global system matrices. To easily obtain the global system matrices, the self-identified global edge-related basis functions in the first order rotational space are defined as

$$\boldsymbol{a}_{ij} = \lambda_i \nabla \lambda_j - \lambda_j \nabla \lambda_i, \quad (i, j = 0, 1, 2, 3;\ i \neq j), \tag{7.2.1}$$

where i and j are local node numbers. The order of (i, j) can determine the direction of the global edge and also the global basis function. With respect to the system matrices $[R_{mn}]$, the curls of the global edge-related basis functions are calculated as

$$\begin{aligned} \nabla \times \boldsymbol{a}_{ij} &= \nabla \times (\lambda_i \nabla \lambda_j - \lambda_j \nabla \lambda_i) \\ &= \lambda_i \underbrace{\nabla \times (\nabla \lambda_j)}_{0} + \nabla \lambda_i \times \nabla \lambda_j - \lambda_j \underbrace{\nabla \times (\nabla \lambda_i)}_{0} - \nabla \lambda_j \times \nabla \lambda_i \\ &= 2 \nabla \lambda_i \times \nabla \lambda_j, \quad (i, j = 0, 1, 2, 3;\ i \neq j). \end{aligned} \tag{7.2.2}$$

With (6.3.9) and (6.3.11) into (7.2.1) and (7.2.2), it is shown that

$$\boldsymbol{a}_{ij} = \frac{1}{3V_T}(\lambda_i \boldsymbol{A}_j - \lambda_j \boldsymbol{A}_i), \tag{7.2.3}$$

$$\nabla \times \boldsymbol{a}_{ij} = \frac{2}{9V_T^2}(\boldsymbol{A}_i \times \boldsymbol{A}_j), \quad (i, j = 0, 1, 2, 3;\ i \neq j). \tag{7.2.4}$$

From (7.2.1) to (7.2.4), it is found that the node index of (i, j) can determine six edge-related basis functions in a single FE.

7.3 The First Order Gradient Space

The first order gradient space (1st order) is also a subspace of $\boldsymbol{\alpha}_n$, constructed by edge-related basis functions in the FEs and represented by $\boldsymbol{b}$. The curls of the basis functions

in the gradient space are zero. The system matrices $[R_{mn}]$ vanish as they are relevant to the curl of the basis functions. The system matrices $[S_{mn}]$ and $[w_m]$ have to be computed dependent on the basis functions. Moreover, on the boundary surfaces, the tangential components of the basis functions are utilized to compute the $[T_{mn}]$ system matrices. At the face and edge boundaries of the FEs, the tangential components are continuous. However, the orthogonal components of the basis functions are not required to be continuous. Then, the system matrices $[T_{mn}]$ are also compliant with BI.

The definitions of the basis functions in the 1st order gradient space also take advantage of the nodes of edges. The node order determines the direction of the edge, while, the directions of the basis functions follow the corresponding directions of the global edges. Then, the system matrices derived from the local FEs have to be transformed into the global system matrices. To easily obtain the global system matrices, the self-identified global edge-related basis functions in the first order of gradient space are defined as

$$\boldsymbol{b}_{ij} = \lambda_i \nabla \lambda_j + \lambda_j \nabla \lambda_i, \quad (i, j = 0, 1, 2, 3;\, i \neq j), \tag{7.3.1}$$

With respect to the system matrices $[R_{mn}]$, the curls of the global edge-related basis functions are computed as

$$\begin{aligned} \nabla \times \boldsymbol{b}_{ij} &= \nabla \times (\lambda_i \nabla \lambda_j + \lambda_j \nabla \lambda_i) \\ &= \lambda_i \underbrace{\nabla \times (\nabla \lambda_j)}_{0} + \nabla \lambda_i \times \nabla \lambda_j + \lambda_j \underbrace{\nabla \times (\nabla \lambda_i)}_{0} + \nabla \lambda_j \times \nabla \lambda_i \\ &= \mathbf{0}, \quad (i, j = 0, 1, 2, 3;\, i \neq j). \end{aligned} \tag{7.3.2}$$

With (7.3.2) into (6.4.3), it gives

$$[R_{mn}] = 0. \tag{7.3.3}$$

From (7.3.3), it is shown that the system matrices $[R_{mn}]$ are zero when the mutual couplings are related to the first order of gradient space.

7.4 The Second Order Rotational Space

The second order rotational space (2nd order) is a subspace of $\boldsymbol{\alpha}_n$, constructed by face-associated basis functions in the FEs and represented by $\boldsymbol{c}$ and $\boldsymbol{d}$. The curls of the basis functions are not zero. So the system matrices $[R_{mn}]$ have to be calculated dependent on the curl of the basis functions. The system matrices $[S_{mn}]$ and $[w_m]$ rely on the basis functions and also have to be computed. Moreover, on the boundary surfaces, the tangential components of the basis functions are utilized to compute $[T_{mn}]$. At the face and edge boundaries of the FEs, the tangential components are continuous. Then, the system matrices $[T_{mn}]$ are also compliant with the BI method.

The definitions of the basis functions take advantage of the nodes of faces in the second order rotational space. The node orders of the FE faces determine the directions of their unit normal vectors, the directions of the basis functions follow the corresponding global node orders. Then, the system matrices derived from the local FEs have to be transformed into

the global system matrices. To easily obtain the global system matrices, the self-identified global face-associated basis functions in the second order rotational space are defined as

$$\begin{aligned}\boldsymbol{c}_{rst} &= \lambda_r\lambda_s\nabla\lambda_t - 2\lambda_r\lambda_t\nabla\lambda_s + \lambda_s\lambda_t\nabla\lambda_r \\ &= \frac{1}{3V_T}(\lambda_r\lambda_s\boldsymbol{A}_t - 2\lambda_r\lambda_t\boldsymbol{A}_s + \lambda_s\lambda_t\boldsymbol{A}_r), \quad (r,s,t=0,1,2,3;\ r\neq s\neq t), \qquad (7.4.1)\\ \boldsymbol{d}_{rst} &= \lambda_r\lambda_s\nabla\lambda_t - \lambda_s\lambda_t\nabla\lambda_r \\ &= \frac{1}{3V_T}(\lambda_r\lambda_s\boldsymbol{A}_t - \lambda_s\lambda_t\boldsymbol{A}_r), \qquad (r,s,t=0,1,2,3;\ r\neq s\neq t). \qquad (7.4.2)\end{aligned}$$

With respect to the system matrices $[R_{mn}]$, the curls of the global face-associated basis functions are computed as

$$\begin{aligned}\nabla\times\boldsymbol{c}_{rst} =& 3\lambda_r\nabla\lambda_s\times\nabla\lambda_t - 3\lambda_t\nabla\lambda_r\times\nabla\lambda_s \\ =& \frac{1}{3V_T^2}(\lambda_r\boldsymbol{A}_s\times\boldsymbol{A}_t - \lambda_t\boldsymbol{A}_r\times\boldsymbol{A}_s), \quad (r,s,t=0,1,2,3;\ r\neq s\neq t), \qquad (7.4.3)\\ \nabla\times\boldsymbol{d}_{rst} =& \lambda_r\nabla\lambda_s\times\nabla\lambda_t + 2\lambda_s\nabla\lambda_r\times\nabla\lambda_t + \lambda_t\nabla\lambda_r\times\nabla\lambda_s \\ =& \frac{1}{9V_T^2}(\lambda_r\boldsymbol{A}_s\times\boldsymbol{A}_t + 2\lambda_s\boldsymbol{A}_r\times\boldsymbol{A}_t + \lambda_t\boldsymbol{A}_r\times\boldsymbol{A}_s), \\ & (r,s,t=0,1,2,3;\ r\neq s\neq t). \qquad (7.4.4)\end{aligned}$$

From (7.4.1) to (7.4.4), it can be noticed that the node index (r, s, t) can determine four face-associated basis functions in a single FE for each $\boldsymbol{c}_{rst}$ and $\boldsymbol{d}_{rst}$. Thus, there are eight unknowns for the second order rotational space in each single FE.

7.5 The Second Order Gradient Space

The second order gradient space (3rd order) is a subspace of $\boldsymbol{\alpha}_n$, constructed by both edge-related and also face-associated basis functions in the FEs and represented by $\boldsymbol{e}$ and $\boldsymbol{f}$ respectively. The curls of the basis functions are zero in the 2nd order gradient space. The system matrices $[R_{mn}]$ vanish due to the curl of the basis functions. The system matrices $[S_{mn}]$ and $[w_m]$ have to be computed. Moreover, on the boundary surfaces, the tangential components of the basis functions are utilized to compute the $[T_{mn}]$ system matrices. At the face and edge boundaries of the FEs, the tangential components are continuous. However, the orthogonal components of the basis functions are not required to be continuous. Then, the system matrices $[T_{mn}]$ are also compliant with BI.

The definitions of the basis functions take advantage of the nodes in the FEs for the second order gradient space. The node orders of the edges determine the directions of the edge-related basis functions. The directions of the basis functions follow the corresponding global edge directions. The node orders of the faces determine the directions of the face-associated basis functions. Then, the system matrices derived from the local FEs have to be transformed into the global system matrices. To easily obtain the global system matrices, the self-identified global edge-related and face-associated basis functions in the second order

gradient space are defined as

$$\begin{aligned}\boldsymbol{e}_{ij} &= (2\lambda_j - \lambda_i)\lambda_i \nabla\lambda_j - (2\lambda_i - \lambda_j)\lambda_j \nabla\lambda_i \\ &= \frac{1}{3V_T}[(2\lambda_j - \lambda_i)\lambda_i \boldsymbol{A}_j - (2\lambda_i - \lambda_j)\lambda_j \boldsymbol{A}_i], \quad (i,j = 0,1,2,3;\ i \neq j), \qquad (7.5.1) \\ \boldsymbol{f}_{rst} &= \lambda_r\lambda_s\nabla\lambda_t + \lambda_r\lambda_t\nabla\lambda_s + \lambda_s\lambda_t\nabla\lambda_r \\ &= \frac{1}{3V_T}(\lambda_r\lambda_s\boldsymbol{A}_t + \lambda_r\lambda_t\boldsymbol{A}_s + \lambda_s\lambda_t\boldsymbol{A}_r), \quad (r,s,t = 0,1,2,3;\ r \neq s \neq t). \qquad (7.5.2)\end{aligned}$$

With respect to the system matrices $[R_{mn}]$, the curls of the basis functions are calculated as

$$\nabla \times \boldsymbol{e}_{ij} = \nabla \times \boldsymbol{f}_{rst} = \boldsymbol{0}. \qquad (7.5.3)$$

It gives that

$$[R_{mn}] = 0. \qquad (7.5.4)$$

From (7.5.3), it is shown that the system matrices $[R_{mn}]$ are zero when the mutual couplings are related to the second order gradient space.

7.6 The Third Order Rotational Space

The third order rotational space (4th order) is a subspace of $\boldsymbol{\alpha}_n$, constructed by both face-associated and volume-associated basis functions in the FEs. The face-associated basis functions are represented by $\boldsymbol{g}$, $\boldsymbol{h}$ and $\boldsymbol{i}$. The volume-associated basis functions are represented by $\boldsymbol{j}$, $\boldsymbol{k}$ and $\boldsymbol{l}$. The curls of the basis functions are not zero in the third order rotational space. The system matrices $[R_{mn}]$ have to be calculated with the curl of the basis functions. The system matrices $[S_{mn}]$ and $[w_m]$ have to be computed dependent on the basis functions. Moreover, on the boundary surfaces, the tangential components of the basis functions are utilized to compute the $[T_{mn}]$ in the third order rotational space. At the face and edge boundaries of the FEs, the tangential components are continuous. Then, the system matrices $[T_{mn}]$ are also compliant with BI.

The definitions of the basis functions take advantage of the nodes of faces and the volume in the third order rotational space. The node orders of the FE faces determine the directions of their unit normal vectors, the directions of the basis functions follow the corresponding global node orders. Then, the system matrices derived from the face-associated basis functions have to be transformed into the global system matrices. However, the volume-associated basis functions vanish at the boundaries of the FEs, so the local node number can be directly utilized for the system matrices. To easily obtain the global system matrices, the self-identified global face-associated basis functions in the third order

rotational space are defined as

$$\begin{aligned}
\boldsymbol{g}_{rst} &= (\lambda_r - \lambda_s)\lambda_r\lambda_s\nabla\lambda_t - (\lambda_t - \lambda_s)\lambda_s\lambda_t\nabla\lambda_r + (\lambda_t - \lambda_r)\lambda_r\lambda_t\nabla\lambda_s \\
&= \frac{1}{3V_T}[(\lambda_r - \lambda_s)\lambda_r\lambda_s\boldsymbol{A}_t - (\lambda_t - \lambda_s)\lambda_s\lambda_t\boldsymbol{A}_r + (\lambda_t - \lambda_r)\lambda_r\lambda_t\boldsymbol{A}_s], \\
&\quad (r, s, t = 0, 1, 2, 3;\ r \neq s \neq t), \qquad (7.6.1) \\
\boldsymbol{h}_{rst} &= (393\lambda_t + 80\lambda_r - 212\lambda_s)\lambda_r\lambda_s\nabla\lambda_t - (393\lambda_r + 80\lambda_t - 212\lambda_s)\lambda_s\lambda_t\nabla\lambda_r \\
&\quad + (-292\lambda_t + 292\lambda_r)\lambda_r\lambda_t\nabla\lambda_s \\
&= \frac{1}{3V_T}[(393\lambda_t + 80\lambda_r - 212\lambda_s)\lambda_r\lambda_s\boldsymbol{A}_t - (393\lambda_r + 80\lambda_t - 212\lambda_s)\lambda_s\lambda_t\boldsymbol{A}_r \\
&\quad + (-292\lambda_t + 292\lambda_r)\lambda_r\lambda_t\boldsymbol{A}_s], \qquad (r, s, t = 0, 1, 2, 3;\ r \neq s \neq t), \qquad (7.6.2) \\
\boldsymbol{i}_{rst} &= (-131\lambda_t + 168\lambda_r - 124\lambda_s)\lambda_r\lambda_s\nabla\lambda_t + (-131\lambda_r + 168\lambda_t - 124\lambda_s)\lambda_s\lambda_t\nabla\lambda_r \\
&\quad + (-44\lambda_t - 44\lambda_r + 262\lambda_s)\lambda_r\lambda_t\nabla\lambda_s \\
&= \frac{1}{3V_T}[(-131\lambda_t + 168\lambda_r - 124\lambda_s)\lambda_r\lambda_s\boldsymbol{A}_t + (-131\lambda_r + 168\lambda_t - 124\lambda_s)\lambda_s\lambda_t\boldsymbol{A}_r \\
&\quad + (-44\lambda_t - 44\lambda_r + 262\lambda_s)\lambda_r\lambda_t\boldsymbol{A}_s], \qquad (r, s, t = 0, 1, 2, 3;\ r \neq s \neq t), \qquad (7.6.3)
\end{aligned}$$

The volume-associated basis functions are written as

$$\begin{aligned}
\boldsymbol{j}_{0123} &= \lambda_1\lambda_2\lambda_3\nabla\lambda_0 + \lambda_0\lambda_2\lambda_3\nabla\lambda_1 - \lambda_0\lambda_1\lambda_3\nabla\lambda_2 - \lambda_0\lambda_1\lambda_2\nabla\lambda_3 \\
&= \frac{1}{3V_T}(\lambda_1\lambda_2\lambda_3\boldsymbol{A}_0 + \lambda_0\lambda_2\lambda_3\boldsymbol{A}_1 - \lambda_0\lambda_1\lambda_3\boldsymbol{A}_2 - \lambda_0\lambda_1\lambda_2\boldsymbol{A}_3), \qquad (7.6.4) \\
\boldsymbol{k}_{0123} &= \lambda_0\lambda_1\lambda_3\nabla\lambda_2 - \lambda_0\lambda_1\lambda_2\nabla\lambda_3 \\
&= \frac{1}{3V_T}(\lambda_0\lambda_1\lambda_3\boldsymbol{A}_2 - \lambda_0\lambda_1\lambda_2\boldsymbol{A}_3), \qquad (7.6.5) \\
\boldsymbol{l}_{0123} &= \lambda_1\lambda_2\lambda_3\nabla\lambda_0 - \lambda_0\lambda_2\lambda_3\nabla\lambda_1 \\
&= \frac{1}{3V_T}(\lambda_1\lambda_2\lambda_3\boldsymbol{A}_0 - \lambda_0\lambda_2\lambda_3\boldsymbol{A}_1). \qquad (7.6.6)
\end{aligned}$$

With respect to the system matrices $[R_{mn}]$, the curl property of the basis functions in the

third order rotational space are computed as

$$\begin{aligned}
\nabla \times \boldsymbol{g}_{rst} &= 2[(\lambda_r \cancel{\lambda_s} \cancel{\lambda_t})\lambda_r \nabla\lambda_s \times \nabla\lambda_t - (\lambda_s \cancel{\lambda_r} \cancel{\lambda_t})\lambda_s \nabla\lambda_r \times \nabla\lambda_t + (\lambda_t \cancel{\lambda_r} \cancel{\lambda_s})\lambda_t \nabla\lambda_r \times \nabla\lambda_s] \\
&= \frac{2}{9V_T^2}[(\lambda_r \cancel{\lambda_s} \cancel{\lambda_t})\lambda_r \boldsymbol{A}_s \times \boldsymbol{A}_t - (\lambda_s \cancel{\lambda_r} \cancel{\lambda_t})\lambda_s \boldsymbol{A}_r \times \boldsymbol{A}_t + (\lambda_t \cancel{\lambda_r} \cancel{\lambda_s})\lambda_t \boldsymbol{A}_r \times \boldsymbol{A}_s], \\
&\quad (r,s,t = 0,1,2,3;\ r \neq s \neq t), \qquad (7.6.7) \\
\nabla \times \boldsymbol{h}_{rst} &= (977\lambda_t \cancel{-424\lambda_s} - 212\lambda_r)\lambda_r \nabla\lambda_s \times \nabla\lambda_t + (533\lambda_t + 533\lambda_r - 424\lambda_s)\lambda_s \nabla\lambda_r \times \nabla\lambda_t \\
&\quad + (977\lambda_r \cancel{-424\lambda_s} - 212\lambda_t)\lambda_t \nabla\lambda_r \times \nabla\lambda_s \\
&= \frac{1}{9V_T^2}[(977\lambda_t \cancel{-424\lambda_s} - 212\lambda_r)\lambda_r \boldsymbol{A}_s \times \boldsymbol{A}_t + (533\lambda_t + 533\lambda_r - 424\lambda_s)\lambda_s \boldsymbol{A}_r \times \boldsymbol{A}_t \\
&\quad + (977\lambda_r \cancel{-424\lambda_s} - 212\lambda_t)\lambda_t \boldsymbol{A}_r \times \boldsymbol{A}_s], \quad (r,s,t = 0,1,2,3;\ r \neq s \neq t), \qquad (7.6.8) \\
\nabla \times \boldsymbol{i}_{rst} &= (-43\lambda_t \cancel{-510\lambda_s} + 212\lambda_r)\lambda_r \nabla\lambda_s \times \nabla\lambda_t + (-467\lambda_t + 467\lambda_r)\lambda_s \nabla\lambda_r \times \nabla\lambda_t \\
&\quad + (43\lambda_r \cancel{+510\lambda_s} - 212\lambda_t)\lambda_t \nabla\lambda_r \times \nabla\lambda_s \\
&= \frac{1}{9V_T^2}[(-43\lambda_t \cancel{-510\lambda_s} + 212\lambda_r)\lambda_r \boldsymbol{A}_s \times \boldsymbol{A}_t + (-467\lambda_t + 467\lambda_r)\lambda_s \boldsymbol{A}_r \times \boldsymbol{A}_t \\
&\quad + (43\lambda_r + 510\lambda_s - 212\lambda_t)\lambda_t \boldsymbol{A}_r \times \boldsymbol{A}_s], \quad (r,s,t = 0,1,2,3;\ r \neq s \neq t), \qquad (7.6.9) \\
\nabla \times \boldsymbol{j}_{0123} &= -2(\lambda_1\lambda_2 \nabla\lambda_0 \times \nabla\lambda_3 + \lambda_1\lambda_3 \nabla\lambda_0 \times \nabla\lambda_2 + \lambda_0\lambda_2 \nabla\lambda_1 \times \nabla\lambda_3 + \lambda_0\lambda_3 \nabla\lambda_1 \times \nabla\lambda_2) \\
&= \frac{-2}{9V_T^2}[(\lambda_1\lambda_2 \boldsymbol{A}_0 \times \boldsymbol{A}_3 + \lambda_1\lambda_3 \boldsymbol{A}_0 \times \boldsymbol{A}_2 + \lambda_0\lambda_2 \boldsymbol{A}_1 \times \boldsymbol{A}_3 + \lambda_0\lambda_3 \boldsymbol{A}_1 \times \boldsymbol{A}_2)], \\
&\qquad (7.6.10) \\
\nabla \times \boldsymbol{k}_{0123} &= \lambda_0\lambda_3 \nabla\lambda_1 \times \nabla\lambda_2 + \lambda_1\lambda_3 \nabla\lambda_0 \times \nabla\lambda_2 - \lambda_0\lambda_2 \nabla\lambda_1 \times \nabla\lambda_3 \\
&\quad - \lambda_1\lambda_2 \nabla\lambda_0 \times \nabla\lambda_3 - 2\lambda_0\lambda_1 \nabla\lambda_2 \times \nabla\lambda_3 \\
&= \frac{1}{9V_T^2}(\lambda_0\lambda_3 \boldsymbol{A}_1 \times \boldsymbol{A}_2 + \lambda_1\lambda_3 \boldsymbol{A}_0 \times \boldsymbol{A}_2 - \lambda_0\lambda_2 \boldsymbol{A}_1 \times \boldsymbol{A}_3 \\
&\quad - \lambda_1\lambda_2 \boldsymbol{A}_0 \times \boldsymbol{A}_3 - 2\lambda_0\lambda_1 \boldsymbol{A}_2 \times \boldsymbol{A}_3), \qquad (7.6.11) \\
\nabla \times \boldsymbol{l}_{0123} &= -\lambda_1\lambda_2 \nabla\lambda_0 \times \nabla\lambda_3 - \lambda_1\lambda_3 \nabla\lambda_0 \times \nabla\lambda_2 + \lambda_0\lambda_2 \nabla\lambda_1 \times \nabla\lambda_3 \\
&\quad + \lambda_0\lambda_3 \nabla\lambda_1 \times \nabla\lambda_2 - 2\lambda_2\lambda_3 \nabla\lambda_0 \times \nabla\lambda_1 \\
&= \frac{1}{9V_T^2}(-\lambda_1\lambda_2 \boldsymbol{A}_0 \times \boldsymbol{A}_3 - \lambda_1\lambda_3 \boldsymbol{A}_0 \times \boldsymbol{A}_2 + \lambda_0\lambda_2 \boldsymbol{A}_1 \times \boldsymbol{A}_3 \\
&\quad + \lambda_0\lambda_3 \boldsymbol{A}_1 \times \boldsymbol{A}_2 - 2\lambda_2\lambda_3 \boldsymbol{A}_0 \times \boldsymbol{A}_1). \qquad (7.6.12)
\end{aligned}$$

From (7.6.1) to (7.6.12), $\boldsymbol{g}_{rst}$, $\boldsymbol{h}_{rst}$, $\boldsymbol{i}_{rst}$ and their curls are face-associated, $\boldsymbol{j}_{0123}$, $\boldsymbol{k}_{0123}$, $\boldsymbol{l}_{0123}$ and their curls are volume-associated. Each face-associated basis function represents four unknowns for the system matrices, while each volume-associated basis function produces only one unknown. The third order rotational space together with the other spaces can improve the accuracy with increasing frequencies.

Table 4: Hierarchical Basis Functions and Properties for a Tetrahedron.

		FE Vector Basis Functions $\boldsymbol{\alpha_i}$		$\nabla \times \boldsymbol{\alpha_i}$	
R^1	$\boldsymbol{a}_1$	$\lambda_i \nabla \lambda_j - \lambda_j \nabla \lambda_i$	$\frac{\lambda_i \boldsymbol{A}_j - \lambda_j \boldsymbol{A}_i}{3V_T}$	$2\nabla\lambda_i \times \nabla\lambda_j$	$\frac{2}{9V_T^2}(\boldsymbol{A}_i \times \boldsymbol{A}_j)$
G^1	$\boldsymbol{b}_1$	$\lambda_i \nabla \lambda_j + \lambda_j \nabla \lambda_i$	$\frac{\lambda_i \boldsymbol{A}_j + \lambda_j \boldsymbol{A}_i}{3V_T}$	$\mathbf{0}$	$\mathbf{0}$
R^2	$\boldsymbol{c}_2$	$\lambda_r\lambda_s\nabla\lambda_t + \lambda_s\lambda_t\nabla\lambda_r - 2\lambda_r\lambda_t\nabla\lambda_s$	$\frac{\lambda_r\lambda_s\boldsymbol{A}_t + \lambda_s\lambda_t\boldsymbol{A}_r - 2\lambda_r\lambda_t\boldsymbol{A}_s}{3V_T}$	$3\lambda_r\nabla\lambda_s \times \nabla\lambda_t - 3\lambda_t\nabla\lambda_r \times \nabla\lambda_s$	$\frac{1}{3V_T^2}(\lambda_r\boldsymbol{A}_s \times \boldsymbol{A}_t - \lambda_t\boldsymbol{A}_r \times \boldsymbol{A}_s)$
	$\boldsymbol{d}_2$	$\lambda_r\lambda_s\nabla\lambda_t - \lambda_s\lambda_t\nabla\lambda_r$	$\frac{\lambda_r\lambda_s\boldsymbol{A}_t - \lambda_s\lambda_t\boldsymbol{A}_r}{3V_T}$	$\lambda_r\nabla\lambda_s \times \nabla\lambda_t + 2\lambda_s\nabla\lambda_r \times \nabla\lambda_t + \lambda_t\nabla\lambda_r \times \nabla\lambda_s$	$\frac{1}{9V_T^2}(\lambda_r\boldsymbol{A}_s \times \boldsymbol{A}_t + 2\lambda_s\boldsymbol{A}_r \times \boldsymbol{A}_t + \lambda_t\boldsymbol{A}_r \times \boldsymbol{A}_s)$
G^2	$\boldsymbol{e}_2$	$(2\lambda_j - \lambda_i)\lambda_i\nabla\lambda_j - (2\lambda_i - \lambda_j)\lambda_j\nabla\lambda_i$	$\frac{(2\lambda_j - \lambda_i)\lambda_i\boldsymbol{A}_j - (2\lambda_i - \lambda_j)\lambda_j\boldsymbol{A}_i}{3V_T}$	$\mathbf{0}$	$\mathbf{0}$
	$\boldsymbol{f}_2$	$\lambda_r\lambda_s\nabla\lambda_t + \lambda_s\lambda_t\nabla\lambda_r + \lambda_r\lambda_t\nabla\lambda_s$	$\frac{\lambda_r\lambda_s\boldsymbol{A}_t + \lambda_s\lambda_t\boldsymbol{A}_r + \lambda_r\lambda_t\boldsymbol{A}_s}{3V_T}$	$\mathbf{0}$	$\mathbf{0}$
R^3	$\boldsymbol{g}_3$	$(\lambda_r - \lambda_s)\lambda_r\lambda_s\nabla\lambda_t - (\lambda_t - \lambda_s)\lambda_s\lambda_t\nabla\lambda_r + (\lambda_t - \lambda_r)\lambda_r\lambda_t\nabla\lambda_s$	$\frac{1}{3V_T}[(\lambda_r - \lambda_s)\lambda_r\lambda_s\boldsymbol{A}_t - (\lambda_t - \lambda_s)\lambda_s\lambda_t\boldsymbol{A}_r + (\lambda_t - \lambda_r)\lambda_r\lambda_t\boldsymbol{A}_s]$	$2[(\lambda_r-\lambda_s-\lambda_t)\lambda_r\nabla\lambda_s\times\nabla\lambda_t - (\lambda_s-\lambda_r-\lambda_t)\lambda_s\nabla\lambda_r\times\nabla\lambda_t + (\lambda_t-\lambda_r-\lambda_s)\lambda_t\nabla\lambda_r\times\nabla\lambda_s]$	$\frac{2}{9V_T^2}[(\lambda_r-\lambda_s-\lambda_t)\lambda_r\boldsymbol{A}_s\times\boldsymbol{A}_t - (\lambda_s-\lambda_r-\lambda_t)\lambda_s\boldsymbol{A}_r\times\boldsymbol{A}_t + (\lambda_t-\lambda_r-\lambda_s)\lambda_t\boldsymbol{A}_r\times\boldsymbol{A}_s]$
	$\boldsymbol{h}_3$	$(393\lambda_t+80\lambda_r-212\lambda_s)\lambda_r\lambda_s\nabla\lambda_t - (393\lambda_r+80\lambda_t-212\lambda_s)\lambda_s\lambda_t\nabla\lambda_r + (-292\lambda_t+292\lambda_r)\lambda_r\lambda_t\nabla\lambda_s$	$\frac{1}{3V_T}[(393\lambda_t+80\lambda_r-212\lambda_s)\lambda_r\lambda_s\boldsymbol{A}_t - (393\lambda_r+80\lambda_t-212\lambda_s)\lambda_s\lambda_t\boldsymbol{A}_r + (-292\lambda_t+292\lambda_r)\lambda_r\lambda_t\boldsymbol{A}_s]$	$(977\lambda_t-424\lambda_s-212\lambda_r)\lambda_r\nabla\lambda_s\times\nabla\lambda_t + (533\lambda_t + 533\lambda_r - 424\lambda_s)\lambda_s\nabla\lambda_r\times\nabla\lambda_t + (977\lambda_r-424\lambda_s-212\lambda_t)\lambda_t\nabla\lambda_r\times\nabla\lambda_s$	$\frac{1}{9V_T^2}[(977\lambda_t-424\lambda_s-212\lambda_r)\lambda_r\boldsymbol{A}_s\times\boldsymbol{A}_t + (533\lambda_t + 533\lambda_r - 424\lambda_s)\lambda_s\boldsymbol{A}_r\times\boldsymbol{A}_t + (977\lambda_r-424\lambda_s-212\lambda_t)\lambda_t\boldsymbol{A}_r\times\boldsymbol{A}_s]$
	$\boldsymbol{i}_3$	$(-131\lambda_t+168\lambda_r-124\lambda_s)\lambda_r\lambda_s\nabla\lambda_t + (-131\lambda_r+168\lambda_t-124\lambda_s)\lambda_s\lambda_t\nabla\lambda_r + (-44\lambda_t-44\lambda_r+262\lambda_s)\lambda_r\lambda_t\nabla\lambda_s$	$\frac{1}{3V_T}[(-131\lambda_t+168\lambda_r-124\lambda_s)\lambda_r\lambda_s\boldsymbol{A}_t + (-131\lambda_r+168\lambda_t-124\lambda_s)\lambda_s\lambda_t\boldsymbol{A}_r + (-44\lambda_t-44\lambda_r+262\lambda_s)\lambda_r\lambda_t\boldsymbol{A}_s]$	$(-43\lambda_t-510\lambda_s+212\lambda_r)\lambda_r\nabla\lambda_s\times\nabla\lambda_t + (-467\lambda_t + 467\lambda_r)\lambda_s\nabla\lambda_r\times\nabla\lambda_t + (43\lambda_r+510\lambda_s-212\lambda_t)\lambda_t\nabla\lambda_r\times\nabla\lambda_s$	$\frac{1}{9V_T^2}(-43\lambda_t-510\lambda_s+212\lambda_r)\lambda_r\boldsymbol{A}_s\times\boldsymbol{A}_t + (-467\lambda_t + 467\lambda_r)\lambda_s\boldsymbol{A}_r\times\boldsymbol{A}_t + (43\lambda_r+510\lambda_s-212\lambda_t)\lambda_t\boldsymbol{A}_r\times\boldsymbol{A}_s$
	$\boldsymbol{j}_3$	$\lambda_1\lambda_2\lambda_3\nabla\lambda_0 + \lambda_0\lambda_2\lambda_3\nabla\lambda_1 - \lambda_0\lambda_1\lambda_3\nabla\lambda_2 - \lambda_0\lambda_1\lambda_2\nabla\lambda_3$	$\frac{1}{3V_T}(\lambda_1\lambda_2\lambda_3\boldsymbol{A}_0 + \lambda_0\lambda_2\lambda_3\boldsymbol{A}_1 - \lambda_0\lambda_1\lambda_3\boldsymbol{A}_2 - \lambda_0\lambda_1\lambda_2\boldsymbol{A}_3)$	$-2(\lambda_1\lambda_2\nabla\lambda_0 \times \nabla\lambda_3 + \lambda_1\lambda_3\nabla\lambda_0 \times \nabla\lambda_2 + \lambda_0\lambda_2\nabla\lambda_1 \times \nabla\lambda_3 + \lambda_0\lambda_3\nabla\lambda_1 \times \nabla\lambda_2)$	$\frac{-2}{9V_T^2}(\lambda_1\lambda_2\boldsymbol{A}_0 \times \boldsymbol{A}_3 + \lambda_1\lambda_3\boldsymbol{A}_0 \times \boldsymbol{A}_2 + \lambda_0\lambda_2\boldsymbol{A}_1 \times \boldsymbol{A}_3 + \lambda_0\lambda_3\boldsymbol{A}_1 \times \boldsymbol{A}_2)$
	$\boldsymbol{k}_3$	$\lambda_0\lambda_1\lambda_3\nabla\lambda_2 - \lambda_0\lambda_1\lambda_2\nabla\lambda_3$	$\frac{1}{3V_T}(\lambda_0\lambda_1\lambda_3\boldsymbol{A}_2 - \lambda_0\lambda_1\lambda_2\boldsymbol{A}_3)$	$\lambda_0\lambda_3\nabla\lambda_1 \times \nabla\lambda_2 + \lambda_1\lambda_3\nabla\lambda_0 \times \nabla\lambda_2 - \lambda_0\lambda_2\nabla\lambda_1 \times \nabla\lambda_3 - \lambda_1\lambda_2\nabla\lambda_0 \times \nabla\lambda_3 - 2\lambda_0\lambda_1\nabla\lambda_2 \times \nabla\lambda_3$	$\frac{1}{9V_T^2}(\lambda_0\lambda_3\boldsymbol{A}_1 \times \boldsymbol{A}_2 + \lambda_1\lambda_3\boldsymbol{A}_0 \times \boldsymbol{A}_2 - \lambda_0\lambda_2\boldsymbol{A}_1 \times \boldsymbol{A}_3 - \lambda_1\lambda_2\boldsymbol{A}_0 \times \boldsymbol{A}_3 - 2\lambda_0\lambda_1\boldsymbol{A}_2 \times \boldsymbol{A}_3)$
	$\boldsymbol{l}_3$	$\lambda_1\lambda_2\lambda_3\nabla\lambda_0 - \lambda_0\lambda_2\lambda_3\nabla\lambda_1$	$\frac{1}{3V_T}(\lambda_1\lambda_2\lambda_3\boldsymbol{A}_0 - \lambda_0\lambda_2\lambda_3\boldsymbol{A}_1)$	$-\lambda_1\lambda_2\nabla\lambda_0 \times \nabla\lambda_3 - \lambda_1\lambda_3\nabla\lambda_0 \times \nabla\lambda_2 + \lambda_0\lambda_2\nabla\lambda_1 \times \nabla\lambda_3 + \lambda_0\lambda_3\nabla\lambda_1 \times \nabla\lambda_2 - 2\lambda_2\lambda_3\nabla\lambda_0 \times \nabla\lambda_1$	$\frac{1}{9V_T^2}(-\lambda_1\lambda_2\boldsymbol{A}_0 \times \boldsymbol{A}_3 - \lambda_1\lambda_3\boldsymbol{A}_0 \times \boldsymbol{A}_2 + \lambda_0\lambda_2\boldsymbol{A}_1 \times \boldsymbol{A}_3 + \lambda_0\lambda_3\boldsymbol{A}_1 \times \boldsymbol{A}_2 - 2\lambda_2\lambda_3\boldsymbol{A}_0 \times \boldsymbol{A}_1)$

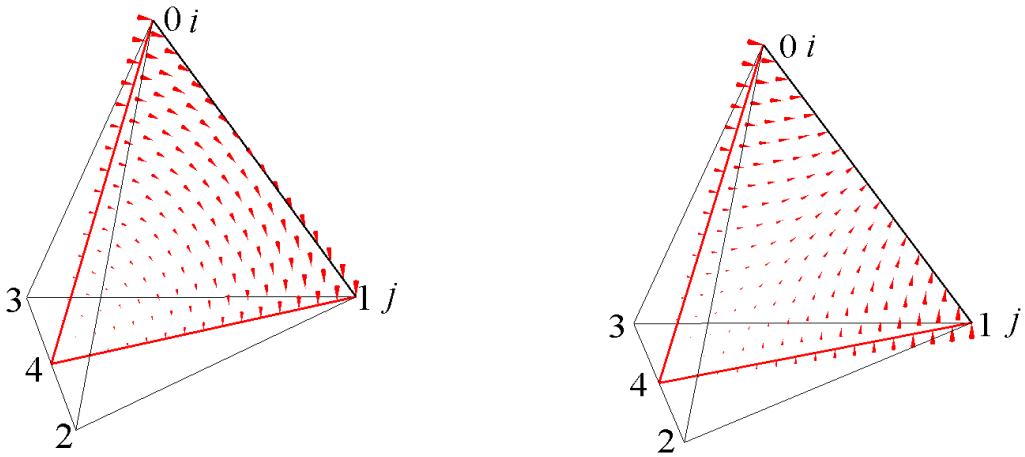

(a) (b)

Figure 50: The basis function distribution of the first order rotational and gradient spaces: (a) The first order rotational space $\boldsymbol{a}_1$, edge related from node $i = 0$ to node $j = 1$. (b) The first order gradient space $\boldsymbol{b}_1$, edge related from node $i = 0$ to node $j = 1$.

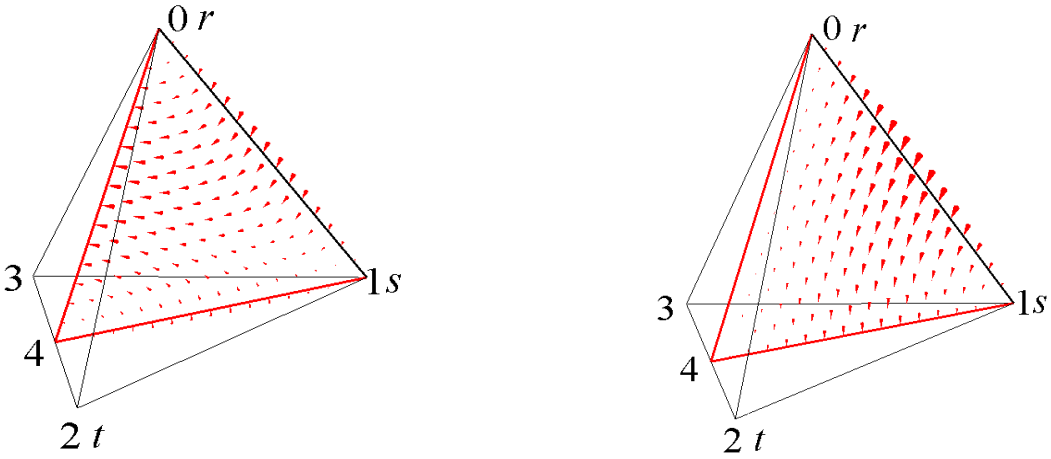

(c) (d)

Figure 51: The basis function distribution of the second order rotational space: (c) The basis function $\boldsymbol{c}_2$, face associated with node order rst ($r = 0$, $s = 1$, $t = 2$). (d) The basis function $\boldsymbol{d}_2$, face associated with node order rst ($r = 0$, $s = 1$, $t = 2$).

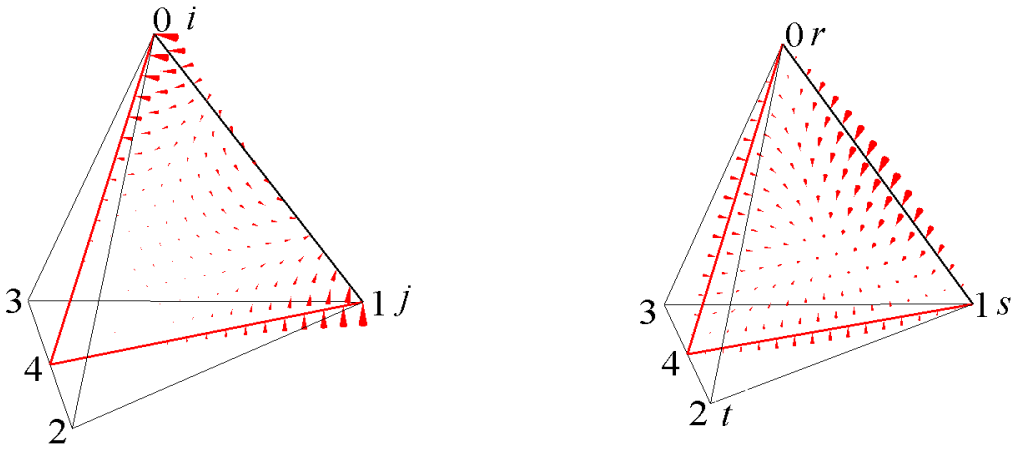

(e) (f)

Figure 52: The basis function distribution of the second order gradient space: (e) The basis function $\boldsymbol{e}_2$, edge related from node $i = 0$ to node $j = 1$. (f) The basis function $\boldsymbol{f}_2$, face associated with node order rst ($r = 0$, $s = 1$, $t = 2$).

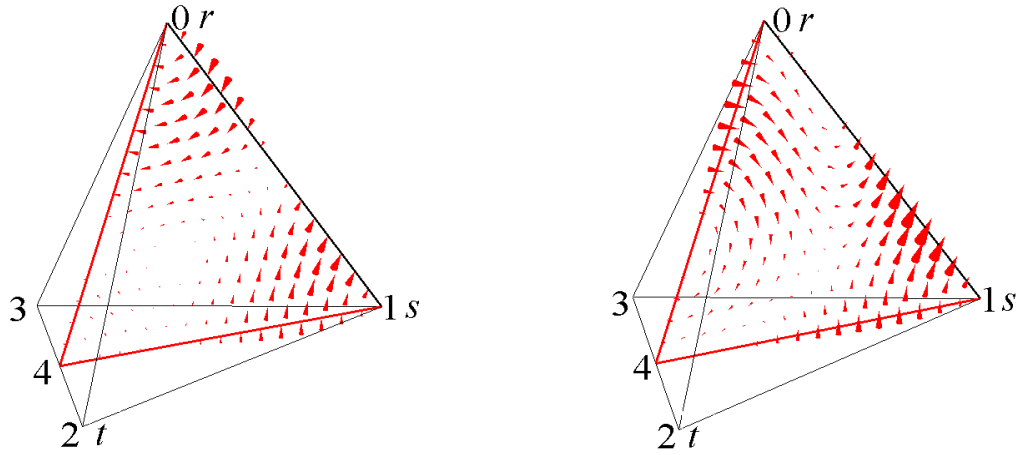

(g) (h)

Figure 53: The basis function distribution of the third order rotational space: (g) The basis function $\boldsymbol{g}_3$, face associated with node order rst ($r = 0$, $s = 1$, $t = 2$). (f) The basis function $\boldsymbol{h}_3$, face associated with node order rst ($r = 0$, $s = 1$, $t = 2$).

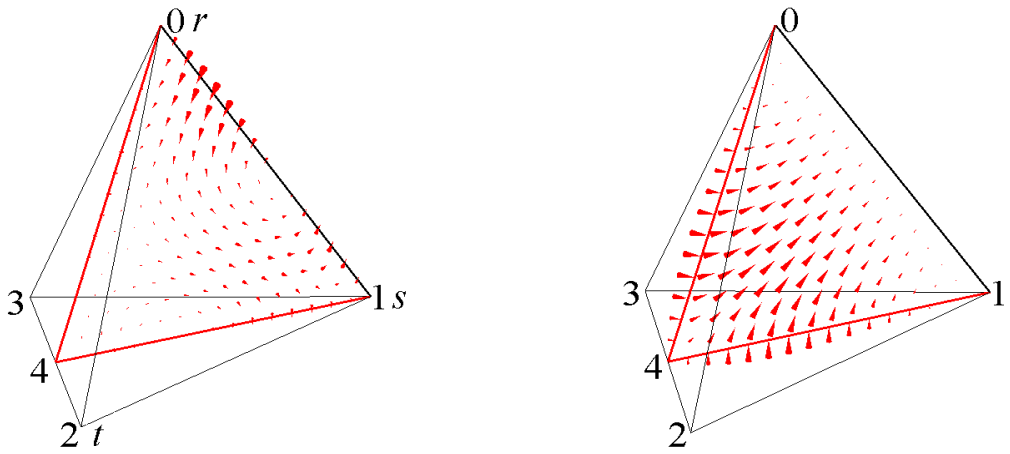

(i) (j)

Figure 54: The basis function distribution of the third order rotational space: (i) The basis function $\boldsymbol{i}_3$, face associated with node order rst ($r = 0$, $s = 1$, $t = 2$). (j) The basis function $\boldsymbol{j}_3$, volume associated with node order 0123.

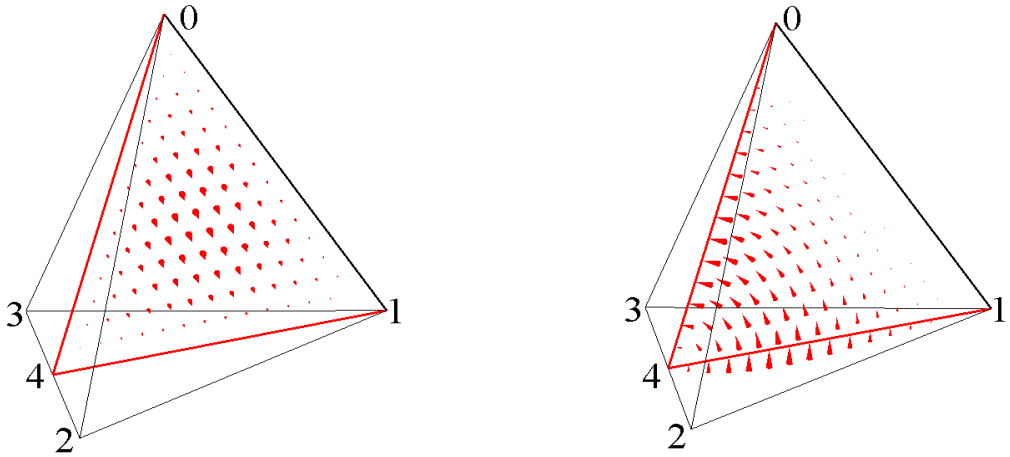

(k) (l)

Figure 55: The basis function distribution of the third order rotational space: (k) The basis function $\boldsymbol{k}_3$, volume associated with node order 0123. (l) The basis function $\boldsymbol{l}_3$, volume associated with node order 0123.

7.7 Numerical Results of the FE-BI Method

To specify the efficacy and accuracy of the analytical matrix elements and the global matrix assembly in the FE-BI method, numerical simulation results are displayed in this section. A convincing demonstration is to take advantage of a coated sphere testing case, where a PEC sphere is enclosed by a layer of dielectric material. The MIE scattering [Balanis, 1989] is a well known analytical RCS solution for this kind of problem. Good matching of the RCS of the numerical method and the analytical solution can verify the efficacy of the FE-BI method. With higher frequencies and finer mesh, more unknowns have to be solved. Moreover, testing cases of FE-BI in very large scale simulations are shown through the RCS of a bomber aircraft and also the Flamme aircraft, where both models are layered with dielectric materials. The 0th order FE-BI method has been verified in many published articles [Eibert, 2007, Eibert and Hansen, 1997, Tzoulis and Eibert, 2005b], it is used as a reference for HO. The efficiency of different orders of self-identified basis functions are presented for the FE-BI method. The sphere model, the bomber aircraft and the Flamme simulations were performed on a 64 bit work station with processor X 5690 @ 3.47 GHz (24 processors), installed memory (RAM) 192 GB.

7.7.1 Coated Sphere

For the coated sphere testing case, numerical RCS results from different orders of basis functions are compared with the MIE scattering results. The coated sphere contains a PEC sphere core with radius 1.0 m, the PEC core is enclosed with a dielectric layer with thickness 0.01 m. The properties of the dielectric layer are presented with $\epsilon_r = 2.5 - 0.5j$ and $\mu_r = 1.0$. The incident wave is 2 GHz and propagating toward the $+z$ direction and the electric field is 100 V/m along the x direction ($E_x = 100$ V/m). The results for the real components of the electric currents are shown in Fig. 56 and the RCS is shown in Fig. 57.

The same mesh was utilized for all orders of hierarchical basis functions, the mesh size was set 0.03 m, the mean edge length is 3.108 cm, with minimum edge length 1.0 cm and maximum edge length 5.787 cm. For 0th order, the total unknowns are 127 075. The running time was 37 877.3 s. For 1st order, the total unknowns are 254 150. The running time was 48 949.3 s. For 2nd order, the total unknowns are 608 750. The running time was 50 182.2 s. For 3rd order, the total unknowns are 913 125. The running time was 95 096.3 s. For 4th order, the total unknowns are 1 672 290. The running time was 85 375.7 s.

The numerical RCS results are compared with the MIE scattering results. The mesh size of the layered sphere is roughly $\lambda/3$ within the absorbing material layer. Compared with LO, the number of unknowns for HO is much larger. However, more accurate scattering results can be obtained by HO as shown in Fig. 57. The detailed analysis of the accuracy for different orders of basis functions is proposed in a later chapter.

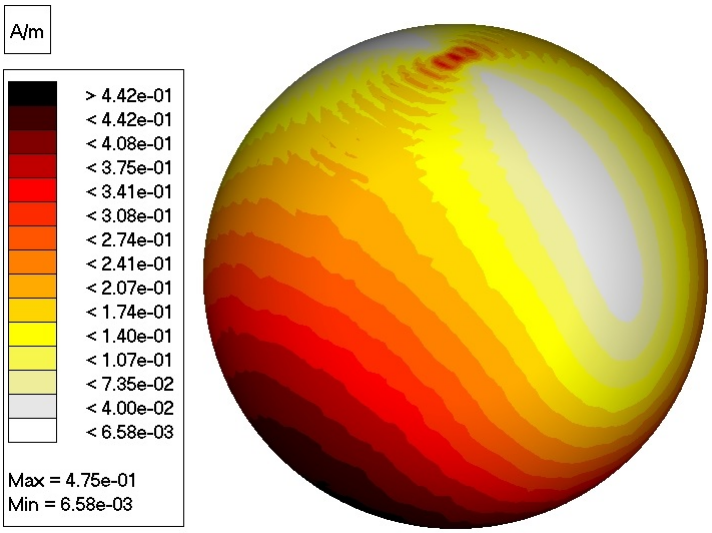

Figure 56: Surface electric current distribution of the coated sphere @ 2 GHz through the 0th order FE-BI method.

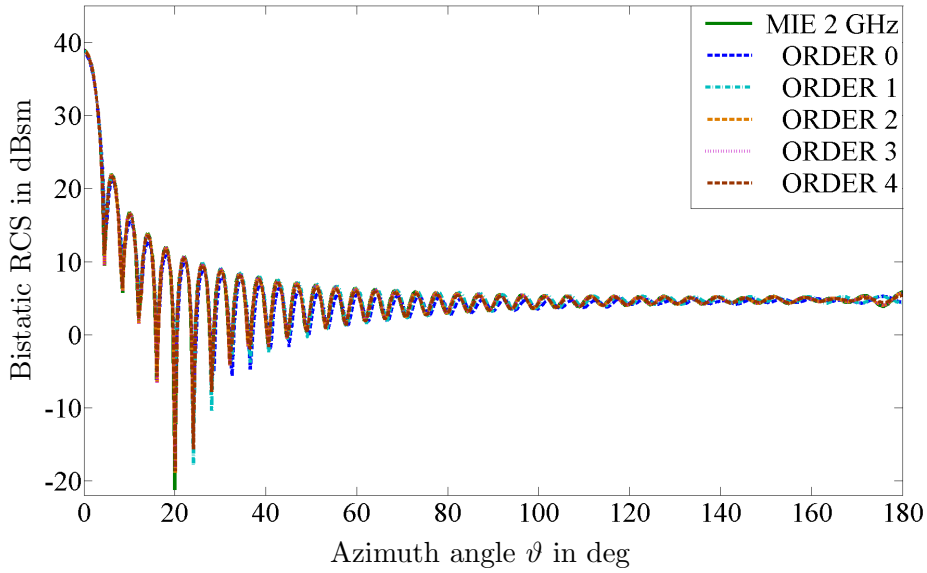

Figure 57: Bistatic RCS of a coated sphere @ 2 GHz on xz cut half plane ($\varphi = 0°$).

7.7.2 Stealth Bomber Aircraft with Absorbing Materials

A stealth B2 aircraft is utilized as an example for EM simulations with the FE-BI method for very large scale applications. The B2 aircraft is located in the xz plane, with nose heading along the $+z$ axis, as shown in Fig. 58. The B2 is enclosed by a layer of lossy dielectric material with thickness approximately 1 cm. The permittivity of the lossy dielectric material is $\epsilon_r = 1.21 - 10j$ and the permeability is $\mu_r = 1$. The simulation frequency is 1.5 GHz. The incident plane wave propagates towards the $-z$ direction, with electric field ($E_x = 100$ V/m). To study the absorbing effects of the lossy dielectric material, a PEC B2 aircraft simulation with the BI method is utilized for comparison.

Figure 58 shows the real components of the surface electric currents for the covered B2. The bistatic RCS of the PEC and the layered B2 aircraft in different cut planes is shown in Figs. 59 - 61. The normalized polar bistatic RCS of the PEC and the layered bomber in different cut planes is shown in Figs. 62 - 64. The PEC B2 is simulated through BI with 4th order of self-identified basis functions, the layered B2 is simulated through FE-BI with 0th, 1st, 2nd, 3rd and 4th order of self-identified basis functions correspondingly. The 0th order has been proven accurate with a finer mesh. The 4th order basis functions for the PEC B2 have also been verified as compared with the 0th order in Figs. 34 - 40. So, the 4th order PEC simulation result is utilized as a reference. The RCS comparison shows that most of the input power goes over the bomber.

The simulation data summary for the layered and PEC B2 is shown in Table 5. TM is the type of model, TB is the type of bases, D is the mesh size set for the model, $\bar{\mathrm{D}}$ is the mean mesh edge length, D_{min} is the minimum mesh edge length, D_{max} is the maximum mesh edge length, N is the total number of unknowns, N_J is the number of BI electric current unknowns, N_M is the number of BI magnetic current unknowns, L is the number of levels for MLFMM, PM is the peak memory consumption and T is the run time of the simulation.

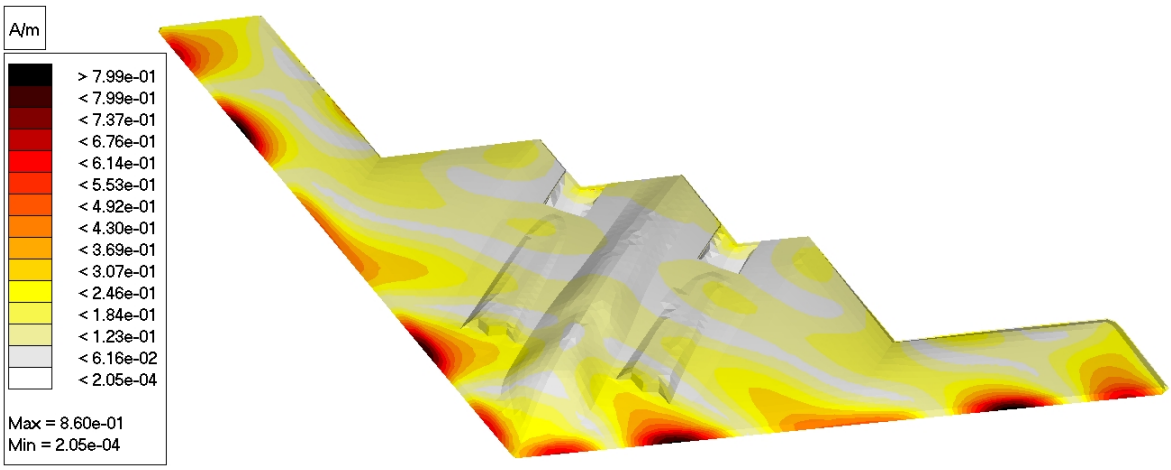

Figure 58: Covered bomber real components of surface electric currents @ 1.5 GHz.

Table 5: The Simulation Results for the PEC and Layered B2

TM	TB	D (m)	$\bar{D}$ (cm)	D_{min} (cm)	D_{max} (cm)	N	N_J	N_M	L	PM (MB)	T (s)
Layered	R^1	0.01	0.980	0.033	2.172	56 489	17 847	16 630	4	690.960	28 640.6
Layered	$R^1 + G^1$	0.01	0.980	0.033	2.172	112 977	35 694	33 260	4	2 084.113	33 161.0
Layered	$R^1 + G^1 + R^2$	0.01	0.980	0.033	2.172	269 063	59 490	55 466	4	5 392.330	48 986.8
Layered	$R^1 + G^1 + R^2 + G^2$	0.01	0.980	0.033	2.172	403 595	89 235	83 199	4	11 145.910	80 806.3
Layered	$R^1 + G^1 + R^2 + G^2 + R^3$	0.01	0.980	0.033	2.172	637 724	124 929	116 508	4	21 132.31	141 412.2
PEC	$R^1 + G^1 + R^2 + G^2 + R^3$	0.01	1.009	0.253	2.172	123 900	123 900	0	4	10 107.25	75 945.1

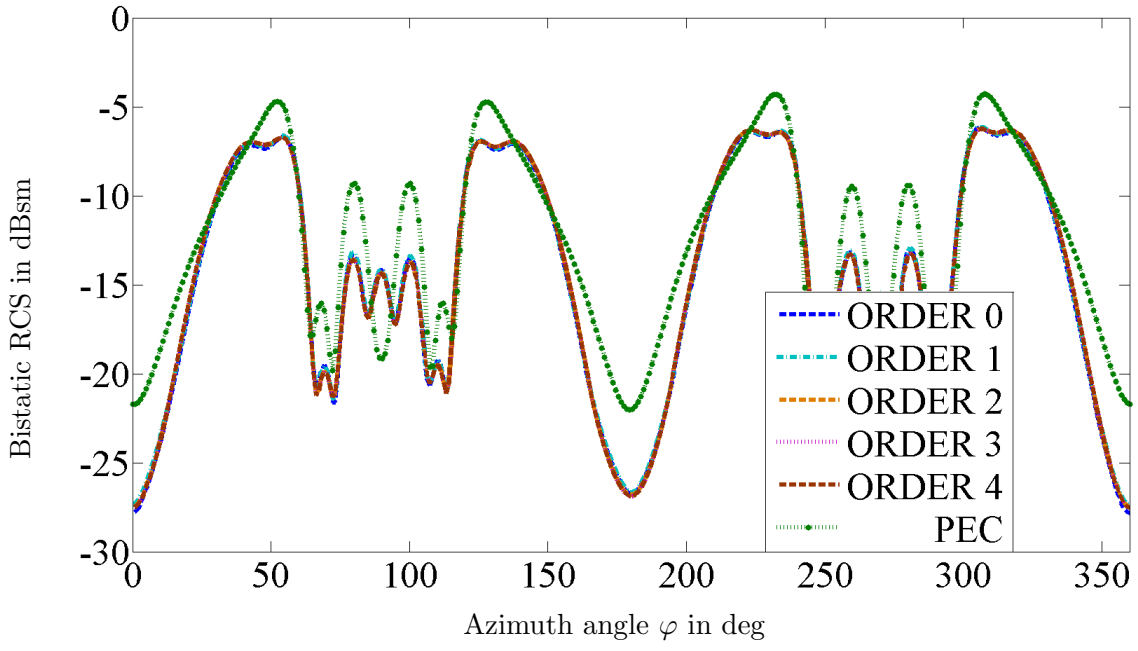

Figure 59: Bistatic RCS of covered bomber @ 1.5 GHz on xy cut plane ($\vartheta = 90°$).

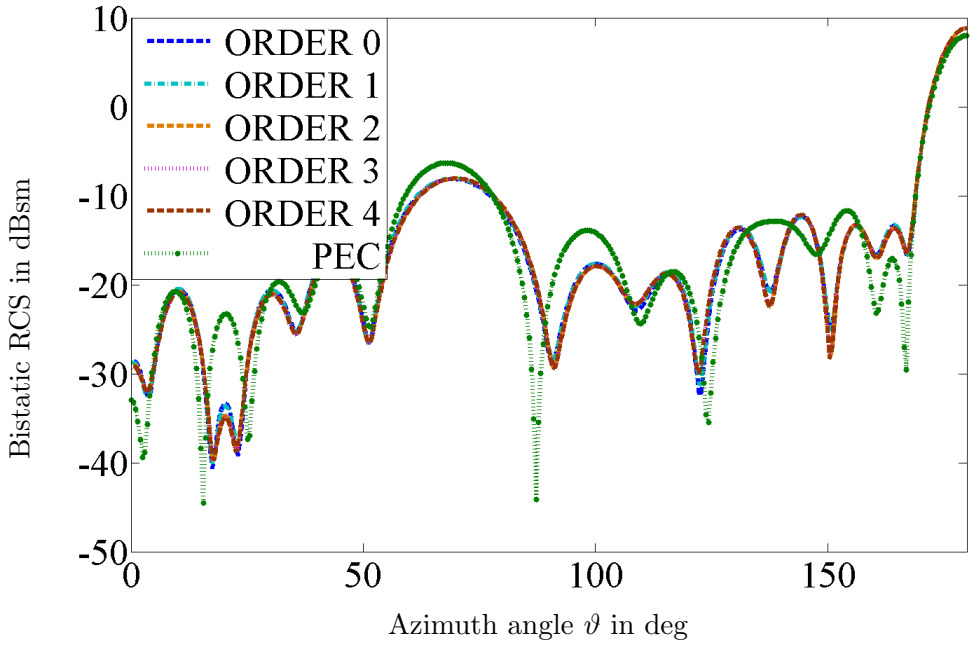

Figure 60: Bistatic RCS of covered bomber @ 1.5 GHz on xz cut half plane ($\varphi = 0°$).

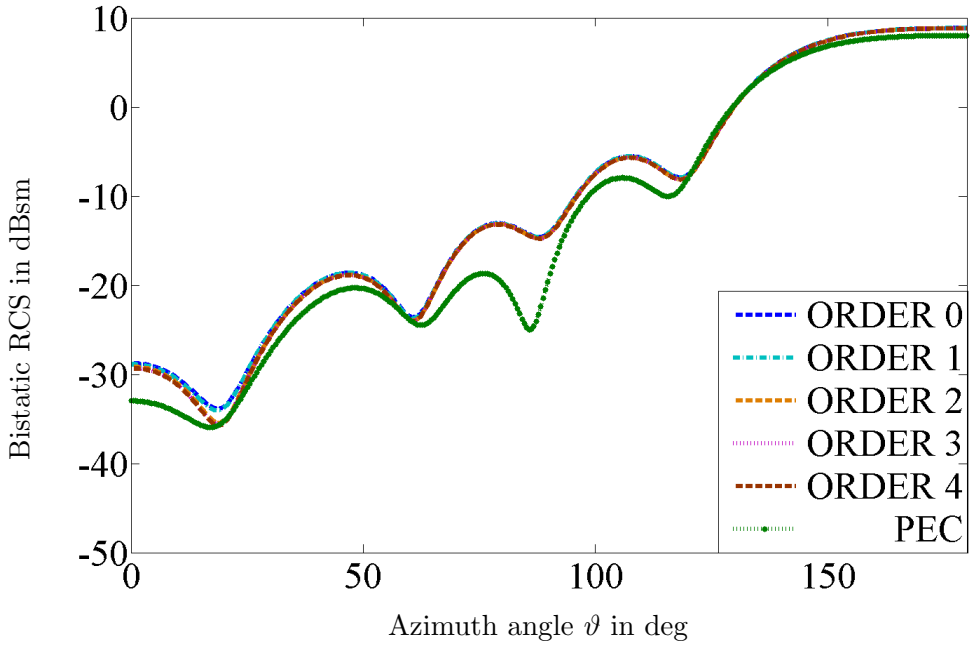

Figure 61: Bistatic RCS of covered bomber @ 1.5 GHz on yz cut half plane ($\varphi = 90°$).

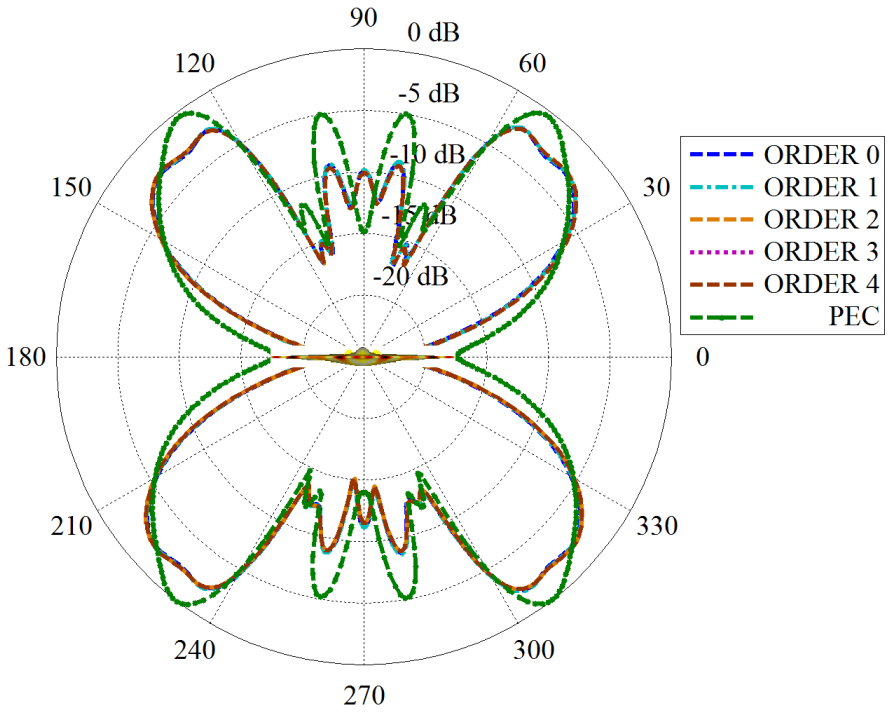

Figure 62: Normalized polar bistatic RCS of covered bomber @ 1.5 GHz on xy cut plane.

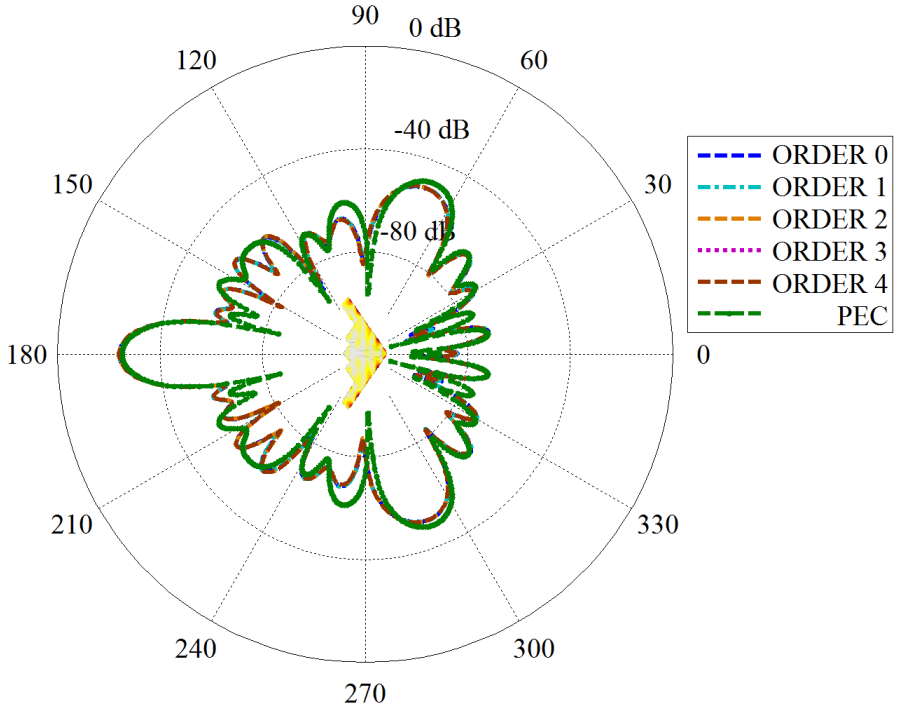

Figure 63: Normalized polar bistatic RCS of covered bomber @ 1.5 GHz on xz cut plane.

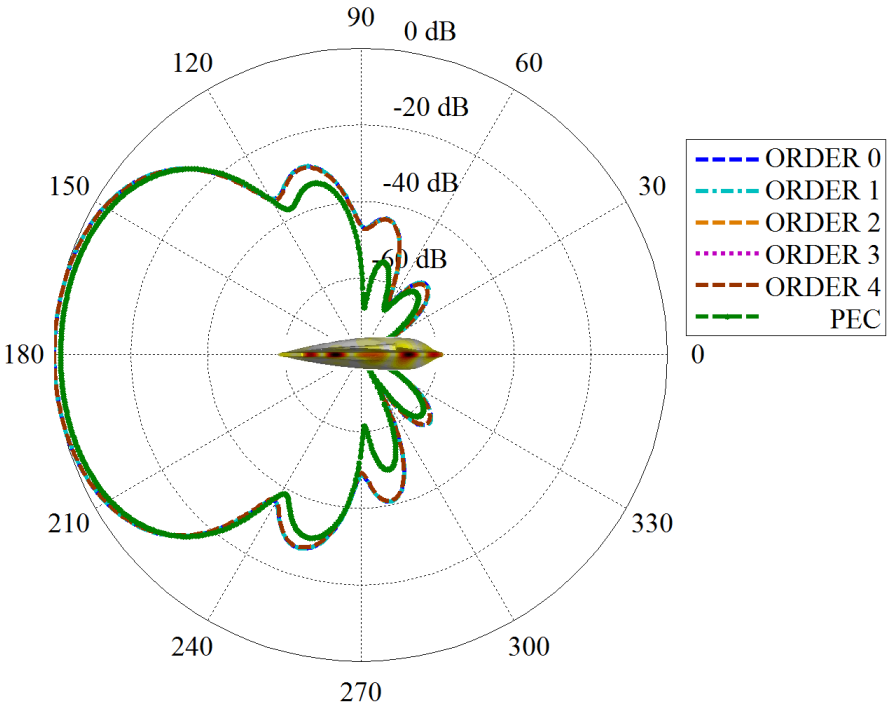

Figure 64: Normalized polar bistatic RCS of covered bomber @ 1.5 GHz on yz cut plane.

7.7.3 Flamme with Absorbing Materials

The layered Flamme case is another application of the FE-BI method for very large scale simulation. The Flamme is located in the xy plane, with nose heading along the $+x$ axis, as shown in Fig. 65. The Flamme is enclosed by a layer of lossy dielectric material with thickness of approximately 1 cm. The permittivity of the dielectric material is $\epsilon_r = 1.21 - 10j$ and the permeability is $\mu_r = 1$. The simulation frequency is 1.0 GHz. The incident plane wave propagates towards $-x$ direction, with electric field ($E_z = 100$ V/m). To visualize absorbing effects of the lossy dielectric material, a PEC Flamme simulated by BI is utilized for comparison.

The real components of the equivalent surface electric currents on the layered Flamme are shown in Fig. 65. The bistatic RCS of the layered Flamme on different cut planes is shown in Figs. 66 - 69. The normalized polar bistatic RCS of the layered Flamme on different cut planes is shown in Figs. 70 - 72. The layered Flamme is simulated through FE-BI with 0th, 1st, 2nd, 3rd and 4th orders of self-identified basis functions. As the efficacy of LO basis functions with finer mesh has been verified, here the 0th order of FE-BI for the layered Flamme together with the 4th order of BI for the PEC flamme simulations are used as references. The RCS comparison shows that most of the input power goes over the layered Flamme.

The simulation data summary for the layered and PEC Flamme is shown in Table 6. TM is the type of model, TB is the type of bases, D is the mesh size set for the model, $\bar{\mathrm{D}}$ is the mean mesh edge length, D_{min} is the minimum mesh edge length, D_{max} is the maximum mesh edge length, N is the total number of unknowns, N_J is the number of BI electric current unknowns, N_M is the number of BI magnetic current unknowns, L is the number of levels for MLFMM, PM is the peak memory consumption and T is the run time of the simulation.

Table 6: The Simulation Results for the PEC and Layered Flamme

TM	TB	D (m)	$\bar{\mathrm{D}}$ (cm)	D_{min} (cm)	D_{max} (cm)	N	N_J	N_M	L	PM (MB)	T (s)
Layered	R^1	0.02	1.783	0.065	3.933	626 498	213 855	180 488	6	8 111.168	410 844.5
Layered	$R^1 + G^1$	0.02	1.783	0.065	3.933	1 252 996	427 710	360 976	6	25 496.380	484 916.1
Layered	$R^1 + G^1 + R^2$	0.07	5.846	0.405	15.216	244 347	58 460	50 128	4	5 609.957	60 852.5
Layered	$R^1 + G^1 + R^2 + G^2$	0.07	5.846	0.405	15.216	366 521	87 690	75 192	4	11 669.280	94 771.3
Layered	$R^1 + G^1 + R^2 + G^2 + R^3$	0.07	5.846	0.405	15.216	577 289	122 766	105 372	4	22 144.43	148 342.1
PEC	$R^1 + G^1 + R^2 + G^2 + R^3$	0.07	5.924	0.405	15.216	118 104	118 104	0	4	10 140.52	57 656.8

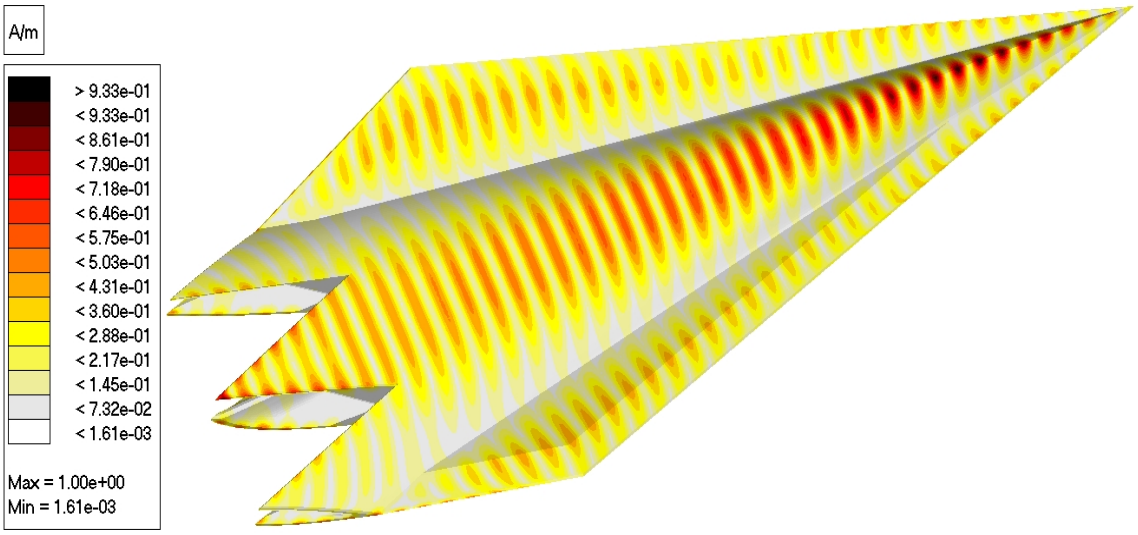

Figure 65: Layered Flamme real components of surface electric currents @ 1 GHz.

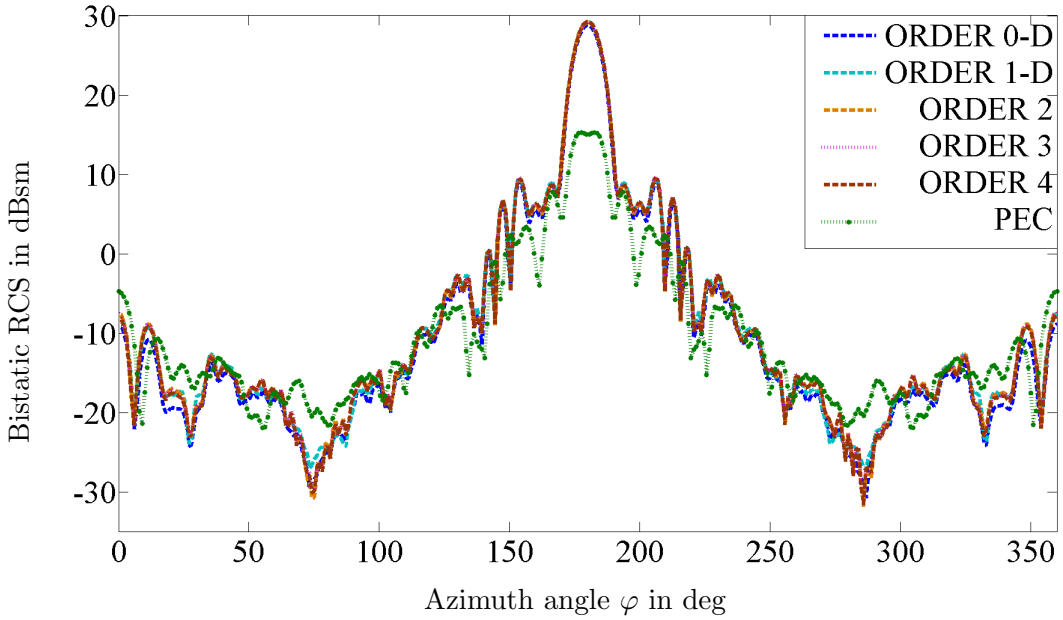

Figure 66: Bistatic RCS of layered Flamme @ 1 GHz on xy cut plane ($\vartheta = 90°$).

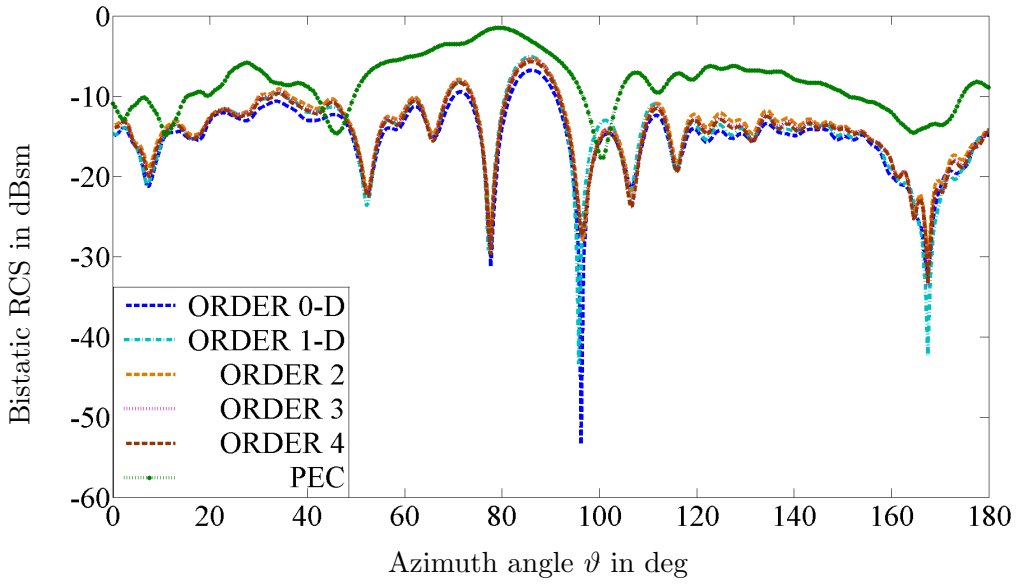

Figure 67: Bistatic RCS of layered Flamme @ 1 GHz on xz cut half plane ($\varphi = 0°$).

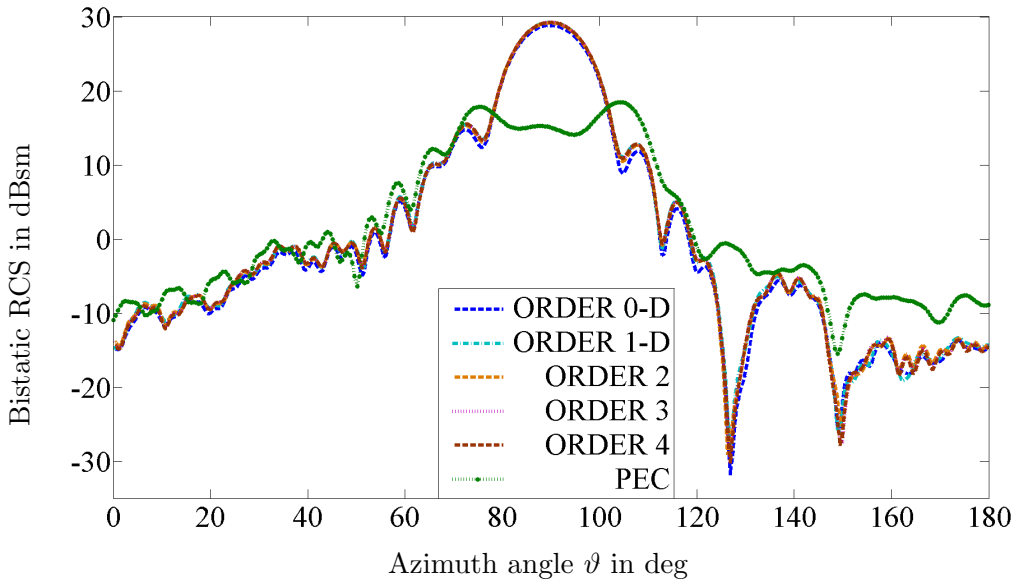

Figure 68: Bistatic RCS of layered Flamme @ 1 GHz on xz cut half plane ($\varphi = 180°$).

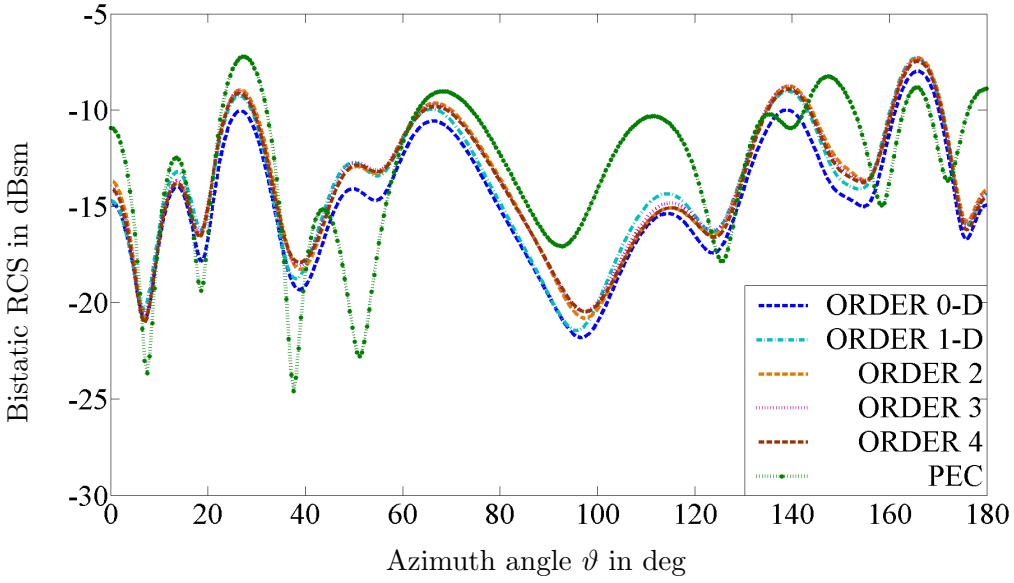

Figure 69: Bistatic RCS of layered Flamme @ 1 GHz on xy cut half plane ($\varphi = 90°$).

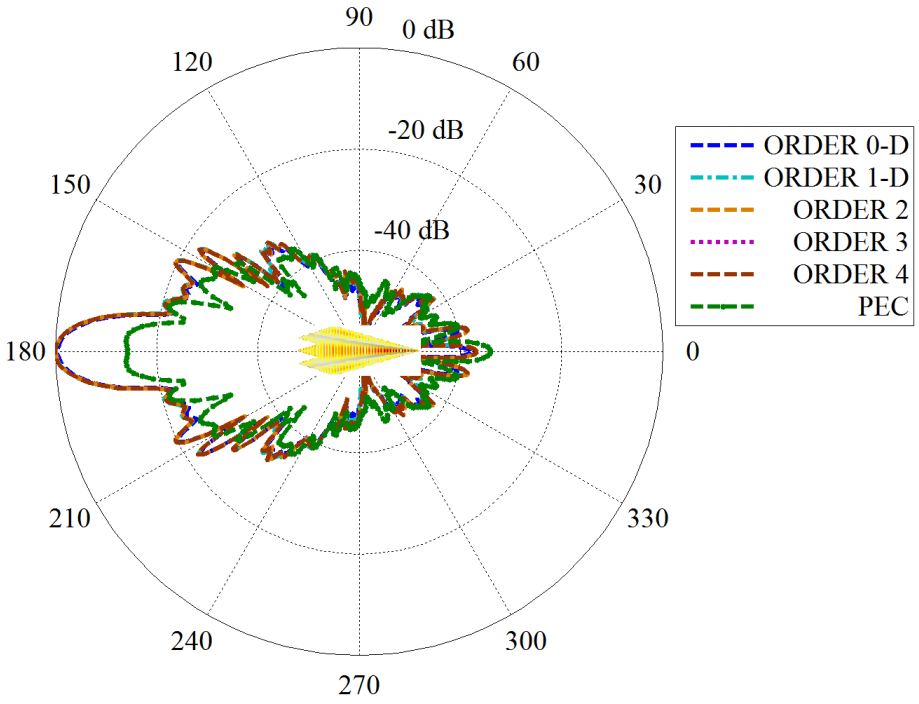

Figure 70: Normalized polar bistatic RCS of layered Flamme @ 1 GHz on xy cut plane.

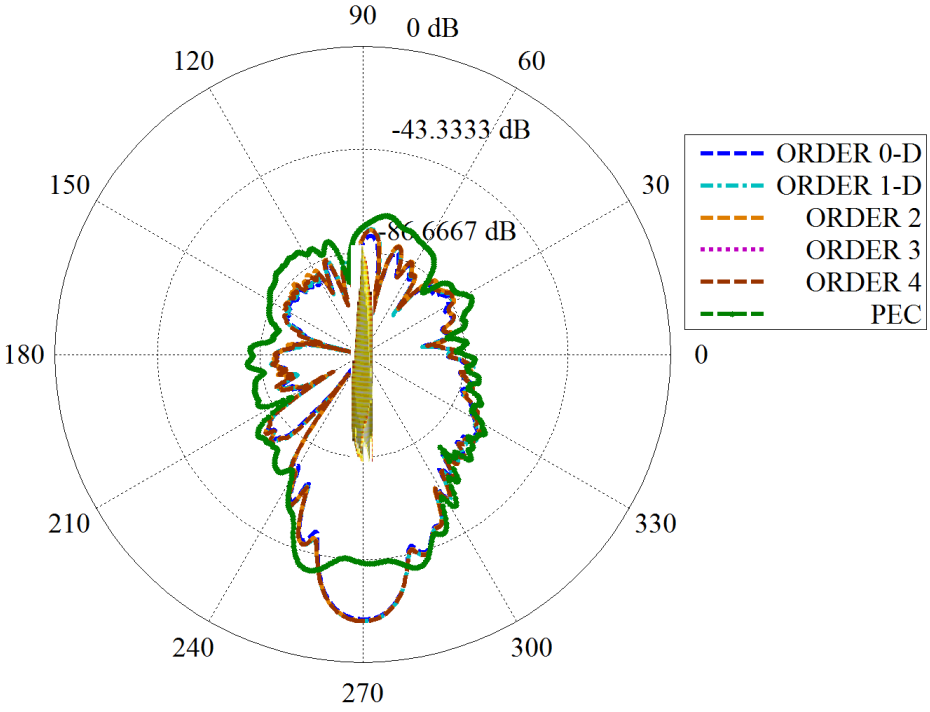

Figure 71: Normalized polar bistatic RCS of layered Flamme @ 1 GHz on xz cut plane.

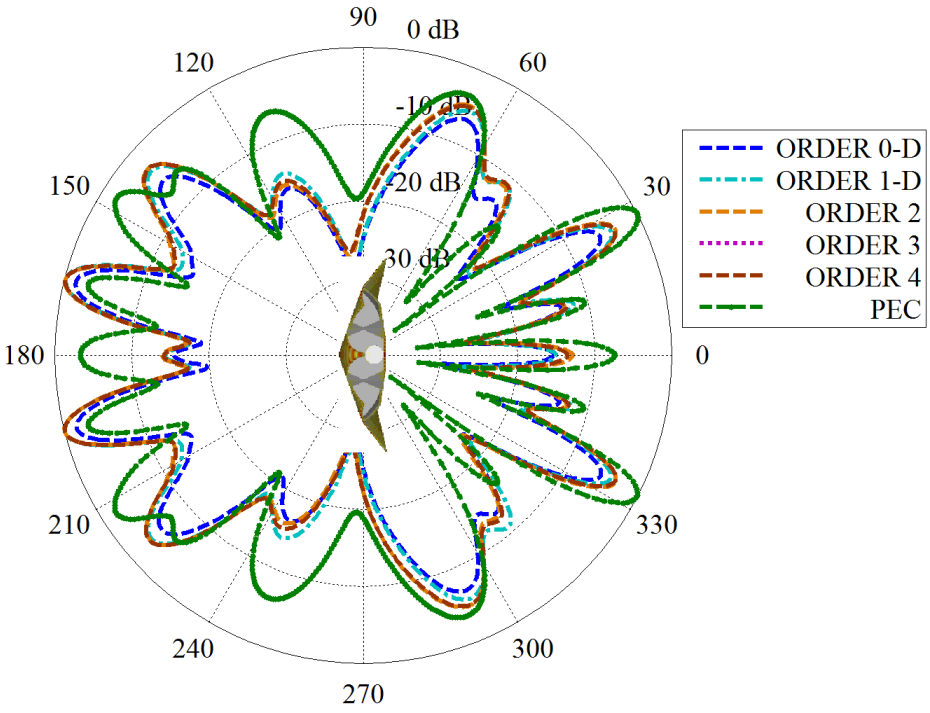

Figure 72: Normalized polar bistatic RCS of layered Flamme @ 1 GHz on yz cut plane.

7.8 Conclusion

Self-identified hierarchical 3D vector basis functions were generated for the finite element method (FEM) and 2D vector basis functions were utilized for the boundary intetgral (BI). Then, the hybrid finite element boundary integral (FE-BI) technique was obtained for EM simulations with hierarchical spaces. For the FEM, analytical solutions for the FE matrix elements have been presented up to 4th order. Self-identified basis functions are feasible for the FEM and effectively compatible with BI. Going from 1st to 4th order, the FE-BI method allows for a mesh size increasing from $\lambda/8$ up to $\lambda/3$. From coated sphere testing results, good accuracy was found, the Bomber and Flamme simulations proved that the FE-BI method based on self-identified basis functions can be utilized for very large scale simulations.

8 Accuracy Analysis of the Finite Element Boundary Integral Method

Numerical electromagnetic (EM) simulations for arbitrarily shaped objects play a significant role in microwave components design. An accuracy analysis of numerical techniques is required to prove the efficacy and for validation of EM simulations. General methods to evaluate the accuracy of the numerical algorithms are proposed. References are selected and compared with numerical simulation results. When the numerical results agree with the references, the algorithms are proven to be valid. Then, an accuracy analysis according to the reference results is employed for the algorithm evaluations.

The approaches to select the reference results are important for an accuracy analysis. Convincing selections of references contain analytical solutions to some simple structural models, the measurement results of the physical objects, the simulation results from different verified algorithms, and so on.

8.1 The Definition of Root Mean Square (RMS) Error

The FE-BI method is very efficient in electromagnetic simulations of PEC objects and also PEC objects coated with dielectric materials. For the PEC models, the electric field is zero inside the PEC objects. The bistatic radar cross section (Bi-RCS) is utilized to illustrate the efficiency and the accuracy of the vector hierarchical basis functions for MoM. For PEC together with dielectric material models, the electric and magnetic fields can be computed inside the volumes of the dielectric materials. So the distributions of the electric and magnetic fields can also be utilized to evaluate the accuracy of FE-BI with vector hierarchical basis functions. The Bi-RCS is produced by the reconstructed electric and magnetic currents, where the currents are computed through MoM. The electric and magnetic fields are distributed inside the volume of the dielectric materials, where the fields are computed through FEM. So an accurate Bi-RCS can also prove the efficacy and analyze the efficiency of the currents on the outside surfaces of the objects. An accurate field computation can be utilized for the accuracy analysis of FE-BI inside the volume of the dielectric materials. In order to evaluate the accuracy through the Bi-RCS and electric and magnetic fields, the root mean square (RMS) error is utilized to measure the accuracy of the solutions. The RMS is defined as

$$RMS = \sqrt{\frac{1}{N}\sum_{i=1}^{N} |\Phi_T - \Phi_R|^2}, \tag{8.1.1}$$

where N is the total number of testing points. For the Bi-RCS, N is the number of sampling directions. For electric and magnetic fields, N is the number of sampling points inside the volume of the dielectric materials. Φ_R are the reference values from the reference solutions, including the results from the physical objects, the analytical solutions, the measurement results, the commercial software simulation results or the results from the classic technologies with very fine mesh. Φ_T are the computational results from the FE-BI method with vector hierarchical basis functions. For the surface integral equation solvers,

the normalized residual is set as 10^{-4} and it is usually accurate enough for MoM to obtain accurate simulation results. For the FE-BI method, the normalized residual is set as 10^{-7} and it is accurate enough to obtain accurate simulation results for large scale EM simulations. If a different normalized residual value is utilized for iterative solvers, it will be illustrated in the numerical results. All simulations, unless exceptional illustration, are computed with an X 5690 @ 3.47 GHz workstation with a total memory of 192 GB.

8.2 Accuracy Analysis Against Analytical Models

Analytical models are effective for testing the efficacy of numerical EM solutions. The electric and magnetic fields are exactly known and these results can be utilized as references for new algorithms. A simple analytical solution is given for objects filled with the same material as the surrounding space. The excitation of these models can be plane waves. Then, the electric and magnetic fields inside the object volumes are easy to compute through the plane wave propagation. The numerical results are computed through the FE-BI method. The fields inside the object volume are determined by the expansions of the vector basis functions multiplied with the corresponding solved coefficients. The numerical results are compared with the reference results for the accuracy evaluations.

The *RMS* electric field error is utilized to evaluate the accuracy of the FE-BI method as proposed in (8.1.1). In the selected models, the reference results $\boldsymbol{\Phi}_R(\boldsymbol{r})$ and the computation results $\boldsymbol{\Phi}_T(\boldsymbol{r})$ are vector fields, so the *RMS* electric field error is reorganized as

$$RMS = \sqrt{\frac{1}{N}\sum_{i=1}^{N} |\,\boldsymbol{\Phi}_T - \boldsymbol{\Phi}_R|^2}\,, \tag{8.2.1}$$

where N is the total number of testing points inside the object volumes. The accuracy of the FE-BI method depends on the working frequencies. For LO, fine meshes are required, but for HO, the mesh size can be extended. So the *RMS* electric field error with different frequencies can illustrate the accuracy and performance of the FE-BI method according to the relevant mesh size. The *RMS* electric field error with the same frequency also shows the accuracy improvements for HO in the FE-BI method. An air block and an air sphere are selected as the models for the accuracy analysis.

8.3 The *RMS* Electric Field Error for the Air Block

The air block model is efficient to study the accuracy of the FE-BI method. The faces of the blocks are planar, so the planar triangular meshes of the faces do not influence the accuracy of the model. The outside boundary surfaces are accurately illustrated by the boundary meshes. To study the accuracy of the FE-BI method for the relevant mesh size, the *RMS* electric field error in (8.2.1) with increasing frequencies is shown. So a fixed mesh of an air block is selected. The input plane waves with different frequencies propagate in the same direction. The EM simulations of the FE-BI method and the *RMS* electric field error are computed separately for different frequencies, the field results are computed within the FEs and compared with the physical model results.

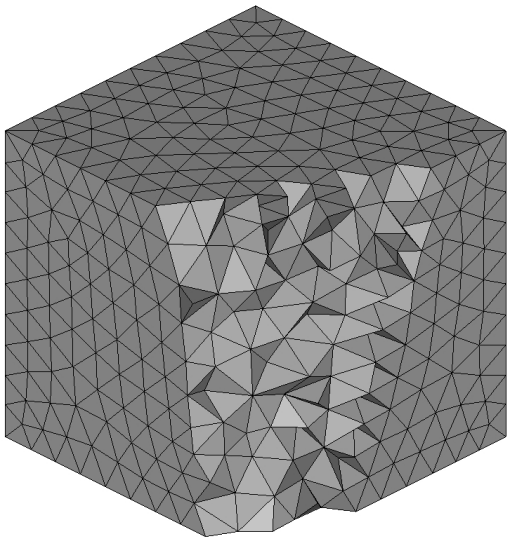

Figure 73: Covered volume mesh of the air cube with mesh size 0.1 m, cube edge length 1 m.

Figure 73 displays the mesh of the cube and parts of the mesh are masked. The edge length of the cube is 1 m. The surfaces of the cube are meshed into triangles and the volume is meshed into tetrahedra. The mesh size is set 0.1 m, the minimum edge length is 6.143 cm, the maximum edge length is 19.072 cm and the mean edge length is 11.713 cm. The excitation plane wave is polarized along the x-axis, $\boldsymbol{E}_x = 100$ V/m, propagates from the bottom towards the top of the cube. The air cube model requires the material inside the cube volume to be the free space, the permittivity ϵ_r and the permeability μ_r inside the tetrahedral FEs are set as $\epsilon_r = \mu_r = 1.0$.

The testing points are distributed uniformly inside the cube volume, where the electric fields are evaluated. In each dimension of the cube, n sampling points are utilized, so the total number of sampling points is $N = n^3$. The positions of the testing points are represented as $\boldsymbol{r}$ in Cartesian coordinates. Then, the reference results on the distributed points $\boldsymbol{r}$ are written as

$$\boldsymbol{E}(\boldsymbol{r}) = \boldsymbol{E}_0 e^{-j\boldsymbol{k}_0 \cdot \boldsymbol{r}}\,, \tag{8.3.1}$$

where $\boldsymbol{E}_0$ is the amplitude vector of the plane wave, $\boldsymbol{k}_0$ is the wave number vector in free space. It represents the propagation direction of the plane wave, $k_0 = |\boldsymbol{k}_0| = \omega\sqrt{\epsilon_0\mu_0}$ is the wave number in free space. ϵ_0 and μ_0 are the permittivity and the permeability of the free space, $\omega = 2\pi f$, where f is the frequency of the plane wave.

With the position $\boldsymbol{r}$, the testing point can be located in the corresponding tetrahedron in the mesh shown in Fig. 73. From the geometrical information of the tetrahedron, the corresponding simplex coordinates of $(\lambda_1, \lambda_2, \lambda_3, \lambda_4,)$ can be computed for $\boldsymbol{r}$. With the FE basis functions in Table 4 and the solved unknowns by FE, the numerical results of the FE-BI method can be obtained through the expansion of the electric field in (6.2.2.1). Then, the *RMS* electric field error in (8.2.1) can be computed with the electric field from (8.3.1)

and compared with the numerical electric field from the FE-BI method.

The *RMS* electric field error is shown in Fig. 74 with changing frequency for different orders of basis functions. The *RMS* electric field error is evaluated in dB and the frequencies are shown in logarithmic scale. The sampling points in each dimension of the cube is $n = 50$, so the total number of sampling points is $N = 125\,000$. It is shown in Fig. 74 that the accuracy of all orders of basis functions increases with decreasing frequency.

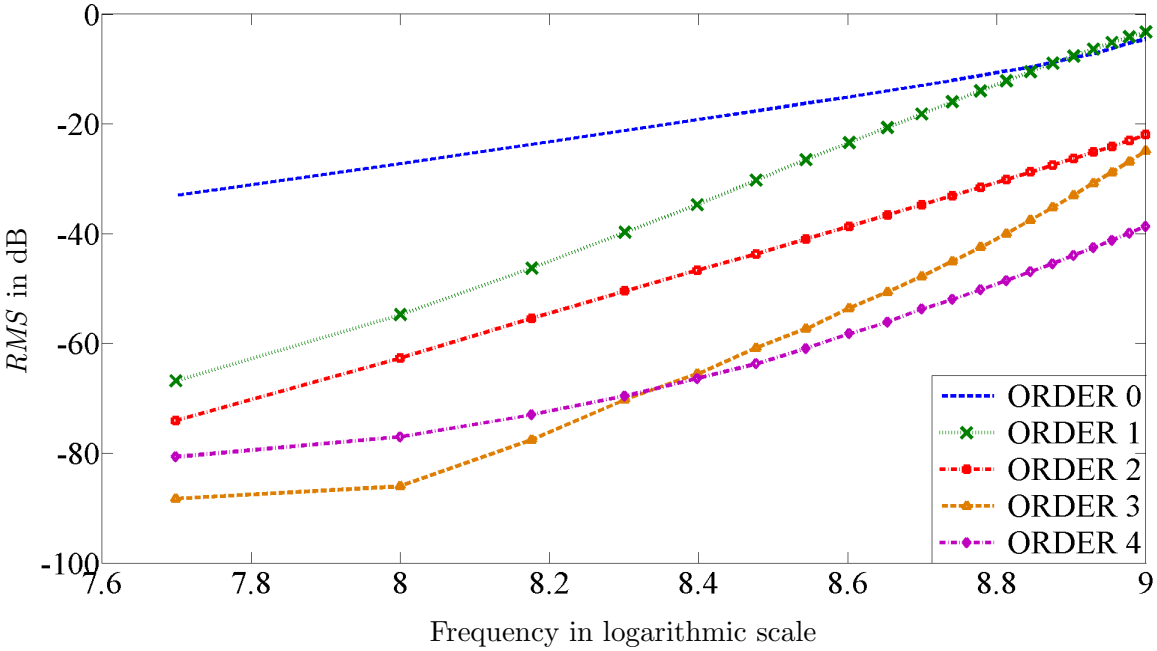

Figure 74: The *RMS* electric field error in dB versus the logarithmic frequency for the air cube.

8.4 The *RMS* Electric Field Error for Air Spheres

The air sphere is also utilized to study the accuracy of the FE-BI method. The spherical surface is curvilinear, so the planar triangular mesh cells are required to be sufficiently small for the accuracy of the model. To study the accuracy of the FE-BI method, the *RMS* in (8.2.1) with increasing frequencies are also shown. A fixed mesh of an air sphere is selected. The input plane waves with different frequencies propagate in the same direction. The EM simulations of the FE-BI method and the *RMS* are computed separately for different frequencies, the simulation results are computed within the FEs and compared with the analytical model results.

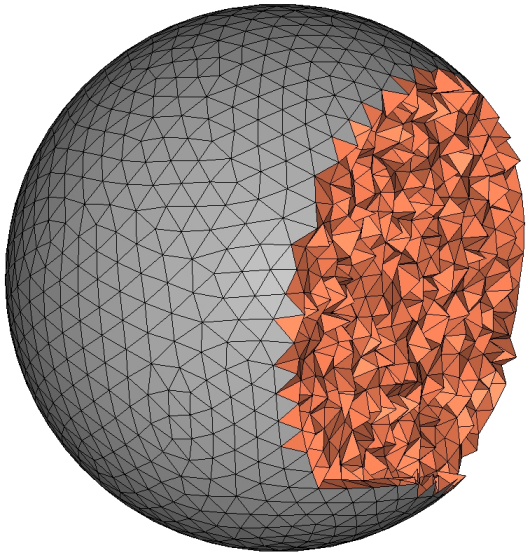

Figure 75: Covered volume mesh of the air sphere with mesh size 0.1 m, radius 1 m.

Figure 75 displays the mesh of an air sphere and parts of the mesh are masked. The radius of the sphere is 1 m. The surface of the sphere is meshed into triangles and the volume is meshed into tetrahedra. The mesh size is set to 0.1 m, the minimum edge length is 3.436 cm, the maximum edge length is 16.194 cm and the mean edge length is 10.419 cm. The input plane waves are polarized along the x-axis, $\boldsymbol{E}_x = 100$ V/m and propagate from the bottom towards the top of the sphere. The air sphere physical model requires the material inside the spherical volume to be free space, the permittivity ϵ_r and the permeability μ_r inside the tetrahedral FEs are set as $\epsilon_r = \mu_r = 1.0$.

The testing points are distributed inside the spherical volume, where the electric field is evaluated. The testing points are illustrated through a Spherical Coordinate System $(\rho, \vartheta, \varphi)$, where ρ is the radial distance, ϑ is the polar angle and φ is the azimuthal angle. n_ρ is the number of sampling points along ρ, n_ϑ is the number of sampling points in ϑ and n_φ is the number of sampling points in φ. So the total number of sampling points is $N = n_\rho n_\vartheta n_\varphi$. The positions of the testing points in Cartesian coordinates are represented as $\boldsymbol{r} = (\rho \sin\vartheta \cos\varphi, \rho \sin\vartheta \cos\varphi, \rho \cos\vartheta)$. Then, (8.3.1) is also utilized as reference result.

The *RMS* electric field error is shown in Fig. 76 with changing frequencies for different orders of basis functions. The *RMS* electric field error is evaluated in dB and the frequencies are computed in logarithmic scale. The sampling points in all dimensions of the sphere are $n_\rho = 30$, $n_\vartheta = 91$, $n_\varphi = 180$. The total number of sampling points is $N = 491\,400$. It is shown in Fig. 76 that the accuracy of all orders of basis functions increases with the decreasing frequencies. A nearly linear accuracy performance of *RMS* electric field error is obtained with respect to the selected frequencies in logarithmic scale. In general, higher order basis functions achieve higher accuracy at some selected frequencies. Better accuracy is obtained at lower frequencies for each order basis function. The performance of LO and HO basis functions is clearly shown for the selected frequencies. Further improvement in accuracy can also be obtained with better Gauss Legendre quadrature performance.

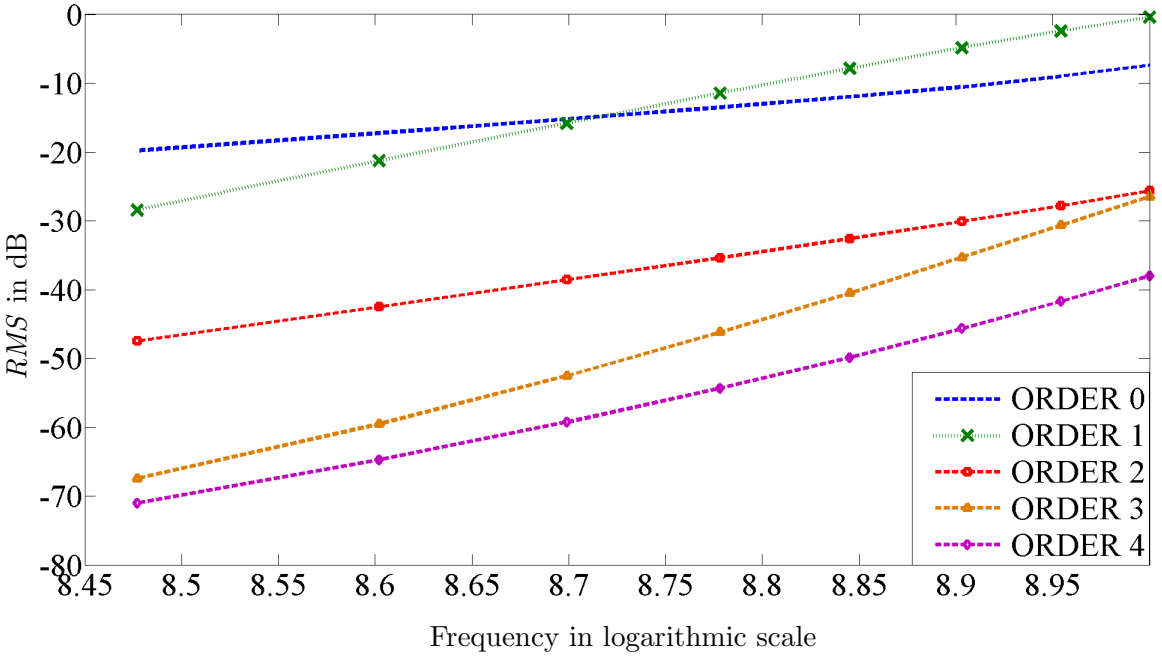

Figure 76: The *RMS* electric field error in dB versus the logarithmic frequencies for the air sphere.

9 Summary and Conclusion

The hybrid FE-BI formulations have been proven to be efficient and accurate for radiation and scattering simulations in electromagnetics, where the variational formulation for the method of finite elements and the governing integral equations for the method of moments have been converted into a system of linear equations. The FE method utilizes the Ritz approach with tetrahedral hierarchical vector basis functions and analytical solutions for system matrices have been obtained. The BI method utilizes the method of moments, where MoM employs the Galerkin process with triangular hierarchical vector basis functions and treats singularities in mutual coupling integrals adaptively. The MLFMM with spherical harmonics expansions has also been implemented into fast iterative solvers for unknown computations through linear equations, where the FE-BI method has been considered powerful and versatile for simulations of antennas and electromagnetic scattering for arbitrarily shaped components.

The accuracy of the FE-BI method relies on both FE and BI. High accuracy of FE can be obtained as the system matrices are computed analytically. The accuracy of MoM solutions of integral equations are significantly dependent on the precision of mutual couplings, including singular kernels in near couplings. Special numerical treatments of singular integrals are required, as quadrature rules are not applicable to neighboring source and testing domains directly. A fully numerical treatment of singular integrals inherits the adaptive singularity cancellation technique and good efficiency and accuracy are also obtained. For singularity cancellation techniques, a new family of radial-angular-R^n transformations have been proposed in this work based on the variable separation method. General solutions are provided for the variable separation method. Thus, a family of transformation schemes are obtained for different orders of singularity cancellations. The 1st order transformation schemes are valid for $1/R$ - type singular kernels, 2nd and 3rd order transformation schemes are effective for $\boldsymbol{R}/R^3$ - type singular kernels. Moreover, good performance of radial-angular-R^n transformations has also been obtained for deformed triangles. High efficiency and accuracy are acquired by the new transformation schemes. Additionally, for the inside projection configuration, traditional transformation schemes are sensitive to the projection height of the observation point to the source domain plain. For extremely small projection height, a large number of sampling points are required for the traditional schemes to achieve good accuracy. The new proposed transformations successfully and efficiently cancel out the effects of the projection height and excellent accuracy convergence has been obtained with a significantly limited number of quadrature points. Improved efficiency and accuracy of near-coupling evaluations have been obtained.

Hierarchical spaces for the hybrid FE-BI formulations provide efficient and important solutions to the development of powerful algorithms for computational electromagnetics. The low order RWG basis functions are well applied in the expansion of surface currents, however, the RWG basis functions suffer from the fundamental shortcoming that the accuracy is limited for dense geometrical discretization. To achieve better accuracy, nearly orthogonal hierarchical HO basis functions have been employed in the mixed order spaces and implemented into the FE-BI formulations. Furthermore, the HO basis functions achieve the same good accuracy as the LO counterparts with sufficient reduction in the number

of unknowns for given models. Proper fast solvers are necessarily required for numerical solutions to large scale EM simulations with the hybrid FE-BI formulations. The global system matrix from FE is highly sparse since interactions only involve neighboring elements. Thus, additional boundary conditions are utilized to arrive at a unique solution. The global system matrix from BI is dense since a traversal of all elements take place in mutual couplings. However, traditional MLFMM approaches turn to be less efficient for HO due to their hierarchical element dimensions. The SE-MLFMM has been proven considerably efficient in terms of memory requirements and computation time even for HO basis functions, where the $\hat{k}$ - space integral computations of the individual basis functions tremendously reduce the RAM storage and hence raise up the efficiency of iterative solvers for the resulting equation system. Thus, the SE-MLFMM technique accelerates the MoM solution for the SIE formulations.

The new proposed radial-angular-R^n transformation schemes have been utilized in various EM simulations for practical models incorporated with the adaptive singularity cancellation technique and higher-order surface current modeling. The efficacy of the hybrid FE-BI method has been proven through comparisons between simulation results and simple testing cases of physical models and analytical solutions. Bomber and Flamme aircraft models have been detailed studied in terms of scattering for PEC configurations and PEC configurations covered with dielectric absorbing materials. The hybrid FE-BI method provides accurate predictions of current distributions on the envelopes of objects and radiation pattern in free space. Furthermore, the accuracy analysis of the hybrid FE-BI method demonstrates that HO basis functions provide more accurate simulation results for increasing frequencies with respect to the corresponding model meshes.

Appendix A

System Matrices of the Finite Element Formulation based on Self-Identification Technique

In this appendix, the system matrices of the finite element formulation in (6.4.2) are listed. The system matrices have been derived from the 3-D hierarchical vector basis functions, where the basis functions are defined with the self-identification technique. The matrices can be directly linked into the system solvers. In Appendix A.2, $< \alpha_m, \alpha_n >$ means the system matrix element relevant to the basis functions $\boldsymbol{\alpha}_m$ and $\boldsymbol{\alpha}_n$.

A.1. Parameters for the System Matrices

The parameters are defined on a single tetrahedron shown in Fig. 49. It gives that

$$I_{ij} = \boldsymbol{A}_i \cdot \boldsymbol{A}_j \tag{A.1.1}$$

$$\boldsymbol{T}_{ij} = \boldsymbol{A}_i \times \boldsymbol{A}_j, \quad (i \neq j) = (0, 1, 2, 3), \tag{A.1.2}$$

and

$$v9 = 1.0/(9.0 * v), \tag{A.1.3}$$

$$v180 = 180.0 * v, \tag{A.1.4}$$

$$v36 = 1.0/(36.0 * v), \tag{A.1.5}$$

$$v24 = 1.0/(24.0 * v), \tag{A.1.6}$$

$$v72 = 1.0/(72.0 * v), \tag{A.1.7}$$

$$v80 = 1.0/(80.0 * v), \tag{A.1.8}$$

$$v240 = 1.0/(240.0 * v), \tag{A.1.9}$$

$$v720 = 1.0/(720.0 * v), \tag{A.1.10}$$

$$v1080 = 1.0/(1080.0 * v), \tag{A.1.11}$$

$$v7560 = 1.0/(7560.0 * v), \tag{A.1.12}$$

$$v180k02 = k02/(180.0 * v), \tag{A.1.13}$$

$$v1080k02 = k02/(1080 * v), \tag{A.1.14}$$

$$v7560k02 = k02/(7560 * v), \tag{A.1.15}$$

$$v60480k02 = k02/(60480 * v), \tag{A.1.16}$$

$$v544320k02 = k02/(544320 * v), \tag{A.1.17}$$

$$v3\_81\_4 = 4.0/(81.0 * v^3), \tag{A.1.18}$$
$$v3\_54 = 1.0/(54.0 * v^3), \tag{A.1.19}$$
$$v3\_162 = 1.0/(162.0 * v^3), \tag{A.1.20}$$
$$v3\_180 = 1.0/(180.0 * v^3), \tag{A.1.21}$$
$$v3\_540 = 1.0/(540.0 * v^3), \tag{A.1.22}$$
$$v3\_1620 = 1.0/(1620.0 * v^3), \tag{A.1.23}$$
$$v3\_4860 = 1.0/(4860.0 * v^3), \tag{A.1.24}$$
$$v3\_17010 = 1.0/(17010.0 * v^3), \tag{A.1.25}$$
$$v3\_810 = 1.0/(810.0 * v^3), \tag{A.1.26}$$
$$v3\_3240 = 1.0/(3240.0 * v^3), \tag{A.1.27}$$
$$v3\_9720 = 1.0/(9720.0 * v^3), \tag{A.1.28}$$
$$v3\_34020 = 1.0/(34020.0 * v^3), \tag{A.1.29}$$
$$v3\_68040 = 1.0/(68040.0 * v^3), \tag{A.1.30}$$

where v is the volume of the corresponding tetrahedron, $k02 = k_0^2 = \omega^2\epsilon_0\mu_0$, k_0 is the wave number in free space, ϵ_0 and μ_0 are the permittivity and permeability of the free space.

With (6.3.7) and (6.3.8), the coefficients for the system matrices can be determined.

$$\begin{aligned}
&for \quad j = 1 : J \\
&\quad k_i = 0; \\
&\quad for \quad i = 0 : 3 \\
&\qquad if\,(n_j == i) \quad k_i + +; \\
&\quad end \\
&\quad L_j(\{n_j\}) = \prod_{i=0}^{3} k_i!\,; \\
&end
\end{aligned}$$

where j is the number of the nodes relevant to the coefficients, n_j is the node number indexed in the basis functions, $\{n_j\}$ represents all nodes utilized for the coefficient, i is the node index of the tetrahedron, k_i is the number of index times of node i and L_j is the corresponding coefficient for the matrix mutual couplings.

A.2. R_{mn} and S_{mn} Matrix based on Self-Identification Technique

$$
\begin{aligned}
&< a_{1m}, a_{1n} > \\
&\quad R_{mn} = v3\_81\_4 \boldsymbol{T}_{m_i m_j} \cdot \boldsymbol{T}_{n_i n_j}, \\
&\quad S_{mn} = v180k02(L_2(m_i, n_i) I_{m_j, n_j} - L_2(m_i, n_j) I_{m_j n_i} - L_2(m_j n_i) I_{m_i n_j} + L_2(m_j, n_j) I_{m_i n_i}). \\
&< a_{1m}, b_{1n} > \\
&\quad R_{mn} = 0.0, \\
&\quad S_{mn} = v180k02(L_2(m_i, n_i) I_{m_j n_j} + L_2(m_i, n_j) I_{m_j n_i} - L_2(m_j, n_i) I_{m_i n_j} - L_2(m_j, n_j) I_{m_i n_i}). \\
&< a_{1m}, c_{2n} > \\
&\quad R_{mn} = v3\_54(\boldsymbol{T}_{m_i m_j} \cdot \boldsymbol{T}_{n_y n_z} - \boldsymbol{T}_{m_i m_j} \cdot \boldsymbol{T}_{n_x n_y}), \\
&\quad S_{mn} = v1080k02(L_3(m_i, n_x, n_y) I_{m_j n_z} + L_3(m_i, n_y, n_z) I_{m_j n_x} - 2.0 L_3(m_i, n_x, n_z) I_{m_j n_y} \\
&\qquad - L_3(m_j, n_x, n_y) I_{m_i n_z} - L_3(m_j, n_y, n_z) I_{m_i n_x} + 2.0 L_3(m_j, n_x, n_z) I_{m_i n_y}). \\
&< a_{1m}, d_{2n} > \\
&\quad R_{mn} = v3\_162(\boldsymbol{T}_{m_i m_j} \cdot \boldsymbol{T}_{n_y n_z} + 2.0 \boldsymbol{T}_{m_i m_j}\ cdot \boldsymbol{T}_{n_x n_z} + \boldsymbol{T}_{m_i m_j} \cdot \boldsymbol{T}_{n_x n_y}), \\
&\quad S_{mn} = v1080k02(L_3(m_i, n_x, n_y) I_{m_j n_z} - L_3(m_i, n_y, n_z) I_{m_j n_x} - L_3(m_j, n_x, n_y) I_{m_i n_z} \\
&\qquad + L_3(m_j, n_y, n_z) I_{m_i n_x}). \\
&< a_{1m}, e_{2n} > \\
&\quad R_{mn} = 0.0, \\
&\quad S_{mn} = v1080k02(2.0 L_3(m_i, n_i, n_j) I_{m_j n_j} - L_2(m_i, n_i) I_{m_j n_j} - 2.0 L_3(m_j, n_i, n_j) I_{m_i n_j} \\
&\qquad + L_2(m_j, n_i) I_{m_i n_j} - 2.0 L_3(m_i, n_i, n_j) I_{m_j n_i} + L_2(m_i, n_j) I_{m_j n_i} \\
&\qquad + 2.0 L_3(m_j, n_i, n_j) I_{m_i n_i} - L_2(m_j, n_j) I_{m_i n_i}). \\
&< a_{1m}, f_{2n} > \\
&\quad R_{mn} = 0.0, \\
&\quad S_{mn} = v1080k02(L_3(m_i, n_x, n_y) I_{m_j n_z} + L_3(m_i, n_y, n_z) I_{m_j n_x} + L_3(m_i, n_x, n_z) I_{m_j n_y} \\
&\qquad - L_3(m_j, n_x, n_y) I_{m_i n_z} - L_3(m_j, n_y, n_z) I_{m_i n_x} - L_3(m_j, n_x, n_z) I_{m_i n_y}). \\
&< a_{1m}, g_{3n} > \\
&\quad R_{mn} = 0, \\
&\quad S_{mn} = v7560k02(-I_{m_i n_x} L_4(m_j, n_y, n_y, n_z) + I_{m_i n_x} L_4(m_j, n_y, n_z, n_z) \\
&\qquad + I_{m_i n_y} L_4(m_j, n_x, n_x, n_z) - I_{m_i n_y} L_4(m_j, n_x, n_z, n_z) - I_{m_i n_z} L_4(m_j, n_x, n_x, n_y) \\
&\qquad + I_{m_i n_z} L_4(m_j, n_x, n_y, n_y) + I_{m_j n_x} L_4(m_i, n_y, n_y, n_z) - I_{m_j n_x} L_4(m_i, n_y, n_z, n_z) \\
&\qquad - I_{m_j n_y} L_4(m_i, n_x, n_x, n_z) + I_{m_j n_y} L_4(m_i, n_x, n_z, n_z) + I_{m_j n_z} L_4(m_i, n_x, n_x, n_y) \\
&\qquad - I_{m_j n_z} L_4(m_i, n_x, n_y, n_y)).
\end{aligned}
$$

$< a_{1m}, h_{3n} >$

$$
\begin{aligned}
R_{mn} =& v3\_810(977(\boldsymbol{T}_{m_i m_j} \cdot \boldsymbol{T}_{n_x n_y}) L_2(n_x, n_z) - 424(\boldsymbol{T}_{m_i m_j} \cdot \boldsymbol{T}_{n_x n_y}) L_2(n_y, n_z) \\
& - 212(\boldsymbol{T}_{m_i m_j} \cdot \boldsymbol{T}_{n_x n_y}) L_2(n_z, n_z) + 553(\boldsymbol{T}_{m_i m_j} \cdot \boldsymbol{T}_{n_x n_z}) L_2(n_x, n_y) \\
& - 424(\boldsymbol{T}_{m_i m_j} \cdot \boldsymbol{T}_{n_x n_z}) L_2(n_y, n_y) + 553(\boldsymbol{T}_{m_i m_j} \cdot \boldsymbol{T}_{n_x n_z}) L_2(n_y, n_z) \\
& - 212(\boldsymbol{T}_{m_i m_j} \cdot \boldsymbol{T}_{n_y n_z}) L_2(n_x, n_x) - 424(\boldsymbol{T}_{m_i m_j} \cdot \boldsymbol{T}_{n_y n_z}) L_2(n_x, n_y) \\
& + 977(\boldsymbol{T}_{m_i m_j} \cdot \boldsymbol{T}_{n_y n_z}) L_2(n_x, n_z)), \\
S_{mn} =& v7560k02(393 I_{m_i n_x} L_4(m_j, n_x, n_y, n_z) - 212 I_{m_i n_x} L_4(m_j, n_y, n_y, n_z) \\
& + 80 I_{m_i n_x} L_4(m_j, n_y, n_z, n_z) - 292 I_{m_i n_y} L_4(m_j, n_x, n_x, n_z) \\
& + 292 I_{m_i n_y} L_4(m_j, n_x, n_z, n_z) - 80 I_{m_i n_z} L_4(m_j, n_x, n_x, n_y) \\
& + 212 I_{m_i n_z} L_4(m_j, n_x, n_y, n_y) - 393 I_{m_i n_z} L_4(m_j, n_x, n_y, n_z) \\
& - 393 I_{m_j n_x} L_4(m_i, n_x, n_y, n_z) + 212 I_{m_j n_x} L_4(m_i, n_y, n_y, n_z) \\
& - 80 I_{m_j n_x} L_4(m_i, n_y, n_z, n_z) + 292 I_{m_j n_y} L_4(m_i, n_x, n_x, n_z) \\
& - 292 I_{m_j n_y} L_4(m_i, n_x, n_z, n_z) + 80 I_{m_j n_z} L_4(m_i, n_x, n_x, n_y) \\
& - 212 I_{m_j n_z} L_4(m_i, n_x, n_y, n_y) + 393 I_{m_j n_z} L_4(m_i, n_x, n_y, n_z)).
\end{aligned}
$$

$< a_{1m}, i_{3n} >$

$$
\begin{aligned}
R_{mn} =& v3\_810(43(\boldsymbol{T}_{m_i m_j} \cdot \boldsymbol{T}_{n_x n_y}) L_2(n_x, n_z) + 510(\boldsymbol{T}_{m_i m_j} \cdot \boldsymbol{T}_{n_x n_y}) L_2(n_y, n_z) \\
& - 212(\boldsymbol{T}_{m_i m_j} \cdot \boldsymbol{T}_{n_x n_y}) L_2(n_z, n_z) + 467(\boldsymbol{T}_{m_i m_j} \cdot \boldsymbol{T}_{n_x n_z}) L_2(n_x, n_y) \\
& - 467(\boldsymbol{T}_{m_i m_j} \cdot \boldsymbol{T}_{n_x n_z}) L_2(n_y, n_z) + 212(\boldsymbol{T}_{m_i m_j} \cdot \boldsymbol{T}_{n_y n_z}) L_2(n_x, n_x) \\
& - 510(\boldsymbol{T}_{m_i m_j} \cdot \boldsymbol{T}_{n_y n_z}) L_2(n_x, n_y) - 43(\boldsymbol{T}_{m_i m_j} \cdot \boldsymbol{T}_{n_y n_z}) L_2(n_x, n_z)), \\
S_{mn} =& v7560k02(131 I_{m_i n_x} L_4(m_j, n_x, n_y, n_z) + 124 I_{m_i n_x} L_4(m_j, n_y, n_y, n_z) \\
& - 168 I_{m_i n_x} L_4(m_j, n_y, n_z, n_z) + 44 I_{m_i n_y} L_4(m_j, n_x, n_x, n_z) \\
& - 262 I_{m_i n_y} L_4(m_j, n_x, n_y, n_z) + 44 I_{m_i n_y} L_4(m_j, n_x, n_z, n_z) \\
& - 168 I_{m_i n_z} L_4(m_j, n_x, n_x, n_y) + 124 I_{m_i n_z} L_4(m_j, n_x, n_y, n_y) \\
& + 131 I_{m_i n_z} L_4(m_j, n_x, n_y, n_z) - 131 I_{m_j n_x} L_4(m_i, n_x, n_y, n_z) \\
& - 124 I_{m_j n_x} L_4(m_i, n_y, n_y, n_z) + 168 I_{m_j n_x} L_4(m_i, n_y, n_z, n_z) \\
& - 44 I_{m_j n_y} L_4(m_i, n_x, n_x, n_z) + 262 I_{m_j n_y} L_4(m_i, n_x, n_y, n_z) \\
& - 44 I_{m_j n_y} L_4(m_i, n_x, n_z, n_z) + 168 I_{m_j n_z} L_4(m_i, n_x, n_x, n_y) \\
& - 124 I_{m_j n_z} L_4(m_i, n_x, n_y, n_y) - 131 I_{m_j n_z} L_4(m_i, n_x, n_y, n_z)).
\end{aligned}
$$

$$
\begin{aligned}
&< a_{1m}, j_{3n} > \\
&\quad R_{mn} = & & v3\_810 \\
&\qquad & & (-2(\boldsymbol{T}_{m_i m_j} \cdot \boldsymbol{T}_{n_0 n_2}) L_2(n_1, n_3) - 2(\boldsymbol{T}_{m_i m_j} \cdot \boldsymbol{T}_{n_0 n_3}) L_2(n_1, n_2) \\
&\qquad & & - 2(\boldsymbol{T}_{m_i m_j} \cdot \boldsymbol{T}_{n_1 n_2}) L_2(n_0, n_3) - 2(\boldsymbol{T}_{m_i m_j} \cdot \boldsymbol{T}_{n_1 n_3}) L_2(n_0, n_2)), \\
&\quad S_{mn} = & & v7560k02 \\
&\qquad & & (-I_{m_i n_0} L_4(m_j, n_1, n_2, n_3) - I_{m_i n_1} L_4(m_j, n_0, n_2, n_3) \\
&\qquad & & + I_{m_i n_2} L_4(m_j, n_0, n_1, n_3) + I_{m_i n_3} L_4(m_j, n_0, n_1, n_2) \\
&\qquad & & + I_{m_j n_0} L_4(m_i, n_1, n_2, n_3) + I_{m_j n_1} L_4(m_i, n_0, n_2, n_3) \\
&\qquad & & - I_{m_j n_2} L_4(m_i, n_0, n_1, n_3) - I_{m_j n_3} L_4(m_i, n_0, n_1, n_2)).
\end{aligned}
$$

$$
\begin{aligned}
&< a_{1m}, k_{3n} > \\
&\quad R_{mn} = & & v3\_810 \\
&\qquad & & ((\boldsymbol{T}_{m_i m_j} \cdot \boldsymbol{T}_{n_0 n_2}) L_2(n_1, n_3) - (\boldsymbol{T}_{m_i m_j} \cdot \boldsymbol{T}_{n_0 n_3}) L_2(n_1, n_2) \\
&\qquad & & + (\boldsymbol{T}_{m_i m_j} \cdot \boldsymbol{T}_{n_1 n_2}) L_2(n_0, n_3) - (\boldsymbol{T}_{m_i m_j} \cdot \boldsymbol{T}_{n_1 n_3}) L_2(n_0, n_2) \\
&\qquad & & - 2(\boldsymbol{T}_{m_i m_j} \cdot \boldsymbol{T}_{n_2 n_3}) L_2(n_0, n_1)), \\
&\quad S_{mn} = & & v7560k02 \\
&\qquad & & (-I_{m_i n_2} L_4(m_j, n_0, n_1, n_3) + I_{m_i n_3} L_4(m_j, n_0, n_1, n_2) \\
&\qquad & & + I_{m_j n_2} L_4(m_i, n_0, n_1, n_3) - I_{m_j n_3} L_4(m_i, n_0, n_1, n_2)).
\end{aligned}
$$

$$
\begin{aligned}
&< a_{1m}, l_{3n} > \\
&\quad R_{mn} = & & v3\_810 \\
&\qquad & & (-2(\boldsymbol{T}_{m_i m_j} \cdot \boldsymbol{T}_{n_0 n_1}) L_2(n_2, n_3) - (\boldsymbol{T}_{m_i m_j} \cdot \boldsymbol{T}_{n_0 n_2}) L_2(n_1, n_3) \\
&\qquad & & - (\boldsymbol{T}_{m_i m_j} \cdot \boldsymbol{T}_{n_0 n_3}) L_2(n_1, n_2) + (\boldsymbol{T}_{m_i m_j} \cdot \boldsymbol{T}_{n_1 n_2}) L_2(n_0, n_3) \\
&\qquad & & + (\boldsymbol{T}_{m_i m_j} \cdot \boldsymbol{T}_{n_1 n_3}) L_2(n_0, n_2)), \\
&\quad S_{mn} = & & v7560k02 \\
&\qquad & & (-I_{m_i n_0} L_4(m_j, n_1, n_2, n_3) + I_{m_i n_1} L_4(m_j, n_0, n_2, n_3) \\
&\qquad & & + I_{m_j n_0} L_4(m_i, n_1, n_2, n_3) - I_{m_j n_1} L_4(m_i, n_0, n_2, n_3)).
\end{aligned}
$$

$$
\begin{aligned}
&< b_{1m}, c_{2n} > \\
&\quad R_{mn} = & & 0.0, \\
&\quad S_{mn} = & & v1080k02(L_3(m_i, n_x, n_y) I_{m_j n_z} + L_3(m_i, n_y, n_z) I_{m_j n_x} - 2.0 L_3(m_i, n_x, n_z) I_{m_j n_y} \\
&\qquad & & + L_3(m_j, n_x, n_y) I_{m_i n_z} + L_3(m_j, n_y, n_z) I_{m_i n_x} - 2.0 L_3(m_j, n_x, n_z) I_{m_i n_y}).
\end{aligned}
$$

$$
\begin{aligned}
&< b_{1m}, d_{2n} > \\
&\quad R_{mn} = & & 0.0, \\
&\quad S_{mn} = & & v1080k02(L_3(m_i, n_x, n_y) I_{m_j n_z} - L_3(m_i, n_y, n_z) I_{m_j n_x} + L_3(m_j, n_x, n_y) I_{m_i n_z} \\
&\qquad & & - L_3(m_j, n_y, n_z) I_{m_i n_x}).
\end{aligned}
$$

$$
\begin{aligned}
&< b_{1m}, e_{2n} > \\
&\quad R_{mn} = 0.0, \\
&\quad S_{mn} = v1080k02(2.0L_3(m_i, n_i, n_j)I_{m_j n_j} - L_2(m_i, n_i)I_{m_j n_j} + 2.0L_3(m_j, n_i, n_j)I_{m_i n_j} \\
&\qquad - L_2(m_j, n_i)I_{m_i n_j} - 2.0L_3(m_i, n_i, n_j)I_{m_j n_i} + L_2(m_i, n_j)I_{m_j n_i} \\
&\qquad - 2.0L_3(m_j, n_i, n_j)I_{m_i n_i} + L_2(m_j, n_j)I_{m_i n_i}).
\end{aligned}
$$

$$
\begin{aligned}
&< b_{1m}, f_{2n} > \\
&\quad R_{mn} = 0.0, \\
&\quad S_{mn} = v1080k02(L_3(m_i, n_x, n_y)I_{m_j n_z} + L_3(m_i, n_y, n_z)I_{m_j n_x} + L_3(m_i, n_x, n_z)I_{m_j n_y} \\
&\qquad + L_3(m_j, n_x, n_y)I_{m_i n_z} + L_3(m_j, n_y, n_z)I_{m_i n_x} + L_3(m_j, n_x, n_z)I_{m_i n_y}).
\end{aligned}
$$

$$
\begin{aligned}
&< b_{1m}, g_{3n} > \\
&\quad R_{mn} = 0, \\
&\quad S_{mn} = v7560k02(+I_{m_i n_x}L_4(m_j, n_y, n_y, n_z) - I_{m_i n_x}L_4(m_j, n_y, n_z, n_z) \\
&\qquad - I_{m_i n_y}L_4(m_j, n_x, n_x, n_z) + I_{m_i n_y}L_4(m_j, n_x, n_z, n_z) \\
&\qquad + I_{m_i n_z}L_4(m_j, n_x, n_x, n_y) - I_{m_i n_z}L_4(m_j, n_x, n_y, n_y) \\
&\qquad + I_{m_j n_x}L_4(m_i, n_y, n_y, n_z) - I_{m_j n_x}L_4(m_i, n_y, n_z, n_z) \\
&\qquad - I_{m_j n_y}L_4(m_i, n_x, n_x, n_z) + I_{m_j n_y}L_4(m_i, n_x, n_z, n_z) \\
&\qquad + I_{m_j n_z}L_4(m_i, n_x, n_x, n_y) - I_{m_j n_z}L_4(m_i, n_x, n_y, n_y)).
\end{aligned}
$$

$$
\begin{aligned}
&< b_{1m}, h_{3n} > \\
&\quad R_{mn} = 0, \\
&\quad S_{mn} = v7560k02(-393I_{m_i n_x}L_4(m_j, n_x, n_y, n_z) + 212I_{m_i n_x}L_4(m_j, n_y, n_y, n_z) \\
&\qquad - 80I_{m_i n_x}L_4(m_j, n_y, n_z, n_z) + 292I_{m_i n_y}L_4(m_j, n_x, n_x, n_z) \\
&\qquad - 292I_{m_i n_y}L_4(m_j, n_x, n_z, n_z) + 80I_{m_i n_z}L_4(m_j, n_x, n_x, n_y) \\
&\qquad - 212I_{m_i n_z}L_4(m_j, n_x, n_y, n_y) + 393I_{m_i n_z}L_4(m_j, n_x, n_y, n_z) \\
&\qquad - 393I_{m_j n_x}L_4(m_i, n_x, n_y, n_z) + 212I_{m_j n_x}L_4(m_i, n_y, n_y, n_z) \\
&\qquad - 80I_{m_j n_x}L_4(m_i, n_y, n_z, n_z) + 292I_{m_j n_y}L_4(m_i, n_x, n_x, n_z) \\
&\qquad - 292I_{m_j n_y}L_4(m_i, n_x, n_z, n_z) + 80I_{m_j n_z}L_4(m_i, n_x, n_x, n_y) \\
&\qquad - 212I_{m_j n_z}L_4(m_i, n_x, n_y, n_y) + 393I_{m_j n_z}L_4(m_i, n_x, n_y, n_z)).
\end{aligned}
$$

$$
\begin{aligned}
&< b_{1m}, i_{3n} > \\
&\quad R_{mn} = 0, \\
&\quad S_{mn} = v7560k02(-131 I_{m_i n_x} L_4(m_j, n_x, n_y, n_z) - 124 I_{m_i n_x} L_4(m_j, n_y, n_y, n_z) \\
&\qquad + 168 I_{m_i n_x} L_4(m_j, n_y, n_z, n_z) - 44 I_{m_i n_y} L_4(m_j, n_x, n_x, n_z) \\
&\qquad + 262 I_{m_i n_y} L_4(m_j, n_x, n_y, n_z) - 44 I_{m_i n_y} L_4(m_j, n_x, n_z, n_z) \\
&\qquad + 168 I_{m_i n_z} L_4(m_j, n_x, n_x, n_y) - 124 I_{m_i n_z} L_4(m_j, n_x, n_y, n_y) \\
&\qquad - 131 I_{m_i n_z} L_4(m_j, n_x, n_y, n_z) - 131 I_{m_j n_x} L_4(m_i, n_x, n_y, n_z) \\
&\qquad - 124 I_{m_j n_x} L_4(m_i, n_y, n_y, n_z) + 168 I_{m_j n_x} L_4(m_i, n_y, n_z, n_z) \\
&\qquad - 44 I_{m_j n_y} L_4(m_i, n_x, n_x, n_z) + 262 I_{m_j n_y} L_4(m_i, n_x, n_y, n_z) \\
&\qquad - 44 I_{m_j n_y} L_4(m_i, n_x, n_z, n_z) + 168 I_{m_j n_z} L_4(m_i, n_x, n_x, n_y) \\
&\qquad - 124 I_{m_j n_z} L_4(m_i, n_x, n_y, n_y) - 131 I_{m_j n_z} L_4(m_i, n_x, n_y, n_z)).
\end{aligned}
$$

$$
\begin{aligned}
&< b_{1m}, j_{3n} > \\
&\quad R_{mn} = 0, \\
&\quad S_{mn} = v7560k02 \\
&\qquad (I_{m_i n_0} L_4(m_j, n_1, n_2, n_3) + I_{m_i n_1} L_4(m_j, n_0, n_2, n_3) \\
&\qquad - I_{m_i n_2} L_4(m_j, n_0, n_1, n_3) - I_{m_i n_3} L_4(m_j, n_0, n_1, n_2) \\
&\qquad + I_{m_j n_0} L_4(m_i, n_1, n_2, n_3) + I_{m_j n_1} L_4(m_i, n_0, n_2, n_3) \\
&\qquad - I_{m_j n_2} L_4(m_i, n_0, n_1, n_3) - I_{m_j n_3} L_4(m_i, n_0, n_1, n_2)).
\end{aligned}
$$

$$
\begin{aligned}
&< b_{1m}, k_{3n} > \\
&\quad R_{mn} = 0, \\
&\quad S_{mn} = v7560k02 \\
&\qquad (+ I_{m_i n_2} L_4(m_j, n_0, n_1, n_3) - I_{m_i n_3} L_4(m_j, n_0, n_1, n_2) \\
&\qquad + I_{m_j n_2} L_4(m_i, n_0, n_1, n_3) - I_{m_j n_3} L_4(m_i, n_0, n_1, n_2)).
\end{aligned}
$$

$$
\begin{aligned}
&< b_{1m}, l_{3n} > \\
&\quad R_{mn} = 0, \\
&\quad S_{mn} = v7560k02 \\
&\qquad (I_{m_i n_0} L_4(m_j, n_1, n_2, n_3) - I_{m_i n_1} L_4(m_j, n_0, n_2, n_3) \\
&\qquad + I_{m_j n_0} L_4(m_i, n_1, n_2, n_3) - I_{m_j n_1} L_4(m_i, n_0, n_2, n_3)).
\end{aligned}
$$

$< c_{2m}, c_{2n} >$

$$
\begin{aligned}
R_{mn} =& v3\_180(L_2(m_x, n_x)\boldsymbol{T}_{m_y m_z} \cdot \boldsymbol{T}_{n_y n_z} - L_2(m_x, n_z)\boldsymbol{T}_{m_y m_z} \cdot \boldsymbol{T}_{n_x n_y} \\
& - L_2(m_z, n_x)\boldsymbol{T}_{m_x m_y} \cdot \boldsymbol{T}_{n_y n_z} + L_2(m_z, n_z)\boldsymbol{T}_{m_x m_y} \cdot \boldsymbol{T}_{n_x n_y}), \\
S_{mn} =& v7560k02(L_4(m_x, m_y, n_x, n_y)I_{m_z n_z} + L_4(m_x, m_y, n_y, n_z)I_{m_z n_x} \\
& - 2.0L_4(m_x, m_y, n_x, n_z)I_{m_z n_y} + L_4(m_y, m_z, n_x, n_y)I_{m_x n_z} \\
& + L_4(m_y, m_z, n_y, n_z)I_{m_x n_x} - 2.0L_4(m_y, m_z, n_x, n_z)I_{m_x n_y} \\
& - 2.0L_4(m_x, m_z, n_x, n_y)I_{m_y n_z} - 2.0L_4(m_x, m_z, n_y, n_z)I_{m_y n_x} \\
& + 4.0L_4(m_x, m_z, n_x, n_z)I_{m_y n_y}).
\end{aligned}
$$

$< c_{2m}, d_{2n} >$

$$
\begin{aligned}
R_{mn} =& v3\_540(L_2(m_x, n_x)\boldsymbol{T}_{m_y m_z} \cdot \boldsymbol{T}_{n_y n_z} + 2.0L_2(m_x, n_y)\boldsymbol{T}_{m_y m_z} \cdot \boldsymbol{T}_{n_x n_z} \\
& + L_2(m_x, n_z)\boldsymbol{T}_{m_y m_z} \cdot \boldsymbol{T}_{n_x n_y} - L_2(m_z, n_x)\boldsymbol{T}_{m_x m_y} \cdot \boldsymbol{T}_{n_y n_z} \\
& - 2.0L_2(m_z, n_y)\boldsymbol{T}_{m_x m_y} \cdot \boldsymbol{T}_{n_x n_z} - L_2(m_z, n_z)\boldsymbol{T}_{m_x m_y} \cdot \boldsymbol{T}_{n_x n_y}), \\
S_{mn} =& v7560k02(L_4(m_x, m_y, n_x, n_y)I_{m_z n_z} - L_4(m_x, m_y, n_y, n_z)I_{m_z n_x} \\
& + L_4(m_y, m_z, n_x, n_y)I_{m_x n_z} - L_4(m_y, m_z, n_y, n_z)I_{m_x n_x} \\
& - 2.0L_4(m_x, m_z, n_x, n_y)I_{m_y n_z} + 2.0L_4(m_x, m_z, n_y, n_z)I_{m_y n_x}).
\end{aligned}
$$

$< c_{2m}, e_{2n} >$

$$
\begin{aligned}
R_{mn} =& 0.0, \\
S_{mn} =& v7560k02(2.0L_4(m_x, m_y, n_i, n_j)I_{m_z n_j} - L_3(m_x, m_y, n_i)I_{m_z n_j} \\
& - 2.0L_4(m_x, m_y, n_i, n_j)I_{m_z n_i} + L_3(m_x, m_y, n_j)I_{m_z n_i} \\
& + 2.0L_4(m_y, m_z, n_i, n_j)I_{m_x n_j} - L_3(m_y, m_z, n_i)I_{m_x n_j} \\
& - 2.0L_4(m_y, m_z, n_i, n_j)I_{m_x n_i} + L_3(m_y, m_z, n_j)I_{m_x n_i} \\
& - 4.0L_4(m_x, m_z, n_i, n_j)I_{m_y n_j} + 2.0L_3(m_x, m_z, n_i)I_{m_y n_j} \\
& + 4.0L_4(m_x, m_z, n_i, n_j)I_{m_y n_i} - 2.0L_3(m_x, m_z, n_j)I_{m_y n_i}).
\end{aligned}
$$

$< c_{2m}, f_{2n} >$

$$
\begin{aligned}
R_{mn} =& 0.0, \\
S_{mn} =& v7560k02(L_4(m_x, m_y, n_x, n_y)I_{m_z n_z} + L_4(m_x, m_y, n_y, n_z)I_{m_z n_x} \\
& + L_4(m_x, m_y, n_x, n_z)I_{m_z n_y} + L_4(m_y, m_z, n_x, n_y)I_{m_x n_z} \\
& + L_4(m_y, m_z, n_y, n_z)I_{m_x n_x} + L_4(m_y, m_z, n_x, n_z)I_{m_x n_y} \\
& - 2.0L_4(m_x, m_z, n_x, n_y)I_{m_y n_z} - 2.0L_4(m_x, m_z, n_y, n_z)I_{m_y n_x} \\
& - 2.0L_4(m_x, m_z, n_x, n_z)I_{m_y n_y}).
\end{aligned}
$$

$$
\begin{aligned}
< c_{2m}, g_{3n} > \\
R_{mn} =& v3\_1620((\boldsymbol{T}_{m_x m_y} \cdot \boldsymbol{T}_{n_x n_y}) L_3(m_z, n_x, n_z) + (\boldsymbol{T}_{m_x m_y} \cdot \boldsymbol{T}_{n_x n_y}) L_3(m_z, n_y, n_z) \\
& - (\boldsymbol{T}_{m_x m_y} \cdot \boldsymbol{T}_{n_x n_y}) L_3(m_z, n_z, n_z) - (\boldsymbol{T}_{m_x m_y} \cdot \boldsymbol{T}_{n_x n_z}) L_3(m_z, n_x, n_y) \\
& + (\boldsymbol{T}_{m_x m_y} \cdot \boldsymbol{T}_{n_x n_z}) L_3(m_z, n_y, n_y) - (\boldsymbol{T}_{m_x m_y} \cdot \boldsymbol{T}_{n_x n_z}) L_3(m_z, n_y, n_z) \\
& - (\boldsymbol{T}_{m_x m_y} \cdot \boldsymbol{T}_{n_y n_z}) L_3(m_z, n_x, n_x) + (\boldsymbol{T}_{m_x m_y} \cdot \boldsymbol{T}_{n_y n_z}) L_3(m_z, n_x, n_y) \\
& + (\boldsymbol{T}_{m_x m_y} \cdot \boldsymbol{T}_{n_y n_z}) L_3(m_z, n_x, n_z) - (\boldsymbol{T}_{m_y m_z} \cdot \boldsymbol{T}_{n_x n_y}) L_3(m_x, n_x, n_z) \\
& - (\boldsymbol{T}_{m_y m_z} \cdot \boldsymbol{T}_{n_x n_y}) L_3(m_x, n_y, n_z) + (\boldsymbol{T}_{m_y m_z} \cdot \boldsymbol{T}_{n_x n_y}) L_3(m_x, n_z, n_z) \\
& + (\boldsymbol{T}_{m_y m_z} \cdot \boldsymbol{T}_{n_x n_z}) L_3(m_x, n_x, n_y) - (\boldsymbol{T}_{m_y m_z} \cdot \boldsymbol{T}_{n_x n_z}) L_3(m_x, n_y, n_y) \\
& + (\boldsymbol{T}_{m_y m_z} \cdot \boldsymbol{T}_{n_x n_z}) L_3(m_x, n_y, n_z) + (\boldsymbol{T}_{m_y m_z} \cdot \boldsymbol{T}_{n_y n_z}) L_3(m_x, n_x, n_x) \\
& - (\boldsymbol{T}_{m_y m_z} \cdot \boldsymbol{T}_{n_y n_z}) L_3(m_x, n_x, n_y) - (\boldsymbol{T}_{m_y m_z} \cdot \boldsymbol{T}_{n_y n_z}) L_3(m_x, n_x, n_z)), \\
S_{mn} =& v60480k02(I_{m_x n_x} L_5(m_y, m_z, n_y, n_y, n_z) - I_{m_x n_x} L_5(m_y, m_z, n_y, n_z, n_z) \\
& - I_{m_x n_y} L_5(m_y, m_z, n_x, n_x, n_z) + I_{m_x n_y} L_5(m_y, m_z, n_x, n_z, n_z) \\
& + I_{m_x n_z} L_5(m_y, m_z, n_x, n_x, n_y) - I_{m_x n_z} L_5(m_y, m_z, n_x, n_y, n_y) \\
& - 2I_{m_y n_x} L_5(m_x, m_z, n_y, n_y, n_z) + 2I_{m_y n_x} L_5(m_x, m_z, n_y, n_z, n_z) \\
& + 2I_{m_y n_y} L_5(m_x, m_z, n_x, n_x, n_z) - 2I_{m_y n_y} L_5(m_x, m_z, n_x, n_z, n_z) \\
& - 2I_{m_y n_z} L_5(m_x, m_z, n_x, n_x, n_y) + 2I_{m_y n_z} L_5(m_x, m_z, n_x, n_y, n_y) \\
& + I_{m_z n_x} L_5(m_x, m_y, n_y, n_y, n_z) - I_{m_z n_x} L_5(m_x, m_y, n_y, n_z, n_z) \\
& - I_{m_z n_y} L_5(m_x, m_y, n_x, n_x, n_z) + I_{m_z n_y} L_5(m_x, m_y, n_x, n_z, n_z) \\
& + I_{m_z n_z} L_5(m_x, m_y, n_x, n_x, n_y) - I_{m_z n_z} L_5(m_x, m_y, n_x, n_y, n_y)).
\end{aligned}
$$

$< c_{2m}, h_{3n} >$

$$
\begin{aligned}
R_{mn} =& v3\_3240(-977(\boldsymbol{T}_{m_xm_y} \cdot \boldsymbol{T}_{n_xn_y})L_3(m_z, n_x, n_z) + 424(\boldsymbol{T}_{m_xm_y} \cdot \boldsymbol{T}_{n_xn_y})L_3(m_z, n_y, n_z) \\
&+ 212(\boldsymbol{T}_{m_xm_y} \cdot \boldsymbol{T}_{n_xn_y})L_3(m_z, n_z, n_z) - 553(\boldsymbol{T}_{m_xm_y} \cdot \boldsymbol{T}_{n_xn_z})L_3(m_z, n_x, n_y) \\
&+ 424(\boldsymbol{T}_{m_xm_y} \cdot \boldsymbol{T}_{n_xn_z})L_3(m_z, n_y, n_y) - 553(\boldsymbol{T}_{m_xm_y} \cdot \boldsymbol{T}_{n_xn_z})L_3(m_z, n_y, n_z) \\
&+ 212(\boldsymbol{T}_{m_xm_y} \cdot \boldsymbol{T}_{n_yn_z})L_3(m_z, n_x, n_x) + 424(\boldsymbol{T}_{m_xm_y} \cdot \boldsymbol{T}_{n_yn_z})L_3(m_z, n_x, n_y) \\
&- 977(\boldsymbol{T}_{m_xm_y} \cdot \boldsymbol{T}_{n_yn_z})L_3(m_z, n_x, n_z) + 977(\boldsymbol{T}_{m_ym_z} \cdot \boldsymbol{T}_{n_xn_y})L_3(m_x, n_x, n_z) \\
&- 424(\boldsymbol{T}_{m_ym_z} \cdot \boldsymbol{T}_{n_xn_y})L_3(m_x, n_y, n_z) - 212(\boldsymbol{T}_{m_ym_z} \cdot \boldsymbol{T}_{n_xn_y})L_3(m_x, n_z, n_z) \\
&+ 553(\boldsymbol{T}_{m_ym_z} \cdot \boldsymbol{T}_{n_xn_z})L_3(m_x, n_x, n_y) - 424(\boldsymbol{T}_{m_ym_z} \cdot \boldsymbol{T}_{n_xn_z})L_3(m_x, n_y, n_y) \\
&+ 553(\boldsymbol{T}_{m_ym_z} \cdot \boldsymbol{T}_{n_xn_z})L_3(m_x, n_y, n_z) - 212(\boldsymbol{T}_{m_ym_z} \cdot \boldsymbol{T}_{n_yn_z})L_3(m_x, n_x, n_x) \\
&- 424(\boldsymbol{T}_{m_ym_z} \cdot \boldsymbol{T}_{n_yn_z})L_3(m_x, n_x, n_y) + 977(\boldsymbol{T}_{m_ym_z} \cdot \boldsymbol{T}_{n_yn_z})L_3(m_x, n_x, n_z)), \\
S_{mn} =& v60480k02(-393I_{m_xn_x}L_5(m_y, m_z, n_x, n_y, n_z) + 212I_{m_xn_x}L_5(m_y, m_z, n_y, n_y, n_z) \\
&- 80I_{m_xn_x}L_5(m_y, m_z, n_y, n_z, n_z) + 292I_{m_xn_y}L_5(m_y, m_z, n_x, n_x, n_z) \\
&- 292I_{m_xn_y}L_5(m_y, m_z, n_x, n_z, n_z) + 80I_{m_xn_z}L_5(m_y, m_z, n_x, n_x, n_y) \\
&- 212I_{m_xn_z}L_5(m_y, m_z, n_x, n_y, n_y) + 393I_{m_xn_z}L_5(m_y, m_z, n_x, n_y, n_z) \\
&+ 786I_{m_yn_x}L_5(m_x, m_z, n_x, n_y, n_z) - 424I_{m_yn_x}L_5(m_x, m_z, n_y, n_y, n_z) \\
&+ 160I_{m_yn_x}L_5(m_x, m_z, n_y, n_z, n_z) - 584I_{m_yn_y}L_5(m_x, m_z, n_x, n_x, n_z) \\
&+ 584I_{m_yn_y}L_5(m_x, m_z, n_x, n_z, n_z) - 160I_{m_yn_z}L_5(m_x, m_z, n_x, n_x, n_y) \\
&+ 424I_{m_yn_z}L_5(m_x, m_z, n_x, n_y, n_y) - 786I_{m_yn_z}L_5(m_x, m_z, n_x, n_y, n_z) \\
&- 393I_{m_zn_x}L_5(m_x, m_y, n_x, n_y, n_z) + 212I_{m_zn_x}L_5(m_x, m_y, n_y, n_y, n_z) \\
&- 80I_{m_zn_x}L_5(m_x, m_y, n_y, n_z, n_z) + 292I_{m_zn_y}L_5(m_x, m_y, n_x, n_x, n_z) \\
&- 292I_{m_zn_y}L_5(m_x, m_y, n_x, n_z, n_z) + 80I_{m_zn_z}L_5(m_x, m_y, n_x, n_x, n_y) \\
&- 212I_{m_zn_z}L_5(m_x, m_y, n_x, n_y, n_y) + 393I_{m_zn_z}L_5(m_x, m_y, n_x, n_y, n_z)).
\end{aligned}
$$

$< c_{2m}, i_{3n} >$

$$
\begin{aligned}
R_{mn} =& v3\_3240(-43(\boldsymbol{T}_{m_xm_y} \cdot \boldsymbol{T}_{n_xn_y})L_3(m_z, n_x, n_z) - 510(\boldsymbol{T}_{m_xm_y} \cdot \boldsymbol{T}_{n_xn_y})L_3(m_z, n_y, n_z) \\
&+ 212(\boldsymbol{T}_{m_xm_y} \cdot \boldsymbol{T}_{n_xn_y})L_3(m_z, n_z, n_z) - 467(\boldsymbol{T}_{m_xm_y} \cdot \boldsymbol{T}_{n_xn_z})L_3(m_z, n_x, n_y) \\
&+ 467(\boldsymbol{T}_{m_xm_y} \cdot \boldsymbol{T}_{n_xn_z})L_3(m_z, n_y, n_z) - 212(\boldsymbol{T}_{m_xm_y} \cdot \boldsymbol{T}_{n_yn_z})L_3(m_z, n_x, n_x) \\
&+ 510(\boldsymbol{T}_{m_xm_y} \cdot \boldsymbol{T}_{n_yn_z})L_3(m_z, n_x, n_y) + 43(\boldsymbol{T}_{m_xm_y} \cdot \boldsymbol{T}_{n_yn_z})L_3(m_z, n_x, n_z) \\
&+ 43(\boldsymbol{T}_{m_ym_z} \cdot \boldsymbol{T}_{n_xn_y})L_3(m_x, n_x, n_z) + 510(\boldsymbol{T}_{m_ym_z} \cdot \boldsymbol{T}_{n_xn_y})L_3(m_x, n_y, n_z) \\
&- 212(\boldsymbol{T}_{m_ym_z} \cdot \boldsymbol{T}_{n_xn_y})L_3(m_x, n_z, n_z) + 467(\boldsymbol{T}_{m_ym_z} \cdot \boldsymbol{T}_{n_xn_z})L_3(m_x, n_x, n_y) \\
&- 467(\boldsymbol{T}_{m_ym_z} \cdot \boldsymbol{T}_{n_xn_z})L_3(m_x, n_y, n_z) + 212(\boldsymbol{T}_{m_ym_z} \cdot \boldsymbol{T}_{n_yn_z})L_3(m_x, n_x, n_x) \\
&- 510(\boldsymbol{T}_{m_ym_z} \cdot \boldsymbol{T}_{n_yn_z})L_3(m_x, n_x, n_y) - 43(\boldsymbol{T}_{m_ym_z} \cdot \boldsymbol{T}_{n_yn_z})L_3(m_x, n_x, n_z)),
\end{aligned}
$$

$$
\begin{aligned}
S_{mn} =& v60480k02(-131I_{m_xn_x}L_5(m_y,m_z,n_x,n_y,n_z) - 124I_{m_xn_x}L_5(m_y,m_z,n_y,n_y,n_z)\\
&+ 168I_{m_xn_x}L_5(m_y,m_z,n_y,n_z,n_z) - 44I_{m_xn_y}L_5(m_y,m_z,n_x,n_x,n_z)\\
&+ 262I_{m_xn_y}L_5(m_y,m_z,n_x,n_y,n_z) - 44I_{m_xn_y}L_5(m_y,m_z,n_x,n_z,n_z)\\
&+ 168I_{m_xn_z}L_5(m_y,m_z,n_x,n_x,n_y) - 124I_{m_xn_z}L_5(m_y,m_z,n_x,n_y,n_y)\\
&- 131I_{m_xn_z}L_5(m_y,m_z,n_x,n_y,n_z) + 262I_{m_yn_x}L_5(m_x,m_z,n_x,n_y,n_z)\\
&+ 248I_{m_yn_x}L_5(m_x,m_z,n_y,n_y,n_z) - 336I_{m_yn_x}L_5(m_x,m_z,n_y,n_z,n_z)\\
&+ 88I_{m_yn_y}L_5(m_x,m_z,n_x,n_x,n_z) - 524I_{m_yn_y}L_5(m_x,m_z,n_x,n_y,n_z)\\
&+ 88I_{m_yn_y}L_5(m_x,m_z,n_x,n_z,n_z) - 336I_{m_yn_z}L_5(m_x,m_z,n_x,n_x,n_y)\\
&+ 248I_{m_yn_z}L_5(m_x,m_z,n_x,n_y,n_y) + 262I_{m_yn_z}L_5(m_x,m_z,n_x,n_y,n_z)\\
&- 131I_{m_zn_x}L_5(m_x,m_y,n_x,n_y,n_z) - 124I_{m_zn_x}L_5(m_x,m_y,n_y,n_y,n_z)\\
&+ 168I_{m_zn_x}L_5(m_x,m_y,n_y,n_z,n_z) - 44I_{m_zn_y}L_5(m_x,m_y,n_x,n_x,n_z)\\
&+ 262I_{m_zn_y}L_5(m_x,m_y,n_x,n_y,n_z) - 44I_{m_zn_y}L_5(m_x,m_y,n_x,n_z,n_z)\\
&+ 168I_{m_zn_z}L_5(m_x,m_y,n_x,n_x,n_y) - 124I_{m_zn_z}L_5(m_x,m_y,n_x,n_y,n_y)\\
&- 131I_{m_zn_z}L_5(m_x,m_y,n_x,n_y,n_z)).
\end{aligned}
$$

$$
\begin{aligned}
&< c_{2m}, j_{3n} >\\
&\quad R_{mn} = v3\_3240\\
&\qquad (2(\boldsymbol{T}_{m_xm_y}\cdot\boldsymbol{T}_{n_0n_2})L_3(m_z,n_1,n_3) + 2(\boldsymbol{T}_{m_xm_y}\cdot\boldsymbol{T}_{n_0n_3})L_3(m_z,n_1,n_2)\\
&\qquad + 2(\boldsymbol{T}_{m_xm_y}\cdot\boldsymbol{T}_{n_1n_2})L_3(m_z,n_0,n_3) + 2(\boldsymbol{T}_{m_xm_y}\cdot\boldsymbol{T}_{n_1n_3})L_3(m_z,n_0,n_2)\\
&\qquad - 2(\boldsymbol{T}_{m_ym_z}\cdot\boldsymbol{T}_{n_0n_2})L_3(m_x,n_1,n_3) - 2(\boldsymbol{T}_{m_ym_z}\cdot\boldsymbol{T}_{n_0n_3})L_3(m_x,n_1,n_2)\\
&\qquad - 2(\boldsymbol{T}_{m_ym_z}\cdot\boldsymbol{T}_{n_1n_2})L_3(m_x,n_0,n_3) - 2(\boldsymbol{T}_{m_ym_z}\cdot\boldsymbol{T}_{n_1n_3})L_3(m_x,n_0,n_2)),\\
&\quad S_{mn} = v60480k02\\
&\qquad (I_{m_xn_0}L_5(m_y,m_z,n_1,n_2,n_3) + I_{m_xn_1}L_5(m_y,m_z,n_0,n_2,n_3)\\
&\qquad - I_{m_xn_2}L_5(m_y,m_z,n_0,n_1,n_3) - I_{m_xn_3}L_5(m_y,m_z,n_0,n_1,n_2)\\
&\qquad - 2I_{m_yn_0}L_5(m_x,m_z,n_1,n_2,n_3) - 2I_{m_yn_1}L_5(m_x,m_z,n_0,n_2,n_3)\\
&\qquad + 2I_{m_yn_2}L_5(m_x,m_z,n_0,n_1,n_3) + 2I_{m_yn_3}L_5(m_x,m_z,n_0,n_1,n_2)\\
&\qquad + I_{m_zn_0}L_5(m_x,m_y,n_1,n_2,n_3) + I_{m_zn_1}L_5(m_x,m_y,n_0,n_2,n_3)\\
&\qquad - I_{m_zn_2}L_5(m_x,m_y,n_0,n_1,n_3) - I_{m_zn_3}L_5(m_x,m_y,n_0,n_1,n_2)).
\end{aligned}
$$

$< c_{2m}, k_{3n} >$

$$
\begin{aligned}
R_{mn} =& v3\_3240 \\
& (-(\boldsymbol{T}_{m_x m_y} \cdot \boldsymbol{T}_{n_0 n_2}) L_3(m_z, n_1, n_3) + (\boldsymbol{T}_{m_x m_y} \cdot \boldsymbol{T}_{n_0 n_3}) L_3(m_z, n_1, n_2) \\
& - (\boldsymbol{T}_{m_x m_y} \cdot \boldsymbol{T}_{n_1 n_2}) L_3(m_z, n_0, n_3) + (\boldsymbol{T}_{m_x m_y} \cdot \boldsymbol{T}_{n_1 n_3}) L_3(m_z, n_0, n_2) \\
& + 2(\boldsymbol{T}_{m_x m_y} \cdot \boldsymbol{T}_{n_2 n_3}) L_3(m_z, n_0, n_1) + (\boldsymbol{T}_{m_y m_z} \cdot \boldsymbol{T}_{n_0 n_2}) L_3(m_x, n_1, n_3) \\
& - (\boldsymbol{T}_{m_y m_z} \cdot \boldsymbol{T}_{n_0 n_3}) L_3(m_x, n_1, n_2) + (\boldsymbol{T}_{m_y m_z} \cdot \boldsymbol{T}_{n_1 n_2}) L_3(m_x, n_0, n_3) \\
& - (\boldsymbol{T}_{m_y m_z} \cdot \boldsymbol{T}_{n_1 n_3}) L_3(m_x, n_0, n_2) - 2(\boldsymbol{T}_{m_y m_z} \cdot \boldsymbol{T}_{n_2 n_3}) L_3(m_x, n_0, n_1)), \\
S_{mn} =& v60480k02 \\
& (I_{m_x n_2} L_5(m_y, m_z, n_0, n_1, n_3) - I_{m_x n_3} L_5(m_y, m_z, n_0, n_1, n_2) \\
& - 2I_{m_y n_2} L_5(m_x, m_z, n_0, n_1, n_3) + 2I_{m_y n_3} L_5(m_x, m_z, n_0, n_1, n_2) \\
& + I_{m_z n_2} L_5(m_x, m_y, n_0, n_1, n_3) - I_{m_z n_3} L_5(m_x, m_y, n_0, n_1, n_2)).
\end{aligned}
$$

$< c_{2m}, l_{3n} >$

$$
\begin{aligned}
R_{mn} =& v3\_3240 \\
& (2(\boldsymbol{T}_{m_x m_y} \cdot \boldsymbol{T}_{n_0 n_1}) L_3(m_z, n_2, n_3) + (\boldsymbol{T}_{m_x m_y} \cdot \boldsymbol{T}_{n_0 n_2}) L_3(m_z, n_1, n_3) \\
& + (\boldsymbol{T}_{m_x m_y} \cdot \boldsymbol{T}_{n_0 n_3}) L_3(m_z, n_1, n_2) - (\boldsymbol{T}_{m_x m_y} \cdot \boldsymbol{T}_{n_1 n_2}) L_3(m_z, n_0, n_3) \\
& - (\boldsymbol{T}_{m_x m_y} \cdot \boldsymbol{T}_{n_1 n_3}) L_3(m_z, n_0, n_2) - 2(\boldsymbol{T}_{m_y m_z} \cdot \boldsymbol{T}_{n_0 n_1}) L_3(m_x, n_2, n_3) \\
& - (\boldsymbol{T}_{m_y m_z} \cdot \boldsymbol{T}_{n_0 n_2}) L_3(m_x, n_1, n_3) - (\boldsymbol{T}_{m_y m_z} \cdot \boldsymbol{T}_{n_0 n_3}) L_3(m_x, n_1, n_2) \\
& + (\boldsymbol{T}_{m_y m_z} \cdot \boldsymbol{T}_{n_1 n_2}) L_3(m_x, n_0, n_3) + (\boldsymbol{T}_{m_y m_z} \cdot \boldsymbol{T}_{n_1 n_3}) L_3(m_x, n_0, n_2)), \\
S_{mn} =& v60480k02(I_{m_x n_0} L_5(m_y, m_z, n_1, n_2, n_3) - I_{m_x n_1} L_5(m_y, m_z, n_0, n_2, n_3) \\
& - 2I_{m_y n_0} L_5(m_x, m_z, n_1, n_2, n_3) + 2I_{m_y n_1} L_5(m_x, m_z, n_0, n_2, n_3) \\
& + I_{m_z n_0} L_5(m_x, m_y, n_1, n_2, n_3) - I_{m_z n_1} L_5(m_x, m_y, n_0, n_2, n_3)).
\end{aligned}
$$

$< d_{2m}, d_{2n} >$

$$
\begin{aligned}
R_{mn} =& v3\_1620(L_2(m_x, n_x) \boldsymbol{T}_{m_y m_z} \cdot \boldsymbol{T}_{n_y n_z} + 2.0 L_2(m_x, n_y) \boldsymbol{T}_{m_y m_z} \cdot \boldsymbol{T}_{n_x n_z} \\
& + L_2(m_x, n_z) \boldsymbol{T}_{m_y m_z} \cdot \boldsymbol{T}_{n_x n_y} + 2.0 L_2(m_y, n_x) \boldsymbol{T}_{m_x m_z} \cdot \boldsymbol{T}_{n_y n_z} \\
& + 4.0 L_2(m_y, n_y) \boldsymbol{T}_{m_x m_z} \cdot \boldsymbol{T}_{n_x n_z} + 2.0 L_2(m_y, n_z) \boldsymbol{T}_{m_x m_z} \cdot \boldsymbol{T}_{n_x n_y} \\
& + L_2(m_z, n_x) \boldsymbol{T}_{m_x m_y} \cdot \boldsymbol{T}_{n_y n_z} + 2.0 L_2(m_z, n_y) \boldsymbol{T}_{m_x m_y} \cdot \boldsymbol{T}_{n_x n_z} \\
& + L_2(m_z, n_z) \boldsymbol{T}_{m_x m_y} \cdot \boldsymbol{T}_{n_x n_y}), \\
S_{mn} =& v7560k02(L_4(m_x, m_y, n_x, n_y) I_{m_z n_z} - L_4(m_x, m_y, n_y, n_z) I_{m_z n_x} \\
& - L_4(m_y, m_z, n_x, n_y) I_{m_x n_z} + L_4(m_y, m_z, n_y, n_z) I_{m_x n_x}).
\end{aligned}
$$

$< d_{2m}, e_{2n} >$

$$
\begin{aligned}
R_{mn} =& 0.0, \\
S_{mn} =& v7560k02(2.0 L_4(m_x, m_y, n_i, n_j) I_{m_z n_j} - L_3(m_x, m_y, n_i) I_{m_z n_j} \\
& - 2.0 L_4(m_x, m_y, n_i, n_j) I_{m_z n_i} + L_3(m_x, m_y, n_j) I_{m_z n_i} \\
& - 2.0 L_4(m_y, m_z, n_i, n_j) I_{m_x n_j} + L_3(m_y, m_z, n_i) I_{m_x n_j} \\
& + 2.0 L_4(m_y, m_z, n_i, n_j) I_{m_x n_i} - L_3(m_y, m_z, n_j) I_{m_x n_i}).
\end{aligned}
$$

$$
\begin{aligned}
&< d_{2m}, f_{2n} > \\
&\quad R_{mn} = 0.0, \\
&\quad S_{mn} = v7560k02(L_4(m_x, m_y, n_x, n_y) I_{m_z n_z} + L_4(m_x, m_y, n_y, n_z) I_{m_z n_x} \\
&\qquad + L_4(m_x, m_y, n_x, n_z) I_{m_z n_y} - L_4(m_y, m_z, n_x, n_y) I_{m_x n_z} \\
&\qquad - L_4(m_y, m_z, n_y, n_z) I_{m_x n_x} - L_4(m_y, m_z, n_x, n_z) I_{m_x n_y}).
\end{aligned}
$$

$$
\begin{aligned}
&< d_{2m}, g_{3n} > \\
&\quad R_{mn} = v3\_4860(-(\boldsymbol{T}_{m_x m_y} \cdot \boldsymbol{T}_{n_x n_y}) L_3(m_z, n_x, n_z) - (\boldsymbol{T}_{m_x m_y} \cdot \boldsymbol{T}_{n_x n_y}) L_3(m_z, n_y, n_z) \\
&\qquad + (\boldsymbol{T}_{m_x m_y} \cdot \boldsymbol{T}_{n_x n_y}) L_3(m_z, n_z, n_z) + (\boldsymbol{T}_{m_x m_y} \cdot \boldsymbol{T}_{n_x n_z}) L_3(m_z, n_x, n_y) \\
&\qquad - (\boldsymbol{T}_{m_x m_y} \cdot \boldsymbol{T}_{n_x n_z}) L_3(m_z, n_y, n_y) + (\boldsymbol{T}_{m_x m_y} \cdot \boldsymbol{T}_{n_x n_z}) L_3(m_z, n_y, n_z) \\
&\qquad + (\boldsymbol{T}_{m_x m_y} \cdot \boldsymbol{T}_{n_y n_z}) L_3(m_z, n_x, n_x) - (\boldsymbol{T}_{m_x m_y} \cdot \boldsymbol{T}_{n_y n_z}) L_3(m_z, n_x, n_y) \\
&\qquad - (\boldsymbol{T}_{m_x m_y} \cdot \boldsymbol{T}_{n_y n_z}) L_3(m_z, n_x, n_z) - 2(\boldsymbol{T}_{m_x m_z} \cdot \boldsymbol{T}_{n_x n_y}) L_3(m_y, n_x, n_z) \\
&\qquad - 2(\boldsymbol{T}_{m_x m_z} \cdot \boldsymbol{T}_{n_x n_y}) L_3(m_y, n_y, n_z) + 2(\boldsymbol{T}_{m_x m_z} \cdot \boldsymbol{T}_{n_x n_y}) L_3(m_y, n_z, n_z) \\
&\qquad + 2(\boldsymbol{T}_{m_x m_z} \cdot \boldsymbol{T}_{n_x n_z}) L_3(m_y, n_x, n_y) - 2(\boldsymbol{T}_{m_x m_z} \cdot \boldsymbol{T}_{n_x n_z}) L_3(m_y, n_y, n_y) \\
&\qquad + 2(\boldsymbol{T}_{m_x m_z} \cdot \boldsymbol{T}_{n_x n_z}) L_3(m_y, n_y, n_z) + 2(\boldsymbol{T}_{m_x m_z} \cdot \boldsymbol{T}_{n_y n_z}) L_3(m_y, n_x, n_x) \\
&\qquad - 2(\boldsymbol{T}_{m_x m_z} \cdot \boldsymbol{T}_{n_y n_z}) L_3(m_y, n_x, n_y) - 2(\boldsymbol{T}_{m_x m_z} \cdot \boldsymbol{T}_{n_y n_z}) L_3(m_y, n_x, n_z) \\
&\qquad - (\boldsymbol{T}_{m_y m_z} \cdot \boldsymbol{T}_{n_x n_y}) L_3(m_x, n_x, n_z) - (\boldsymbol{T}_{m_y m_z} \cdot \boldsymbol{T}_{n_x n_y}) L_3(m_x, n_y, n_z) \\
&\qquad + (\boldsymbol{T}_{m_y m_z} \cdot \boldsymbol{T}_{n_x n_y}) L_3(m_x, n_z, n_z) + (\boldsymbol{T}_{m_y m_z} \cdot \boldsymbol{T}_{n_x n_z}) L_3(m_x, n_x, n_y) \\
&\qquad - (\boldsymbol{T}_{m_y m_z} \cdot \boldsymbol{T}_{n_x n_z}) L_3(m_x, n_y, n_y) + (\boldsymbol{T}_{m_y m_z} \cdot \boldsymbol{T}_{n_x n_z}) L_3(m_x, n_y, n_z) \\
&\qquad + (\boldsymbol{T}_{m_y m_z} \cdot \boldsymbol{T}_{n_y n_z}) L_3(m_x, n_x, n_x) - (\boldsymbol{T}_{m_y m_z} \cdot \boldsymbol{T}_{n_y n_z}) L_3(m_x, n_x, n_y) \\
&\qquad - (\boldsymbol{T}_{m_y m_z} \cdot \boldsymbol{T}_{n_y n_z}) L_3(m_x, n_x, n_z)), \\
&\quad S_{mn} = v60480k02(-I_{m_x n_x} L_5(m_y, m_z, n_y, n_y, n_z) + I_{m_x n_x} L_5(m_y, m_z, n_y, n_z, n_z) \\
&\qquad + I_{m_x n_y} L_5(m_y, m_z, n_x, n_x, n_z) - I_{m_x n_y} L_5(m_y, m_z, n_x, n_z, n_z) \\
&\qquad - I_{m_x n_z} L_5(m_y, m_z, n_x, n_x, n_y) + I_{m_x n_z} L_5(m_y, m_z, n_x, n_y, n_y) \\
&\qquad + I_{m_z n_x} L_5(m_x, m_y, n_y, n_y, n_z) - I_{m_z n_x} L_5(m_x, m_y, n_y, n_z, n_z) \\
&\qquad - I_{m_z n_y} L_5(m_x, m_y, n_x, n_x, n_z) + I_{m_z n_y} L_5(m_x, m_y, n_x, n_z, n_z) \\
&\qquad + I_{m_z n_z} L_5(m_x, m_y, n_x, n_x, n_y) - I_{m_z n_z} L_5(m_x, m_y, n_x, n_y, n_y)).
\end{aligned}
$$

$< d_{2m}, h_{3n} >$

$$
\begin{aligned}
R_{mn} =& v3\_9720(977(\boldsymbol{T}_{m_xm_y} \cdot \boldsymbol{T}_{n_xn_y})L_3(m_z, n_x, n_z) - 424(\boldsymbol{T}_{m_xm_y} \cdot \boldsymbol{T}_{n_xn_y})L_3(m_z, n_y, n_z) \\
&- 212(\boldsymbol{T}_{m_xm_y} \cdot \boldsymbol{T}_{n_xn_y})L_3(m_z, n_z, n_z) + 553(\boldsymbol{T}_{m_xm_y} \cdot \boldsymbol{T}_{n_xn_z})L_3(m_z, n_x, n_y) \\
&- 424(\boldsymbol{T}_{m_xm_y} \cdot \boldsymbol{T}_{n_xn_z})L_3(m_z, n_y, n_y) + 553(\boldsymbol{T}_{m_xm_y} \cdot \boldsymbol{T}_{n_xn_z})L_3(m_z, n_y, n_z) \\
&- 212(\boldsymbol{T}_{m_xm_y} \cdot \boldsymbol{T}_{n_yn_z})L_3(m_z, n_x, n_x) - 424(\boldsymbol{T}_{m_xm_y} \cdot \boldsymbol{T}_{n_yn_z})L_3(m_z, n_x, n_y) \\
&+ 977(\boldsymbol{T}_{m_xm_y} \cdot \boldsymbol{T}_{n_yn_z})L_3(m_z, n_x, n_z) + 1954(\boldsymbol{T}_{m_xm_z} \cdot \boldsymbol{T}_{n_xn_y})L_3(m_y, n_x, n_z) \\
&- 848(\boldsymbol{T}_{m_xm_z} \cdot \boldsymbol{T}_{n_xn_y})L_3(m_y, n_y, n_z) - 424(\boldsymbol{T}_{m_xm_z} \cdot \boldsymbol{T}_{n_xn_y})L_3(m_y, n_z, n_z) \\
&+ 1106(\boldsymbol{T}_{m_xm_z} \cdot \boldsymbol{T}_{n_xn_z})L_3(m_y, n_x, n_y) - 848(\boldsymbol{T}_{m_xm_z} \cdot \boldsymbol{T}_{n_xn_z})L_3(m_y, n_y, n_y) \\
&+ 1106(\boldsymbol{T}_{m_xm_z} \cdot \boldsymbol{T}_{n_xn_z})L_3(m_y, n_y, n_z) - 424(\boldsymbol{T}_{m_xm_z} \cdot \boldsymbol{T}_{n_yn_z})L_3(m_y, n_x, n_x) \\
&- 848(\boldsymbol{T}_{m_xm_z} \cdot \boldsymbol{T}_{n_yn_z})L_3(m_y, n_x, n_y) + 1954(\boldsymbol{T}_{m_xm_z} \cdot \boldsymbol{T}_{n_yn_z})L_3(m_y, n_x, n_z) \\
&+ 977(\boldsymbol{T}_{m_ym_z} \cdot \boldsymbol{T}_{n_xn_y})L_3(m_x, n_x, n_z) - 424(\boldsymbol{T}_{m_ym_z} \cdot \boldsymbol{T}_{n_xn_y})L_3(m_x, n_y, n_z) \\
&- 212(\boldsymbol{T}_{m_ym_z} \cdot \boldsymbol{T}_{n_xn_y})L_3(m_x, n_z, n_z) + 553(\boldsymbol{T}_{m_ym_z} \cdot \boldsymbol{T}_{n_xn_z})L_3(m_x, n_x, n_y) \\
&- 424(\boldsymbol{T}_{m_ym_z} \cdot \boldsymbol{T}_{n_xn_z})L_3(m_x, n_y, n_y) + 553(\boldsymbol{T}_{m_ym_z} \cdot \boldsymbol{T}_{n_xn_z})L_3(m_x, n_y, n_z) \\
&- 212(\boldsymbol{T}_{m_ym_z} \cdot \boldsymbol{T}_{n_yn_z})L_3(m_x, n_x, n_x) - 424(\boldsymbol{T}_{m_ym_z} \cdot \boldsymbol{T}_{n_yn_z})L_3(m_x, n_x, n_y) \\
&+ 977(\boldsymbol{T}_{m_ym_z} \cdot \boldsymbol{T}_{n_yn_z})L_3(m_x, n_x, n_z)), \\
S_{mn} =& v60480k02(393I_{m_xn_x}L_5(m_y, m_z, n_x, n_y, n_z) - 212I_{m_xn_x}L_5(m_y, m_z, n_y, n_y, n_z) \\
&+ 80I_{m_xn_x}L_5(m_y, m_z, n_y, n_z, n_z) - 292I_{m_xn_y}L_5(m_y, m_z, n_x, n_x, n_z) \\
&+ 292I_{m_xn_y}L_5(m_y, m_z, n_x, n_z, n_z) - 80I_{m_xn_z}L_5(m_y, m_z, n_x, n_x, n_y) \\
&+ 212I_{m_xn_z}L_5(m_y, m_z, n_x, n_y, n_y) - 393I_{m_xn_z}L_5(m_y, m_z, n_x, n_y, n_z) \\
&- 393I_{m_zn_x}L_5(m_x, m_y, n_x, n_y, n_z) + 212I_{m_zn_x}L_5(m_x, m_y, n_y, n_y, n_z) \\
&- 80I_{m_zn_x}L_5(m_x, m_y, n_y, n_z, n_z) + 292I_{m_zn_y}L_5(m_x, m_y, n_x, n_x, n_z) \\
&- 292I_{m_zn_y}L_5(m_x, m_y, n_x, n_z, n_z) + 80I_{m_zn_z}L_5(m_x, m_y, n_x, n_x, n_y) \\
&- 212I_{m_zn_z}L_5(m_x, m_y, n_x, n_y, n_y) + 393I_{m_zn_z}L_5(m_x, m_y, n_x, n_y, n_z)).
\end{aligned}
$$

$< d_{2m}, i_{3n} >$

$$
\begin{aligned}
R_{mn} =& v3\_9720(43(\boldsymbol{T}_{m_xm_y} \cdot \boldsymbol{T}_{n_xn_y})L_3(m_z, n_x, n_z) + 510(\boldsymbol{T}_{m_xm_y} \cdot \boldsymbol{T}_{n_xn_y})L_3(m_z, n_y, n_z) \\
&- 212(\boldsymbol{T}_{m_xm_y} \cdot \boldsymbol{T}_{n_xn_y})L_3(m_z, n_z, n_z) + 467(\boldsymbol{T}_{m_xm_y} \cdot \boldsymbol{T}_{n_xn_z})L_3(m_z, n_x, n_y) \\
&- 467(\boldsymbol{T}_{m_xm_y} \cdot \boldsymbol{T}_{n_xn_z})L_3(m_z, n_y, n_z) + 212(\boldsymbol{T}_{m_xm_y} \cdot \boldsymbol{T}_{n_yn_z})L_3(m_z, n_x, n_x) \\
&- 510(\boldsymbol{T}_{m_xm_y} \cdot \boldsymbol{T}_{n_yn_z})L_3(m_z, n_x, n_y) - 43(\boldsymbol{T}_{m_xm_y} \cdot \boldsymbol{T}_{n_yn_z})L_3(m_z, n_x, n_z) \\
&+ 86(\boldsymbol{T}_{m_xm_z} \cdot \boldsymbol{T}_{n_xn_y})L_3(m_y, n_x, n_z) + 1020(\boldsymbol{T}_{m_xm_z} \cdot \boldsymbol{T}_{n_xn_y})L_3(m_y, n_y, n_z) \\
&- 424(\boldsymbol{T}_{m_xm_z} \cdot \boldsymbol{T}_{n_xn_y})L_3(m_y, n_z, n_z) + 934(\boldsymbol{T}_{m_xm_z} \cdot \boldsymbol{T}_{n_xn_z})L_3(m_y, n_x, n_y) \\
&- 934(\boldsymbol{T}_{m_xm_z} \cdot \boldsymbol{T}_{n_xn_z})L_3(m_y, n_y, n_z) + 424(\boldsymbol{T}_{m_xm_z} \cdot \boldsymbol{T}_{n_yn_z})L_3(m_y, n_x, n_x) \\
&- 1020(\boldsymbol{T}_{m_xm_z} \cdot \boldsymbol{T}_{n_yn_z})L_3(m_y, n_x, n_y) - 86(\boldsymbol{T}_{m_xm_z} \cdot \boldsymbol{T}_{n_yn_z})L_3(m_y, n_x, n_z) \\
&+ 43(\boldsymbol{T}_{m_ym_z} \cdot \boldsymbol{T}_{n_xn_y})L_3(m_x, n_x, n_z) + 510(\boldsymbol{T}_{m_ym_z} \cdot \boldsymbol{T}_{n_xn_y})L_3(m_x, n_y, n_z) \\
&- 212(\boldsymbol{T}_{m_ym_z} \cdot \boldsymbol{T}_{n_xn_y})L_3(m_x, n_z, n_z) + 467(\boldsymbol{T}_{m_ym_z} \cdot \boldsymbol{T}_{n_xn_z})L_3(m_x, n_x, n_y) \\
&- 467(\boldsymbol{T}_{m_ym_z} \cdot \boldsymbol{T}_{n_xn_z})L_3(m_x, n_y, n_z) + 212(\boldsymbol{T}_{m_ym_z} \cdot \boldsymbol{T}_{n_yn_z})L_3(m_x, n_x, n_x) \\
&- 510(\boldsymbol{T}_{m_ym_z} \cdot \boldsymbol{T}_{n_yn_z})L_3(m_x, n_x, n_y) - 43(\boldsymbol{T}_{m_ym_z} \cdot \boldsymbol{T}_{n_yn_z})L_3(m_x, n_x, n_z)),
\end{aligned}
$$

$$
\begin{aligned}
S_{mn} =& v60480k02(131I_{m_xn_x}L_5(m_y,m_z,n_x,n_y,n_z) + 124I_{m_xn_x}L_5(m_y,m_z,n_y,n_y,n_z)\\
&- 168I_{m_xn_x}L_5(m_y,m_z,n_y,n_z,n_z) + 44I_{m_xn_y}L_5(m_y,m_z,n_x,n_x,n_z)\\
&- 262I_{m_xn_y}L_5(m_y,m_z,n_x,n_y,n_z) + 44I_{m_xn_y}L_5(m_y,m_z,n_x,n_z,n_z)\\
&- 168I_{m_xn_z}L_5(m_y,m_z,n_x,n_x,n_y) + 124I_{m_xn_z}L_5(m_y,m_z,n_x,n_y,n_y)\\
&+ 131I_{m_xn_z}L_5(m_y,m_z,n_x,n_y,n_z) - 131I_{m_zn_x}L_5(m_x,m_y,n_x,n_y,n_z)\\
&- 124I_{m_zn_x}L_5(m_x,m_y,n_y,n_y,n_z) + 168I_{m_zn_x}L_5(m_x,m_y,n_y,n_z,n_z)\\
&- 44I_{m_zn_y}L_5(m_x,m_y,n_x,n_x,n_z) + 262I_{m_zn_y}L_5(m_x,m_y,n_x,n_y,n_z)\\
&- 44I_{m_zn_y}L_5(m_x,m_y,n_x,n_z,n_z) + 168I_{m_zn_z}L_5(m_x,m_y,n_x,n_x,n_y)\\
&- 124I_{m_zn_z}L_5(m_x,m_y,n_x,n_y,n_y) - 131I_{m_zn_z}L_5(m_x,m_y,n_x,n_y,n_z)).
\end{aligned}
$$

$< d_{2m}, j_{3n} >$

$$
\begin{aligned}
R_{mn} =& v3\_9720\\
&(-2(\boldsymbol{T}_{m_xm_y}\cdot\boldsymbol{T}_{n_0n_2})L_3(m_z,n_1,n_3) - 2(\boldsymbol{T}_{m_xm_y}\cdot\boldsymbol{T}_{n_0n_3})L_3(m_z,n_1,n_2)\\
&- 2(\boldsymbol{T}_{m_xm_y}\cdot\boldsymbol{T}_{n_1n_2})L_3(m_z,n_0,n_3) - 2(\boldsymbol{T}_{m_xm_y}\cdot\boldsymbol{T}_{n_1n_3})L_3(m_z,n_0,n_2)\\
&- 4(\boldsymbol{T}_{m_xm_z}\cdot\boldsymbol{T}_{n_0n_2})L_3(m_y,n_1,n_3) - 4(\boldsymbol{T}_{m_xm_z}\cdot\boldsymbol{T}_{n_0n_3})L_3(m_y,n_1,n_2)\\
&- 4(\boldsymbol{T}_{m_xm_z}\cdot\boldsymbol{T}_{n_1n_2})L_3(m_y,n_0,n_3) - 4(\boldsymbol{T}_{m_xm_z}\cdot\boldsymbol{T}_{n_1n_3})L_3(m_y,n_0,n_2)\\
&- 2(\boldsymbol{T}_{m_ym_z}\cdot\boldsymbol{T}_{n_0n_2})L_3(m_x,n_1,n_3) - 2(\boldsymbol{T}_{m_ym_z}\cdot\boldsymbol{T}_{n_0n_3})L_3(m_x,n_1,n_2)\\
&- 2(\boldsymbol{T}_{m_ym_z}\cdot\boldsymbol{T}_{n_1n_2})L_3(m_x,n_0,n_3) - 2(\boldsymbol{T}_{m_ym_z}\cdot\boldsymbol{T}_{n_1n_3})L_3(m_x,n_0,n_2)),\\
S_{mn} =& v60480k02\\
&(-I_{m_xn_0}L_5(m_y,m_z,n_1,n_2,n_3) - I_{m_xn_1}L_5(m_y,m_z,n_0,n_2,n_3)\\
&+ I_{m_xn_2}L_5(m_y,m_z,n_0,n_1,n_3) + I_{m_xn_3}L_5(m_y,m_z,n_0,n_1,n_2)\\
&+ I_{m_zn_0}L_5(m_x,m_y,n_1,n_2,n_3) + I_{m_zn_1}L_5(m_x,m_y,n_0,n_2,n_3)\\
&- I_{m_zn_2}L_5(m_x,m_y,n_0,n_1,n_3) - I_{m_zn_3}L_5(m_x,m_y,n_0,n_1,n_2));
\end{aligned}
$$

$< d_{2m}, k_{3n} >$

$$
\begin{aligned}
R_{mn} =& v3\_9720\\
&((\boldsymbol{T}_{m_xm_y}\cdot\boldsymbol{T}_{n_0n_2})L_3(m_z,n_1,n_3) - (\boldsymbol{T}_{m_xm_y}\cdot\boldsymbol{T}_{n_0n_3})L_3(m_z,n_1,n_2)\\
&+ (\boldsymbol{T}_{m_xm_y}\cdot\boldsymbol{T}_{n_1n_2})L_3(m_z,n_0,n_3) - (\boldsymbol{T}_{m_xm_y}\cdot\boldsymbol{T}_{n_1n_3})L_3(m_z,n_0,n_2)\\
&- 2(\boldsymbol{T}_{m_xm_y}\cdot\boldsymbol{T}_{n_2n_3})L_3(m_z,n_0,n_1) + 2(\boldsymbol{T}_{m_xm_z}\cdot\boldsymbol{T}_{n_0n_2})L_3(m_y,n_1,n_3)\\
&- 2(\boldsymbol{T}_{m_xm_z}\cdot\boldsymbol{T}_{n_0n_3})L_3(m_y,n_1,n_2) + 2(\boldsymbol{T}_{m_xm_z}\cdot\boldsymbol{T}_{n_1n_2})L_3(m_y,n_0,n_3)\\
&- 2(\boldsymbol{T}_{m_xm_z}\cdot\boldsymbol{T}_{n_1n_3})L_3(m_y,n_0,n_2) - 4(\boldsymbol{T}_{m_xm_z}\cdot\boldsymbol{T}_{n_2n_3})L_3(m_y,n_0,n_1)\\
&+ (\boldsymbol{T}_{m_ym_z}\cdot\boldsymbol{T}_{n_0n_2})L_3(m_x,n_1,n_3) - (\boldsymbol{T}_{m_ym_z}\cdot\boldsymbol{T}_{n_0n_3})L_3(m_x,n_1,n_2)\\
&+ (\boldsymbol{T}_{m_ym_z}\cdot\boldsymbol{T}_{n_1n_2})L_3(m_x,n_0,n_3) - (\boldsymbol{T}_{m_ym_z}\cdot\boldsymbol{T}_{n_1n_3})L_3(m_x,n_0,n_2)\\
&- 2(\boldsymbol{T}_{m_ym_z}\cdot\boldsymbol{T}_{n_2n_3})L_3(m_x,n_0,n_1)),\\
S_{mn} =& v60480k02\\
&(-I_{m_xn_2}L_5(m_y,m_z,n_0,n_1,n_3) + I_{m_xn_3}L_5(m_y,m_z,n_0,n_1,n_2)\\
&+ I_{m_zn_2}L_5(m_x,m_y,n_0,n_1,n_3) - I_{m_zn_3}L_5(m_x,m_y,n_0,n_1,n_2)).
\end{aligned}
$$

$< d_{2m}, l_{3n} >$

$$
\begin{aligned}
R_{mn} =& v3\_9720 \\
& (-2(\boldsymbol{T}_{m_x m_y} \cdot \boldsymbol{T}_{n_0 n_1}) L_3(m_z, n_2, n_3) - (\boldsymbol{T}_{m_x m_y} \cdot \boldsymbol{T}_{n_0 n_2}) L_3(m_z, n_1, n_3) \\
& - (\boldsymbol{T}_{m_x m_y} \cdot \boldsymbol{T}_{n_0 n_3}) L_3(m_z, n_1, n_2) + (\boldsymbol{T}_{m_x m_y} \cdot \boldsymbol{T}_{n_1 n_2}) L_3(m_z, n_0, n_3) \\
& + (\boldsymbol{T}_{m_x m_y} \cdot \boldsymbol{T}_{n_1 n_3}) L_3(m_z, n_0, n_2) - 4(\boldsymbol{T}_{m_x m_z} \cdot \boldsymbol{T}_{n_0 n_1}) L_3(m_y, n_2, n_3) \\
& - 2(\boldsymbol{T}_{m_x m_z} \cdot \boldsymbol{T}_{n_0 n_2}) L_3(m_y, n_1, n_3) - 2(\boldsymbol{T}_{m_x m_z} \cdot \boldsymbol{T}_{n_0 n_3}) L_3(m_y, n_1, n_2) \\
& + 2(\boldsymbol{T}_{m_x m_z} \cdot \boldsymbol{T}_{n_1 n_2}) L_3(m_y, n_0, n_3) + 2(\boldsymbol{T}_{m_x m_z} \cdot \boldsymbol{T}_{n_1 n_3}) L_3(m_y, n_0, n_2) \\
& - 2(\boldsymbol{T}_{m_y m_z} \cdot \boldsymbol{T}_{n_0 n_1}) L_3(m_x, n_2, n_3) - (\boldsymbol{T}_{m_y m_z} \cdot \boldsymbol{T}_{n_0 n_2}) L_3(m_x, n_1, n_3) \\
& - (\boldsymbol{T}_{m_y m_z} \cdot \boldsymbol{T}_{n_0 n_3}) L_3(m_x, n_1, n_2) + (\boldsymbol{T}_{m_y m_z} \cdot \boldsymbol{T}_{n_1 n_2}) L_3(m_x, n_0, n_3) \\
& + (\boldsymbol{T}_{m_y m_z} \cdot \boldsymbol{T}_{n_1 n_3}) L_3(m_x, n_0, n_2)), \\
S_{mn} =& v60480k02 \\
& (-I_{m_x n_0} L_5(m_y, m_z, n_1, n_2, n_3) + I_{m_x n_1} L_5(m_y, m_z, n_0, n_2, n_3) \\
& + I_{m_z n_0} L_5(m_x, m_y, n_1, n_2, n_3) - I_{m_z n_1} L_5(m_x, m_y, n_0, n_2, n_3)).
\end{aligned}
$$

$< e_{2m}, e_{2n} >$

$$
\begin{aligned}
R_{mn} =& 0.0, \\
S_{mn} =& v7560k02((4.0L_4(m_i, m_j, n_i, n_j) - 2.0L_3(m_i, m_j, n_i) \\
& - 2.0L_3(m_i, n_i, n_j) + L_2(m_i, n_i)) I_{m_j n_j} \\
& - (4.0L_4(m_i, m_j, n_i, n_j) - 2.0L_3(m_i, m_j, n_j) \\
& - 2.0L_3(m_i, n_i, n_j) + L_2(m_i, n_j)) I_{m_j n_i} \\
& - (4.0L_4(m_i, m_j, n_i, n_j) - 2.0L_3(m_i, m_j, n_i) \\
& - 2.0L_3(m_j, n_i, n_j) + L_2(m_j, n_i)) I_{m_i n_j} \\
& + (4.0L_4(m_i, m_j, n_i, n_j) - 2.0L_3(m_i, m_j, n_j) \\
& - 2.0L_3(m_j, n_i, n_j) + L_2(m_j, n_j)) I_{m_i n_i}).
\end{aligned}
$$

$< e_{2m}, f_{2n} >$

$$
\begin{aligned}
R_{mn} =& 0.0, \\
S_{mn} =& v7560k02((2.0L_4(m_i, m_j, n_x, n_y) - L_3(m_i, n_x, n_y)) I_{m_j n_z} \\
& + (2.0L_4(m_i, m_j, n_y, n_z) - L_3(m_i, n_y, n_z)) I_{m_j n_x} \\
& + (2.0L_4(m_i, m_j, n_x, n_z) - L_3(m_i, n_x, n_z)) I_{m_j n_y} \\
& - (2.0L_4(m_i, m_j, n_x, n_y) - L_3(m_j, n_x, n_y)) I_{m_i n_z} \\
& - (2.0L_4(m_i, m_j, n_y, n_z) - L_3(m_j, n_y, n_z)) I_{m_i n_x} \\
& - (2.0L_4(m_i, m_j, n_x, n_z) - L_3(m_j, n_x, n_z)) I_{m_i n_y}).
\end{aligned}
$$

$< e_{2m}, g_{3n} >$

$$
\begin{aligned}
R_{mn} =& 0, \\
S_{mn} =& v60480k02(-2I_{m_in_x}L_5(m_i,m_j,n_y,n_y,n_z) + 2I_{m_in_x}L_5(m_i,m_j,n_y,n_z,n_z) \\
&+ I_{m_in_x}L_5(m_j,m_j,n_y,n_y,n_z) - I_{m_in_x}L_5(m_j,m_j,n_y,n_z,n_z) \\
&+ 2I_{m_in_y}L_5(m_i,m_j,n_x,n_x,n_z) - 2I_{m_in_y}L_5(m_i,m_j,n_x,n_z,n_z) \\
&- I_{m_in_y}L_5(m_j,m_j,n_x,n_x,n_z) + I_{m_in_y}L_5(m_j,m_j,n_x,n_z,n_z) \\
&- 2I_{m_in_z}L_5(m_i,m_j,n_x,n_x,n_y) + 2I_{m_in_z}L_5(m_i,m_j,n_x,n_y,n_y) \\
&+ I_{m_in_z}L_5(m_j,m_j,n_x,n_x,n_y) - I_{m_in_z}L_5(m_j,m_j,n_x,n_y,n_y) \\
&- I_{m_jn_x}L_5(m_i,m_i,n_y,n_y,n_z) + I_{m_jn_x}L_5(m_i,m_i,n_y,n_z,n_z) \\
&+ 2I_{m_jn_x}L_5(m_i,m_j,n_y,n_y,n_z) - 2I_{m_jn_x}L_5(m_i,m_j,n_y,n_z,n_z) \\
&+ I_{m_jn_y}L_5(m_i,m_i,n_x,n_x,n_z) - I_{m_jn_y}L_5(m_i,m_i,n_x,n_z,n_z) \\
&- 2I_{m_jn_y}L_5(m_i,m_j,n_x,n_x,n_z) + 2I_{m_jn_y}L_5(m_i,m_j,n_x,n_z,n_z) \\
&- I_{m_jn_z}L_5(m_i,m_i,n_x,n_x,n_y) + I_{m_jn_z}L_5(m_i,m_i,n_x,n_y,n_y) \\
&+ 2I_{m_jn_z}L_5(m_i,m_j,n_x,n_x,n_y) - 2I_{m_jn_z}L_5(m_i,m_j,n_x,n_y,n_y)).
\end{aligned}
$$

$< e_{2m}, h_{3n} >$

$$
\begin{aligned}
R_{mn} =& 0, \\
S_{mn} =& v60480k02(786I_{m_in_x}L_5(m_i,m_j,n_x,n_y,n_z) - 424I_{m_in_x}L_5(m_i,m_j,n_y,n_y,n_z) \\
&+ 160I_{m_in_x}L_5(m_i,m_j,n_y,n_z,n_z) - 393I_{m_in_x}L_5(m_j,m_j,n_x,n_y,n_z) \\
&+ 212I_{m_in_x}L_5(m_j,m_j,n_y,n_y,n_z) - 80I_{m_in_x}L_5(m_j,m_j,n_y,n_z,n_z) \\
&- 584I_{m_in_y}L_5(m_i,m_j,n_x,n_x,n_z) + 584I_{m_in_y}L_5(m_i,m_j,n_x,n_z,n_z) \\
&+ 292I_{m_in_y}L_5(m_j,m_j,n_x,n_x,n_z) - 292I_{m_in_y}L_5(m_j,m_j,n_x,n_z,n_z) \\
&- 160I_{m_in_z}L_5(m_i,m_j,n_x,n_x,n_y) + 424I_{m_in_z}L_5(m_i,m_j,n_x,n_y,n_y) \\
&- 786I_{m_in_z}L_5(m_i,m_j,n_x,n_y,n_z) + 80I_{m_in_z}L_5(m_j,m_j,n_x,n_x,n_y) \\
&- 212I_{m_in_z}L_5(m_j,m_j,n_x,n_y,n_y) + 393I_{m_in_z}L_5(m_j,m_j,n_x,n_y,n_z) \\
&+ 393I_{m_jn_x}L_5(m_i,m_i,n_x,n_y,n_z) - 212I_{m_jn_x}L_5(m_i,m_i,n_y,n_y,n_z) \\
&+ 80I_{m_jn_x}L_5(m_i,m_i,n_y,n_z,n_z) - 786I_{m_jn_x}L_5(m_i,m_j,n_x,n_y,n_z) \\
&+ 424I_{m_jn_x}L_5(m_i,m_j,n_y,n_y,n_z) - 160I_{m_jn_x}L_5(m_i,m_j,n_y,n_z,n_z) \\
&- 292I_{m_jn_y}L_5(m_i,m_i,n_x,n_x,n_z) + 292I_{m_jn_y}L_5(m_i,m_i,n_x,n_z,n_z) \\
&+ 584I_{m_jn_y}L_5(m_i,m_j,n_x,n_x,n_z) - 584I_{m_jn_y}L_5(m_i,m_j,n_x,n_z,n_z) \\
&- 80I_{m_jn_z}L_5(m_i,m_i,n_x,n_x,n_y) + 212I_{m_jn_z}L_5(m_i,m_i,n_x,n_y,n_y) \\
&- 393I_{m_jn_z}L_5(m_i,m_i,n_x,n_y,n_z) + 160I_{m_jn_z}L_5(m_i,m_j,n_x,n_x,n_y) \\
&- 424I_{m_jn_z}L_5(m_i,m_j,n_x,n_y,n_y) + 786I_{m_jn_z}L_5(m_i,m_j,n_x,n_y,n_z)).
\end{aligned}
$$

$$
\begin{aligned}
&< e_{2m}, i_{3n} > \\
&\quad R_{mn} = 0, \\
&\quad S_{mn} = v60480k02(262I_{m_in_x}L_5(m_i,m_j,n_x,n_y,n_z) + 248I_{m_in_x}L_5(m_i,m_j,n_y,n_y,n_z) \\
&\qquad - 336I_{m_in_x}L_5(m_i,m_j,n_y,n_z,n_z) - 131I_{m_in_x}L_5(m_j,m_j,n_x,n_y,n_z) \\
&\qquad - 124I_{m_in_x}L_5(m_j,m_j,n_y,n_y,n_z) + 168I_{m_in_x}L_5(m_j,m_j,n_y,n_z,n_z) \\
&\qquad + 88I_{m_in_y}L_5(m_i,m_j,n_x,n_x,n_z) - 524I_{m_in_y}L_5(m_i,m_j,n_x,n_y,n_z) \\
&\qquad + 88I_{m_in_y}L_5(m_i,m_j,n_x,n_z,n_z) - 44I_{m_in_y}L_5(m_j,m_j,n_x,n_x,n_z) \\
&\qquad + 262I_{m_in_y}L_5(m_j,m_j,n_x,n_y,n_z) - 44I_{m_in_y}L_5(m_j,m_j,n_x,n_z,n_z) \\
&\qquad - 336I_{m_in_z}L_5(m_i,m_j,n_x,n_x,n_y) + 248I_{m_in_z}L_5(m_i,m_j,n_x,n_y,n_y) \\
&\qquad + 262I_{m_in_z}L_5(m_i,m_j,n_x,n_y,n_z) + 168I_{m_in_z}L_5(m_j,m_j,n_x,n_x,n_y) \\
&\qquad - 124I_{m_in_z}L_5(m_j,m_j,n_x,n_y,n_y) - 131I_{m_in_z}L_5(m_j,m_j,n_x,n_y,n_z) \\
&\qquad + 131I_{m_jn_x}L_5(m_i,m_i,n_x,n_y,n_z) + 124I_{m_jn_x}L_5(m_i,m_i,n_y,n_y,n_z) \\
&\qquad - 168I_{m_jn_x}L_5(m_i,m_i,n_y,n_z,n_z) - 262I_{m_jn_x}L_5(m_i,m_j,n_x,n_y,n_z) \\
&\qquad - 248I_{m_jn_x}L_5(m_i,m_j,n_y,n_y,n_z) + 336I_{m_jn_x}L_5(m_i,m_j,n_y,n_z,n_z) \\
&\qquad + 44I_{m_jn_y}L_5(m_i,m_i,n_x,n_x,n_z) - 262I_{m_jn_y}L_5(m_i,m_i,n_x,n_y,n_z) \\
&\qquad + 44I_{m_jn_y}L_5(m_i,m_i,n_x,n_z,n_z) - 88I_{m_jn_y}L_5(m_i,m_j,n_x,n_x,n_z) \\
&\qquad + 524I_{m_jn_y}L_5(m_i,m_j,n_x,n_y,n_z) - 88I_{m_jn_y}L_5(m_i,m_j,n_x,n_z,n_z) \\
&\qquad - 168I_{m_jn_z}L_5(m_i,m_i,n_x,n_x,n_y) + 124I_{m_jn_z}L_5(m_i,m_i,n_x,n_y,n_y) \\
&\qquad + 131I_{m_jn_z}L_5(m_i,m_i,n_x,n_y,n_z) + 336I_{m_jn_z}L_5(m_i,m_j,n_x,n_x,n_y) \\
&\qquad - 248I_{m_jn_z}L_5(m_i,m_j,n_x,n_y,n_y) - 262I_{m_jn_z}L_5(m_i,m_j,n_x,n_y,n_z)).
\end{aligned}
$$

$$
\begin{aligned}
&< e_{2m}, j_{3n} > \\
&\quad R_{mn} = 0, \\
&\quad S_{mn} = v60480k02 \\
&\qquad (-2I_{m_in_0}L_5(m_i,m_j,n_1,n_2,n_3) + I_{m_in_0}L_5(m_j,m_j,n_1,n_2,n_3) \\
&\qquad - 2I_{m_in_1}L_5(m_i,m_j,n_0,n_2,n_3) + I_{m_in_1}L_5(m_j,m_j,n_0,n_2,n_3) \\
&\qquad + 2I_{m_in_2}L_5(m_i,m_j,n_0,n_1,n_3) - I_{m_in_2}L_5(m_j,m_j,n_0,n_1,n_3) \\
&\qquad + 2I_{m_in_3}L_5(m_i,m_j,n_0,n_1,n_2) - I_{m_in_3}L_5(m_j,m_j,n_0,n_1,n_2) \\
&\qquad - I_{m_jn_0}L_5(m_i,m_i,n_1,n_2,n_3) + 2I_{m_jn_0}L_5(m_i,m_j,n_1,n_2,n_3) \\
&\qquad - I_{m_jn_1}L_5(m_i,m_i,n_0,n_2,n_3) + 2I_{m_jn_1}L_5(m_i,m_j,n_0,n_2,n_3) \\
&\qquad + I_{m_jn_2}L_5(m_i,m_i,n_0,n_1,n_3) - 2I_{m_jn_2}L_5(m_i,m_j,n_0,n_1,n_3) \\
&\qquad + I_{m_jn_3}L_5(m_i,m_i,n_0,n_1,n_2) - 2I_{m_jn_3}L_5(m_i,m_j,n_0,n_1,n_2)).
\end{aligned}
$$

$$
\begin{aligned}
&< e_{2m}, k_{3n} > \\
&\quad R_{mn} =0, \\
&\quad S_{mn} =v60480k02 \\
&\qquad (-2I_{m_in_2}L_5(m_i,m_j,n_0,n_1,n_3) + I_{m_in_2}L_5(m_j,m_j,n_0,n_1,n_3) \\
&\qquad + 2I_{m_in_3}L_5(m_i,m_j,n_0,n_1,n_2) - I_{m_in_3}L_5(m_j,m_j,n_0,n_1,n_2) \\
&\qquad - I_{m_jn_2}L_5(m_i,m_i,n_0,n_1,n_3) + 2I_{m_jn_2}L_5(m_i,m_j,n_0,n_1,n_3) \\
&\qquad + I_{m_jn_3}L_5(m_i,m_i,n_0,n_1,n_2) - 2I_{m_jn_3}L_5(m_i,m_j,n_0,n_1,n_2)).
\end{aligned}
$$

$$
\begin{aligned}
&< e_{2m}, l_{3n} > \\
&\quad R_{mn} =0, \\
&\quad S_{mn} =v60480k02 \\
&\qquad (-2I_{m_in_0}L_5(m_i,m_j,n_1,n_2,n_3) + I_{m_in_0}L_5(m_j,m_j,n_1,n_2,n_3) \\
&\qquad + 2I_{m_in_1}L_5(m_i,m_j,n_0,n_2,n_3) - I_{m_in_1}L_5(m_j,m_j,n_0,n_2,n_3) \\
&\qquad - I_{m_jn_0}L_5(m_i,m_i,n_1,n_2,n_3) + 2I_{m_jn_0}L_5(m_i,m_j,n_1,n_2,n_3) \\
&\qquad + I_{m_jn_1}L_5(m_i,m_i,n_0,n_2,n_3) - 2I_{m_jn_1}L_5(m_i,m_j,n_0,n_2,n_3)).
\end{aligned}
$$

$$
\begin{aligned}
&< f_{2m}, f_{2n} > \\
&\quad R_{mn} =0.0, \\
&\quad S_{mn} =v7560k02(L_4(m_x,m_y,n_x,n_y)I_{m_zn_z} + L_4(m_x,m_y,n_y,n_z)I_{m_zn_x} \\
&\qquad + L_4(m_x,m_y,n_x,n_z)I_{m_zn_y} + L_4(m_y,m_z,n_x,n_y)I_{m_xn_z} \\
&\qquad + L_4(m_y,m_z,n_y,n_z)I_{m_xn_x} + L_4(m_y,m_z,n_x,n_z)I_{m_xn_y} \\
&\qquad + L_4(m_x,m_z,n_x,n_y)I_{m_yn_z} + L_4(m_x,m_z,n_y,n_z)I_{m_yn_x} \\
&\qquad + L_4(m_x,m_z,n_x,n_z)I_{m_yn_y}).
\end{aligned}
$$

$$
\begin{aligned}
&< f_{2m}, g_{3n} > \\
&\quad R_{mn} =0, \\
&\quad S_{mn} =v60480k02(I_{m_xn_x}L_5(m_y,m_z,n_y,n_y,n_z) - I_{m_xn_x}L_5(m_y,m_z,n_y,n_z,n_z) \\
&\qquad - I_{m_xn_y}L_5(m_y,m_z,n_x,n_x,n_z) + I_{m_xn_y}L_5(m_y,m_z,n_x,n_z,n_z) \\
&\qquad + I_{m_xn_z}L_5(m_y,m_z,n_x,n_x,n_y) - I_{m_xn_z}L_5(m_y,m_z,n_x,n_y,n_y) \\
&\qquad + I_{m_yn_x}L_5(m_x,m_z,n_y,n_y,n_z) - I_{m_yn_x}L_5(m_x,m_z,n_y,n_z,n_z) \\
&\qquad - I_{m_yn_y}L_5(m_x,m_z,n_x,n_x,n_z) + I_{m_yn_y}L_5(m_x,m_z,n_x,n_z,n_z) \\
&\qquad + I_{m_yn_z}L_5(m_x,m_z,n_x,n_x,n_y) - I_{m_yn_z}L_5(m_x,m_z,n_x,n_y,n_y) \\
&\qquad + I_{m_zn_x}L_5(m_x,m_y,n_y,n_y,n_z) - I_{m_zn_x}L_5(m_x,m_y,n_y,n_z,n_z) \\
&\qquad - I_{m_zn_y}L_5(m_x,m_y,n_x,n_x,n_z) + I_{m_zn_y}L_5(m_x,m_y,n_x,n_z,n_z) \\
&\qquad + I_{m_zn_z}L_5(m_x,m_y,n_x,n_x,n_y) - I_{m_zn_z}L_5(m_x,m_y,n_x,n_y,n_y)).
\end{aligned}
$$

$< f_{2m}, h_{3n} >$

$$
\begin{aligned}
R_{mn} =& 0, \\
S_{mn} =& v60480k02(-393I_{m_x n_x} L_5(m_y, m_z, n_x, n_y, n_z) + 212I_{m_x n_x} L_5(m_y, m_z, n_y, n_y, n_z) \\
& - 80I_{m_x n_x} L_5(m_y, m_z, n_y, n_z, n_z) + 292I_{m_x n_y} L_5(m_y, m_z, n_x, n_x, n_z) \\
& - 292I_{m_x n_y} L_5(m_y, m_z, n_x, n_z, n_z) + 80I_{m_x n_z} L_5(m_y, m_z, n_x, n_x, n_y) \\
& - 212I_{m_x n_z} L_5(m_y, m_z, n_x, n_y, n_y) + 393I_{m_x n_z} L_5(m_y, m_z, n_x, n_y, n_z) \\
& - 393I_{m_y n_x} L_5(m_x, m_z, n_x, n_y, n_z) + 212I_{m_y n_x} L_5(m_x, m_z, n_y, n_y, n_z) \\
& - 80I_{m_y n_x} L_5(m_x, m_z, n_y, n_z, n_z) + 292I_{m_y n_y} L_5(m_x, m_z, n_x, n_x, n_z) \\
& - 292I_{m_y n_y} L_5(m_x, m_z, n_x, n_z, n_z) + 80I_{m_y n_z} L_5(m_x, m_z, n_x, n_x, n_y) \\
& - 212I_{m_y n_z} L_5(m_x, m_z, n_x, n_y, n_y) + 393I_{m_y n_z} L_5(m_x, m_z, n_x, n_y, n_z) \\
& - 393I_{m_z n_x} L_5(m_x, m_y, n_x, n_y, n_z) + 212I_{m_z n_x} L_5(m_x, m_y, n_y, n_y, n_z) \\
& - 80I_{m_z n_x} L_5(m_x, m_y, n_y, n_z, n_z) + 292I_{m_z n_y} L_5(m_x, m_y, n_x, n_x, n_z) \\
& - 292I_{m_z n_y} L_5(m_x, m_y, n_x, n_z, n_z) + 80I_{m_z n_z} L_5(m_x, m_y, n_x, n_x, n_y) \\
& - 212I_{m_z n_z} L_5(m_x, m_y, n_x, n_y, n_y) + 393I_{m_z n_z} L_5(m_x, m_y, n_x, n_y, n_z)).
\end{aligned}
$$

$< f_{2m}, i_{3n} >$

$$
\begin{aligned}
R_{mn} =& 0, \\
S_{mn} =& v60480k02(-131I_{m_x n_x} L_5(m_y, m_z, n_x, n_y, n_z) - 124I_{m_x n_x} L_5(m_y, m_z, n_y, n_y, n_z) \\
& + 168I_{m_x n_x} L_5(m_y, m_z, n_y, n_z, n_z) - 44I_{m_x n_y} L_5(m_y, m_z, n_x, n_x, n_z) \\
& + 262I_{m_x n_y} L_5(m_y, m_z, n_x, n_y, n_z) - 44I_{m_x n_y} L_5(m_y, m_z, n_x, n_z, n_z) \\
& + 168I_{m_x n_z} L_5(m_y, m_z, n_x, n_x, n_y) - 124I_{m_x n_z} L_5(m_y, m_z, n_x, n_y, n_y) \\
& - 131I_{m_x n_z} L_5(m_y, m_z, n_x, n_y, n_z) - 131I_{m_y n_x} L_5(m_x, m_z, n_x, n_y, n_z) \\
& - 124I_{m_y n_x} L_5(m_x, m_z, n_y, n_y, n_z) + 168I_{m_y n_x} L_5(m_x, m_z, n_y, n_z, n_z) \\
& - 44I_{m_y n_y} L_5(m_x, m_z, n_x, n_x, n_z) + 262I_{m_y n_y} L_5(m_x, m_z, n_x, n_y, n_z) \\
& - 44I_{m_y n_y} L_5(m_x, m_z, n_x, n_z, n_z) + 168I_{m_y n_z} L_5(m_x, m_z, n_x, n_x, n_y) \\
& - 124I_{m_y n_z} L_5(m_x, m_z, n_x, n_y, n_y) - 131I_{m_y n_z} L_5(m_x, m_z, n_x, n_y, n_z) \\
& - 131I_{m_z n_x} L_5(m_x, m_y, n_x, n_y, n_z) - 124I_{m_z n_x} L_5(m_x, m_y, n_y, n_y, n_z) \\
& + 168I_{m_z n_x} L_5(m_x, m_y, n_y, n_z, n_z) - 44I_{m_z n_y} L_5(m_x, m_y, n_x, n_x, n_z) \\
& + 262I_{m_z n_y} L_5(m_x, m_y, n_x, n_y, n_z) - 44I_{m_z n_y} L_5(m_x, m_y, n_x, n_z, n_z) \\
& + 168I_{m_z n_z} L_5(m_x, m_y, n_x, n_x, n_y) - 124I_{m_z n_z} L_5(m_x, m_y, n_x, n_y, n_y) \\
& - 131I_{m_z n_z} L_5(m_x, m_y, n_x, n_y, n_z)).
\end{aligned}
$$

$< f_{2m}, j_{3n} >$

$$R_{mn} = 0,$$

$$\begin{aligned} S_{mn} =& v60480k02 \\ & (I_{m_x n_0} L_5(m_y, m_z, n_1, n_2, n_3) + I_{m_x n_1} L_5(m_y, m_z, n_0, n_2, n_3) \\ & - I_{m_x n_2} L_5(m_y, m_z, n_0, n_1, n_3) - I_{m_x n_3} L_5(m_y, m_z, n_0, n_1, n_2) \\ & + I_{m_y n_0} L_5(m_x, m_z, n_1, n_2, n_3) + I_{m_y n_1} L_5(m_x, m_z, n_0, n_2, n_3) \\ & - I_{m_y n_2} L_5(m_x, m_z, n_0, n_1, n_3) - I_{m_y n_3} L_5(m_x, m_z, n_0, n_1, n_2) \\ & + I_{m_z n_0} L_5(m_x, m_y, n_1, n_2, n_3) + I_{m_z n_1} L_5(m_x, m_y, n_0, n_2, n_3) \\ & - I_{m_z n_2} L_5(m_x, m_y, n_0, n_1, n_3) - I_{m_z n_3} L_5(m_x, m_y, n_0, n_1, n_2)). \end{aligned}$$

$< f_{2m}, k_{3n} >$

$$R_{mn} = 0,$$

$$\begin{aligned} S_{mn} =& v60480k02 \\ & (I_{m_x n_2} L_5(m_y, m_z, n_0, n_1, n_3) - I_{m_x n_3} L_5(m_y, m_z, n_0, n_1, n_2) \\ & + I_{m_y n_2} L_5(m_x, m_z, n_0, n_1, n_3) - I_{m_y n_3} L_5(m_x, m_z, n_0, n_1, n_2) \\ & + I_{m_z n_2} L_5(m_x, m_y, n_0, n_1, n_3) - I_{m_z n_3} L_5(m_x, m_y, n_0, n_1, n_2)). \end{aligned}$$

$< f_{2m}, l_{3n} >$

$$R_{mn} = 0,$$

$$\begin{aligned} S_{mn} =& v60480k02 \\ & (I_{m_x n_0} L_5(m_y, m_z, n_1, n_2, n_3) - I_{m_x n_1} L_5(m_y, m_z, n_0, n_2, n_3) \\ & + I_{m_y n_0} L_5(m_x, m_z, n_1, n_2, n_3) - I_{m_y n_1} L_5(m_x, m_z, n_0, n_2, n_3) \\ & + I_{m_z n_0} L_5(m_x, m_y, n_1, n_2, n_3) - I_{m_z n_1} L_5(m_x, m_y, n_0, n_2, n_3)). \end{aligned}$$

$$
\begin{aligned}
&< g_{3m}, h_{3n} > \\
&\quad R_{mn} = v3\_34020(\alpha+\beta+\gamma), \\
&\quad\quad \alpha = -977(\boldsymbol{T}_{m_xm_y}, \boldsymbol{T}_{n_xn_y})L_4(m_x, m_z, n_x, n_z) + 424(\boldsymbol{T}_{m_xm_y}, \boldsymbol{T}_{n_xn_y})L_4(m_x, m_z, n_y, n_z) \\
&\quad\quad\quad + 212(\boldsymbol{T}_{m_xm_y}, \boldsymbol{T}_{n_xn_y})L_4(m_x, m_z, n_z, n_z) - 977(\boldsymbol{T}_{m_xm_y}, \boldsymbol{T}_{n_xn_y})L_4(m_y, m_z, n_x, n_z) \\
&\quad\quad\quad + 424(\boldsymbol{T}_{m_xm_y}, \boldsymbol{T}_{n_xn_y})L_4(m_y, m_z, n_y, n_z) + 212(\boldsymbol{T}_{m_xm_y}, \boldsymbol{T}_{n_xn_y})L_4(m_y, m_z, n_z, n_z) \\
&\quad\quad\quad + 977(\boldsymbol{T}_{m_xm_y}, \boldsymbol{T}_{n_xn_y})L_4(m_z, m_z, n_x, n_z) - 424(\boldsymbol{T}_{m_xm_y}, \boldsymbol{T}_{n_xn_y})L_4(m_z, m_z, n_y, n_z) \\
&\quad\quad\quad - 212(\boldsymbol{T}_{m_xm_y}, \boldsymbol{T}_{n_xn_y})L_4(m_z, m_z, n_z, n_z) - 553(\boldsymbol{T}_{m_xm_y}, \boldsymbol{T}_{n_xn_z})L_4(m_x, m_z, n_x, n_y) \\
&\quad\quad\quad + 424(\boldsymbol{T}_{m_xm_y}, \boldsymbol{T}_{n_xn_z})L_4(m_x, m_z, n_y, n_y) - 553(\boldsymbol{T}_{m_xm_y}, \boldsymbol{T}_{n_xn_z})L_4(m_x, m_z, n_y, n_z) \\
&\quad\quad\quad - 553(\boldsymbol{T}_{m_xm_y}, \boldsymbol{T}_{n_xn_z})L_4(m_y, m_z, n_x, n_y) + 424(\boldsymbol{T}_{m_xm_y}, \boldsymbol{T}_{n_xn_z})L_4(m_y, m_z, n_y, n_y) \\
&\quad\quad\quad - 553(\boldsymbol{T}_{m_xm_y}, \boldsymbol{T}_{n_xn_z})L_4(m_y, m_z, n_y, n_z) + 553(\boldsymbol{T}_{m_xm_y}, \boldsymbol{T}_{n_xn_z})L_4(m_z, m_z, n_x, n_y) \\
&\quad\quad\quad - 424(\boldsymbol{T}_{m_xm_y}, \boldsymbol{T}_{n_xn_z})L_4(m_z, m_z, n_y, n_y) + 553(\boldsymbol{T}_{m_xm_y}, \boldsymbol{T}_{n_xn_z})L_4(m_z, m_z, n_y, n_z) \\
&\quad\quad\quad + 212(\boldsymbol{T}_{m_xm_y}, \boldsymbol{T}_{n_yn_z})L_4(m_x, m_z, n_x, n_x) + 424(\boldsymbol{T}_{m_xm_y}, \boldsymbol{T}_{n_yn_z})L_4(m_x, m_z, n_x, n_y) \\
&\quad\quad\quad - 977(\boldsymbol{T}_{m_xm_y}, \boldsymbol{T}_{n_yn_z})L_4(m_x, m_z, n_x, n_z) + 212(\boldsymbol{T}_{m_xm_y}, \boldsymbol{T}_{n_yn_z})L_4(m_y, m_z, n_x, n_x) \\
&\quad\quad\quad + 424(\boldsymbol{T}_{m_xm_y}, \boldsymbol{T}_{n_yn_z})L_4(m_y, m_z, n_x, n_y) - 977(\boldsymbol{T}_{m_xm_y}, \boldsymbol{T}_{n_yn_z})L_4(m_y, m_z, n_x, n_z) \\
&\quad\quad\quad - 212(\boldsymbol{T}_{m_xm_y}, \boldsymbol{T}_{n_yn_z})L_4(m_z, m_z, n_x, n_x) - 424(\boldsymbol{T}_{m_xm_y}, \boldsymbol{T}_{n_yn_z})L_4(m_z, m_z, n_x, n_y) \\
&\quad\quad\quad + 977(\boldsymbol{T}_{m_xm_y}, \boldsymbol{T}_{n_yn_z})L_4(m_z, m_z, n_x, n_z) + 977(\boldsymbol{T}_{m_xm_z}, \boldsymbol{T}_{n_xn_y})L_4(m_x, m_y, n_x, n_z) \\
&\quad\quad\quad - 424(\boldsymbol{T}_{m_xm_z}, \boldsymbol{T}_{n_xn_y})L_4(m_x, m_y, n_y, n_z) - 212(\boldsymbol{T}_{m_xm_z}, \boldsymbol{T}_{n_xn_y})L_4(m_x, m_y, n_z, n_z) \\
&\quad\quad\quad - 977(\boldsymbol{T}_{m_xm_z}, \boldsymbol{T}_{n_xn_y})L_4(m_y, m_y, n_x, n_z) + 424(\boldsymbol{T}_{m_xm_z}, \boldsymbol{T}_{n_xn_y})L_4(m_y, m_y, n_y, n_z) \\
&\quad\quad\quad + 212(\boldsymbol{T}_{m_xm_z}, \boldsymbol{T}_{n_xn_y})L_4(m_y, m_y, n_z, n_z) + 977(\boldsymbol{T}_{m_xm_z}, \boldsymbol{T}_{n_xn_y})L_4(m_y, m_z, n_x, n_z), \\
&\quad\quad \beta = -424(\boldsymbol{T}_{m_xm_z}, \boldsymbol{T}_{n_xn_y})L_4(m_y, m_z, n_y, n_z) - 212(\boldsymbol{T}_{m_xm_z}, \boldsymbol{T}_{n_xn_y})L_4(m_y, m_z, n_z, n_z) \\
&\quad\quad\quad + 553(\boldsymbol{T}_{m_xm_z}, \boldsymbol{T}_{n_xn_z})L_4(m_x, m_y, n_x, n_y) - 424(\boldsymbol{T}_{m_xm_z}, \boldsymbol{T}_{n_xn_z})L_4(m_x, m_y, n_y, n_y) \\
&\quad\quad\quad + 553(\boldsymbol{T}_{m_xm_z}, \boldsymbol{T}_{n_xn_z})L_4(m_x, m_y, n_y, n_z) - 553(\boldsymbol{T}_{m_xm_z}, \boldsymbol{T}_{n_xn_z})L_4(m_y, m_y, n_x, n_y) \\
&\quad\quad\quad + 424(\boldsymbol{T}_{m_xm_z}, \boldsymbol{T}_{n_xn_z})L_4(m_y, m_y, n_y, n_y) - 553(\boldsymbol{T}_{m_xm_z}, \boldsymbol{T}_{n_xn_z})L_4(m_y, m_y, n_y, n_z) \\
&\quad\quad\quad + 553(\boldsymbol{T}_{m_xm_z}, \boldsymbol{T}_{n_xn_z})L_4(m_y, m_z, n_x, n_y) - 424(\boldsymbol{T}_{m_xm_z}, \boldsymbol{T}_{n_xn_z})L_4(m_y, m_z, n_y, n_y) \\
&\quad\quad\quad + 553(\boldsymbol{T}_{m_xm_z}, \boldsymbol{T}_{n_xn_z})L_4(m_y, m_z, n_y, n_z) - 212(\boldsymbol{T}_{m_xm_z}, \boldsymbol{T}_{n_yn_z})L_4(m_x, m_y, n_x, n_x) \\
&\quad\quad\quad - 424(\boldsymbol{T}_{m_xm_z}, \boldsymbol{T}_{n_yn_z})L_4(m_x, m_y, n_x, n_y) + 977(\boldsymbol{T}_{m_xm_z}, \boldsymbol{T}_{n_yn_z})L_4(m_x, m_y, n_x, n_z) \\
&\quad\quad\quad + 212(\boldsymbol{T}_{m_xm_z}, \boldsymbol{T}_{n_yn_z})L_4(m_y, m_y, n_x, n_x) + 424(\boldsymbol{T}_{m_xm_z}, \boldsymbol{T}_{n_yn_z})L_4(m_y, m_y, n_x, n_y) \\
&\quad\quad\quad - 977(\boldsymbol{T}_{m_xm_z}, \boldsymbol{T}_{n_yn_z})L_4(m_y, m_y, n_x, n_z) - 212(\boldsymbol{T}_{m_xm_z}, \boldsymbol{T}_{n_yn_z})L_4(m_y, m_z, n_x, n_x) \\
&\quad\quad\quad - 424(\boldsymbol{T}_{m_xm_z}, \boldsymbol{T}_{n_yn_z})L_4(m_y, m_z, n_x, n_y) + 977(\boldsymbol{T}_{m_xm_z}, \boldsymbol{T}_{n_yn_z})L_4(m_y, m_z, n_x, n_z) \\
&\quad\quad\quad + 977(\boldsymbol{T}_{m_ym_z}, \boldsymbol{T}_{n_xn_y})L_4(m_x, m_x, n_x, n_z) - 424(\boldsymbol{T}_{m_ym_z}, \boldsymbol{T}_{n_xn_y})L_4(m_x, m_x, n_y, n_z) \\
&\quad\quad\quad - 212(\boldsymbol{T}_{m_ym_z}, \boldsymbol{T}_{n_xn_y})L_4(m_x, m_x, n_z, n_z) - 977(\boldsymbol{T}_{m_ym_z}, \boldsymbol{T}_{n_xn_y})L_4(m_x, m_y, n_x, n_z) \\
&\quad\quad\quad + 424(\boldsymbol{T}_{m_ym_z}, \boldsymbol{T}_{n_xn_y})L_4(m_x, m_y, n_y, n_z) + 212(\boldsymbol{T}_{m_ym_z}, \boldsymbol{T}_{n_xn_y})L_4(m_x, m_y, n_z, n_z) \\
&\quad\quad\quad - 977(\boldsymbol{T}_{m_ym_z}, \boldsymbol{T}_{n_xn_y})L_4(m_x, m_z, n_x, n_z) + 424(\boldsymbol{T}_{m_ym_z}, \boldsymbol{T}_{n_xn_y})L_4(m_x, m_z, n_y, n_z) \\
&\quad\quad\quad + 212(\boldsymbol{T}_{m_ym_z}, \boldsymbol{T}_{n_xn_y})L_4(m_x, m_z, n_z, n_z) + 553(\boldsymbol{T}_{m_ym_z}, \boldsymbol{T}_{n_xn_z})L_4(m_x, m_x, n_x, n_y) \\
&\quad\quad\quad - 424(\boldsymbol{T}_{m_ym_z}, \boldsymbol{T}_{n_xn_z})L_4(m_x, m_x, n_y, n_y) + 553(\boldsymbol{T}_{m_ym_z}, \boldsymbol{T}_{n_xn_z})L_4(m_x, m_x, n_y, n_z) \\
&\quad\quad\quad - 553(\boldsymbol{T}_{m_ym_z}, \boldsymbol{T}_{n_xn_z})L_4(m_x, m_y, n_x, n_y) + 424(\boldsymbol{T}_{m_ym_z}, \boldsymbol{T}_{n_xn_z})L_4(m_x, m_y, n_y, n_y) \\
&\quad\quad\quad - 553(\boldsymbol{T}_{m_ym_z}, \boldsymbol{T}_{n_xn_z})L_4(m_x, m_y, n_y, n_z) - 553(\boldsymbol{T}_{m_ym_z}, \boldsymbol{T}_{n_xn_z})L_4(m_x, m_z, n_x, n_y) \\
&\quad\quad\quad + 424(\boldsymbol{T}_{m_ym_z}, \boldsymbol{T}_{n_xn_z})L_4(m_x, m_z, n_y, n_y) - 553(\boldsymbol{T}_{m_ym_z}, \boldsymbol{T}_{n_xn_z})L_4(m_x, m_z, n_y, n_z),
\end{aligned}
$$

$$
\begin{aligned}
\gamma = &- 212(\boldsymbol{T}_{m_y m_z}, \boldsymbol{T}_{n_y n_z}) L_4(m_x, m_x, n_x, n_x) - 424(\boldsymbol{T}_{m_y m_z}, \boldsymbol{T}_{n_y n_z}) L_4(m_x, m_x, n_x, n_y) \\
&+ 977(\boldsymbol{T}_{m_y m_z}, \boldsymbol{T}_{n_y n_z}) L_4(m_x, m_x, n_x, n_z) + 212(\boldsymbol{T}_{m_y m_z}, \boldsymbol{T}_{n_y n_z}) L_4(m_x, m_y, n_x, n_x) \\
&+ 424(\boldsymbol{T}_{m_y m_z}, \boldsymbol{T}_{n_y n_z}) L_4(m_x, m_y, n_x, n_y) - 977(\boldsymbol{T}_{m_y m_z}, \boldsymbol{T}_{n_y n_z}) L_4(m_x, m_y, n_x, n_z) \\
&+ 212(\boldsymbol{T}_{m_y m_z}, \boldsymbol{T}_{n_y n_z}) L_4(m_x, m_z, n_x, n_x) + 424(\boldsymbol{T}_{m_y m_z}, \boldsymbol{T}_{n_y n_z}) L_4(m_x, m_z, n_x, n_y) \\
&- 977(\boldsymbol{T}_{m_y m_z}, \boldsymbol{T}_{n_y n_z}) L_4(m_x, m_z, n_x, n_z),
\end{aligned}
$$

$$
\begin{aligned}
S_{mn} = &v544320k02(-393 I_{m_x n_x} L_6(m_y, m_y, m_z, n_x, n_y, n_z) + 212 I_{m_x n_x} L_6(m_y, m_y, m_z, n_y, n_y, n_z) \\
&- 80 I_{m_x n_x} L_6(m_y, m_y, m_z, n_y, n_z, n_z) + 393 I_{m_x n_x} L_6(m_y, m_z, m_z, n_x, n_y, n_z) \\
&- 212 I_{m_x n_x} L_6(m_y, m_z, m_z, n_y, n_y, n_z) + 80 I_{m_x n_x} L_6(m_y, m_z, m_z, n_y, n_z, n_z) \\
&+ 292 I_{m_x n_y} L_6(m_y, m_y, m_z, n_x, n_x, n_z) - 292 I_{m_x n_y} L_6(m_y, m_y, m_z, n_x, n_z, n_z) \\
&- 292 I_{m_x n_y} L_6(m_y, m_z, m_z, n_x, n_x, n_z) + 292 I_{m_x n_y} L_6(m_y, m_z, m_z, n_x, n_z, n_z) \\
&+ 80 I_{m_x n_z} L_6(m_y, m_y, m_z, n_x, n_x, n_y) - 212 I_{m_x n_z} L_6(m_y, m_y, m_z, n_x, n_y, n_y) \\
&+ 393 I_{m_x n_z} L_6(m_y, m_y, m_z, n_x, n_y, n_z) - 80 I_{m_x n_z} L_6(m_y, m_z, m_z, n_x, n_x, n_y) \\
&+ 212 I_{m_x n_z} L_6(m_y, m_z, m_z, n_x, n_y, n_y) - 393 I_{m_x n_z} L_6(m_y, m_z, m_z, n_x, n_y, n_z) \\
&+ 393 I_{m_y n_x} L_6(m_x, m_x, m_z, n_x, n_y, n_z) - 212 I_{m_y n_x} L_6(m_x, m_x, m_z, n_y, n_y, n_z) \\
&+ 80 I_{m_y n_x} L_6(m_x, m_x, m_z, n_y, n_z, n_z) - 393 I_{m_y n_x} L_6(m_x, m_z, m_z, n_x, n_y, n_z) \\
&+ 212 I_{m_y n_x} L_6(m_x, m_z, m_z, n_y, n_y, n_z) - 80 I_{m_y n_x} L_6(m_x, m_z, m_z, n_y, n_z, n_z) \\
&- 292 I_{m_y n_y} L_6(m_x, m_x, m_z, n_x, n_x, n_z) + 292 I_{m_y n_y} L_6(m_x, m_x, m_z, n_x, n_z, n_z) \\
&+ 292 I_{m_y n_y} L_6(m_x, m_z, m_z, n_x, n_x, n_z) - 292 I_{m_y n_y} L_6(m_x, m_z, m_z, n_x, n_z, n_z) \\
&- 80 I_{m_y n_z} L_6(m_x, m_x, m_z, n_x, n_x, n_y) + 212 I_{m_y n_z} L_6(m_x, m_x, m_z, n_x, n_y, n_y) \\
&- 393 I_{m_y n_z} L_6(m_x, m_x, m_z, n_x, n_y, n_z) + 80 I_{m_y n_z} L_6(m_x, m_z, m_z, n_x, n_x, n_y) \\
&- 212 I_{m_y n_z} L_6(m_x, m_z, m_z, n_x, n_y, n_y) + 393 I_{m_y n_z} L_6(m_x, m_z, m_z, n_x, n_y, n_z) \\
&- 393 I_{m_z n_x} L_6(m_x, m_x, m_y, n_x, n_y, n_z) + 212 I_{m_z n_x} L_6(m_x, m_x, m_y, n_y, n_y, n_z) \\
&- 80 I_{m_z n_x} L_6(m_x, m_x, m_y, n_y, n_z, n_z) + 393 I_{m_z n_x} L_6(m_x, m_y, m_y, n_x, n_y, n_z) \\
&- 212 I_{m_z n_x} L_6(m_x, m_y, m_y, n_y, n_y, n_z) + 80 I_{m_z n_x} L_6(m_x, m_y, m_y, n_y, n_z, n_z) \\
&+ 292 I_{m_z n_y} L_6(m_x, m_x, m_y, n_x, n_x, n_z) - 292 I_{m_z n_y} L_6(m_x, m_x, m_y, n_x, n_z, n_z) \\
&- 292 I_{m_z n_y} L_6(m_x, m_y, m_y, n_x, n_x, n_z) + 292 I_{m_z n_y} L_6(m_x, m_y, m_y, n_x, n_z, n_z) \\
&+ 80 I_{m_z n_z} L_6(m_x, m_x, m_y, n_x, n_x, n_y) - 212 I_{m_z n_z} L_6(m_x, m_x, m_y, n_x, n_y, n_y) \\
&+ 393 I_{m_z n_z} L_6(m_x, m_x, m_y, n_x, n_y, n_z) - 80 I_{m_z n_z} L_6(m_x, m_y, m_y, n_x, n_x, n_y) \\
&+ 212 I_{m_z n_z} L_6(m_x, m_y, m_y, n_x, n_y, n_y) - 393 I_{m_z n_z} L_6(m_x, m_y, m_y, n_x, n_y, n_z)).
\end{aligned}
$$

$$
\begin{aligned}
&< g_{3m}, g_{3n} > \\
&\quad R_{mn} = \alpha + \beta + \gamma. \\
&\quad\quad \alpha = v3\_17010((\boldsymbol{T}_{m_x m_y} \cdot \boldsymbol{T}_{n_x n_y}) L_4(m_x, m_z, n_x, n_z) + (\boldsymbol{T}_{m_x m_y} \cdot \boldsymbol{T}_{n_x n_y}) L_4(m_x, m_z, n_y, n_z) \\
&\quad\quad\quad - (\boldsymbol{T}_{m_x m_y} \cdot \boldsymbol{T}_{n_x n_y}) L_4(m_x, m_z, n_z, n_z) + (\boldsymbol{T}_{m_x m_y} \cdot \boldsymbol{T}_{n_x n_y}) L_4(m_y, m_z, n_x, n_z) \\
&\quad\quad\quad + (\boldsymbol{T}_{m_x m_y} \cdot \boldsymbol{T}_{n_x n_y}) L_4(m_y, m_z, n_y, n_z) - (\boldsymbol{T}_{m_x m_y} \cdot \boldsymbol{T}_{n_x n_y}) L_4(m_y, m_z, n_z, n_z) \\
&\quad\quad\quad - (\boldsymbol{T}_{m_x m_y} \cdot \boldsymbol{T}_{n_x n_y}) L_4(m_z, m_z, n_x, n_z) - (\boldsymbol{T}_{m_x m_y} \cdot \boldsymbol{T}_{n_x n_y}) L_4(m_z, m_z, n_y, n_z) \\
&\quad\quad\quad + (\boldsymbol{T}_{m_x m_y} \cdot \boldsymbol{T}_{n_x n_y}) L_4(m_z, m_z, n_z, n_z) - (\boldsymbol{T}_{m_x m_y} \cdot \boldsymbol{T}_{n_x n_z}) L_4(m_x, m_z, n_x, n_y) \\
&\quad\quad\quad + (\boldsymbol{T}_{m_x m_y} \cdot \boldsymbol{T}_{n_x n_z}) L_4(m_x, m_z, n_y, n_y) - (\boldsymbol{T}_{m_x m_y} \cdot \boldsymbol{T}_{n_x n_z}) L_4(m_x, m_z, n_y, n_z) \\
&\quad\quad\quad - (\boldsymbol{T}_{m_x m_y} \cdot \boldsymbol{T}_{n_x n_z}) L_4(m_y, m_z, n_x, n_y) + (\boldsymbol{T}_{m_x m_y} \cdot \boldsymbol{T}_{n_x n_z}) L_4(m_y, m_z, n_y, n_y) \\
&\quad\quad\quad - (\boldsymbol{T}_{m_x m_y} \cdot \boldsymbol{T}_{n_x n_z}) L_4(m_y, m_z, n_y, n_z) + (\boldsymbol{T}_{m_x m_y} \cdot \boldsymbol{T}_{n_x n_z}) L_4(m_z, m_z, n_x, n_y) \\
&\quad\quad\quad - (\boldsymbol{T}_{m_x m_y} \cdot \boldsymbol{T}_{n_x n_z}) L_4(m_z, m_z, n_y, n_y) + (\boldsymbol{T}_{m_x m_y} \cdot \boldsymbol{T}_{n_x n_z}) L_4(m_z, m_z, n_y, n_z) \\
&\quad\quad\quad - (\boldsymbol{T}_{m_x m_y} \cdot \boldsymbol{T}_{n_y n_z}) L_4(m_x, m_z, n_x, n_x) + (\boldsymbol{T}_{m_x m_y} \cdot \boldsymbol{T}_{n_y n_z}) L_4(m_x, m_z, n_x, n_y) \\
&\quad\quad\quad + (\boldsymbol{T}_{m_x m_y} \cdot \boldsymbol{T}_{n_y n_z}) L_4(m_x, m_z, n_x, n_z) - (\boldsymbol{T}_{m_x m_y} \cdot \boldsymbol{T}_{n_y n_z}) L_4(m_y, m_z, n_x, n_x) \\
&\quad\quad\quad + (\boldsymbol{T}_{m_x m_y} \cdot \boldsymbol{T}_{n_y n_z}) L_4(m_y, m_z, n_x, n_y) + (\boldsymbol{T}_{m_x m_y} \cdot \boldsymbol{T}_{n_y n_z}) L_4(m_y, m_z, n_x, n_z) \\
&\quad\quad\quad + (\boldsymbol{T}_{m_x m_y} \cdot \boldsymbol{T}_{n_y n_z}) L_4(m_z, m_z, n_x, n_x) - (\boldsymbol{T}_{m_x m_y} \cdot \boldsymbol{T}_{n_y n_z}) L_4(m_z, m_z, n_x, n_y) \\
&\quad\quad\quad - (\boldsymbol{T}_{m_x m_y} \cdot \boldsymbol{T}_{n_y n_z}) L_4(m_z, m_z, n_x, n_z) - (\boldsymbol{T}_{m_x m_z} \cdot \boldsymbol{T}_{n_x n_y}) L_4(m_x, m_y, n_x, n_z) \\
&\quad\quad\quad - (\boldsymbol{T}_{m_x m_z} \cdot \boldsymbol{T}_{n_x n_y}) L_4(m_x, m_y, n_y, n_z) + (\boldsymbol{T}_{m_x m_z} \cdot \boldsymbol{T}_{n_x n_y}) L_4(m_x, m_y, n_z, n_z) \\
&\quad\quad\quad + (\boldsymbol{T}_{m_x m_z} \cdot \boldsymbol{T}_{n_x n_y}) L_4(m_y, m_y, n_x, n_z) + (\boldsymbol{T}_{m_x m_z} \cdot \boldsymbol{T}_{n_x n_y}) L_4(m_y, m_y, n_y, n_z)), \\
&\quad\quad \beta = v3\_17010(-(\boldsymbol{T}_{m_x m_z} \cdot \boldsymbol{T}_{n_x n_y}) L_4(m_y, m_y, n_z, n_z) - (\boldsymbol{T}_{m_x m_z} \cdot \boldsymbol{T}_{n_x n_y}) L_4(m_y, m_z, n_x, n_z) \\
&\quad\quad\quad - (\boldsymbol{T}_{m_x m_z} \cdot \boldsymbol{T}_{n_x n_y}) L_4(m_y, m_z, n_y, n_z) + (\boldsymbol{T}_{m_x m_z} \cdot \boldsymbol{T}_{n_x n_y}) L_4(m_y, m_z, n_z, n_z) \\
&\quad\quad\quad + (\boldsymbol{T}_{m_x m_z} \cdot \boldsymbol{T}_{n_x n_z}) L_4(m_x, m_y, n_x, n_y) - (\boldsymbol{T}_{m_x m_z} \cdot \boldsymbol{T}_{n_x n_z}) L_4(m_x, m_y, n_y, n_y) \\
&\quad\quad\quad + (\boldsymbol{T}_{m_x m_z} \cdot \boldsymbol{T}_{n_x n_z}) L_4(m_x, m_y, n_y, n_z) - (\boldsymbol{T}_{m_x m_z} \cdot \boldsymbol{T}_{n_x n_z}) L_4(m_y, m_y, n_x, n_y) \\
&\quad\quad\quad + (\boldsymbol{T}_{m_x m_z} \cdot \boldsymbol{T}_{n_x n_z}) L_4(m_y, m_y, n_y, n_y) - (\boldsymbol{T}_{m_x m_z} \cdot \boldsymbol{T}_{n_x n_z}) L_4(m_y, m_y, n_y, n_z) \\
&\quad\quad\quad + (\boldsymbol{T}_{m_x m_z} \cdot \boldsymbol{T}_{n_x n_z}) L_4(m_y, m_z, n_x, n_y) - (\boldsymbol{T}_{m_x m_z} \cdot \boldsymbol{T}_{n_x n_z}) L_4(m_y, m_z, n_y, n_y) \\
&\quad\quad\quad + (\boldsymbol{T}_{m_x m_z} \cdot \boldsymbol{T}_{n_x n_z}) L_4(m_y, m_z, n_y, n_z) + (\boldsymbol{T}_{m_x m_z} \cdot \boldsymbol{T}_{n_y n_z}) L_4(m_x, m_y, n_x, n_x) \\
&\quad\quad\quad - (\boldsymbol{T}_{m_x m_z} \cdot \boldsymbol{T}_{n_y n_z}) L_4(m_x, m_y, n_x, n_y) - (\boldsymbol{T}_{m_x m_z} \cdot \boldsymbol{T}_{n_y n_z}) L_4(m_x, m_y, n_x, n_z) \\
&\quad\quad\quad - (\boldsymbol{T}_{m_x m_z} \cdot \boldsymbol{T}_{n_y n_z}) L_4(m_y, m_y, n_x, n_x) + (\boldsymbol{T}_{m_x m_z} \cdot \boldsymbol{T}_{n_y n_z}) L_4(m_y, m_y, n_x, n_y) \\
&\quad\quad\quad + (\boldsymbol{T}_{m_x m_z} \cdot \boldsymbol{T}_{n_y n_z}) L_4(m_y, m_y, n_x, n_z) + (\boldsymbol{T}_{m_x m_z} \cdot \boldsymbol{T}_{n_y n_z}) L_4(m_y, m_z, n_x, n_x) \\
&\quad\quad\quad - (\boldsymbol{T}_{m_x m_z} \cdot \boldsymbol{T}_{n_y n_z}) L_4(m_y, m_z, n_x, n_y) - (\boldsymbol{T}_{m_x m_z} \cdot \boldsymbol{T}_{n_y n_z}) L_4(m_y, m_z, n_x, n_z) \\
&\quad\quad\quad - (\boldsymbol{T}_{m_y m_z} \cdot \boldsymbol{T}_{n_x n_y}) L_4(m_x, m_x, n_x, n_z) - (\boldsymbol{T}_{m_y m_z} \cdot \boldsymbol{T}_{n_x n_y}) L_4(m_x, m_x, n_y, n_z) \\
&\quad\quad\quad + (\boldsymbol{T}_{m_y m_z} \cdot \boldsymbol{T}_{n_x n_y}) L_4(m_x, m_x, n_z, n_z) + (\boldsymbol{T}_{m_y m_z} \cdot \boldsymbol{T}_{n_x n_y}) L_4(m_x, m_y, n_x, n_z) \\
&\quad\quad\quad + (\boldsymbol{T}_{m_y m_z} \cdot \boldsymbol{T}_{n_x n_y}) L_4(m_x, m_y, n_y, n_z) - (\boldsymbol{T}_{m_y m_z} \cdot \boldsymbol{T}_{n_x n_y}) L_4(m_x, m_y, n_z, n_z) \\
&\quad\quad\quad + (\boldsymbol{T}_{m_y m_z} \cdot \boldsymbol{T}_{n_x n_y}) L_4(m_x, m_z, n_x, n_z) + (\boldsymbol{T}_{m_y m_z} \cdot \boldsymbol{T}_{n_x n_y}) L_4(m_x, m_z, n_y, n_z) \\
&\quad\quad\quad - (\boldsymbol{T}_{m_y m_z} \cdot \boldsymbol{T}_{n_x n_y}) L_4(m_x, m_z, n_z, n_z) + (\boldsymbol{T}_{m_y m_z} \cdot \boldsymbol{T}_{n_x n_z}) L_4(m_x, m_x, n_x, n_y) \\
&\quad\quad\quad - (\boldsymbol{T}_{m_y m_z} \cdot \boldsymbol{T}_{n_x n_z}) L_4(m_x, m_x, n_y, n_y) + (\boldsymbol{T}_{m_y m_z} \cdot \boldsymbol{T}_{n_x n_z}) L_4(m_x, m_x, n_y, n_z) \\
&\quad\quad\quad - (\boldsymbol{T}_{m_y m_z} \cdot \boldsymbol{T}_{n_x n_z}) L_4(m_x, m_y, n_x, n_y) + (\boldsymbol{T}_{m_y m_z} \cdot \boldsymbol{T}_{n_x n_z}) L_4(m_x, m_y, n_y, n_y)),
\end{aligned}
$$

$$
\begin{aligned}
\gamma =& v3\_17010(-(\boldsymbol{T}_{m_y m_z} \cdot \boldsymbol{T}_{n_x n_z}) L_4(m_x, m_y, n_y, n_z) - (\boldsymbol{T}_{m_y m_z} \cdot \boldsymbol{T}_{n_x n_z}) L_4(m_x, m_z, n_x, n_y) \\
&+ (\boldsymbol{T}_{m_y m_z} \cdot \boldsymbol{T}_{n_x n_z}) L_4(m_x, m_z, n_y, n_y) - (\boldsymbol{T}_{m_y m_z} \cdot \boldsymbol{T}_{n_x n_z}) L_4(m_x, m_z, n_y, n_z) \\
&+ (\boldsymbol{T}_{m_y m_z} \cdot \boldsymbol{T}_{n_y n_z}) L_4(m_x, m_x, n_x, n_x) - (\boldsymbol{T}_{m_y m_z} \cdot \boldsymbol{T}_{n_y n_z}) L_4(m_x, m_x, n_x, n_y) \\
&- (\boldsymbol{T}_{m_y m_z} \cdot \boldsymbol{T}_{n_y n_z}) L_4(m_x, m_x, n_x, n_z) - (\boldsymbol{T}_{m_y m_z} \cdot \boldsymbol{T}_{n_y n_z}) L_4(m_x, m_y, n_x, n_x) \\
&+ (\boldsymbol{T}_{m_y m_z} \cdot \boldsymbol{T}_{n_y n_z}) L_4(m_x, m_y, n_x, n_y) + (\boldsymbol{T}_{m_y m_z} \cdot \boldsymbol{T}_{n_y n_z}) L_4(m_x, m_y, n_x, n_z) \\
&- (\boldsymbol{T}_{m_y m_z} \cdot \boldsymbol{T}_{n_y n_z}) L_4(m_x, m_z, n_x, n_x) + (\boldsymbol{T}_{m_y m_z} \cdot \boldsymbol{T}_{n_y n_z}) L_4(m_x, m_z, n_x, n_y) \\
&+ (\boldsymbol{T}_{m_y m_z} \cdot \boldsymbol{T}_{n_y n_z}) L_4(m_x, m_z, n_x, n_z)),
\end{aligned}
$$

$$
\begin{aligned}
S_{mn} =& v544320k02(I_{m_x n_x} L_6(m_y, m_y, m_z, n_y, n_y, n_z) - I_{m_x n_x} L_6(m_y, m_y, m_z, n_y, n_z, n_z) \\
&- I_{m_x n_x} L_6(m_y, m_z, m_z, n_y, n_y, n_z) + I_{m_x n_x} L_6(m_y, m_z, m_z, n_y, n_z, n_z) \\
&- I_{m_x n_y} L_6(m_y, m_y, m_z, n_x, n_x, n_z) + I_{m_x n_y} L_6(m_y, m_y, m_z, n_x, n_z, n_z) \\
&+ I_{m_x n_y} L_6(m_y, m_z, m_z, n_x, n_x, n_z) - I_{m_x n_y} L_6(m_y, m_z, m_z, n_x, n_z, n_z) \\
&+ I_{m_x n_z} L_6(m_y, m_y, m_z, n_x, n_x, n_y) - I_{m_x n_z} L_6(m_y, m_y, m_z, n_x, n_y, n_y) \\
&- I_{m_x n_z} L_6(m_y, m_z, m_z, n_x, n_x, n_y) + I_{m_x n_z} L_6(m_y, m_z, m_z, n_x, n_y, n_y) \\
&- I_{m_y n_x} L_6(m_x, m_x, m_z, n_y, n_y, n_z) + I_{m_y n_x} L_6(m_x, m_x, m_z, n_y, n_z, n_z) \\
&+ I_{m_y n_x} L_6(m_x, m_z, m_z, n_y, n_y, n_z) - I_{m_y n_x} L_6(m_x, m_z, m_z, n_y, n_z, n_z) \\
&+ I_{m_y n_y} L_6(m_x, m_x, m_z, n_x, n_x, n_z) - I_{m_y n_y} L_6(m_x, m_x, m_z, n_x, n_z, n_z) \\
&- I_{m_y n_y} L_6(m_x, m_z, m_z, n_x, n_x, n_z) + I_{m_y n_y} L_6(m_x, m_z, m_z, n_x, n_z, n_z) \\
&- I_{m_y n_z} L_6(m_x, m_x, m_z, n_x, n_x, n_y) + I_{m_y n_z} L_6(m_x, m_x, m_z, n_x, n_y, n_y) \\
&+ I_{m_y n_z} L_6(m_x, m_z, m_z, n_x, n_x, n_y) - I_{m_y n_z} L_6(m_x, m_z, m_z, n_x, n_y, n_y) \\
&+ I_{m_z n_x} L_6(m_x, m_x, m_y, n_y, n_y, n_z) - I_{m_z n_x} L_6(m_x, m_x, m_y, n_y, n_z, n_z) \\
&- I_{m_z n_x} L_6(m_x, m_y, m_y, n_y, n_y, n_z) + I_{m_z n_x} L_6(m_x, m_y, m_y, n_y, n_z, n_z) \\
&- I_{m_z n_y} L_6(m_x, m_x, m_y, n_x, n_x, n_z) + I_{m_z n_y} L_6(m_x, m_x, m_y, n_x, n_z, n_z) \\
&+ I_{m_z n_y} L_6(m_x, m_y, m_y, n_x, n_x, n_z) - I_{m_z n_y} L_6(m_x, m_y, m_y, n_x, n_z, n_z) \\
&+ I_{m_z n_z} L_6(m_x, m_x, m_y, n_x, n_x, n_y) - I_{m_z n_z} L_6(m_x, m_x, m_y, n_x, n_y, n_y) \\
&- I_{m_z n_z} L_6(m_x, m_y, m_y, n_x, n_x, n_y) + I_{m_z n_z} L_6(m_x, m_y, m_y, n_x, n_y, n_y)).
\end{aligned}
$$

$$
\begin{aligned}
&< g_{3m}, h_{3n} > \\
&\quad R_{mn} = \alpha + \beta + \gamma, \\
&\quad \alpha = v3\_34020(-977(\boldsymbol{T}_{m_x m_y} \cdot \boldsymbol{T}_{n_x n_y}) L_4(m_x, m_z, n_x, n_z) + 424(\boldsymbol{T}_{m_x m_y} \cdot \boldsymbol{T}_{n_x n_y}) L_4(m_x, m_z, n_y, n_z) \\
&\qquad + 212(\boldsymbol{T}_{m_x m_y} \cdot \boldsymbol{T}_{n_x n_y}) L_4(m_x, m_z, n_z, n_z) - 977(\boldsymbol{T}_{m_x m_y} \cdot \boldsymbol{T}_{n_x n_y}) L_4(m_y, m_z, n_x, n_z) \\
&\qquad + 424(\boldsymbol{T}_{m_x m_y} \cdot \boldsymbol{T}_{n_x n_y}) L_4(m_y, m_z, n_y, n_z) + 212(\boldsymbol{T}_{m_x m_y} \cdot \boldsymbol{T}_{n_x n_y}) L_4(m_y, m_z, n_z, n_z) \\
&\qquad + 977(\boldsymbol{T}_{m_x m_y} \cdot \boldsymbol{T}_{n_x n_y}) L_4(m_z, m_z, n_x, n_z) - 424(\boldsymbol{T}_{m_x m_y} \cdot \boldsymbol{T}_{n_x n_y}) L_4(m_z, m_z, n_y, n_z) \\
&\qquad - 212(\boldsymbol{T}_{m_x m_y} \cdot \boldsymbol{T}_{n_x n_y}) L_4(m_z, m_z, n_z, n_z) - 553(\boldsymbol{T}_{m_x m_y} \cdot \boldsymbol{T}_{n_x n_z}) L_4(m_x, m_z, n_x, n_y) \\
&\qquad + 424(\boldsymbol{T}_{m_x m_y} \cdot \boldsymbol{T}_{n_x n_z}) L_4(m_x, m_z, n_y, n_y) - 553(\boldsymbol{T}_{m_x m_y} \cdot \boldsymbol{T}_{n_x n_z}) L_4(m_x, m_z, n_y, n_z) \\
&\qquad - 553(\boldsymbol{T}_{m_x m_y} \cdot \boldsymbol{T}_{n_x n_z}) L_4(m_y, m_z, n_x, n_y) + 424(\boldsymbol{T}_{m_x m_y} \cdot \boldsymbol{T}_{n_x n_z}) L_4(m_y, m_z, n_y, n_y) \\
&\qquad - 553(\boldsymbol{T}_{m_x m_y} \cdot \boldsymbol{T}_{n_x n_z}) L_4(m_y, m_z, n_y, n_z) + 553(\boldsymbol{T}_{m_x m_y} \cdot \boldsymbol{T}_{n_x n_z}) L_4(m_z, m_z, n_x, n_y) \\
&\qquad - 424(\boldsymbol{T}_{m_x m_y} \cdot \boldsymbol{T}_{n_x n_z}) L_4(m_z, m_z, n_y, n_y) + 553(\boldsymbol{T}_{m_x m_y} \cdot \boldsymbol{T}_{n_x n_z}) L_4(m_z, m_z, n_y, n_z) \\
&\qquad + 212(\boldsymbol{T}_{m_x m_y} \cdot \boldsymbol{T}_{n_y n_z}) L_4(m_x, m_z, n_x, n_x) + 424(\boldsymbol{T}_{m_x m_y} \cdot \boldsymbol{T}_{n_y n_z}) L_4(m_x, m_z, n_x, n_y) \\
&\qquad - 977(\boldsymbol{T}_{m_x m_y} \cdot \boldsymbol{T}_{n_y n_z}) L_4(m_x, m_z, n_x, n_z) + 212(\boldsymbol{T}_{m_x m_y} \cdot \boldsymbol{T}_{n_y n_z}) L_4(m_y, m_z, n_x, n_x) \\
&\qquad + 424(\boldsymbol{T}_{m_x m_y} \cdot \boldsymbol{T}_{n_y n_z}) L_4(m_y, m_z, n_x, n_y) - 977(\boldsymbol{T}_{m_x m_y} \cdot \boldsymbol{T}_{n_y n_z}) L_4(m_y, m_z, n_x, n_z) \\
&\qquad - 212(\boldsymbol{T}_{m_x m_y} \cdot \boldsymbol{T}_{n_y n_z}) L_4(m_z, m_z, n_x, n_x) - 424(\boldsymbol{T}_{m_x m_y} \cdot \boldsymbol{T}_{n_y n_z}) L_4(m_z, m_z, n_x, n_y) \\
&\qquad + 977(\boldsymbol{T}_{m_x m_y} \cdot \boldsymbol{T}_{n_y n_z}) L_4(m_z, m_z, n_x, n_z) + 977(\boldsymbol{T}_{m_x m_z} \cdot \boldsymbol{T}_{n_x n_y}) L_4(m_x, m_y, n_x, n_z) \\
&\qquad - 424(\boldsymbol{T}_{m_x m_z} \cdot \boldsymbol{T}_{n_x n_y}) L_4(m_x, m_y, n_y, n_z) - 212(\boldsymbol{T}_{m_x m_z} \cdot \boldsymbol{T}_{n_x n_y}) L_4(m_x, m_y, n_z, n_z) \\
&\qquad - 977(\boldsymbol{T}_{m_x m_z} \cdot \boldsymbol{T}_{n_x n_y}) L_4(m_y, m_y, n_x, n_z) + 424(\boldsymbol{T}_{m_x m_z} \cdot \boldsymbol{T}_{n_x n_y}) L_4(m_y, m_y, n_y, n_z) \\
&\qquad + 212(\boldsymbol{T}_{m_x m_z} \cdot \boldsymbol{T}_{n_x n_y}) L_4(m_y, m_y, n_z, n_z) + 977(\boldsymbol{T}_{m_x m_z} \cdot \boldsymbol{T}_{n_x n_y}) L_4(m_y, m_z, n_x, n_z) \\
&\qquad - 424(\boldsymbol{T}_{m_x m_z} \cdot \boldsymbol{T}_{n_x n_y}) L_4(m_y, m_z, n_y, n_z) - 212(\boldsymbol{T}_{m_x m_z} \cdot \boldsymbol{T}_{n_x n_y}) L_4(m_y, m_z, n_z, n_z)) \\
&\quad \beta = v3\_34020(+553(\boldsymbol{T}_{m_x m_z} \cdot \boldsymbol{T}_{n_x n_z}) L_4(m_x, m_y, n_x, n_y) - 424(\boldsymbol{T}_{m_x m_z} \cdot \boldsymbol{T}_{n_x n_z}) L_4(m_x, m_y, n_y, n_y) \\
&\qquad + 553(\boldsymbol{T}_{m_x m_z} \cdot \boldsymbol{T}_{n_x n_z}) L_4(m_x, m_y, n_y, n_z) - 553(\boldsymbol{T}_{m_x m_z} \cdot \boldsymbol{T}_{n_x n_z}) L_4(m_y, m_y, n_x, n_y) \\
&\qquad + 424(\boldsymbol{T}_{m_x m_z} \cdot \boldsymbol{T}_{n_x n_z}) L_4(m_y, m_y, n_y, n_y) - 553(\boldsymbol{T}_{m_x m_z} \cdot \boldsymbol{T}_{n_x n_z}) L_4(m_y, m_y, n_y, n_z) \\
&\qquad + 553(\boldsymbol{T}_{m_x m_z} \cdot \boldsymbol{T}_{n_x n_z}) L_4(m_y, m_z, n_x, n_y) - 424(\boldsymbol{T}_{m_x m_z} \cdot \boldsymbol{T}_{n_x n_z}) L_4(m_y, m_z, n_y, n_y) \\
&\qquad + 553(\boldsymbol{T}_{m_x m_z} \cdot \boldsymbol{T}_{n_x n_z}) L_4(m_y, m_z, n_y, n_z) - 212(\boldsymbol{T}_{m_x m_z} \cdot \boldsymbol{T}_{n_y n_z}) L_4(m_x, m_y, n_x, n_x) \\
&\qquad - 424(\boldsymbol{T}_{m_x m_z} \cdot \boldsymbol{T}_{n_y n_z}) L_4(m_x, m_y, n_x, n_y) + 977(\boldsymbol{T}_{m_x m_z} \cdot \boldsymbol{T}_{n_y n_z}) L_4(m_x, m_y, n_x, n_z) \\
&\qquad + 212(\boldsymbol{T}_{m_x m_z} \cdot \boldsymbol{T}_{n_y n_z}) L_4(m_y, m_y, n_x, n_x) + 424(\boldsymbol{T}_{m_x m_z} \cdot \boldsymbol{T}_{n_y n_z}) L_4(m_y, m_y, n_x, n_y) \\
&\qquad - 977(\boldsymbol{T}_{m_x m_z} \cdot \boldsymbol{T}_{n_y n_z}) L_4(m_y, m_y, n_x, n_z) - 212(\boldsymbol{T}_{m_x m_z} \cdot \boldsymbol{T}_{n_y n_z}) L_4(m_y, m_z, n_x, n_x) \\
&\qquad - 424(\boldsymbol{T}_{m_x m_z} \cdot \boldsymbol{T}_{n_y n_z}) L_4(m_y, m_z, n_x, n_y) + 977(\boldsymbol{T}_{m_x m_z} \cdot \boldsymbol{T}_{n_y n_z}) L_4(m_y, m_z, n_x, n_z) \\
&\qquad + 977(\boldsymbol{T}_{m_y m_z} \cdot \boldsymbol{T}_{n_x n_y}) L_4(m_x, m_x, n_x, n_z) - 424(\boldsymbol{T}_{m_y m_z} \cdot \boldsymbol{T}_{n_x n_y}) L_4(m_x, m_x, n_y, n_z) \\
&\qquad - 212(\boldsymbol{T}_{m_y m_z} \cdot \boldsymbol{T}_{n_x n_y}) L_4(m_x, m_x, n_z, n_z) - 977(\boldsymbol{T}_{m_y m_z} \cdot \boldsymbol{T}_{n_x n_y}) L_4(m_x, m_y, n_x, n_z) \\
&\qquad + 424(\boldsymbol{T}_{m_y m_z} \cdot \boldsymbol{T}_{n_x n_y}) L_4(m_x, m_y, n_y, n_z) + 212(\boldsymbol{T}_{m_y m_z} \cdot \boldsymbol{T}_{n_x n_y}) L_4(m_x, m_y, n_z, n_z) \\
&\qquad - 977(\boldsymbol{T}_{m_y m_z} \cdot \boldsymbol{T}_{n_x n_y}) L_4(m_x, m_z, n_x, n_z) + 424(\boldsymbol{T}_{m_y m_z} \cdot \boldsymbol{T}_{n_x n_y}) L_4(m_x, m_z, n_y, n_z) \\
&\qquad + 212(\boldsymbol{T}_{m_y m_z} \cdot \boldsymbol{T}_{n_x n_y}) L_4(m_x, m_z, n_z, n_z) + 553(\boldsymbol{T}_{m_y m_z} \cdot \boldsymbol{T}_{n_x n_z}) L_4(m_x, m_x, n_x, n_y) \\
&\qquad - 424(\boldsymbol{T}_{m_y m_z} \cdot \boldsymbol{T}_{n_x n_z}) L_4(m_x, m_x, n_y, n_y) + 553(\boldsymbol{T}_{m_y m_z} \cdot \boldsymbol{T}_{n_x n_z}) L_4(m_x, m_x, n_y, n_z) \\
&\qquad - 553(\boldsymbol{T}_{m_y m_z} \cdot \boldsymbol{T}_{n_x n_z}) L_4(m_x, m_y, n_x, n_y) + 424(\boldsymbol{T}_{m_y m_z} \cdot \boldsymbol{T}_{n_x n_z}) L_4(m_x, m_y, n_y, n_y) \\
&\qquad - 553(\boldsymbol{T}_{m_y m_z} \cdot \boldsymbol{T}_{n_x n_z}) L_4(m_x, m_y, n_y, n_z) - 553(\boldsymbol{T}_{m_y m_z} \cdot \boldsymbol{T}_{n_x n_z}) L_4(m_x, m_z, n_x, n_y) \\
&\qquad + 424(\boldsymbol{T}_{m_y m_z} \cdot \boldsymbol{T}_{n_x n_z}) L_4(m_x, m_z, n_y, n_y) - 553(\boldsymbol{T}_{m_y m_z} \cdot \boldsymbol{T}_{n_x n_z}) L_4(m_x, m_z, n_y, n_z)),
\end{aligned}
$$

$$
\begin{aligned}
\gamma =& v3\_34020(-212(\boldsymbol{T}_{m_ym_z}\cdot\boldsymbol{T}_{n_yn_z})L_4(m_x,m_x,n_x,n_x)-424(\boldsymbol{T}_{m_ym_z}\cdot\boldsymbol{T}_{n_yn_z})L_4(m_x,m_x,n_x,n_y)\\
&+977(\boldsymbol{T}_{m_ym_z}\cdot\boldsymbol{T}_{n_yn_z})L_4(m_x,m_x,n_x,n_z)+212(\boldsymbol{T}_{m_ym_z}\cdot\boldsymbol{T}_{n_yn_z})L_4(m_x,m_y,n_x,n_x)\\
&+424(\boldsymbol{T}_{m_ym_z}\cdot\boldsymbol{T}_{n_yn_z})L_4(m_x,m_y,n_x,n_y)-977(\boldsymbol{T}_{m_ym_z}\cdot\boldsymbol{T}_{n_yn_z})L_4(m_x,m_y,n_x,n_z)\\
&+212(\boldsymbol{T}_{m_ym_z}\cdot\boldsymbol{T}_{n_yn_z})L_4(m_x,m_z,n_x,n_x)+424(\boldsymbol{T}_{m_ym_z}\cdot\boldsymbol{T}_{n_yn_z})L_4(m_x,m_z,n_x,n_y)\\
&-977(\boldsymbol{T}_{m_ym_z}\cdot\boldsymbol{T}_{n_yn_z})L_4(m_x,m_z,n_x,n_z)),
\end{aligned}
$$

$$
\begin{aligned}
S_{mn} =& v544320k02(-393I_{m_xn_x}L_6(m_y,m_y,m_z,n_x,n_y,n_z)+212I_{m_xn_x}L_6(m_y,m_y,m_z,n_y,n_y,n_z)\\
&-80I_{m_xn_x}L_6(m_y,m_y,m_z,n_y,n_z,n_z)+393I_{m_xn_x}L_6(m_y,m_z,m_z,n_x,n_y,n_z)\\
&-212I_{m_xn_x}L_6(m_y,m_z,m_z,n_y,n_y,n_z)+80I_{m_xn_x}L_6(m_y,m_z,m_z,n_y,n_z,n_z)\\
&+292I_{m_xn_y}L_6(m_y,m_y,m_z,n_x,n_x,n_z)-292I_{m_xn_y}L_6(m_y,m_y,m_z,n_x,n_z,n_z)\\
&-292I_{m_xn_y}L_6(m_y,m_z,m_z,n_x,n_x,n_z)+292I_{m_xn_y}L_6(m_y,m_z,m_z,n_x,n_z,n_z)\\
&+80I_{m_xn_z}L_6(m_y,m_y,m_z,n_x,n_x,n_y)-212I_{m_xn_z}L_6(m_y,m_y,m_z,n_x,n_y,n_y)\\
&+393I_{m_xn_z}L_6(m_y,m_y,m_z,n_x,n_y,n_z)-80I_{m_xn_z}L_6(m_y,m_z,m_z,n_x,n_x,n_y)\\
&+212I_{m_xn_z}L_6(m_y,m_z,m_z,n_x,n_y,n_y)-393I_{m_xn_z}L_6(m_y,m_z,m_z,n_x,n_y,n_z)\\
&+393I_{m_yn_x}L_6(m_x,m_x,m_z,n_x,n_y,n_z)-212I_{m_yn_x}L_6(m_x,m_x,m_z,n_y,n_y,n_z)\\
&+80I_{m_yn_x}L_6(m_x,m_x,m_z,n_y,n_z,n_z)-393I_{m_yn_x}L_6(m_x,m_z,m_z,n_x,n_y,n_z)\\
&+212I_{m_yn_x}L_6(m_x,m_z,m_z,n_y,n_y,n_z)-80I_{m_yn_x}L_6(m_x,m_z,m_z,n_y,n_z,n_z)\\
&-292I_{m_yn_y}L_6(m_x,m_x,m_z,n_x,n_x,n_z)+292I_{m_yn_y}L_6(m_x,m_x,m_z,n_x,n_z,n_z)\\
&+292I_{m_yn_y}L_6(m_x,m_z,m_z,n_x,n_x,n_z)-292I_{m_yn_y}L_6(m_x,m_z,m_z,n_x,n_z,n_z)\\
&-80I_{m_yn_z}L_6(m_x,m_x,m_z,n_x,n_x,n_y)+212I_{m_yn_z}L_6(m_x,m_x,m_z,n_x,n_y,n_y)\\
&-393I_{m_yn_z}L_6(m_x,m_x,m_z,n_x,n_y,n_z)+80I_{m_yn_z}L_6(m_x,m_z,m_z,n_x,n_x,n_y)\\
&-212I_{m_yn_z}L_6(m_x,m_z,m_z,n_x,n_y,n_y)+393I_{m_yn_z}L_6(m_x,m_z,m_z,n_x,n_y,n_z)\\
&-393I_{m_zn_x}L_6(m_x,m_x,m_y,n_x,n_y,n_z)+212I_{m_zn_x}L_6(m_x,m_x,m_y,n_y,n_y,n_z)\\
&-80I_{m_zn_x}L_6(m_x,m_x,m_y,n_y,n_z,n_z)+393I_{m_zn_x}L_6(m_x,m_y,m_y,n_x,n_y,n_z)\\
&-212I_{m_zn_x}L_6(m_x,m_y,m_y,n_y,n_y,n_z)+80I_{m_zn_x}L_6(m_x,m_y,m_y,n_y,n_z,n_z)\\
&+292I_{m_zn_y}L_6(m_x,m_x,m_y,n_x,n_x,n_z)-292I_{m_zn_y}L_6(m_x,m_x,m_y,n_x,n_z,n_z)\\
&-292I_{m_zn_y}L_6(m_x,m_y,m_y,n_x,n_x,n_z)+292I_{m_zn_y}L_6(m_x,m_y,m_y,n_x,n_z,n_z)\\
&+80I_{m_zn_z}L_6(m_x,m_x,m_y,n_x,n_x,n_y)-212I_{m_zn_z}L_6(m_x,m_x,m_y,n_x,n_y,n_y)\\
&+393I_{m_zn_z}L_6(m_x,m_x,m_y,n_x,n_y,n_z)-80I_{m_zn_z}L_6(m_x,m_y,m_y,n_x,n_x,n_y)\\
&+212I_{m_zn_z}L_6(m_x,m_y,m_y,n_x,n_y,n_y)-393I_{m_zn_z}L_6(m_x,m_y,m_y,n_x,n_y,n_z)).
\end{aligned}
$$

$$
\begin{aligned}
&< g_{3m}, i_{3n} > \\
&\quad R_{mn} = v3\_34020 \\
&\qquad (-43(\boldsymbol{T}_{m_x m_y} \cdot \boldsymbol{T}_{n_x n_y}) L_4(m_x, m_z, n_x, n_z) - 510(\boldsymbol{T}_{m_x m_y} \cdot \boldsymbol{T}_{n_x n_y}) L_4(m_x, m_z, n_y, n_z) \\
&\qquad + 212(\boldsymbol{T}_{m_x m_y} \cdot \boldsymbol{T}_{n_x n_y}) L_4(m_x, m_z, n_z, n_z) - 43(\boldsymbol{T}_{m_x m_y} \cdot \boldsymbol{T}_{n_x n_y}) L_4(m_y, m_z, n_x, n_z) \\
&\qquad - 510(\boldsymbol{T}_{m_x m_y} \cdot \boldsymbol{T}_{n_x n_y}) L_4(m_y, m_z, n_y, n_z) + 212(\boldsymbol{T}_{m_x m_y} \cdot \boldsymbol{T}_{n_x n_y}) L_4(m_y, m_z, n_z, n_z) \\
&\qquad + 43(\boldsymbol{T}_{m_x m_y} \cdot \boldsymbol{T}_{n_x n_y}) L_4(m_z, m_z, n_x, n_z) + 510(\boldsymbol{T}_{m_x m_y} \cdot \boldsymbol{T}_{n_x n_y}) L_4(m_z, m_z, n_y, n_z) \\
&\qquad - 212(\boldsymbol{T}_{m_x m_y} \cdot \boldsymbol{T}_{n_x n_y}) L_4(m_z, m_z, n_z, n_z) - 467(\boldsymbol{T}_{m_x m_y} \cdot \boldsymbol{T}_{n_x n_z}) L_4(m_x, m_z, n_x, n_y) \\
&\qquad + 467(\boldsymbol{T}_{m_x m_y} \cdot \boldsymbol{T}_{n_x n_z}) L_4(m_x, m_z, n_y, n_z) - 467(\boldsymbol{T}_{m_x m_y} \cdot \boldsymbol{T}_{n_x n_z}) L_4(m_y, m_z, n_x, n_y) \\
&\qquad + 467(\boldsymbol{T}_{m_x m_y} \cdot \boldsymbol{T}_{n_x n_z}) L_4(m_y, m_z, n_y, n_z) + 467(\boldsymbol{T}_{m_x m_y} \cdot \boldsymbol{T}_{n_x n_z}) L_4(m_z, m_z, n_x, n_y) \\
&\qquad - 467(\boldsymbol{T}_{m_x m_y} \cdot \boldsymbol{T}_{n_x n_z}) L_4(m_z, m_z, n_y, n_z) - 212(\boldsymbol{T}_{m_x m_y} \cdot \boldsymbol{T}_{n_y n_z}) L_4(m_x, m_z, n_x, n_x) \\
&\qquad + 510(\boldsymbol{T}_{m_x m_y} \cdot \boldsymbol{T}_{n_y n_z}) L_4(m_x, m_z, n_x, n_y) + 43(\boldsymbol{T}_{m_x m_y} \cdot \boldsymbol{T}_{n_y n_z}) L_4(m_x, m_z, n_x, n_z) \\
&\qquad - 212(\boldsymbol{T}_{m_x m_y} \cdot \boldsymbol{T}_{n_y n_z}) L_4(m_y, m_z, n_x, n_x) + 510(\boldsymbol{T}_{m_x m_y} \cdot \boldsymbol{T}_{n_y n_z}) L_4(m_y, m_z, n_x, n_y) \\
&\qquad + 43(\boldsymbol{T}_{m_x m_y} \cdot \boldsymbol{T}_{n_y n_z}) L_4(m_y, m_z, n_x, n_z) + 212(\boldsymbol{T}_{m_x m_y} \cdot \boldsymbol{T}_{n_y n_z}) L_4(m_z, m_z, n_x, n_x) \\
&\qquad - 510(\boldsymbol{T}_{m_x m_y} \cdot \boldsymbol{T}_{n_y n_z}) L_4(m_z, m_z, n_x, n_y) - 43(\boldsymbol{T}_{m_x m_y} \cdot \boldsymbol{T}_{n_y n_z}) L_4(m_z, m_z, n_x, n_z) \\
&\qquad + 43(\boldsymbol{T}_{m_x m_z} \cdot \boldsymbol{T}_{n_x n_y}) L_4(m_x, m_y, n_x, n_z) + 510(\boldsymbol{T}_{m_x m_z} \cdot \boldsymbol{T}_{n_x n_y}) L_4(m_x, m_y, n_y, n_z) \\
&\qquad - 212(\boldsymbol{T}_{m_x m_z} \cdot \boldsymbol{T}_{n_x n_y}) L_4(m_x, m_y, n_z, n_z) - 43(\boldsymbol{T}_{m_x m_z} \cdot \boldsymbol{T}_{n_x n_y}) L_4(m_y, m_y, n_x, n_z) \\
&\qquad - 510(\boldsymbol{T}_{m_x m_z} \cdot \boldsymbol{T}_{n_x n_y}) L_4(m_y, m_y, n_y, n_z) + 212(\boldsymbol{T}_{m_x m_z} \cdot \boldsymbol{T}_{n_x n_y}) L_4(m_y, m_y, n_z, n_z) \\
&\qquad + 43(\boldsymbol{T}_{m_x m_z} \cdot \boldsymbol{T}_{n_x n_y}) L_4(m_y, m_z, n_x, n_z) + 510(\boldsymbol{T}_{m_x m_z} \cdot \boldsymbol{T}_{n_x n_y}) L_4(m_y, m_z, n_y, n_z) \\
&\qquad - 212(\boldsymbol{T}_{m_x m_z} \cdot \boldsymbol{T}_{n_x n_y}) L_4(m_y, m_z, n_z, n_z) + 467(\boldsymbol{T}_{m_x m_z} \cdot \boldsymbol{T}_{n_x n_z}) L_4(m_x, m_y, n_x, n_y) \\
&\qquad - 467(\boldsymbol{T}_{m_x m_z} \cdot \boldsymbol{T}_{n_x n_z}) L_4(m_x, m_y, n_y, n_z) - 467(\boldsymbol{T}_{m_x m_z} \cdot \boldsymbol{T}_{n_x n_z}) L_4(m_y, m_y, n_x, n_y) \\
&\qquad + 467(\boldsymbol{T}_{m_x m_z} \cdot \boldsymbol{T}_{n_x n_z}) L_4(m_y, m_y, n_y, n_z) + 467(\boldsymbol{T}_{m_x m_z} \cdot \boldsymbol{T}_{n_x n_z}) L_4(m_y, m_z, n_x, n_y) \\
&\qquad - 467(\boldsymbol{T}_{m_x m_z} \cdot \boldsymbol{T}_{n_x n_z}) L_4(m_y, m_z, n_y, n_z) + 212(\boldsymbol{T}_{m_x m_z} \cdot \boldsymbol{T}_{n_y n_z}) L_4(m_x, m_y, n_x, n_x) \\
&\qquad - 510(\boldsymbol{T}_{m_x m_z} \cdot \boldsymbol{T}_{n_y n_z}) L_4(m_x, m_y, n_x, n_y) - 43(\boldsymbol{T}_{m_x m_z} \cdot \boldsymbol{T}_{n_y n_z}) L_4(m_x, m_y, n_x, n_z) \\
&\qquad - 212(\boldsymbol{T}_{m_x m_z} \cdot \boldsymbol{T}_{n_y n_z}) L_4(m_y, m_y, n_x, n_x) + 510(\boldsymbol{T}_{m_x m_z} \cdot \boldsymbol{T}_{n_y n_z}) L_4(m_y, m_y, n_x, n_y) \\
&\qquad + 43(\boldsymbol{T}_{m_x m_z} \cdot \boldsymbol{T}_{n_y n_z}) L_4(m_y, m_y, n_x, n_z) + 212(\boldsymbol{T}_{m_x m_z} \cdot \boldsymbol{T}_{n_y n_z}) L_4(m_y, m_z, n_x, n_x) \\
&\qquad - 510(\boldsymbol{T}_{m_x m_z} \cdot \boldsymbol{T}_{n_y n_z}) L_4(m_y, m_z, n_x, n_y) - 43(\boldsymbol{T}_{m_x m_z} \cdot \boldsymbol{T}_{n_y n_z}) L_4(m_y, m_z, n_x, n_z) \\
&\qquad + 43(\boldsymbol{T}_{m_y m_z} \cdot \boldsymbol{T}_{n_x n_y}) L_4(m_x, m_x, n_x, n_z) + 510(\boldsymbol{T}_{m_y m_z} \cdot \boldsymbol{T}_{n_x n_y}) L_4(m_x, m_x, n_y, n_z) \\
&\qquad - 212(\boldsymbol{T}_{m_y m_z} \cdot \boldsymbol{T}_{n_x n_y}) L_4(m_x, m_x, n_z, n_z) - 43(\boldsymbol{T}_{m_y m_z} \cdot \boldsymbol{T}_{n_x n_y}) L_4(m_x, m_y, n_x, n_z) \\
&\qquad - 510(\boldsymbol{T}_{m_y m_z} \cdot \boldsymbol{T}_{n_x n_y}) L_4(m_x, m_y, n_y, n_z) + 212(\boldsymbol{T}_{m_y m_z} \cdot \boldsymbol{T}_{n_x n_y}) L_4(m_x, m_y, n_z, n_z) \\
&\qquad - 43(\boldsymbol{T}_{m_y m_z} \cdot \boldsymbol{T}_{n_x n_y}) L_4(m_x, m_z, n_x, n_z) - 510(\boldsymbol{T}_{m_y m_z} \cdot \boldsymbol{T}_{n_x n_y}) L_4(m_x, m_z, n_y, n_z) \\
&\qquad + 212(\boldsymbol{T}_{m_y m_z} \cdot \boldsymbol{T}_{n_x n_y}) L_4(m_x, m_z, n_z, n_z) + 467(\boldsymbol{T}_{m_y m_z} \cdot \boldsymbol{T}_{n_x n_z}) L_4(m_x, m_x, n_x, n_y) \\
&\qquad - 467(\boldsymbol{T}_{m_y m_z} \cdot \boldsymbol{T}_{n_x n_z}) L_4(m_x, m_x, n_y, n_z) - 467(\boldsymbol{T}_{m_y m_z} \cdot \boldsymbol{T}_{n_x n_z}) L_4(m_x, m_y, n_x, n_y) \\
&\qquad + 467(\boldsymbol{T}_{m_y m_z} \cdot \boldsymbol{T}_{n_x n_z}) L_4(m_x, m_y, n_y, n_z) - 467(\boldsymbol{T}_{m_y m_z} \cdot \boldsymbol{T}_{n_x n_z}) L_4(m_x, m_z, n_x, n_y) \\
&\qquad + 467(\boldsymbol{T}_{m_y m_z} \cdot \boldsymbol{T}_{n_x n_z}) L_4(m_x, m_z, n_y, n_z) + 212(\boldsymbol{T}_{m_y m_z} \cdot \boldsymbol{T}_{n_y n_z}) L_4(m_x, m_x, n_x, n_x) \\
&\qquad - 510(\boldsymbol{T}_{m_y m_z} \cdot \boldsymbol{T}_{n_y n_z}) L_4(m_x, m_x, n_x, n_y) - 43(\boldsymbol{T}_{m_y m_z} \cdot \boldsymbol{T}_{n_y n_z}) L_4(m_x, m_x, n_x, n_z) \\
&\qquad - 212(\boldsymbol{T}_{m_y m_z} \cdot \boldsymbol{T}_{n_y n_z}) L_4(m_x, m_y, n_x, n_x) + 510(\boldsymbol{T}_{m_y m_z} \cdot \boldsymbol{T}_{n_y n_z}) L_4(m_x, m_y, n_x, n_y) \\
&\qquad + 43(\boldsymbol{T}_{m_y m_z} \cdot \boldsymbol{T}_{n_y n_z}) L_4(m_x, m_y, n_x, n_z) - 212(\boldsymbol{T}_{m_y m_z} \cdot \boldsymbol{T}_{n_y n_z}) L_4(m_x, m_z, n_x, n_x) \\
&\qquad + 510(\boldsymbol{T}_{m_y m_z} \cdot \boldsymbol{T}_{n_y n_z}) L_4(m_x, m_z, n_x, n_y) + 43(\boldsymbol{T}_{m_y m_z} \cdot \boldsymbol{T}_{n_y n_z}) L_4(m_x, m_z, n_x, n_z)),
\end{aligned}
$$

$$
\begin{aligned}
S_{mn} =& v544320k02 \\
&(-131I_{m_xn_x}L_6(m_y,m_y,m_z,n_x,n_y,n_z) - 124I_{m_xn_x}L_6(m_y,m_y,m_z,n_y,n_y,n_z) \\
&+ 168I_{m_xn_x}L_6(m_y,m_y,m_z,n_y,n_z,n_z) + 131I_{m_xn_x}L_6(m_y,m_z,m_z,n_x,n_y,n_z) \\
&+ 124I_{m_xn_x}L_6(m_y,m_z,m_z,n_y,n_y,n_z) - 168I_{m_xn_x}L_6(m_y,m_z,m_z,n_y,n_z,n_z) \\
&- 44I_{m_xn_y}L_6(m_y,m_y,m_z,n_x,n_x,n_z) + 262I_{m_xn_y}L_6(m_y,m_y,m_z,n_x,n_y,n_z) \\
&- 44I_{m_xn_y}L_6(m_y,m_y,m_z,n_x,n_z,n_z) + 44I_{m_xn_y}L_6(m_y,m_z,m_z,n_x,n_x,n_z) \\
&- 262I_{m_xn_y}L_6(m_y,m_z,m_z,n_x,n_y,n_z) + 44I_{m_xn_y}L_6(m_y,m_z,m_z,n_x,n_z,n_z) \\
&+ 168I_{m_xn_z}L_6(m_y,m_y,m_z,n_x,n_x,n_y) - 124I_{m_xn_z}L_6(m_y,m_y,m_z,n_x,n_y,n_y) \\
&- 131I_{m_xn_z}L_6(m_y,m_y,m_z,n_x,n_y,n_z) - 168I_{m_xn_z}L_6(m_y,m_z,m_z,n_x,n_x,n_y) \\
&+ 124I_{m_xn_z}L_6(m_y,m_z,m_z,n_x,n_y,n_y) + 131I_{m_xn_z}L_6(m_y,m_z,m_z,n_x,n_y,n_z) \\
&+ 131I_{m_yn_x}L_6(m_x,m_x,m_z,n_x,n_y,n_z) + 124I_{m_yn_x}L_6(m_x,m_x,m_z,n_y,n_y,n_z) \\
&- 168I_{m_yn_x}L_6(m_x,m_x,m_z,n_y,n_z,n_z) - 131I_{m_yn_x}L_6(m_x,m_z,m_z,n_x,n_y,n_z) \\
&- 124I_{m_yn_x}L_6(m_x,m_z,m_z,n_y,n_y,n_z) + 168I_{m_yn_x}L_6(m_x,m_z,m_z,n_y,n_z,n_z) \\
&+ 44I_{m_yn_y}L_6(m_x,m_x,m_z,n_x,n_x,n_z) - 262I_{m_yn_y}L_6(m_x,m_x,m_z,n_x,n_y,n_z) \\
&+ 44I_{m_yn_y}L_6(m_x,m_x,m_z,n_x,n_z,n_z) - 44I_{m_yn_y}L_6(m_x,m_z,m_z,n_x,n_x,n_z) \\
&+ 262I_{m_yn_y}L_6(m_x,m_z,m_z,n_x,n_y,n_z) - 44I_{m_yn_y}L_6(m_x,m_z,m_z,n_x,n_z,n_z) \\
&- 168I_{m_yn_z}L_6(m_x,m_x,m_z,n_x,n_x,n_y) + 124I_{m_yn_z}L_6(m_x,m_x,m_z,n_x,n_y,n_y) \\
&+ 131I_{m_yn_z}L_6(m_x,m_x,m_z,n_x,n_y,n_z) + 168I_{m_yn_z}L_6(m_x,m_z,m_z,n_x,n_x,n_y) \\
&- 124I_{m_yn_z}L_6(m_x,m_z,m_z,n_x,n_y,n_y) - 131I_{m_yn_z}L_6(m_x,m_z,m_z,n_x,n_y,n_z) \\
&- 131I_{m_zn_x}L_6(m_x,m_x,m_y,n_x,n_y,n_z) - 124I_{m_zn_x}L_6(m_x,m_x,m_y,n_y,n_y,n_z) \\
&+ 168I_{m_zn_x}L_6(m_x,m_x,m_y,n_y,n_z,n_z) + 131I_{m_zn_x}L_6(m_x,m_y,m_y,n_x,n_y,n_z) \\
&+ 124I_{m_zn_x}L_6(m_x,m_y,m_y,n_y,n_y,n_z) - 168I_{m_zn_x}L_6(m_x,m_y,m_y,n_y,n_z,n_z) \\
&- 44I_{m_zn_y}L_6(m_x,m_x,m_y,n_x,n_x,n_z) + 262I_{m_zn_y}L_6(m_x,m_x,m_y,n_x,n_y,n_z) \\
&- 44I_{m_zn_y}L_6(m_x,m_x,m_y,n_x,n_z,n_z) + 44I_{m_zn_y}L_6(m_x,m_y,m_y,n_x,n_x,n_z) \\
&- 262I_{m_zn_y}L_6(m_x,m_y,m_y,n_x,n_y,n_z) + 44I_{m_zn_y}L_6(m_x,m_y,m_y,n_x,n_z,n_z) \\
&+ 168I_{m_zn_z}L_6(m_x,m_x,m_y,n_x,n_x,n_y) - 124I_{m_zn_z}L_6(m_x,m_x,m_y,n_x,n_y,n_y) \\
&- 131I_{m_zn_z}L_6(m_x,m_x,m_y,n_x,n_y,n_z) - 168I_{m_zn_z}L_6(m_x,m_y,m_y,n_x,n_x,n_y) \\
&+ 124I_{m_zn_z}L_6(m_x,m_y,m_y,n_x,n_y,n_y) + 131I_{m_zn_z}L_6(m_x,m_y,m_y,n_x,n_y,n_z)).
\end{aligned}
$$

$< g_{3m}, j_{3n} >$

$$
\begin{aligned}
R_{mn} =& v3\_34020 \\
& (2(\boldsymbol{T}_{m_x m_y}, \boldsymbol{T}_{n_0 n_2}) L_4(m_x, m_z, n_1, n_3) + 2(\boldsymbol{T}_{m_x m_y}, \boldsymbol{T}_{n_0 n_2}) L_4(m_y, m_z, n_1, n_3) \\
& - 2(\boldsymbol{T}_{m_x m_y}, \boldsymbol{T}_{n_0 n_2}) L_4(m_z, m_z, n_1, n_3) + 2(\boldsymbol{T}_{m_x m_y}, \boldsymbol{T}_{n_0 n_3}) L_4(m_x, m_z, n_1, n_2) \\
& + 2(\boldsymbol{T}_{m_x m_y}, \boldsymbol{T}_{n_0 n_3}) L_4(m_y, m_z, n_1, n_2) - 2(\boldsymbol{T}_{m_x m_y}, \boldsymbol{T}_{n_0 n_3}) L_4(m_z, m_z, n_1, n_2) \\
& + 2(\boldsymbol{T}_{m_x m_y}, \boldsymbol{T}_{n_1 n_2}) L_4(m_x, m_z, n_0, n_3) + 2(\boldsymbol{T}_{m_x m_y}, \boldsymbol{T}_{n_1 n_2}) L_4(m_y, m_z, n_0, n_3) \\
& - 2(\boldsymbol{T}_{m_x m_y}, \boldsymbol{T}_{n_1 n_2}) L_4(m_z, m_z, n_0, n_3) + 2(\boldsymbol{T}_{m_x m_y}, \boldsymbol{T}_{n_1 n_3}) L_4(m_x, m_z, n_0, n_2) \\
& + 2(\boldsymbol{T}_{m_x m_y}, \boldsymbol{T}_{n_1 n_3}) L_4(m_y, m_z, n_0, n_2) - 2(\boldsymbol{T}_{m_x m_y}, \boldsymbol{T}_{n_1 n_3}) L_4(m_z, m_z, n_0, n_2) \\
& - 2(\boldsymbol{T}_{m_x m_z}, \boldsymbol{T}_{n_0 n_2}) L_4(m_x, m_y, n_1, n_3) + 2(\boldsymbol{T}_{m_x m_z}, \boldsymbol{T}_{n_0 n_2}) L_4(m_y, m_y, n_1, n_3) \\
& - 2(\boldsymbol{T}_{m_x m_z}, \boldsymbol{T}_{n_0 n_2}) L_4(m_y, m_z, n_1, n_3) - 2(\boldsymbol{T}_{m_x m_z}, \boldsymbol{T}_{n_0 n_3}) L_4(m_x, m_y, n_1, n_2) \\
& + 2(\boldsymbol{T}_{m_x m_z}, \boldsymbol{T}_{n_0 n_3}) L_4(m_y, m_y, n_1, n_2) - 2(\boldsymbol{T}_{m_x m_z}, \boldsymbol{T}_{n_0 n_3}) L_4(m_y, m_z, n_1, n_2) \\
& - 2(\boldsymbol{T}_{m_x m_z}, \boldsymbol{T}_{n_1 n_2}) L_4(m_x, m_y, n_0, n_3) + 2(\boldsymbol{T}_{m_x m_z}, \boldsymbol{T}_{n_1 n_2}) L_4(m_y, m_y, n_0, n_3) \\
& - 2(\boldsymbol{T}_{m_x m_z}, \boldsymbol{T}_{n_1 n_2}) L_4(m_y, m_z, n_0, n_3) - 2(\boldsymbol{T}_{m_x m_z}, \boldsymbol{T}_{n_1 n_3}) L_4(m_x, m_y, n_0, n_2) \\
& + 2(\boldsymbol{T}_{m_x m_z}, \boldsymbol{T}_{n_1 n_3}) L_4(m_y, m_y, n_0, n_2) - 2(\boldsymbol{T}_{m_x m_z}, \boldsymbol{T}_{n_1 n_3}) L_4(m_y, m_z, n_0, n_2) \\
& - 2(\boldsymbol{T}_{m_y m_z}, \boldsymbol{T}_{n_0 n_2}) L_4(m_x, m_x, n_1, n_3) + 2(\boldsymbol{T}_{m_y m_z}, \boldsymbol{T}_{n_0 n_2}) L_4(m_x, m_y, n_1, n_3) \\
& + 2(\boldsymbol{T}_{m_y m_z}, \boldsymbol{T}_{n_0 n_2}) L_4(m_x, m_z, n_1, n_3) - 2(\boldsymbol{T}_{m_y m_z}, \boldsymbol{T}_{n_0 n_3}) L_4(m_x, m_x, n_1, n_2) \\
& + 2(\boldsymbol{T}_{m_y m_z}, \boldsymbol{T}_{n_0 n_3}) L_4(m_x, m_y, n_1, n_2) + 2(\boldsymbol{T}_{m_y m_z}, \boldsymbol{T}_{n_0 n_3}) L_4(m_x, m_z, n_1, n_2) \\
& - 2(\boldsymbol{T}_{m_y m_z}, \boldsymbol{T}_{n_1 n_2}) L_4(m_x, m_x, n_0, n_3) + 2(\boldsymbol{T}_{m_y m_z}, \boldsymbol{T}_{n_1 n_2}) L_4(m_x, m_y, n_0, n_3) \\
& + 2(\boldsymbol{T}_{m_y m_z}, \boldsymbol{T}_{n_1 n_2}) L_4(m_x, m_z, n_0, n_3) - 2(\boldsymbol{T}_{m_y m_z}, \boldsymbol{T}_{n_1 n_3}) L_4(m_x, m_x, n_0, n_2) \\
& + 2(\boldsymbol{T}_{m_y m_z}, \boldsymbol{T}_{n_1 n_3}) L_4(m_x, m_y, n_0, n_2) + 2(\boldsymbol{T}_{m_y m_z}, \boldsymbol{T}_{n_1 n_3}) L_4(m_x, m_z, n_0, n_2)), \\
S_{mn} =& v544320k02 \\
& (I_{m_x n_0} L_6(m_y, m_y, m_z, n_1, n_2, n_3) - I_{m_x n_0} L_6(m_y, m_z, m_z, n_1, n_2, n_3) \\
& + I_{m_x n_1} L_6(m_y, m_y, m_z, n_0, n_2, n_3) - I_{m_x n_1} L_6(m_y, m_z, m_z, n_0, n_2, n_3) \\
& - I_{m_x n_2} L_6(m_y, m_y, m_z, n_0, n_1, n_3) + I_{m_x n_2} L_6(m_y, m_z, m_z, n_0, n_1, n_3) \\
& - I_{m_x n_3} L_6(m_y, m_y, m_z, n_0, n_1, n_2) + I_{m_x n_3} L_6(m_y, m_z, m_z, n_0, n_1, n_2) \\
& - I_{m_y n_0} L_6(m_x, m_x, m_z, n_1, n_2, n_3) + I_{m_y n_0} L_6(m_x, m_z, m_z, n_1, n_2, n_3) \\
& - I_{m_y n_1} L_6(m_x, m_x, m_z, n_0, n_2, n_3) + I_{m_y n_1} L_6(m_x, m_z, m_z, n_0, n_2, n_3) \\
& + I_{m_y n_2} L_6(m_x, m_x, m_z, n_0, n_1, n_3) - I_{m_y n_2} L_6(m_x, m_z, m_z, n_0, n_1, n_3) \\
& + I_{m_y n_3} L_6(m_x, m_x, m_z, n_0, n_1, n_2) - I_{m_y n_3} L_6(m_x, m_z, m_z, n_0, n_1, n_2) \\
& + I_{m_z n_0} L_6(m_x, m_x, m_y, n_1, n_2, n_3) - I_{m_z n_0} L_6(m_x, m_y, m_y, n_1, n_2, n_3) \\
& + I_{m_z n_1} L_6(m_x, m_x, m_y, n_0, n_2, n_3) - I_{m_z n_1} L_6(m_x, m_y, m_y, n_0, n_2, n_3) \\
& - I_{m_z n_2} L_6(m_x, m_x, m_y, n_0, n_1, n_3) + I_{m_z n_2} L_6(m_x, m_y, m_y, n_0, n_1, n_3) \\
& - I_{m_z n_3} L_6(m_x, m_x, m_y, n_0, n_1, n_2) + I_{m_z n_3} L_6(m_x, m_y, m_y, n_0, n_1, n_2)).
\end{aligned}
$$

$< g_{3m}, k_{3n} >$

$R_{mn} = v3\_34020$

$$
\begin{aligned}
&(-(\boldsymbol{T}_{m_xm_y} \cdot \boldsymbol{T}_{n_0n_2})L_4(m_x, m_z, n_1, n_3) - (\boldsymbol{T}_{m_xm_y} \cdot \boldsymbol{T}_{n_0n_2})L_4(m_y, m_z, n_1, n_3)\\
&+ (\boldsymbol{T}_{m_xm_y} \cdot \boldsymbol{T}_{n_0n_2})L_4(m_z, m_z, n_1, n_3) + (\boldsymbol{T}_{m_xm_y} \cdot \boldsymbol{T}_{n_0n_3})L_4(m_x, m_z, n_1, n_2)\\
&+ (\boldsymbol{T}_{m_xm_y} \cdot \boldsymbol{T}_{n_0n_3})L_4(m_y, m_z, n_1, n_2) - (\boldsymbol{T}_{m_xm_y} \cdot \boldsymbol{T}_{n_0n_3})L_4(m_z, m_z, n_1, n_2)\\
&- (\boldsymbol{T}_{m_xm_y} \cdot \boldsymbol{T}_{n_1n_2})L_4(m_x, m_z, n_0, n_3) - (\boldsymbol{T}_{m_xm_y} \cdot \boldsymbol{T}_{n_1n_2})L_4(m_y, m_z, n_0, n_3)\\
&+ (\boldsymbol{T}_{m_xm_y} \cdot \boldsymbol{T}_{n_1n_2})L_4(m_z, m_z, n_0, n_3) + (\boldsymbol{T}_{m_xm_y} \cdot \boldsymbol{T}_{n_1n_3})L_4(m_x, m_z, n_0, n_2)\\
&+ (\boldsymbol{T}_{m_xm_y} \cdot \boldsymbol{T}_{n_1n_3})L_4(m_y, m_z, n_0, n_2) - (\boldsymbol{T}_{m_xm_y} \cdot \boldsymbol{T}_{n_1n_3})L_4(m_z, m_z, n_0, n_2)\\
&+ 2(\boldsymbol{T}_{m_xm_y} \cdot \boldsymbol{T}_{n_2n_3})L_4(m_x, m_z, n_0, n_1) + 2(\boldsymbol{T}_{m_xm_y} \cdot \boldsymbol{T}_{n_2n_3})L_4(m_y, m_z, n_0, n_1)\\
&- 2(\boldsymbol{T}_{m_xm_y} \cdot \boldsymbol{T}_{n_2n_3})L_4(m_z, m_z, n_0, n_1) + (\boldsymbol{T}_{m_xm_z} \cdot \boldsymbol{T}_{n_0n_2})L_4(m_x, m_y, n_1, n_3)\\
&- (\boldsymbol{T}_{m_xm_z} \cdot \boldsymbol{T}_{n_0n_2})L_4(m_y, m_y, n_1, n_3) + (\boldsymbol{T}_{m_xm_z} \cdot \boldsymbol{T}_{n_0n_2})L_4(m_y, m_z, n_1, n_3)\\
&- (\boldsymbol{T}_{m_xm_z} \cdot \boldsymbol{T}_{n_0n_3})L_4(m_x, m_y, n_1, n_2) + (\boldsymbol{T}_{m_xm_z} \cdot \boldsymbol{T}_{n_0n_3})L_4(m_y, m_y, n_1, n_2)\\
&- (\boldsymbol{T}_{m_xm_z} \cdot \boldsymbol{T}_{n_0n_3})L_4(m_y, m_z, n_1, n_2) + (\boldsymbol{T}_{m_xm_z} \cdot \boldsymbol{T}_{n_1n_2})L_4(m_x, m_y, n_0, n_3)\\
&- (\boldsymbol{T}_{m_xm_z} \cdot \boldsymbol{T}_{n_1n_2})L_4(m_y, m_y, n_0, n_3) + (\boldsymbol{T}_{m_xm_z} \cdot \boldsymbol{T}_{n_1n_2})L_4(m_y, m_z, n_0, n_3)\\
&- (\boldsymbol{T}_{m_xm_z} \cdot \boldsymbol{T}_{n_1n_3})L_4(m_x, m_y, n_0, n_2) + (\boldsymbol{T}_{m_xm_z} \cdot \boldsymbol{T}_{n_1n_3})L_4(m_y, m_y, n_0, n_2)\\
&- (\boldsymbol{T}_{m_xm_z} \cdot \boldsymbol{T}_{n_1n_3})L_4(m_y, m_z, n_0, n_2) - 2(\boldsymbol{T}_{m_xm_z} \cdot \boldsymbol{T}_{n_2n_3})L_4(m_x, m_y, n_0, n_1)\\
&+ 2(\boldsymbol{T}_{m_xm_z} \cdot \boldsymbol{T}_{n_2n_3})L_4(m_y, m_y, n_0, n_1) - 2(\boldsymbol{T}_{m_xm_z} \cdot \boldsymbol{T}_{n_2n_3})L_4(m_y, m_z, n_0, n_1)\\
&+ (\boldsymbol{T}_{m_ym_z} \cdot \boldsymbol{T}_{n_0n_2})L_4(m_x, m_x, n_1, n_3) - (\boldsymbol{T}_{m_ym_z} \cdot \boldsymbol{T}_{n_0n_2})L_4(m_x, m_y, n_1, n_3)\\
&- (\boldsymbol{T}_{m_ym_z} \cdot \boldsymbol{T}_{n_0n_2})L_4(m_x, m_z, n_1, n_3) - (\boldsymbol{T}_{m_ym_z} \cdot \boldsymbol{T}_{n_0n_3})L_4(m_x, m_x, n_1, n_2)\\
&+ (\boldsymbol{T}_{m_ym_z} \cdot \boldsymbol{T}_{n_0n_3})L_4(m_x, m_y, n_1, n_2) + (\boldsymbol{T}_{m_ym_z} \cdot \boldsymbol{T}_{n_0n_3})L_4(m_x, m_z, n_1, n_2)\\
&+ (\boldsymbol{T}_{m_ym_z} \cdot \boldsymbol{T}_{n_1n_2})L_4(m_x, m_x, n_0, n_3) - (\boldsymbol{T}_{m_ym_z} \cdot \boldsymbol{T}_{n_1n_2})L_4(m_x, m_y, n_0, n_3)\\
&- (\boldsymbol{T}_{m_ym_z} \cdot \boldsymbol{T}_{n_1n_2})L_4(m_x, m_z, n_0, n_3) - (\boldsymbol{T}_{m_ym_z} \cdot \boldsymbol{T}_{n_1n_3})L_4(m_x, m_x, n_0, n_2)\\
&+ (\boldsymbol{T}_{m_ym_z} \cdot \boldsymbol{T}_{n_1n_3})L_4(m_x, m_y, n_0, n_2) + (\boldsymbol{T}_{m_ym_z} \cdot \boldsymbol{T}_{n_1n_3})L_4(m_x, m_z, n_0, n_2)\\
&- 2(\boldsymbol{T}_{m_ym_z} \cdot \boldsymbol{T}_{n_2n_3})L_4(m_x, m_x, n_0, n_1) + 2(\boldsymbol{T}_{m_ym_z} \cdot \boldsymbol{T}_{n_2n_3})L_4(m_x, m_y, n_0, n_1)\\
&+ 2(\boldsymbol{T}_{m_ym_z} \cdot \boldsymbol{T}_{n_2n_3})L_4(m_x, m_z, n_0, n_1)),
\end{aligned}
$$

$S_{mn} = v544320k02$

$$
\begin{aligned}
&(I_{m_xn_2}L_6(m_y, m_y, m_z, n_0, n_1, n_3) - I_{m_xn_2}L_6(m_y, m_z, m_z, n_0, n_1, n_3)\\
&- I_{m_xn_3}L_6(m_y, m_y, m_z, n_0, n_1, n_2) + I_{m_xn_3}L_6(m_y, m_z, m_z, n_0, n_1, n_2)\\
&- I_{m_yn_2}L_6(m_x, m_x, m_z, n_0, n_1, n_3) + I_{m_yn_2}L_6(m_x, m_z, m_z, n_0, n_1, n_3)\\
&+ I_{m_yn_3}L_6(m_x, m_x, m_z, n_0, n_1, n_2) - I_{m_yn_3}L_6(m_x, m_z, m_z, n_0, n_1, n_2)\\
&+ I_{m_zn_2}L_6(m_x, m_x, m_y, n_0, n_1, n_3) - I_{m_zn_2}L_6(m_x, m_y, m_y, n_0, n_1, n_3)\\
&- I_{m_zn_3}L_6(m_x, m_x, m_y, n_0, n_1, n_2) + I_{m_zn_3}L_6(m_x, m_y, m_y, n_0, n_1, n_2)).
\end{aligned}
$$

$< g_{3m}, l_{3n} >$

$R_{mn} = v3\_34020$

$(2(\boldsymbol{T}_{m_x m_y} \cdot \boldsymbol{T}_{n_0 n_1}) L_4(m_x, m_z, n_2, n_3) + 2(\boldsymbol{T}_{m_x m_y} \cdot \boldsymbol{T}_{n_0 n_1}) L_4(m_y, m_z, n_2, n_3)$
$- 2(\boldsymbol{T}_{m_x m_y} \cdot \boldsymbol{T}_{n_0 n_1}) L_4(m_z, m_z, n_2, n_3) + (\boldsymbol{T}_{m_x m_y} \cdot \boldsymbol{T}_{n_0 n_2}) L_4(m_x, m_z, n_1, n_3)$
$+ (\boldsymbol{T}_{m_x m_y} \cdot \boldsymbol{T}_{n_0 n_2}) L_4(m_y, m_z, n_1, n_3) - (\boldsymbol{T}_{m_x m_y} \cdot \boldsymbol{T}_{n_0 n_2}) L_4(m_z, m_z, n_1, n_3)$
$+ (\boldsymbol{T}_{m_x m_y} \cdot \boldsymbol{T}_{n_0 n_3}) L_4(m_x, m_z, n_1, n_2) + (\boldsymbol{T}_{m_x m_y} \cdot \boldsymbol{T}_{n_0 n_3}) L_4(m_y, m_z, n_1, n_2)$
$- (\boldsymbol{T}_{m_x m_y} \cdot \boldsymbol{T}_{n_0 n_3}) L_4(m_z, m_z, n_1, n_2) - (\boldsymbol{T}_{m_x m_y} \cdot \boldsymbol{T}_{n_1 n_2}) L_4(m_x, m_z, n_0, n_3)$
$- (\boldsymbol{T}_{m_x m_y} \cdot \boldsymbol{T}_{n_1 n_2}) L_4(m_y, m_z, n_0, n_3) + (\boldsymbol{T}_{m_x m_y} \cdot \boldsymbol{T}_{n_1 n_2}) L_4(m_z, m_z, n_0, n_3)$
$- (\boldsymbol{T}_{m_x m_y} \cdot \boldsymbol{T}_{n_1 n_3}) L_4(m_x, m_z, n_0, n_2) - (\boldsymbol{T}_{m_x m_y} \cdot \boldsymbol{T}_{n_1 n_3}) L_4(m_y, m_z, n_0, n_2)$
$+ (\boldsymbol{T}_{m_x m_y} \cdot \boldsymbol{T}_{n_1 n_3}) L_4(m_z, m_z, n_0, n_2) - 2(\boldsymbol{T}_{m_x m_z} \cdot \boldsymbol{T}_{n_0 n_1}) L_4(m_x, m_y, n_2, n_3)$
$+ 2(\boldsymbol{T}_{m_x m_z} \cdot \boldsymbol{T}_{n_0 n_1}) L_4(m_y, m_y, n_2, n_3) - 2(\boldsymbol{T}_{m_x m_z} \cdot \boldsymbol{T}_{n_0 n_1}) L_4(m_y, m_z, n_2, n_3)$
$- (\boldsymbol{T}_{m_x m_z} \cdot \boldsymbol{T}_{n_0 n_2}) L_4(m_x, m_y, n_1, n_3) + (\boldsymbol{T}_{m_x m_z} \cdot \boldsymbol{T}_{n_0 n_2}) L_4(m_y, m_y, n_1, n_3)$
$- (\boldsymbol{T}_{m_x m_z} \cdot \boldsymbol{T}_{n_0 n_2}) L_4(m_y, m_z, n_1, n_3) - (\boldsymbol{T}_{m_x m_z} \cdot \boldsymbol{T}_{n_0 n_3}) L_4(m_x, m_y, n_1, n_2)$
$+ (\boldsymbol{T}_{m_x m_z} \cdot \boldsymbol{T}_{n_0 n_3}) L_4(m_y, m_y, n_1, n_2) - (\boldsymbol{T}_{m_x m_z} \cdot \boldsymbol{T}_{n_0 n_3}) L_4(m_y, m_z, n_1, n_2)$
$+ (\boldsymbol{T}_{m_x m_z} \cdot \boldsymbol{T}_{n_1 n_2}) L_4(m_x, m_y, n_0, n_3) - (\boldsymbol{T}_{m_x m_z} \cdot \boldsymbol{T}_{n_1 n_2}) L_4(m_y, m_y, n_0, n_3)$
$+ (\boldsymbol{T}_{m_x m_z} \cdot \boldsymbol{T}_{n_1 n_2}) L_4(m_y, m_z, n_0, n_3) + (\boldsymbol{T}_{m_x m_z} \cdot \boldsymbol{T}_{n_1 n_3}) L_4(m_x, m_y, n_0, n_2)$
$- (\boldsymbol{T}_{m_x m_z} \cdot \boldsymbol{T}_{n_1 n_3}) L_4(m_y, m_y, n_0, n_2) + (\boldsymbol{T}_{m_x m_z} \cdot \boldsymbol{T}_{n_1 n_3}) L_4(m_y, m_z, n_0, n_2)$
$- 2(\boldsymbol{T}_{m_y m_z} \cdot \boldsymbol{T}_{n_0 n_1}) L_4(m_x, m_x, n_2, n_3) + 2(\boldsymbol{T}_{m_y m_z} \cdot \boldsymbol{T}_{n_0 n_1}) L_4(m_x, m_y, n_2, n_3)$
$+ 2(\boldsymbol{T}_{m_y m_z} \cdot \boldsymbol{T}_{n_0 n_1}) L_4(m_x, m_z, n_2, n_3) - (\boldsymbol{T}_{m_y m_z} \cdot \boldsymbol{T}_{n_0 n_2}) L_4(m_x, m_x, n_1, n_3)$
$+ (\boldsymbol{T}_{m_y m_z} \cdot \boldsymbol{T}_{n_0 n_2}) L_4(m_x, m_y, n_1, n_3) + (\boldsymbol{T}_{m_y m_z} \cdot \boldsymbol{T}_{n_0 n_2}) L_4(m_x, m_z, n_1, n_3)$
$- (\boldsymbol{T}_{m_y m_z} \cdot \boldsymbol{T}_{n_0 n_3}) L_4(m_x, m_x, n_1, n_2) + (\boldsymbol{T}_{m_y m_z} \cdot \boldsymbol{T}_{n_0 n_3}) L_4(m_x, m_y, n_1, n_2)$
$+ (\boldsymbol{T}_{m_y m_z} \cdot \boldsymbol{T}_{n_0 n_3}) L_4(m_x, m_z, n_1, n_2) + (\boldsymbol{T}_{m_y m_z} \cdot \boldsymbol{T}_{n_1 n_2}) L_4(m_x, m_x, n_0, n_3)$
$- (\boldsymbol{T}_{m_y m_z} \cdot \boldsymbol{T}_{n_1 n_2}) L_4(m_x, m_y, n_0, n_3) - (\boldsymbol{T}_{m_y m_z} \cdot \boldsymbol{T}_{n_1 n_2}) L_4(m_x, m_z, n_0, n_3)$
$+ (\boldsymbol{T}_{m_y m_z} \cdot \boldsymbol{T}_{n_1 n_3}) L_4(m_x, m_x, n_0, n_2) - (\boldsymbol{T}_{m_y m_z} \cdot \boldsymbol{T}_{n_1 n_3}) L_4(m_x, m_y, n_0, n_2)$
$- (\boldsymbol{T}_{m_y m_z} \cdot \boldsymbol{T}_{n_1 n_3}) L_4(m_x, m_z, n_0, n_2)),$

$S_{mn} = v544320k02$

$(I_{m_x n_0} L_6(m_y, m_y, m_z, n_1, n_2, n_3) - I_{m_x n_0} L_6(m_y, m_z, m_z, n_1, n_2, n_3)$
$- I_{m_x n_1} L_6(m_y, m_y, m_z, n_0, n_2, n_3) + I_{m_x n_1} L_6(m_y, m_z, m_z, n_0, n_2, n_3)$
$- I_{m_y n_0} L_6(m_x, m_x, m_z, n_1, n_2, n_3) + I_{m_y n_0} L_6(m_x, m_z, m_z, n_1, n_2, n_3)$
$+ I_{m_y n_1} L_6(m_x, m_x, m_z, n_0, n_2, n_3) - I_{m_y n_1} L_6(m_x, m_z, m_z, n_0, n_2, n_3)$
$+ I_{m_z n_0} L_6(m_x, m_x, m_y, n_1, n_2, n_3) - I_{m_z n_0} L_6(m_x, m_y, m_y, n_1, n_2, n_3)$
$- I_{m_z n_1} L_6(m_x, m_x, m_y, n_0, n_2, n_3) + I_{m_z n_1} L_6(m_x, m_y, m_y, n_0, n_2, n_3)).$

$$
\begin{aligned}
&< h_{3m}, h_{3n} > \\
&\quad R_{mn} = v3\_68040(\alpha+\beta+\gamma), \\
&\quad\quad \alpha = 954529(\boldsymbol{T}_{m_xm_y}\cdot\boldsymbol{T}_{n_xn_y})L_4(m_x,m_z,n_x,n_z) - 414248(\boldsymbol{T}_{m_xm_y}\cdot\boldsymbol{T}_{n_xn_y})L_4(m_x,m_z,n_y,n_z) \\
&\quad\quad\quad - 207124(\boldsymbol{T}_{m_xm_y}\cdot\boldsymbol{T}_{n_xn_y})L_4(m_x,m_z,n_z,n_z) - 414248(\boldsymbol{T}_{m_xm_y}\cdot\boldsymbol{T}_{n_xn_y})L_4(m_y,m_z,n_x,n_z) \\
&\quad\quad\quad + 179776(\boldsymbol{T}_{m_xm_y}\cdot\boldsymbol{T}_{n_xn_y})L_4(m_y,m_z,n_y,n_z) + 89888(\boldsymbol{T}_{m_xm_y}\cdot\boldsymbol{T}_{n_xn_y})L_4(m_y,m_z,n_z,n_z) \\
&\quad\quad\quad - 207124(\boldsymbol{T}_{m_xm_y}\cdot\boldsymbol{T}_{n_xn_y})L_4(m_z,m_z,n_x,n_z) + 89888(\boldsymbol{T}_{m_xm_y}\cdot\boldsymbol{T}_{n_xn_y})L_4(m_z,m_z,n_y,n_z) \\
&\quad\quad\quad + 44944(\boldsymbol{T}_{m_xm_y}\cdot\boldsymbol{T}_{n_xn_y})L_4(m_z,m_z,n_z,n_z) + 540281(\boldsymbol{T}_{m_xm_y}\cdot\boldsymbol{T}_{n_xn_z})L_4(m_x,m_z,n_x,n_y) \\
&\quad\quad\quad - 414248(\boldsymbol{T}_{m_xm_y}\cdot\boldsymbol{T}_{n_xn_z})L_4(m_x,m_z,n_y,n_y) + 540281(\boldsymbol{T}_{m_xm_y}\cdot\boldsymbol{T}_{n_xn_z})L_4(m_x,m_z,n_y,n_z) \\
&\quad\quad\quad - 234472(\boldsymbol{T}_{m_xm_y}\cdot\boldsymbol{T}_{n_xn_z})L_4(m_y,m_z,n_x,n_y) + 179776(\boldsymbol{T}_{m_xm_y}\cdot\boldsymbol{T}_{n_xn_z})L_4(m_y,m_z,n_y,n_y) \\
&\quad\quad\quad - 234472(\boldsymbol{T}_{m_xm_y}\cdot\boldsymbol{T}_{n_xn_z})L_4(m_y,m_z,n_y,n_z) - 117236(\boldsymbol{T}_{m_xm_y}\cdot\boldsymbol{T}_{n_xn_z})L_4(m_z,m_z,n_x,n_y) \\
&\quad\quad\quad + 89888(\boldsymbol{T}_{m_xm_y}\cdot\boldsymbol{T}_{n_xn_z})L_4(m_z,m_z,n_y,n_y) - 117236(\boldsymbol{T}_{m_xm_y}\cdot\boldsymbol{T}_{n_xn_z})L_4(m_z,m_z,n_y,n_z) \\
&\quad\quad\quad - 207124(\boldsymbol{T}_{m_xm_y}\cdot\boldsymbol{T}_{n_yn_z})L_4(m_x,m_z,n_x,n_x) - 414248(\boldsymbol{T}_{m_xm_y}\cdot\boldsymbol{T}_{n_yn_z})L_4(m_x,m_z,n_x,n_y) \\
&\quad\quad\quad + 954529(\boldsymbol{T}_{m_xm_y}\cdot\boldsymbol{T}_{n_yn_z})L_4(m_x,m_z,n_x,n_z) + 89888(\boldsymbol{T}_{m_xm_y}\cdot\boldsymbol{T}_{n_yn_z})L_4(m_y,m_z,n_x,n_x) \\
&\quad\quad\quad + 179776(\boldsymbol{T}_{m_xm_y}\cdot\boldsymbol{T}_{n_yn_z})L_4(m_y,m_z,n_x,n_y) - 414248(\boldsymbol{T}_{m_xm_y}\cdot\boldsymbol{T}_{n_yn_z})L_4(m_y,m_z,n_x,n_z) \\
&\quad\quad\quad + 44944(\boldsymbol{T}_{m_xm_y}\cdot\boldsymbol{T}_{n_yn_z})L_4(m_z,m_z,n_x,n_x) + 89888(\boldsymbol{T}_{m_xm_y}\cdot\boldsymbol{T}_{n_yn_z})L_4(m_z,m_z,n_x,n_y) \\
&\quad\quad\quad - 207124(\boldsymbol{T}_{m_xm_y}\cdot\boldsymbol{T}_{n_yn_z})L_4(m_z,m_z,n_x,n_z) + 540281(\boldsymbol{T}_{m_xm_z}\cdot\boldsymbol{T}_{n_xn_y})L_4(m_x,m_y,n_x,n_z) \\
&\quad\quad\quad - 234472(\boldsymbol{T}_{m_xm_z}\cdot\boldsymbol{T}_{n_xn_y})L_4(m_x,m_y,n_y,n_z) - 117236(\boldsymbol{T}_{m_xm_z}\cdot\boldsymbol{T}_{n_xn_y})L_4(m_x,m_y,n_z,n_z) \\
&\quad\quad\quad - 414248(\boldsymbol{T}_{m_xm_z}\cdot\boldsymbol{T}_{n_xn_y})L_4(m_y,m_y,n_x,n_z) + 179776(\boldsymbol{T}_{m_xm_z}\cdot\boldsymbol{T}_{n_xn_y})L_4(m_y,m_y,n_y,n_z), \\
&\quad\quad \beta = + 89888(\boldsymbol{T}_{m_xm_z}\cdot\boldsymbol{T}_{n_xn_y})L_4(m_y,m_y,n_z,n_z) + 540281(\boldsymbol{T}_{m_xm_z}\cdot\boldsymbol{T}_{n_xn_y})L_4(m_y,m_z,n_x,n_z) \\
&\quad\quad\quad - 234472(\boldsymbol{T}_{m_xm_z}\cdot\boldsymbol{T}_{n_xn_y})L_4(m_y,m_z,n_y,n_z) - 117236(\boldsymbol{T}_{m_xm_z}\cdot\boldsymbol{T}_{n_xn_y})L_4(m_y,m_z,n_z,n_z) \\
&\quad\quad\quad + 305809(\boldsymbol{T}_{m_xm_z}\cdot\boldsymbol{T}_{n_xn_z})L_4(m_x,m_y,n_x,n_y) - 234472(\boldsymbol{T}_{m_xm_z}\cdot\boldsymbol{T}_{n_xn_z})L_4(m_x,m_y,n_y,n_y) \\
&\quad\quad\quad + 305809(\boldsymbol{T}_{m_xm_z}\cdot\boldsymbol{T}_{n_xn_z})L_4(m_x,m_y,n_y,n_z) - 234472(\boldsymbol{T}_{m_xm_z}\cdot\boldsymbol{T}_{n_xn_z})L_4(m_y,m_y,n_x,n_y) \\
&\quad\quad\quad + 179776(\boldsymbol{T}_{m_xm_z}\cdot\boldsymbol{T}_{n_xn_z})L_4(m_y,m_y,n_y,n_y) - 234472(\boldsymbol{T}_{m_xm_z}\cdot\boldsymbol{T}_{n_xn_z})L_4(m_y,m_y,n_y,n_z) \\
&\quad\quad\quad + 305809(\boldsymbol{T}_{m_xm_z}\cdot\boldsymbol{T}_{n_xn_z})L_4(m_y,m_z,n_x,n_y) - 234472(\boldsymbol{T}_{m_xm_z}\cdot\boldsymbol{T}_{n_xn_z})L_4(m_y,m_z,n_y,n_y) \\
&\quad\quad\quad + 305809(\boldsymbol{T}_{m_xm_z}\cdot\boldsymbol{T}_{n_xn_z})L_4(m_y,m_z,n_y,n_z) - 117236(\boldsymbol{T}_{m_xm_z}\cdot\boldsymbol{T}_{n_yn_z})L_4(m_x,m_y,n_x,n_x) \\
&\quad\quad\quad - 234472(\boldsymbol{T}_{m_xm_z}\cdot\boldsymbol{T}_{n_yn_z})L_4(m_x,m_y,n_x,n_y) + 540281(\boldsymbol{T}_{m_xm_z}\cdot\boldsymbol{T}_{n_yn_z})L_4(m_x,m_y,n_x,n_z) \\
&\quad\quad\quad + 89888(\boldsymbol{T}_{m_xm_z}\cdot\boldsymbol{T}_{n_yn_z})L_4(m_y,m_y,n_x,n_x) + 179776(\boldsymbol{T}_{m_xm_z}\cdot\boldsymbol{T}_{n_yn_z})L_4(m_y,m_y,n_x,n_y) \\
&\quad\quad\quad - 414248(\boldsymbol{T}_{m_xm_z}\cdot\boldsymbol{T}_{n_yn_z})L_4(m_y,m_y,n_x,n_z) - 117236(\boldsymbol{T}_{m_xm_z}\cdot\boldsymbol{T}_{n_yn_z})L_4(m_y,m_z,n_x,n_x) \\
&\quad\quad\quad - 234472(\boldsymbol{T}_{m_xm_z}\cdot\boldsymbol{T}_{n_yn_z})L_4(m_y,m_z,n_x,n_y) + 540281(\boldsymbol{T}_{m_xm_z}\cdot\boldsymbol{T}_{n_yn_z})L_4(m_y,m_z,n_x,n_z) \\
&\quad\quad\quad - 207124(\boldsymbol{T}_{m_ym_z}\cdot\boldsymbol{T}_{n_xn_y})L_4(m_x,m_x,n_x,n_z) + 89888(\boldsymbol{T}_{m_ym_z}\cdot\boldsymbol{T}_{n_xn_y})L_4(m_x,m_x,n_y,n_z) \\
&\quad\quad\quad + 44944(\boldsymbol{T}_{m_ym_z}\cdot\boldsymbol{T}_{n_xn_y})L_4(m_x,m_x,n_z,n_z) - 414248(\boldsymbol{T}_{m_ym_z}\cdot\boldsymbol{T}_{n_xn_y})L_4(m_x,m_y,n_x,n_z) \\
&\quad\quad\quad + 179776(\boldsymbol{T}_{m_ym_z}\cdot\boldsymbol{T}_{n_xn_y})L_4(m_x,m_y,n_y,n_z) + 89888(\boldsymbol{T}_{m_ym_z}\cdot\boldsymbol{T}_{n_xn_y})L_4(m_x,m_y,n_z,n_z) \\
&\quad\quad\quad + 954529(\boldsymbol{T}_{m_ym_z}\cdot\boldsymbol{T}_{n_xn_y})L_4(m_x,m_z,n_x,n_z) - 414248(\boldsymbol{T}_{m_ym_z}\cdot\boldsymbol{T}_{n_xn_y})L_4(m_x,m_z,n_y,n_z) \\
&\quad\quad\quad - 207124(\boldsymbol{T}_{m_ym_z}\cdot\boldsymbol{T}_{n_xn_y})L_4(m_x,m_z,n_z,n_z) - 117236(\boldsymbol{T}_{m_ym_z}\cdot\boldsymbol{T}_{n_xn_z})L_4(m_x,m_x,n_x,n_y) \\
&\quad\quad\quad + 89888(\boldsymbol{T}_{m_ym_z}\cdot\boldsymbol{T}_{n_xn_z})L_4(m_x,m_x,n_y,n_y) - 117236(\boldsymbol{T}_{m_ym_z}\cdot\boldsymbol{T}_{n_xn_z})L_4(m_x,m_x,n_y,n_z) \\
&\quad\quad\quad - 234472(\boldsymbol{T}_{m_ym_z}\cdot\boldsymbol{T}_{n_xn_z})L_4(m_x,m_y,n_x,n_y) + 179776(\boldsymbol{T}_{m_ym_z}\cdot\boldsymbol{T}_{n_xn_z})L_4(m_x,m_y,n_y,n_y) \\
&\quad\quad\quad - 234472(\boldsymbol{T}_{m_ym_z}\cdot\boldsymbol{T}_{n_xn_z})L_4(m_x,m_y,n_y,n_z) + 540281(\boldsymbol{T}_{m_ym_z}\cdot\boldsymbol{T}_{n_xn_z})L_4(m_x,m_z,n_x,n_y) \\
&\quad\quad\quad - 414248(\boldsymbol{T}_{m_ym_z}\cdot\boldsymbol{T}_{n_xn_z})L_4(m_x,m_z,n_y,n_y) + 540281(\boldsymbol{T}_{m_ym_z}\cdot\boldsymbol{T}_{n_xn_z})L_4(m_x,m_z,n_y,n_z),
\end{aligned}
$$

$$
\begin{aligned}
\gamma = &+ 44944(\boldsymbol{T}_{m_y m_z} \cdot \boldsymbol{T}_{n_y n_z}) L_4(m_x, m_x, n_x, n_x) + 89888(\boldsymbol{T}_{m_y m_z} \cdot \boldsymbol{T}_{n_y n_z}) L_4(m_x, m_x, n_x, n_y) \\
&- 207124(\boldsymbol{T}_{m_y m_z} \cdot \boldsymbol{T}_{n_y n_z}) L_4(m_x, m_x, n_x, n_z) + 89888(\boldsymbol{T}_{m_y m_z} \cdot \boldsymbol{T}_{n_y n_z}) L_4(m_x, m_y, n_x, n_x) \\
&+ 179776(\boldsymbol{T}_{m_y m_z} \cdot \boldsymbol{T}_{n_y n_z}) L_4(m_x, m_y, n_x, n_y) - 414248(\boldsymbol{T}_{m_y m_z} \cdot \boldsymbol{T}_{n_y n_z}) L_4(m_x, m_y, n_x, n_z) \\
&- 207124(\boldsymbol{T}_{m_y m_z} \cdot \boldsymbol{T}_{n_y n_z}) L_4(m_x, m_z, n_x, n_x) - 414248(\boldsymbol{T}_{m_y m_z} \cdot \boldsymbol{T}_{n_y n_z}) L_4(m_x, m_z, n_x, n_y) \\
&+ 954529(\boldsymbol{T}_{m_y m_z} \cdot \boldsymbol{T}_{n_y n_z}) L_4(m_x, m_z, n_x, n_z),
\end{aligned}
$$

$$
\begin{aligned}
S_{mn} =& v544320k02(154449I_{m_xn_x}L_6(m_x,m_y,m_z,n_x,n_y,n_z) - 83316I_{m_xn_x}L_6(m_x,m_y,m_z,n_y,n_y,n_z)\\
&+ 31440I_{m_xn_x}L_6(m_x,m_y,m_z,n_y,n_z,n_z) - 83316I_{m_xn_x}L_6(m_y,m_y,m_z,n_x,n_y,n_z)\\
&+ 44944I_{m_xn_x}L_6(m_y,m_y,m_z,n_y,n_y,n_z) - 16960I_{m_xn_x}L_6(m_y,m_y,m_z,n_y,n_z,n_z)\\
&+ 31440I_{m_xn_x}L_6(m_y,m_z,m_z,n_x,n_y,n_z) - 16960I_{m_xn_x}L_6(m_y,m_z,m_z,n_y,n_y,n_z)\\
&+ 6400I_{m_xn_x}L_6(m_y,m_z,m_z,n_y,n_z,n_z) - 114756I_{m_xn_y}L_6(m_x,m_y,m_z,n_x,n_x,n_z)\\
&+ 114756I_{m_xn_y}L_6(m_x,m_y,m_z,n_x,n_z,n_z) + 61904I_{m_xn_y}L_6(m_y,m_y,m_z,n_x,n_x,n_z)\\
&- 61904I_{m_xn_y}L_6(m_y,m_y,m_z,n_x,n_z,n_z) - 23360I_{m_xn_y}L_6(m_y,m_z,m_z,n_x,n_x,n_z)\\
&+ 23360I_{m_xn_y}L_6(m_y,m_z,m_z,n_x,n_z,n_z) - 31440I_{m_xn_z}L_6(m_x,m_y,m_z,n_x,n_x,n_y)\\
&+ 83316I_{m_xn_z}L_6(m_x,m_y,m_z,n_x,n_y,n_y) - 154449I_{m_xn_z}L_6(m_x,m_y,m_z,n_x,n_y,n_z)\\
&+ 16960I_{m_xn_z}L_6(m_y,m_y,m_z,n_x,n_x,n_y) - 44944I_{m_xn_z}L_6(m_y,m_y,m_z,n_x,n_y,n_y)\\
&+ 83316I_{m_xn_z}L_6(m_y,m_y,m_z,n_x,n_y,n_z) - 6400I_{m_xn_z}L_6(m_y,m_z,m_z,n_x,n_x,n_y)\\
&+ 16960I_{m_xn_z}L_6(m_y,m_z,m_z,n_x,n_y,n_y) - 31440I_{m_xn_z}L_6(m_y,m_z,m_z,n_x,n_y,n_z)\\
&- 114756I_{m_yn_x}L_6(m_x,m_x,m_z,n_x,n_y,n_z) + 61904I_{m_yn_x}L_6(m_x,m_x,m_z,n_y,n_y,n_z)\\
&- 23360I_{m_yn_x}L_6(m_x,m_x,m_z,n_y,n_z,n_z) + 114756I_{m_yn_x}L_6(m_x,m_z,m_z,n_x,n_y,n_z)\\
&- 61904I_{m_yn_x}L_6(m_x,m_z,m_z,n_y,n_y,n_z) + 23360I_{m_yn_x}L_6(m_x,m_z,m_z,n_y,n_z,n_z)\\
&+ 85264I_{m_yn_y}L_6(m_x,m_x,m_z,n_x,n_x,n_z) - 85264I_{m_yn_y}L_6(m_x,m_x,m_z,n_x,n_z,n_z)\\
&- 85264I_{m_yn_y}L_6(m_x,m_z,m_z,n_x,n_x,n_z) + 85264I_{m_yn_y}L_6(m_x,m_z,m_z,n_x,n_z,n_z)\\
&+ 23360I_{m_yn_z}L_6(m_x,m_x,m_z,n_x,n_x,n_y) - 61904I_{m_yn_z}L_6(m_x,m_x,m_z,n_x,n_y,n_y)\\
&+ 114756I_{m_yn_z}L_6(m_x,m_x,m_z,n_x,n_y,n_z) - 23360I_{m_yn_z}L_6(m_x,m_z,m_z,n_x,n_x,n_y)\\
&+ 61904I_{m_yn_z}L_6(m_x,m_z,m_z,n_x,n_y,n_y) - 114756I_{m_yn_z}L_6(m_x,m_z,m_z,n_x,n_y,n_z)\\
&- 31440I_{m_zn_x}L_6(m_x,m_x,m_y,n_x,n_y,n_z) + 16960I_{m_zn_x}L_6(m_x,m_x,m_y,n_y,n_y,n_z)\\
&- 6400I_{m_zn_x}L_6(m_x,m_x,m_y,n_y,n_z,n_z) + 83316I_{m_zn_x}L_6(m_x,m_y,m_y,n_x,n_y,n_z)\\
&- 44944I_{m_zn_x}L_6(m_x,m_y,m_y,n_y,n_y,n_z) + 16960I_{m_zn_x}L_6(m_x,m_y,m_y,n_y,n_z,n_z)\\
&- 154449I_{m_zn_x}L_6(m_x,m_y,m_z,n_x,n_y,n_z) + 83316I_{m_zn_x}L_6(m_x,m_y,m_z,n_y,n_y,n_z)\\
&- 31440I_{m_zn_x}L_6(m_x,m_y,m_z,n_y,n_z,n_z) + 23360I_{m_zn_y}L_6(m_x,m_x,m_y,n_x,n_x,n_z)\\
&- 23360I_{m_zn_y}L_6(m_x,m_x,m_y,n_x,n_z,n_z) - 61904I_{m_zn_y}L_6(m_x,m_y,m_y,n_x,n_x,n_z)\\
&+ 61904I_{m_zn_y}L_6(m_x,m_y,m_y,n_x,n_z,n_z) + 114756I_{m_zn_y}L_6(m_x,m_y,m_z,n_x,n_x,n_z)\\
&- 114756I_{m_zn_y}L_6(m_x,m_y,m_z,n_x,n_z,n_z) + 6400I_{m_zn_z}L_6(m_x,m_x,m_y,n_x,n_x,n_y)\\
&- 16960I_{m_zn_z}L_6(m_x,m_x,m_y,n_x,n_y,n_y) + 31440I_{m_zn_z}L_6(m_x,m_x,m_y,n_x,n_y,n_z)\\
&- 16960I_{m_zn_z}L_6(m_x,m_y,m_y,n_x,n_x,n_y) + 44944I_{m_zn_z}L_6(m_x,m_y,m_y,n_x,n_y,n_y)\\
&- 83316I_{m_zn_z}L_6(m_x,m_y,m_y,n_x,n_y,n_z) + 31440I_{m_zn_z}L_6(m_x,m_y,m_z,n_x,n_x,n_y)\\
&- 83316I_{m_zn_z}L_6(m_x,m_y,m_z,n_x,n_y,n_y) + 154449I_{m_zn_z}L_6(m_x,m_y,m_z,n_x,n_y,n_z));
\end{aligned}
$$

$$< h_{3m}, i_{3n} >$$
$$R_{mn} = v3\_68040$$
$$(42011(\boldsymbol{T}_{m_xm_y} \cdot \boldsymbol{T}_{n_xn_y})L_4(m_x, m_z, n_x, n_z) + 498270(\boldsymbol{T}_{m_xm_y} \cdot \boldsymbol{T}_{n_xn_y})L_4(m_x, m_z, n_y, n_z)$$
$$- 207124(\boldsymbol{T}_{m_xm_y} \cdot \boldsymbol{T}_{n_xn_y})L_4(m_x, m_z, n_z, n_z) - 18232(\boldsymbol{T}_{m_xm_y} \cdot \boldsymbol{T}_{n_xn_y})L_4(m_y, m_z, n_x, n_z)$$
$$- 216240(\boldsymbol{T}_{m_xm_y} \cdot \boldsymbol{T}_{n_xn_y})L_4(m_y, m_z, n_y, n_z) + 89888(\boldsymbol{T}_{m_xm_y} \cdot \boldsymbol{T}_{n_xn_y})L_4(m_y, m_z, n_z, n_z)$$
$$- 9116(\boldsymbol{T}_{m_xm_y} \cdot \boldsymbol{T}_{n_xn_y})L_4(m_z, m_z, n_x, n_z) - 108120(\boldsymbol{T}_{m_xm_y} \cdot \boldsymbol{T}_{n_xn_y})L_4(m_z, m_z, n_y, n_z)$$
$$+ 44944(\boldsymbol{T}_{m_xm_y} \cdot \boldsymbol{T}_{n_xn_y})L_4(m_z, m_z, n_z, n_z) + 456259(\boldsymbol{T}_{m_xm_y} \cdot \boldsymbol{T}_{n_xn_z})L_4(m_x, m_z, n_x, n_y)$$
$$- 456259(\boldsymbol{T}_{m_xm_y} \cdot \boldsymbol{T}_{n_xn_z})L_4(m_x, m_z, n_y, n_z) - 198008(\boldsymbol{T}_{m_xm_y} \cdot \boldsymbol{T}_{n_xn_z})L_4(m_y, m_z, n_x, n_y)$$
$$+ 198008(\boldsymbol{T}_{m_xm_y} \cdot \boldsymbol{T}_{n_xn_z})L_4(m_y, m_z, n_y, n_z) - 99004(\boldsymbol{T}_{m_xm_y} \cdot \boldsymbol{T}_{n_xn_z})L_4(m_z, m_z, n_x, n_y)$$
$$+ 99004(\boldsymbol{T}_{m_xm_y} \cdot \boldsymbol{T}_{n_xn_z})L_4(m_z, m_z, n_y, n_z) + 207124(\boldsymbol{T}_{m_xm_y} \cdot \boldsymbol{T}_{n_yn_z})L_4(m_x, m_z, n_x, n_x)$$
$$- 498270(\boldsymbol{T}_{m_xm_y} \cdot \boldsymbol{T}_{n_yn_z})L_4(m_x, m_z, n_x, n_y) - 42011(\boldsymbol{T}_{m_xm_y} \cdot \boldsymbol{T}_{n_yn_z})L_4(m_x, m_z, n_x, n_z)$$
$$- 89888(\boldsymbol{T}_{m_xm_y} \cdot \boldsymbol{T}_{n_yn_z})L_4(m_y, m_z, n_x, n_x) + 216240(\boldsymbol{T}_{m_xm_y} \cdot \boldsymbol{T}_{n_yn_z})L_4(m_y, m_z, n_x, n_y)$$
$$+ 18232(\boldsymbol{T}_{m_xm_y} \cdot \boldsymbol{T}_{n_yn_z})L_4(m_y, m_z, n_x, n_z) - 44944(\boldsymbol{T}_{m_xm_y} \cdot \boldsymbol{T}_{n_yn_z})L_4(m_z, m_z, n_x, n_x)$$
$$+ 108120(\boldsymbol{T}_{m_xm_y} \cdot \boldsymbol{T}_{n_yn_z})L_4(m_z, m_z, n_x, n_y) + 9116(\boldsymbol{T}_{m_xm_y} \cdot \boldsymbol{T}_{n_yn_z})L_4(m_z, m_z, n_x, n_z)$$
$$+ 23779(\boldsymbol{T}_{m_xm_z} \cdot \boldsymbol{T}_{n_xn_y})L_4(m_x, m_y, n_x, n_z) + 282030(\boldsymbol{T}_{m_xm_z} \cdot \boldsymbol{T}_{n_xn_y})L_4(m_x, m_y, n_y, n_z)$$
$$- 117236(\boldsymbol{T}_{m_xm_z} \cdot \boldsymbol{T}_{n_xn_y})L_4(m_x, m_y, n_z, n_z) - 18232(\boldsymbol{T}_{m_xm_z} \cdot \boldsymbol{T}_{n_xn_y})L_4(m_y, m_y, n_x, n_z)$$
$$- 216240(\boldsymbol{T}_{m_xm_z} \cdot \boldsymbol{T}_{n_xn_y})L_4(m_y, m_y, n_y, n_z) + 89888(\boldsymbol{T}_{m_xm_z} \cdot \boldsymbol{T}_{n_xn_y})L_4(m_y, m_y, n_z, n_z)$$
$$+ 23779(\boldsymbol{T}_{m_xm_z} \cdot \boldsymbol{T}_{n_xn_y})L_4(m_y, m_z, n_x, n_z) + 282030(\boldsymbol{T}_{m_xm_z} \cdot \boldsymbol{T}_{n_xn_y})L_4(m_y, m_z, n_y, n_z)$$
$$- 117236(\boldsymbol{T}_{m_xm_z} \cdot \boldsymbol{T}_{n_xn_y})L_4(m_y, m_z, n_z, n_z) + 258251(\boldsymbol{T}_{m_xm_z} \cdot \boldsymbol{T}_{n_xn_z})L_4(m_x, m_y, n_x, n_y)$$
$$- 258251(\boldsymbol{T}_{m_xm_z} \cdot \boldsymbol{T}_{n_xn_z})L_4(m_x, m_y, n_y, n_z) - 198008(\boldsymbol{T}_{m_xm_z} \cdot \boldsymbol{T}_{n_xn_z})L_4(m_y, m_y, n_x, n_y)$$
$$+ 198008(\boldsymbol{T}_{m_xm_z} \cdot \boldsymbol{T}_{n_xn_z})L_4(m_y, m_y, n_y, n_z) + 258251(\boldsymbol{T}_{m_xm_z} \cdot \boldsymbol{T}_{n_xn_z})L_4(m_y, m_z, n_x, n_y)$$
$$- 258251(\boldsymbol{T}_{m_xm_z} \cdot \boldsymbol{T}_{n_xn_z})L_4(m_y, m_z, n_y, n_z) + 117236(\boldsymbol{T}_{m_xm_z} \cdot \boldsymbol{T}_{n_yn_z})L_4(m_x, m_y, n_x, n_x)$$
$$- 282030(\boldsymbol{T}_{m_xm_z} \cdot \boldsymbol{T}_{n_yn_z})L_4(m_x, m_y, n_x, n_y) - 23779(\boldsymbol{T}_{m_xm_z} \cdot \boldsymbol{T}_{n_yn_z})L_4(m_x, m_y, n_x, n_z)$$
$$- 89888(\boldsymbol{T}_{m_xm_z} \cdot \boldsymbol{T}_{n_yn_z})L_4(m_y, m_y, n_x, n_x) + 216240(\boldsymbol{T}_{m_xm_z} \cdot \boldsymbol{T}_{n_yn_z})L_4(m_y, m_y, n_x, n_y)$$
$$+ 18232(\boldsymbol{T}_{m_xm_z} \cdot \boldsymbol{T}_{n_yn_z})L_4(m_y, m_y, n_x, n_z) + 117236(\boldsymbol{T}_{m_xm_z} \cdot \boldsymbol{T}_{n_yn_z})L_4(m_y, m_z, n_x, n_x)$$
$$- 282030(\boldsymbol{T}_{m_xm_z} \cdot \boldsymbol{T}_{n_yn_z})L_4(m_y, m_z, n_x, n_y) - 23779(\boldsymbol{T}_{m_xm_z} \cdot \boldsymbol{T}_{n_yn_z})L_4(m_y, m_z, n_x, n_z)$$
$$- 9116(\boldsymbol{T}_{m_ym_z} \cdot \boldsymbol{T}_{n_xn_y})L_4(m_x, m_x, n_x, n_z) - 108120(\boldsymbol{T}_{m_ym_z} \cdot \boldsymbol{T}_{n_xn_y})L_4(m_x, m_x, n_y, n_z)$$
$$+ 44944(\boldsymbol{T}_{m_ym_z} \cdot \boldsymbol{T}_{n_xn_y})L_4(m_x, m_x, n_z, n_z) - 18232(\boldsymbol{T}_{m_ym_z} \cdot \boldsymbol{T}_{n_xn_y})L_4(m_x, m_y, n_x, n_z)$$
$$- 216240(\boldsymbol{T}_{m_ym_z} \cdot \boldsymbol{T}_{n_xn_y})L_4(m_x, m_y, n_y, n_z) + 89888(\boldsymbol{T}_{m_ym_z} \cdot \boldsymbol{T}_{n_xn_y})L_4(m_x, m_y, n_z, n_z)$$
$$+ 42011(\boldsymbol{T}_{m_ym_z} \cdot \boldsymbol{T}_{n_xn_y})L_4(m_x, m_z, n_x, n_z) + 498270(\boldsymbol{T}_{m_ym_z} \cdot \boldsymbol{T}_{n_xn_y})L_4(m_x, m_z, n_y, n_z)$$
$$- 207124(\boldsymbol{T}_{m_ym_z} \cdot \boldsymbol{T}_{n_xn_y})L_4(m_x, m_z, n_z, n_z) - 99004(\boldsymbol{T}_{m_ym_z} \cdot \boldsymbol{T}_{n_xn_z})L_4(m_x, m_x, n_x, n_y)$$
$$+ 99004(\boldsymbol{T}_{m_ym_z} \cdot \boldsymbol{T}_{n_xn_z})L_4(m_x, m_x, n_y, n_z) - 198008(\boldsymbol{T}_{m_ym_z} \cdot \boldsymbol{T}_{n_xn_z})L_4(m_x, m_y, n_x, n_y)$$
$$+ 198008(\boldsymbol{T}_{m_ym_z} \cdot \boldsymbol{T}_{n_xn_z})L_4(m_x, m_y, n_y, n_z) + 456259(\boldsymbol{T}_{m_ym_z} \cdot \boldsymbol{T}_{n_xn_z})L_4(m_x, m_z, n_x, n_y)$$
$$- 456259(\boldsymbol{T}_{m_ym_z} \cdot \boldsymbol{T}_{n_xn_z})L_4(m_x, m_z, n_y, n_z) - 44944(\boldsymbol{T}_{m_ym_z} \cdot \boldsymbol{T}_{n_yn_z})L_4(m_x, m_x, n_x, n_x)$$
$$+ 108120(\boldsymbol{T}_{m_ym_z} \cdot \boldsymbol{T}_{n_yn_z})L_4(m_x, m_x, n_x, n_y) + 9116(\boldsymbol{T}_{m_ym_z} \cdot \boldsymbol{T}_{n_yn_z})L_4(m_x, m_x, n_x, n_z)$$
$$- 89888(\boldsymbol{T}_{m_ym_z} \cdot \boldsymbol{T}_{n_yn_z})L_4(m_x, m_y, n_x, n_x) + 216240(\boldsymbol{T}_{m_ym_z} \cdot \boldsymbol{T}_{n_yn_z})L_4(m_x, m_y, n_x, n_y)$$
$$+ 18232(\boldsymbol{T}_{m_ym_z} \cdot \boldsymbol{T}_{n_yn_z})L_4(m_x, m_y, n_x, n_z) + 207124(\boldsymbol{T}_{m_ym_z} \cdot \boldsymbol{T}_{n_yn_z})L_4(m_x, m_z, n_x, n_x)$$
$$- 498270(\boldsymbol{T}_{m_ym_z} \cdot \boldsymbol{T}_{n_yn_z})L_4(m_x, m_z, n_x, n_y) - 42011(\boldsymbol{T}_{m_ym_z} \cdot \boldsymbol{T}_{n_yn_z})L_4(m_x, m_z, n_x, n_z)),$$

$$
\begin{aligned}
S_{mn} =& v544320k02 \\
&(51483 I_{m_x n_x} L_6(m_x, m_y, m_z, n_x, n_y, n_z) + 48732 I_{m_x n_x} L_6(m_x, m_y, m_z, n_y, n_y, n_z) \\
&- 66024 I_{m_x n_x} L_6(m_x, m_y, m_z, n_y, n_z, n_z) - 27772 I_{m_x n_x} L_6(m_y, m_y, m_z, n_x, n_y, n_z) \\
&- 26288 I_{m_x n_x} L_6(m_y, m_y, m_z, n_y, n_y, n_z) + 35616 I_{m_x n_x} L_6(m_y, m_y, m_z, n_y, n_z, n_z) \\
&+ 10480 I_{m_x n_x} L_6(m_y, m_z, m_z, n_x, n_y, n_z) + 9920 I_{m_x n_x} L_6(m_y, m_z, m_z, n_y, n_y, n_z) \\
&- 13440 I_{m_x n_x} L_6(m_y, m_z, m_z, n_y, n_z, n_z) + 17292 I_{m_x n_y} L_6(m_x, m_y, m_z, n_x, n_x, n_z) \\
&- 102966 I_{m_x n_y} L_6(m_x, m_y, m_z, n_x, n_y, n_z) + 17292 I_{m_x n_y} L_6(m_x, m_y, m_z, n_x, n_z, n_z) \\
&- 9328 I_{m_x n_y} L_6(m_y, m_y, m_z, n_x, n_x, n_z) + 55544 I_{m_x n_y} L_6(m_y, m_y, m_z, n_x, n_y, n_z) \\
&- 9328 I_{m_x n_y} L_6(m_y, m_y, m_z, n_x, n_z, n_z) + 3520 I_{m_x n_y} L_6(m_y, m_z, m_z, n_x, n_x, n_z) \\
&- 20960 I_{m_x n_y} L_6(m_y, m_z, m_z, n_x, n_y, n_z) + 3520 I_{m_x n_y} L_6(m_y, m_z, m_z, n_x, n_z, n_z) \\
&- 66024 I_{m_x n_z} L_6(m_x, m_y, m_z, n_x, n_x, n_y) + 48732 I_{m_x n_z} L_6(m_x, m_y, m_z, n_x, n_y, n_y) \\
&+ 51483 I_{m_x n_z} L_6(m_x, m_y, m_z, n_x, n_y, n_z) + 35616 I_{m_x n_z} L_6(m_y, m_y, m_z, n_x, n_x, n_y) \\
&- 26288 I_{m_x n_z} L_6(m_y, m_y, m_z, n_x, n_y, n_y) - 27772 I_{m_x n_z} L_6(m_y, m_y, m_z, n_x, n_y, n_z) \\
&- 13440 I_{m_x n_z} L_6(m_y, m_z, m_z, n_x, n_x, n_y) + 9920 I_{m_x n_z} L_6(m_y, m_z, m_z, n_x, n_y, n_y) \\
&+ 10480 I_{m_x n_z} L_6(m_y, m_z, m_z, n_x, n_y, n_z) - 38252 I_{m_y n_x} L_6(m_x, m_x, m_z, n_x, n_y, n_z) \\
&- 36208 I_{m_y n_x} L_6(m_x, m_x, m_z, n_y, n_y, n_z) + 49056 I_{m_y n_x} L_6(m_x, m_x, m_z, n_y, n_z, n_z) \\
&+ 38252 I_{m_y n_x} L_6(m_x, m_z, m_z, n_x, n_y, n_z) + 36208 I_{m_y n_x} L_6(m_x, m_z, m_z, n_y, n_y, n_z) \\
&- 49056 I_{m_y n_x} L_6(m_x, m_z, m_z, n_y, n_z, n_z) - 12848 I_{m_y n_y} L_6(m_x, m_x, m_z, n_x, n_x, n_z) \\
&+ 76504 I_{m_y n_y} L_6(m_x, m_x, m_z, n_x, n_y, n_z) - 12848 I_{m_y n_y} L_6(m_x, m_x, m_z, n_x, n_z, n_z) \\
&+ 12848 I_{m_y n_y} L_6(m_x, m_z, m_z, n_x, n_x, n_z) - 76504 I_{m_y n_y} L_6(m_x, m_z, m_z, n_x, n_y, n_z) \\
&+ 12848 I_{m_y n_y} L_6(m_x, m_z, m_z, n_x, n_z, n_z) + 49056 I_{m_y n_z} L_6(m_x, m_x, m_z, n_x, n_x, n_y) \\
&- 36208 I_{m_y n_z} L_6(m_x, m_x, m_z, n_x, n_y, n_y) - 38252 I_{m_y n_z} L_6(m_x, m_x, m_z, n_x, n_y, n_z) \\
&- 49056 I_{m_y n_z} L_6(m_x, m_z, m_z, n_x, n_x, n_y) + 36208 I_{m_y n_z} L_6(m_x, m_z, m_z, n_x, n_y, n_y) \\
&+ 38252 I_{m_y n_z} L_6(m_x, m_z, m_z, n_x, n_y, n_z) - 10480 I_{m_z n_x} L_6(m_x, m_x, m_y, n_x, n_y, n_z) \\
&- 9920 I_{m_z n_x} L_6(m_x, m_x, m_y, n_y, n_y, n_z) + 13440 I_{m_z n_x} L_6(m_x, m_x, m_y, n_y, n_z, n_z) \\
&+ 27772 I_{m_z n_x} L_6(m_x, m_y, m_y, n_x, n_y, n_z) + 26288 I_{m_z n_x} L_6(m_x, m_y, m_y, n_y, n_y, n_z) \\
&- 35616 I_{m_z n_x} L_6(m_x, m_y, m_y, n_y, n_z, n_z) - 51483 I_{m_z n_x} L_6(m_x, m_y, m_z, n_x, n_y, n_z) \\
&- 48732 I_{m_z n_x} L_6(m_x, m_y, m_z, n_y, n_y, n_z) + 66024 I_{m_z n_x} L_6(m_x, m_y, m_z, n_y, n_z, n_z) \\
&- 3520 I_{m_z n_y} L_6(m_x, m_x, m_y, n_x, n_x, n_z) + 20960 I_{m_z n_y} L_6(m_x, m_x, m_y, n_x, n_y, n_z) \\
&- 3520 I_{m_z n_y} L_6(m_x, m_x, m_y, n_x, n_z, n_z) + 9328 I_{m_z n_y} L_6(m_x, m_y, m_y, n_x, n_x, n_z) \\
&- 55544 I_{m_z n_y} L_6(m_x, m_y, m_y, n_x, n_y, n_z) + 9328 I_{m_z n_y} L_6(m_x, m_y, m_y, n_x, n_z, n_z) \\
&- 17292 I_{m_z n_y} L_6(m_x, m_y, m_z, n_x, n_x, n_z) + 102966 I_{m_z n_y} L_6(m_x, m_y, m_z, n_x, n_y, n_z) \\
&- 17292 I_{m_z n_y} L_6(m_x, m_y, m_z, n_x, n_z, n_z) + 13440 I_{m_z n_z} L_6(m_x, m_x, m_y, n_x, n_x, n_y) \\
&- 9920 I_{m_z n_z} L_6(m_x, m_x, m_y, n_x, n_y, n_y) - 10480 I_{m_z n_z} L_6(m_x, m_x, m_y, n_x, n_y, n_z) \\
&- 35616 I_{m_z n_z} L_6(m_x, m_y, m_y, n_x, n_x, n_y) + 26288 I_{m_z n_z} L_6(m_x, m_y, m_y, n_x, n_y, n_y) \\
&+ 27772 I_{m_z n_z} L_6(m_x, m_y, m_y, n_x, n_y, n_z) + 66024 I_{m_z n_z} L_6(m_x, m_y, m_z, n_x, n_x, n_y) \\
&- 48732 I_{m_z n_z} L_6(m_x, m_y, m_z, n_x, n_y, n_y) - 51483 I_{m_z n_z} L_6(m_x, m_y, m_z, n_x, n_y, n_z));
\end{aligned}
$$

$< h_{3m}, j_{3n} >$

$R_{mn} = v3\_68040$

$(-1954(\boldsymbol{T}_{m_x m_y} \cdot \boldsymbol{T}_{n_0 n_2}) L_4(m_x, m_z, n_1, n_3) + 848(\boldsymbol{T}_{m_x m_y} \cdot \boldsymbol{T}_{n_0 n_2}) L_4(m_y, m_z, n_1, n_3)$
$+ 424(\boldsymbol{T}_{m_x m_y} \cdot \boldsymbol{T}_{n_0 n_2}) L_4(m_z, m_z, n_1, n_3) - 1954(\boldsymbol{T}_{m_x m_y} \cdot \boldsymbol{T}_{n_0 n_3}) L_4(m_x, m_z, n_1, n_2)$
$+ 848(\boldsymbol{T}_{m_x m_y} \cdot \boldsymbol{T}_{n_0 n_3}) L_4(m_y, m_z, n_1, n_2) + 424(\boldsymbol{T}_{m_x m_y} \cdot \boldsymbol{T}_{n_0 n_3}) L_4(m_z, m_z, n_1, n_2)$
$- 1954(\boldsymbol{T}_{m_x m_y} \cdot \boldsymbol{T}_{n_1 n_2}) L_4(m_x, m_z, n_0, n_3) + 848(\boldsymbol{T}_{m_x m_y} \cdot \boldsymbol{T}_{n_1 n_2}) L_4(m_y, m_z, n_0, n_3)$
$+ 424(\boldsymbol{T}_{m_x m_y} \cdot \boldsymbol{T}_{n_1 n_2}) L_4(m_z, m_z, n_0, n_3) - 1954(\boldsymbol{T}_{m_x m_y} \cdot \boldsymbol{T}_{n_1 n_3}) L_4(m_x, m_z, n_0, n_2)$
$+ 848(\boldsymbol{T}_{m_x m_y} \cdot \boldsymbol{T}_{n_1 n_3}) L_4(m_y, m_z, n_0, n_2) + 424(\boldsymbol{T}_{m_x m_y} \cdot \boldsymbol{T}_{n_1 n_3}) L_4(m_z, m_z, n_0, n_2)$
$- 1106(\boldsymbol{T}_{m_x m_z} \cdot \boldsymbol{T}_{n_0 n_2}) L_4(m_x, m_y, n_1, n_3) + 848(\boldsymbol{T}_{m_x m_z} \cdot \boldsymbol{T}_{n_0 n_2}) L_4(m_y, m_y, n_1, n_3)$
$- 1106(\boldsymbol{T}_{m_x m_z} \cdot \boldsymbol{T}_{n_0 n_2}) L_4(m_y, m_z, n_1, n_3) - 1106(\boldsymbol{T}_{m_x m_z} \cdot \boldsymbol{T}_{n_0 n_3}) L_4(m_x, m_y, n_1, n_2)$
$+ 848(\boldsymbol{T}_{m_x m_z} \cdot \boldsymbol{T}_{n_0 n_3}) L_4(m_y, m_y, n_1, n_2) - 1106(\boldsymbol{T}_{m_x m_z} \cdot \boldsymbol{T}_{n_0 n_3}) L_4(m_y, m_z, n_1, n_2)$
$- 1106(\boldsymbol{T}_{m_x m_z} \cdot \boldsymbol{T}_{n_1 n_2}) L_4(m_x, m_y, n_0, n_3) + 848(\boldsymbol{T}_{m_x m_z} \cdot \boldsymbol{T}_{n_1 n_2}) L_4(m_y, m_y, n_0, n_3)$
$- 1106(\boldsymbol{T}_{m_x m_z} \cdot \boldsymbol{T}_{n_1 n_2}) L_4(m_y, m_z, n_0, n_3) - 1106(\boldsymbol{T}_{m_x m_z} \cdot \boldsymbol{T}_{n_1 n_3}) L_4(m_x, m_y, n_0, n_2)$
$+ 848(\boldsymbol{T}_{m_x m_z} \cdot \boldsymbol{T}_{n_1 n_3}) L_4(m_y, m_y, n_0, n_2) - 1106(\boldsymbol{T}_{m_x m_z} \cdot \boldsymbol{T}_{n_1 n_3}) L_4(m_y, m_z, n_0, n_2)$
$+ 424(\boldsymbol{T}_{m_y m_z} \cdot \boldsymbol{T}_{n_0 n_2}) L_4(m_x, m_x, n_1, n_3) + 848(\boldsymbol{T}_{m_y m_z} \cdot \boldsymbol{T}_{n_0 n_2}) L_4(m_x, m_y, n_1, n_3)$
$- 1954(\boldsymbol{T}_{m_y m_z} \cdot \boldsymbol{T}_{n_0 n_2}) L_4(m_x, m_z, n_1, n_3) + 424(\boldsymbol{T}_{m_y m_z} \cdot \boldsymbol{T}_{n_0 n_3}) L_4(m_x, m_x, n_1, n_2)$
$+ 848(\boldsymbol{T}_{m_y m_z} \cdot \boldsymbol{T}_{n_0 n_3}) L_4(m_x, m_y, n_1, n_2) - 1954(\boldsymbol{T}_{m_y m_z} \cdot \boldsymbol{T}_{n_0 n_3}) L_4(m_x, m_z, n_1, n_2)$
$+ 424(\boldsymbol{T}_{m_y m_z} \cdot \boldsymbol{T}_{n_1 n_2}) L_4(m_x, m_x, n_0, n_3) + 848(\boldsymbol{T}_{m_y m_z} \cdot \boldsymbol{T}_{n_1 n_2}) L_4(m_x, m_y, n_0, n_3)$
$- 1954(\boldsymbol{T}_{m_y m_z} \cdot \boldsymbol{T}_{n_1 n_2}) L_4(m_x, m_z, n_0, n_3) + 424(\boldsymbol{T}_{m_y m_z} \cdot \boldsymbol{T}_{n_1 n_3}) L_4(m_x, m_x, n_0, n_2)$
$+ 848(\boldsymbol{T}_{m_y m_z} \cdot \boldsymbol{T}_{n_1 n_3}) L_4(m_x, m_y, n_0, n_2) - 1954(\boldsymbol{T}_{m_y m_z} \cdot \boldsymbol{T}_{n_1 n_3}) L_4(m_x, m_z, n_0, n_2)),$

$S_{mn} = v544320k02$

$(-393 I_{m_x n_0} L_6(m_x, m_y, m_z, n_1, n_2, n_3) + 212 I_{m_x n_0} L_6(m_y, m_y, m_z, n_1, n_2, n_3)$
$- 80 I_{m_x n_0} L_6(m_y, m_z, m_z, n_1, n_2, n_3) - 393 I_{m_x n_1} L_6(m_x, m_y, m_z, n_0, n_2, n_3)$
$+ 212 I_{m_x n_1} L_6(m_y, m_y, m_z, n_0, n_2, n_3) - 80 I_{m_x n_1} L_6(m_y, m_z, m_z, n_0, n_2, n_3)$
$+ 393 I_{m_x n_2} L_6(m_x, m_y, m_z, n_0, n_1, n_3) - 212 I_{m_x n_2} L_6(m_y, m_y, m_z, n_0, n_1, n_3)$
$+ 80 I_{m_x n_2} L_6(m_y, m_z, m_z, n_0, n_1, n_3) + 393 I_{m_x n_3} L_6(m_x, m_y, m_z, n_0, n_1, n_2)$
$- 212 I_{m_x n_3} L_6(m_y, m_y, m_z, n_0, n_1, n_2) + 80 I_{m_x n_3} L_6(m_y, m_z, m_z, n_0, n_1, n_2)$
$+ 292 I_{m_y n_0} L_6(m_x, m_x, m_z, n_1, n_2, n_3) - 292 I_{m_y n_0} L_6(m_x, m_z, m_z, n_1, n_2, n_3)$
$+ 292 I_{m_y n_1} L_6(m_x, m_x, m_z, n_0, n_2, n_3) - 292 I_{m_y n_1} L_6(m_x, m_z, m_z, n_0, n_2, n_3)$
$- 292 I_{m_y n_2} L_6(m_x, m_x, m_z, n_0, n_1, n_3) + 292 I_{m_y n_2} L_6(m_x, m_z, m_z, n_0, n_1, n_3)$
$- 292 I_{m_y n_3} L_6(m_x, m_x, m_z, n_0, n_1, n_2) + 292 I_{m_y n_3} L_6(m_x, m_z, m_z, n_0, n_1, n_2)$
$+ 80 I_{m_z n_0} L_6(m_x, m_x, m_y, n_1, n_2, n_3) - 212 I_{m_z n_0} L_6(m_x, m_y, m_y, n_1, n_2, n_3)$
$+ 393 I_{m_z n_0} L_6(m_x, m_y, m_z, n_1, n_2, n_3) + 80 I_{m_z n_1} L_6(m_x, m_x, m_y, n_0, n_2, n_3)$
$- 212 I_{m_z n_1} L_6(m_x, m_y, m_y, n_0, n_2, n_3) + 393 I_{m_z n_1} L_6(m_x, m_y, m_z, n_0, n_2, n_3)$
$- 80 I_{m_z n_2} L_6(m_x, m_x, m_y, n_0, n_1, n_3) + 212 I_{m_z n_2} L_6(m_x, m_y, m_y, n_0, n_1, n_3)$
$- 393 I_{m_z n_2} L_6(m_x, m_y, m_z, n_0, n_1, n_3) - 80 I_{m_z n_3} L_6(m_x, m_x, m_y, n_0, n_1, n_2)$
$+ 212 I_{m_z n_3} L_6(m_x, m_y, m_y, n_0, n_1, n_2) - 393 I_{m_z n_3} L_6(m_x, m_y, m_z, n_0, n_1, n_2)).$

$$
\begin{aligned}
&< h_{3m}, k_{3n} > \\
&\quad R_{mn} = v3\_68040 \\
&\qquad (977(\boldsymbol{T}_{m_xm_y} \cdot \boldsymbol{T}_{n_0n_2})L_4(m_x, m_z, n_1, n_3) - 424(\boldsymbol{T}_{m_xm_y} \cdot \boldsymbol{T}_{n_0n_2})L_4(m_y, m_z, n_1, n_3) \\
&\qquad - 212(\boldsymbol{T}_{m_xm_y} \cdot \boldsymbol{T}_{n_0n_2})L_4(m_z, m_z, n_1, n_3) - 977(\boldsymbol{T}_{m_xm_y} \cdot \boldsymbol{T}_{n_0n_3})L_4(m_x, m_z, n_1, n_2) \\
&\qquad + 424(\boldsymbol{T}_{m_xm_y} \cdot \boldsymbol{T}_{n_0n_3})L_4(m_y, m_z, n_1, n_2) + 212(\boldsymbol{T}_{m_xm_y} \cdot \boldsymbol{T}_{n_0n_3})L_4(m_z, m_z, n_1, n_2) \\
&\qquad + 977(\boldsymbol{T}_{m_xm_y} \cdot \boldsymbol{T}_{n_1n_2})L_4(m_x, m_z, n_0, n_3) - 424(\boldsymbol{T}_{m_xm_y} \cdot \boldsymbol{T}_{n_1n_2})L_4(m_y, m_z, n_0, n_3) \\
&\qquad - 212(\boldsymbol{T}_{m_xm_y} \cdot \boldsymbol{T}_{n_1n_2})L_4(m_z, m_z, n_0, n_3) - 977(\boldsymbol{T}_{m_xm_y} \cdot \boldsymbol{T}_{n_1n_3})L_4(m_x, m_z, n_0, n_2) \\
&\qquad + 424(\boldsymbol{T}_{m_xm_y} \cdot \boldsymbol{T}_{n_1n_3})L_4(m_y, m_z, n_0, n_2) + 212(\boldsymbol{T}_{m_xm_y} \cdot \boldsymbol{T}_{n_1n_3})L_4(m_z, m_z, n_0, n_2) \\
&\qquad - 1954(\boldsymbol{T}_{m_xm_y} \cdot \boldsymbol{T}_{n_2n_3})L_4(m_x, m_z, n_0, n_1) + 848(\boldsymbol{T}_{m_xm_y} \cdot \boldsymbol{T}_{n_2n_3})L_4(m_y, m_z, n_0, n_1) \\
&\qquad + 424(\boldsymbol{T}_{m_xm_y} \cdot \boldsymbol{T}_{n_2n_3})L_4(m_z, m_z, n_0, n_1) + 553(\boldsymbol{T}_{m_xm_z} \cdot \boldsymbol{T}_{n_0n_2})L_4(m_x, m_y, n_1, n_3) \\
&\qquad - 424(\boldsymbol{T}_{m_xm_z} \cdot \boldsymbol{T}_{n_0n_2})L_4(m_y, m_y, n_1, n_3) + 553(\boldsymbol{T}_{m_xm_z} \cdot \boldsymbol{T}_{n_0n_2})L_4(m_y, m_z, n_1, n_3) \\
&\qquad - 553(\boldsymbol{T}_{m_xm_z} \cdot \boldsymbol{T}_{n_0n_3})L_4(m_x, m_y, n_1, n_2) + 424(\boldsymbol{T}_{m_xm_z} \cdot \boldsymbol{T}_{n_0n_3})L_4(m_y, m_y, n_1, n_2) \\
&\qquad - 553(\boldsymbol{T}_{m_xm_z} \cdot \boldsymbol{T}_{n_0n_3})L_4(m_y, m_z, n_1, n_2) + 553(\boldsymbol{T}_{m_xm_z} \cdot \boldsymbol{T}_{n_1n_2})L_4(m_x, m_y, n_0, n_3) \\
&\qquad - 424(\boldsymbol{T}_{m_xm_z} \cdot \boldsymbol{T}_{n_1n_2})L_4(m_y, m_y, n_0, n_3) + 553(\boldsymbol{T}_{m_xm_z} \cdot \boldsymbol{T}_{n_1n_2})L_4(m_y, m_z, n_0, n_3) \\
&\qquad - 553(\boldsymbol{T}_{m_xm_z} \cdot \boldsymbol{T}_{n_1n_3})L_4(m_x, m_y, n_0, n_2) + 424(\boldsymbol{T}_{m_xm_z} \cdot \boldsymbol{T}_{n_1n_3})L_4(m_y, m_y, n_0, n_2) \\
&\qquad - 553(\boldsymbol{T}_{m_xm_z} \cdot \boldsymbol{T}_{n_1n_3})L_4(m_y, m_z, n_0, n_2) - 1106(\boldsymbol{T}_{m_xm_z} \cdot \boldsymbol{T}_{n_2n_3})L_4(m_x, m_y, n_0, n_1) \\
&\qquad + 848(\boldsymbol{T}_{m_xm_z} \cdot \boldsymbol{T}_{n_2n_3})L_4(m_y, m_y, n_0, n_1) - 1106(\boldsymbol{T}_{m_xm_z} \cdot \boldsymbol{T}_{n_2n_3})L_4(m_y, m_z, n_0, n_1) \\
&\qquad - 212(\boldsymbol{T}_{m_ym_z} \cdot \boldsymbol{T}_{n_0n_2})L_4(m_x, m_x, n_1, n_3) - 424(\boldsymbol{T}_{m_ym_z} \cdot \boldsymbol{T}_{n_0n_2})L_4(m_x, m_y, n_1, n_3) \\
&\qquad + 977(\boldsymbol{T}_{m_ym_z} \cdot \boldsymbol{T}_{n_0n_2})L_4(m_x, m_z, n_1, n_3) + 212(\boldsymbol{T}_{m_ym_z} \cdot \boldsymbol{T}_{n_0n_3})L_4(m_x, m_x, n_1, n_2) \\
&\qquad + 424(\boldsymbol{T}_{m_ym_z} \cdot \boldsymbol{T}_{n_0n_3})L_4(m_x, m_y, n_1, n_2) - 977(\boldsymbol{T}_{m_ym_z} \cdot \boldsymbol{T}_{n_0n_3})L_4(m_x, m_z, n_1, n_2) \\
&\qquad - 212(\boldsymbol{T}_{m_ym_z} \cdot \boldsymbol{T}_{n_1n_2})L_4(m_x, m_x, n_0, n_3) - 424(\boldsymbol{T}_{m_ym_z} \cdot \boldsymbol{T}_{n_1n_2})L_4(m_x, m_y, n_0, n_3) \\
&\qquad + 977(\boldsymbol{T}_{m_ym_z} \cdot \boldsymbol{T}_{n_1n_2})L_4(m_x, m_z, n_0, n_3) + 212(\boldsymbol{T}_{m_ym_z} \cdot \boldsymbol{T}_{n_1n_3})L_4(m_x, m_x, n_0, n_2) \\
&\qquad + 424(\boldsymbol{T}_{m_ym_z} \cdot \boldsymbol{T}_{n_1n_3})L_4(m_x, m_y, n_0, n_2) - 977(\boldsymbol{T}_{m_ym_z} \cdot \boldsymbol{T}_{n_1n_3})L_4(m_x, m_z, n_0, n_2) \\
&\qquad + 424(\boldsymbol{T}_{m_ym_z} \cdot \boldsymbol{T}_{n_2n_3})L_4(m_x, m_x, n_0, n_1) + 848(\boldsymbol{T}_{m_ym_z} \cdot \boldsymbol{T}_{n_2n_3})L_4(m_x, m_y, n_0, n_1) \\
&\qquad - 1954(\boldsymbol{T}_{m_ym_z} \cdot \boldsymbol{T}_{n_2n_3})L_4(m_x, m_z, n_0, n_1)), \\
&\quad S_{mn} = v544320k02 \\
&\qquad (-393I_{m_xn_2}L_6(m_x, m_y, m_z, n_0, n_1, n_3) + 212I_{m_xn_2}L_6(m_y, m_y, m_z, n_0, n_1, n_3) \\
&\qquad - 80I_{m_xn_2}L_6(m_y, m_z, m_z, n_0, n_1, n_3) + 393I_{m_xn_3}L_6(m_x, m_y, m_z, n_0, n_1, n_2) \\
&\qquad - 212I_{m_xn_3}L_6(m_y, m_y, m_z, n_0, n_1, n_2) + 80I_{m_xn_3}L_6(m_y, m_z, m_z, n_0, n_1, n_2) \\
&\qquad + 292I_{m_yn_2}L_6(m_x, m_x, m_z, n_0, n_1, n_3) - 292I_{m_yn_2}L_6(m_x, m_z, m_z, n_0, n_1, n_3) \\
&\qquad - 292I_{m_yn_3}L_6(m_x, m_x, m_z, n_0, n_1, n_2) + 292I_{m_yn_3}L_6(m_x, m_z, m_z, n_0, n_1, n_2) \\
&\qquad + 80I_{m_zn_2}L_6(m_x, m_x, m_y, n_0, n_1, n_3) - 212I_{m_zn_2}L_6(m_x, m_y, m_y, n_0, n_1, n_3) \\
&\qquad + 393I_{m_zn_2}L_6(m_x, m_y, m_z, n_0, n_1, n_3) - 80I_{m_zn_3}L_6(m_x, m_x, m_y, n_0, n_1, n_2) \\
&\qquad + 212I_{m_zn_3}L_6(m_x, m_y, m_y, n_0, n_1, n_2) - 393I_{m_zn_3}L_6(m_x, m_y, m_z, n_0, n_1, n_2)).
\end{aligned}
$$

$< h_{3m}, l_{3n} >$

$R_{mn} = v3\_68040$

$(-1954(\boldsymbol{T}_{m_x m_y} \cdot \boldsymbol{T}_{n_0 n_1}) L_4(m_x, m_z, n_2, n_3) + 848(\boldsymbol{T}_{m_x m_y} \cdot \boldsymbol{T}_{n_0 n_1}) L_4(m_y, m_z, n_2, n_3)$
$+ 424(\boldsymbol{T}_{m_x m_y} \cdot \boldsymbol{T}_{n_0 n_1}) L_4(m_z, m_z, n_2, n_3) - 977(\boldsymbol{T}_{m_x m_y} \cdot \boldsymbol{T}_{n_0 n_2}) L_4(m_x, m_z, n_1, n_3)$
$+ 424(\boldsymbol{T}_{m_x m_y} \cdot \boldsymbol{T}_{n_0 n_2}) L_4(m_y, m_z, n_1, n_3) + 212(\boldsymbol{T}_{m_x m_y} \cdot \boldsymbol{T}_{n_0 n_2}) L_4(m_z, m_z, n_1, n_3)$
$- 977(\boldsymbol{T}_{m_x m_y} \cdot \boldsymbol{T}_{n_0 n_3}) L_4(m_x, m_z, n_1, n_2) + 424(\boldsymbol{T}_{m_x m_y} \cdot \boldsymbol{T}_{n_0 n_3}) L_4(m_y, m_z, n_1, n_2)$
$+ 212(\boldsymbol{T}_{m_x m_y} \cdot \boldsymbol{T}_{n_0 n_3}) L_4(m_z, m_z, n_1, n_2) + 977(\boldsymbol{T}_{m_x m_y} \cdot \boldsymbol{T}_{n_1 n_2}) L_4(m_x, m_z, n_0, n_3)$
$- 424(\boldsymbol{T}_{m_x m_y} \cdot \boldsymbol{T}_{n_1 n_2}) L_4(m_y, m_z, n_0, n_3) - 212(\boldsymbol{T}_{m_x m_y} \cdot \boldsymbol{T}_{n_1 n_2}) L_4(m_z, m_z, n_0, n_3)$
$+ 977(\boldsymbol{T}_{m_x m_y} \cdot \boldsymbol{T}_{n_1 n_3}) L_4(m_x, m_z, n_0, n_2) - 424(\boldsymbol{T}_{m_x m_y} \cdot \boldsymbol{T}_{n_1 n_3}) L_4(m_y, m_z, n_0, n_2)$
$- 212(\boldsymbol{T}_{m_x m_y} \cdot \boldsymbol{T}_{n_1 n_3}) L_4(m_z, m_z, n_0, n_2) - 1106(\boldsymbol{T}_{m_x m_z} \cdot \boldsymbol{T}_{n_0 n_1}) L_4(m_x, m_y, n_2, n_3)$
$+ 848(\boldsymbol{T}_{m_x m_z} \cdot \boldsymbol{T}_{n_0 n_1}) L_4(m_y, m_y, n_2, n_3) - 1106(\boldsymbol{T}_{m_x m_z} \cdot \boldsymbol{T}_{n_0 n_1}) L_4(m_y, m_z, n_2, n_3)$
$- 553(\boldsymbol{T}_{m_x m_z} \cdot \boldsymbol{T}_{n_0 n_2}) L_4(m_x, m_y, n_1, n_3) + 424(\boldsymbol{T}_{m_x m_z} \cdot \boldsymbol{T}_{n_0 n_2}) L_4(m_y, m_y, n_1, n_3)$
$- 553(\boldsymbol{T}_{m_x m_z} \cdot \boldsymbol{T}_{n_0 n_2}) L_4(m_y, m_z, n_1, n_3) - 553(\boldsymbol{T}_{m_x m_z} \cdot \boldsymbol{T}_{n_0 n_3}) L_4(m_x, m_y, n_1, n_2)$
$+ 424(\boldsymbol{T}_{m_x m_z} \cdot \boldsymbol{T}_{n_0 n_3}) L_4(m_y, m_y, n_1, n_2) - 553(\boldsymbol{T}_{m_x m_z} \cdot \boldsymbol{T}_{n_0 n_3}) L_4(m_y, m_z, n_1, n_2)$
$+ 553(\boldsymbol{T}_{m_x m_z} \cdot \boldsymbol{T}_{n_1 n_2}) L_4(m_x, m_y, n_0, n_3) - 424(\boldsymbol{T}_{m_x m_z} \cdot \boldsymbol{T}_{n_1 n_2}) L_4(m_y, m_y, n_0, n_3)$
$+ 553(\boldsymbol{T}_{m_x m_z} \cdot \boldsymbol{T}_{n_1 n_2}) L_4(m_y, m_z, n_0, n_3) + 553(\boldsymbol{T}_{m_x m_z} \cdot \boldsymbol{T}_{n_1 n_3}) L_4(m_x, m_y, n_0, n_2)$
$- 424(\boldsymbol{T}_{m_x m_z} \cdot \boldsymbol{T}_{n_1 n_3}) L_4(m_y, m_y, n_0, n_2) + 553(\boldsymbol{T}_{m_x m_z} \cdot \boldsymbol{T}_{n_1 n_3}) L_4(m_y, m_z, n_0, n_2)$
$+ 424(\boldsymbol{T}_{m_y m_z} \cdot \boldsymbol{T}_{n_0 n_1}) L_4(m_x, m_x, n_2, n_3) + 848(\boldsymbol{T}_{m_y m_z} \cdot \boldsymbol{T}_{n_0 n_1}) L_4(m_x, m_y, n_2, n_3)$
$- 1954(\boldsymbol{T}_{m_y m_z} \cdot \boldsymbol{T}_{n_0 n_1}) L_4(m_x, m_z, n_2, n_3) + 212(\boldsymbol{T}_{m_y m_z} \cdot \boldsymbol{T}_{n_0 n_2}) L_4(m_x, m_x, n_1, n_3)$
$+ 424(\boldsymbol{T}_{m_y m_z} \cdot \boldsymbol{T}_{n_0 n_2}) L_4(m_x, m_y, n_1, n_3) - 977(\boldsymbol{T}_{m_y m_z} \cdot \boldsymbol{T}_{n_0 n_2}) L_4(m_x, m_z, n_1, n_3)$
$+ 212(\boldsymbol{T}_{m_y m_z} \cdot \boldsymbol{T}_{n_0 n_3}) L_4(m_x, m_x, n_1, n_2) + 424(\boldsymbol{T}_{m_y m_z} \cdot \boldsymbol{T}_{n_0 n_3}) L_4(m_x, m_y, n_1, n_2)$
$- 977(\boldsymbol{T}_{m_y m_z} \cdot \boldsymbol{T}_{n_0 n_3}) L_4(m_x, m_z, n_1, n_2) - 212(\boldsymbol{T}_{m_y m_z} \cdot \boldsymbol{T}_{n_1 n_2}) L_4(m_x, m_x, n_0, n_3)$
$- 424(\boldsymbol{T}_{m_y m_z} \cdot \boldsymbol{T}_{n_1 n_2}) L_4(m_x, m_y, n_0, n_3) + 977(\boldsymbol{T}_{m_y m_z} \cdot \boldsymbol{T}_{n_1 n_2}) L_4(m_x, m_z, n_0, n_3)$
$- 212(\boldsymbol{T}_{m_y m_z} \cdot \boldsymbol{T}_{n_1 n_3}) L_4(m_x, m_x, n_0, n_2) - 424(\boldsymbol{T}_{m_y m_z} \cdot \boldsymbol{T}_{n_1 n_3}) L_4(m_x, m_y, n_0, n_2)$
$+ 977(\boldsymbol{T}_{m_y m_z} \cdot \boldsymbol{T}_{n_1 n_3}) L_4(m_x, m_z, n_0, n_2)),$

$S_{mn} = v544320k02$

$(-393 I_{m_x n_0} L_6(m_x, m_y, m_z, n_1, n_2, n_3) + 212 I_{m_x n_0} L_6(m_y, m_y, m_z, n_1, n_2, n_3)$
$- 80 I_{m_x n_0} L_6(m_y, m_z, m_z, n_1, n_2, n_3) + 393 I_{m_x n_1} L_6(m_x, m_y, m_z, n_0, n_2, n_3)$
$- 212 I_{m_x n_1} L_6(m_y, m_y, m_z, n_0, n_2, n_3) + 80 I_{m_x n_1} L_6(m_y, m_z, m_z, n_0, n_2, n_3)$
$+ 292 I_{m_y n_0} L_6(m_x, m_x, m_z, n_1, n_2, n_3) - 292 I_{m_y n_0} L_6(m_x, m_z, m_z, n_1, n_2, n_3)$
$- 292 I_{m_y n_1} L_6(m_x, m_x, m_z, n_0, n_2, n_3) + 292 I_{m_y n_1} L_6(m_x, m_z, m_z, n_0, n_2, n_3)$
$+ 80 I_{m_z n_0} L_6(m_x, m_x, m_y, n_1, n_2, n_3) - 212 I_{m_z n_0} L_6(m_x, m_y, m_y, n_1, n_2, n_3)$
$+ 393 I_{m_z n_0} L_6(m_x, m_y, m_z, n_1, n_2, n_3) - 80 I_{m_z n_1} L_6(m_x, m_x, m_y, n_0, n_2, n_3)$
$+ 212 I_{m_z n_1} L_6(m_x, m_y, m_y, n_0, n_2, n_3) - 393 I_{m_z n_1} L_6(m_x, m_y, m_z, n_0, n_2, n_3)).$

$< i_{3m}, i_{3n} >$

$R_{mn} = v3\_68040$

$(1849(\boldsymbol{T}_{m_xm_y} \cdot \boldsymbol{T}_{n_xn_y})L_4(m_x, m_z, n_x, n_z) + 21930(\boldsymbol{T}_{m_xm_y} \cdot \boldsymbol{T}_{n_xn_y})L_4(m_x, m_z, n_y, n_z)$
$- 9116(\boldsymbol{T}_{m_xm_y} \cdot \boldsymbol{T}_{n_xn_y})L_4(m_x, m_z, n_z, n_z) + 21930(\boldsymbol{T}_{m_xm_y} \cdot \boldsymbol{T}_{n_xn_y})L_4(m_y, m_z, n_x, n_z)$
$+ 260100(\boldsymbol{T}_{m_xm_y} \cdot \boldsymbol{T}_{n_xn_y})L_4(m_y, m_z, n_y, n_z) - 108120(\boldsymbol{T}_{m_xm_y} \cdot \boldsymbol{T}_{n_xn_y})L_4(m_y, m_z, n_z, n_z)$
$- 9116(\boldsymbol{T}_{m_xm_y} \cdot \boldsymbol{T}_{n_xn_y})L_4(m_z, m_z, n_x, n_z) - 108120(\boldsymbol{T}_{m_xm_y} \cdot \boldsymbol{T}_{n_xn_y})L_4(m_z, m_z, n_y, n_z)$
$+ 44944(\boldsymbol{T}_{m_xm_y} \cdot \boldsymbol{T}_{n_xn_y})L_4(m_z, m_z, n_z, n_z) + 20081(\boldsymbol{T}_{m_xm_y} \cdot \boldsymbol{T}_{n_xn_z})L_4(m_x, m_z, n_x, n_y)$
$- 20081(\boldsymbol{T}_{m_xm_y} \cdot \boldsymbol{T}_{n_xn_z})L_4(m_x, m_z, n_y, n_z) + 238170(\boldsymbol{T}_{m_xm_y} \cdot \boldsymbol{T}_{n_xn_z})L_4(m_y, m_z, n_x, n_y)$
$- 238170(\boldsymbol{T}_{m_xm_y} \cdot \boldsymbol{T}_{n_xn_z})L_4(m_y, m_z, n_y, n_z) - 99004(\boldsymbol{T}_{m_xm_y} \cdot \boldsymbol{T}_{n_xn_z})L_4(m_z, m_z, n_x, n_y)$
$+ 99004(\boldsymbol{T}_{m_xm_y} \cdot \boldsymbol{T}_{n_xn_z})L_4(m_z, m_z, n_y, n_z) + 9116(\boldsymbol{T}_{m_xm_y} \cdot \boldsymbol{T}_{n_yn_z})L_4(m_x, m_z, n_x, n_x)$
$- 21930(\boldsymbol{T}_{m_xm_y} \cdot \boldsymbol{T}_{n_yn_z})L_4(m_x, m_z, n_x, n_y) - 1849(\boldsymbol{T}_{m_xm_y} \cdot \boldsymbol{T}_{n_yn_z})L_4(m_x, m_z, n_x, n_z)$
$+ 108120(\boldsymbol{T}_{m_xm_y} \cdot \boldsymbol{T}_{n_yn_z})L_4(m_y, m_z, n_x, n_x) - 260100(\boldsymbol{T}_{m_xm_y} \cdot \boldsymbol{T}_{n_yn_z})L_4(m_y, m_z, n_x, n_y)$
$- 21930(\boldsymbol{T}_{m_xm_y} \cdot \boldsymbol{T}_{n_yn_z})L_4(m_y, m_z, n_x, n_z) - 44944(\boldsymbol{T}_{m_xm_y} \cdot \boldsymbol{T}_{n_yn_z})L_4(m_z, m_z, n_x, n_x)$
$+ 108120(\boldsymbol{T}_{m_xm_y} \cdot \boldsymbol{T}_{n_yn_z})L_4(m_z, m_z, n_x, n_y) + 9116(\boldsymbol{T}_{m_xm_y} \cdot \boldsymbol{T}_{n_yn_z})L_4(m_z, m_z, n_x, n_z)$
$+ 20081(\boldsymbol{T}_{m_xm_z} \cdot \boldsymbol{T}_{n_xn_y})L_4(m_x, m_y, n_x, n_z) + 238170(\boldsymbol{T}_{m_xm_z} \cdot \boldsymbol{T}_{n_xn_y})L_4(m_x, m_y, n_y, n_z)$
$- 99004(\boldsymbol{T}_{m_xm_z} \cdot \boldsymbol{T}_{n_xn_y})L_4(m_x, m_y, n_z, n_z) - 20081(\boldsymbol{T}_{m_xm_z} \cdot \boldsymbol{T}_{n_xn_y})L_4(m_y, m_z, n_x, n_z)$
$- 238170(\boldsymbol{T}_{m_xm_z} \cdot \boldsymbol{T}_{n_xn_y})L_4(m_y, m_z, n_y, n_z) + 99004(\boldsymbol{T}_{m_xm_z} \cdot \boldsymbol{T}_{n_xn_y})L_4(m_y, m_z, n_z, n_z)$
$+ 218089(\boldsymbol{T}_{m_xm_z} \cdot \boldsymbol{T}_{n_xn_z})L_4(m_x, m_y, n_x, n_y) - 218089(\boldsymbol{T}_{m_xm_z} \cdot \boldsymbol{T}_{n_xn_z})L_4(m_x, m_y, n_y, n_z)$
$- 218089(\boldsymbol{T}_{m_xm_z} \cdot \boldsymbol{T}_{n_xn_z})L_4(m_y, m_z, n_x, n_y) + 218089(\boldsymbol{T}_{m_xm_z} \cdot \boldsymbol{T}_{n_xn_z})L_4(m_y, m_z, n_y, n_z)$
$+ 99004(\boldsymbol{T}_{m_xm_z} \cdot \boldsymbol{T}_{n_yn_z})L_4(m_x, m_y, n_x, n_x) - 238170(\boldsymbol{T}_{m_xm_z} \cdot \boldsymbol{T}_{n_yn_z})L_4(m_x, m_y, n_x, n_y)$
$- 20081(\boldsymbol{T}_{m_xm_z} \cdot \boldsymbol{T}_{n_yn_z})L_4(m_x, m_y, n_x, n_z) - 99004(\boldsymbol{T}_{m_xm_z} \cdot \boldsymbol{T}_{n_yn_z})L_4(m_y, m_z, n_x, n_x)$
$+ 238170(\boldsymbol{T}_{m_xm_z} \cdot \boldsymbol{T}_{n_yn_z})L_4(m_y, m_z, n_x, n_y) + 20081(\boldsymbol{T}_{m_xm_z} \cdot \boldsymbol{T}_{n_yn_z})L_4(m_y, m_z, n_x, n_z)$
$+ 9116(\boldsymbol{T}_{m_ym_z} \cdot \boldsymbol{T}_{n_xn_y})L_4(m_x, m_x, n_x, n_z) + 108120(\boldsymbol{T}_{m_ym_z} \cdot \boldsymbol{T}_{n_xn_y})L_4(m_x, m_x, n_y, n_z)$
$- 44944(\boldsymbol{T}_{m_ym_z} \cdot \boldsymbol{T}_{n_xn_y})L_4(m_x, m_x, n_z, n_z) - 21930(\boldsymbol{T}_{m_ym_z} \cdot \boldsymbol{T}_{n_xn_y})L_4(m_x, m_y, n_x, n_z)$
$- 260100(\boldsymbol{T}_{m_ym_z} \cdot \boldsymbol{T}_{n_xn_y})L_4(m_x, m_y, n_y, n_z) + 108120(\boldsymbol{T}_{m_ym_z} \cdot \boldsymbol{T}_{n_xn_y})L_4(m_x, m_y, n_z, n_z)$
$- 1849(\boldsymbol{T}_{m_ym_z} \cdot \boldsymbol{T}_{n_xn_y})L_4(m_x, m_z, n_x, n_z) - 21930(\boldsymbol{T}_{m_ym_z} \cdot \boldsymbol{T}_{n_xn_y})L_4(m_x, m_z, n_y, n_z)$
$+ 9116(\boldsymbol{T}_{m_ym_z} \cdot \boldsymbol{T}_{n_xn_y})L_4(m_x, m_z, n_z, n_z) + 99004(\boldsymbol{T}_{m_ym_z} \cdot \boldsymbol{T}_{n_xn_z})L_4(m_x, m_x, n_x, n_y)$
$- 99004(\boldsymbol{T}_{m_ym_z} \cdot \boldsymbol{T}_{n_xn_z})L_4(m_x, m_x, n_y, n_z) - 238170(\boldsymbol{T}_{m_ym_z} \cdot \boldsymbol{T}_{n_xn_z})L_4(m_x, m_y, n_x, n_y)$
$+ 238170(\boldsymbol{T}_{m_ym_z} \cdot \boldsymbol{T}_{n_xn_z})L_4(m_x, m_y, n_y, n_z) - 20081(\boldsymbol{T}_{m_ym_z} \cdot \boldsymbol{T}_{n_xn_z})L_4(m_x, m_z, n_x, n_y)$
$+ 20081(\boldsymbol{T}_{m_ym_z} \cdot \boldsymbol{T}_{n_xn_z})L_4(m_x, m_z, n_y, n_z) + 44944(\boldsymbol{T}_{m_ym_z} \cdot \boldsymbol{T}_{n_yn_z})L_4(m_x, m_x, n_x, n_x)$
$- 108120(\boldsymbol{T}_{m_ym_z} \cdot \boldsymbol{T}_{n_yn_z})L_4(m_x, m_x, n_x, n_y) - 9116(\boldsymbol{T}_{m_ym_z} \cdot \boldsymbol{T}_{n_yn_z})L_4(m_x, m_x, n_x, n_z)$
$- 108120(\boldsymbol{T}_{m_ym_z} \cdot \boldsymbol{T}_{n_yn_z})L_4(m_x, m_y, n_x, n_x) + 260100(\boldsymbol{T}_{m_ym_z} \cdot \boldsymbol{T}_{n_yn_z})L_4(m_x, m_y, n_x, n_y)$
$+ 21930(\boldsymbol{T}_{m_ym_z} \cdot \boldsymbol{T}_{n_yn_z})L_4(m_x, m_y, n_x, n_z) - 9116(\boldsymbol{T}_{m_ym_z} \cdot \boldsymbol{T}_{n_yn_z})L_4(m_x, m_z, n_x, n_x)$
$+ 21930(\boldsymbol{T}_{m_ym_z} \cdot \boldsymbol{T}_{n_yn_z})L_4(m_x, m_z, n_x, n_y) + 1849(\boldsymbol{T}_{m_ym_z} \cdot \boldsymbol{T}_{n_yn_z})L_4(m_x, m_z, n_x, n_z)),$

$$
\begin{aligned}
S_{mn} =& v544320k02(\alpha+\beta+\gamma),\\
\alpha =& 17161I_{m_xn_x}L_6(m_x,m_y,m_z,n_x,n_y,n_z)+16244I_{m_xn_x}L_6(m_x,m_y,m_z,n_y,n_y,n_z)\\
&-22008I_{m_xn_x}L_6(m_x,m_y,m_z,n_y,n_z,n_z)+16244I_{m_xn_x}L_6(m_y,m_y,m_z,n_x,n_y,n_z)\\
&+15376I_{m_xn_x}L_6(m_y,m_y,m_z,n_y,n_y,n_z)-20832I_{m_xn_x}L_6(m_y,m_y,m_z,n_y,n_z,n_z)\\
&-22008I_{m_xn_x}L_6(m_y,m_z,m_z,n_x,n_y,n_z)-20832I_{m_xn_x}L_6(m_y,m_z,m_z,n_y,n_y,n_z)\\
&+28224I_{m_xn_x}L_6(m_y,m_z,m_z,n_y,n_z,n_z)+5764I_{m_xn_y}L_6(m_x,m_y,m_z,n_x,n_x,n_z)\\
&-34322I_{m_xn_y}L_6(m_x,m_y,m_z,n_x,n_y,n_z)+5764I_{m_xn_y}L_6(m_x,m_y,m_z,n_x,n_z,n_z)\\
&+5456I_{m_xn_y}L_6(m_y,m_y,m_z,n_x,n_x,n_z)-32488I_{m_xn_y}L_6(m_y,m_y,m_z,n_x,n_y,n_z)\\
&+5456I_{m_xn_y}L_6(m_y,m_y,m_z,n_x,n_z,n_z)-7392I_{m_xn_y}L_6(m_y,m_z,m_z,n_x,n_x,n_z)\\
&+44016I_{m_xn_y}L_6(m_y,m_z,m_z,n_x,n_y,n_z)-7392I_{m_xn_y}L_6(m_y,m_z,m_z,n_x,n_z,n_z)\\
&-22008I_{m_xn_z}L_6(m_x,m_y,m_z,n_x,n_x,n_y)+16244I_{m_xn_z}L_6(m_x,m_y,m_z,n_x,n_y,n_y)\\
&+17161I_{m_xn_z}L_6(m_x,m_y,m_z,n_x,n_y,n_z)-20832I_{m_xn_z}L_6(m_y,m_y,m_z,n_x,n_x,n_y)\\
&+15376I_{m_xn_z}L_6(m_y,m_y,m_z,n_x,n_y,n_y)+16244I_{m_xn_z}L_6(m_y,m_y,m_z,n_x,n_y,n_z)\\
&+28224I_{m_xn_z}L_6(m_y,m_z,m_z,n_x,n_x,n_y)-20832I_{m_xn_z}L_6(m_y,m_z,m_z,n_x,n_y,n_y)\\
&-22008I_{m_xn_z}L_6(m_y,m_z,m_z,n_x,n_y,n_z)+5764I_{m_yn_x}L_6(m_x,m_x,m_z,n_x,n_y,n_z)\\
&+5456I_{m_yn_x}L_6(m_x,m_x,m_z,n_y,n_y,n_z)-7392I_{m_yn_x}L_6(m_x,m_x,m_z,n_y,n_z,n_z)\\
&-34322I_{m_yn_x}L_6(m_x,m_y,m_z,n_x,n_y,n_z)-32488I_{m_yn_x}L_6(m_x,m_y,m_z,n_y,n_y,n_z),\\
\beta =& +44016I_{m_yn_x}L_6(m_x,m_y,m_z,n_y,n_z,n_z)+5764I_{m_yn_x}L_6(m_x,m_z,m_z,n_x,n_y,n_z)\\
&+5456I_{m_yn_x}L_6(m_x,m_z,m_z,n_y,n_y,n_z)-7392I_{m_yn_x}L_6(m_x,m_z,m_z,n_y,n_z,n_z)\\
&+1936I_{m_yn_y}L_6(m_x,m_x,m_z,n_x,n_x,n_z)-11528I_{m_yn_y}L_6(m_x,m_x,m_z,n_x,n_y,n_z)\\
&+1936I_{m_yn_y}L_6(m_x,m_x,m_z,n_x,n_z,n_z)-11528I_{m_yn_y}L_6(m_x,m_y,m_z,n_x,n_x,n_z)\\
&+68644I_{m_yn_y}L_6(m_x,m_y,m_z,n_x,n_y,n_z)-11528I_{m_yn_y}L_6(m_x,m_y,m_z,n_x,n_z,n_z)\\
&+1936I_{m_yn_y}L_6(m_x,m_z,m_z,n_x,n_x,n_z)-11528I_{m_yn_y}L_6(m_x,m_z,m_z,n_x,n_y,n_z)\\
&+1936I_{m_yn_y}L_6(m_x,m_z,m_z,n_x,n_z,n_z)-7392I_{m_yn_z}L_6(m_x,m_x,m_z,n_x,n_x,n_y)\\
&+5456I_{m_yn_z}L_6(m_x,m_x,m_z,n_x,n_y,n_y)+5764I_{m_yn_z}L_6(m_x,m_x,m_z,n_x,n_y,n_z)\\
&+44016I_{m_yn_z}L_6(m_x,m_y,m_z,n_x,n_x,n_y)-32488I_{m_yn_z}L_6(m_x,m_y,m_z,n_x,n_y,n_y)\\
&-34322I_{m_yn_z}L_6(m_x,m_y,m_z,n_x,n_y,n_z)-7392I_{m_yn_z}L_6(m_x,m_z,m_z,n_x,n_x,n_y)\\
&+5456I_{m_yn_z}L_6(m_x,m_z,m_z,n_x,n_y,n_y)+5764I_{m_yn_z}L_6(m_x,m_z,m_z,n_x,n_y,n_z)\\
&-22008I_{m_zn_x}L_6(m_x,m_x,m_y,n_x,n_y,n_z)-20832I_{m_zn_x}L_6(m_x,m_x,m_y,n_y,n_y,n_z)\\
&+28224I_{m_zn_x}L_6(m_x,m_x,m_y,n_y,n_z,n_z)+16244I_{m_zn_x}L_6(m_x,m_y,m_y,n_x,n_y,n_z)\\
&+15376I_{m_zn_x}L_6(m_x,m_y,m_y,n_y,n_y,n_z)-20832I_{m_zn_x}L_6(m_x,m_y,m_y,n_y,n_z,n_z)\\
&+17161I_{m_zn_x}L_6(m_x,m_y,m_z,n_x,n_y,n_z)+16244I_{m_zn_x}L_6(m_x,m_y,m_z,n_y,n_y,n_z)\\
&-22008I_{m_zn_x}L_6(m_x,m_y,m_z,n_y,n_z,n_z)-7392I_{m_zn_y}L_6(m_x,m_x,m_y,n_x,n_x,n_z)\\
&+44016I_{m_zn_y}L_6(m_x,m_x,m_y,n_x,n_y,n_z)-7392I_{m_zn_y}L_6(m_x,m_x,m_y,n_x,n_z,n_z)\\
&+5456I_{m_zn_y}L_6(m_x,m_y,m_y,n_x,n_x,n_z)-32488I_{m_zn_y}L_6(m_x,m_y,m_y,n_x,n_y,n_z),
\end{aligned}
$$

$$
\begin{aligned}
\gamma = &+ 5456 I_{m_z n_y} L_6(m_x, m_y, m_y, n_x, n_z, n_z) + 5764 I_{m_z n_y} L_6(m_x, m_y, m_z, n_x, n_x, n_z) \\
&- 34322 I_{m_z n_y} L_6(m_x, m_y, m_z, n_x, n_y, n_z) + 5764 I_{m_z n_y} L_6(m_x, m_y, m_z, n_x, n_z, n_z) \\
&+ 28224 I_{m_z n_z} L_6(m_x, m_x, m_y, n_x, n_x, n_y) - 20832 I_{m_z n_z} L_6(m_x, m_x, m_y, n_x, n_y, n_y) \\
&- 22008 I_{m_z n_z} L_6(m_x, m_x, m_y, n_x, n_y, n_z) - 20832 I_{m_z n_z} L_6(m_x, m_y, m_y, n_x, n_x, n_y) \\
&+ 15376 I_{m_z n_z} L_6(m_x, m_y, m_y, n_x, n_y, n_y) + 16244 I_{m_z n_z} L_6(m_x, m_y, m_y, n_x, n_y, n_z) \\
&- 22008 I_{m_z n_z} L_6(m_x, m_y, m_z, n_x, n_x, n_y) + 16244 I_{m_z n_z} L_6(m_x, m_y, m_z, n_x, n_y, n_y) \\
&+ 17161 I_{m_z n_z} L_6(m_x, m_y, m_z, n_x, n_y, n_z).
\end{aligned}
$$

$< i_{3m}, j_{3n} >$

$R_{mn} = v3\_68040$

$(-86(\boldsymbol{T}_{m_xm_y} \cdot \boldsymbol{T}_{n_0n_2})L_4(m_x, m_z, n_1, n_3) - 1020(\boldsymbol{T}_{m_xm_y} \cdot \boldsymbol{T}_{n_0n_2})L_4(m_y, m_z, n_1, n_3)$
$+ 424(\boldsymbol{T}_{m_xm_y} \cdot \boldsymbol{T}_{n_0n_2})L_4(m_z, m_z, n_1, n_3) - 86(\boldsymbol{T}_{m_xm_y} \cdot \boldsymbol{T}_{n_0n_3})L_4(m_x, m_z, n_1, n_2)$
$- 1020(\boldsymbol{T}_{m_xm_y} \cdot \boldsymbol{T}_{n_0n_3})L_4(m_y, m_z, n_1, n_2) + 424(\boldsymbol{T}_{m_xm_y} \cdot \boldsymbol{T}_{n_0n_3})L_4(m_z, m_z, n_1, n_2)$
$- 86(\boldsymbol{T}_{m_xm_y} \cdot \boldsymbol{T}_{n_1n_2})L_4(m_x, m_z, n_0, n_3) - 1020(\boldsymbol{T}_{m_xm_y} \cdot \boldsymbol{T}_{n_1n_2})L_4(m_y, m_z, n_0, n_3)$
$+ 424(\boldsymbol{T}_{m_xm_y} \cdot \boldsymbol{T}_{n_1n_2})L_4(m_z, m_z, n_0, n_3) - 86(\boldsymbol{T}_{m_xm_y} \cdot \boldsymbol{T}_{n_1n_3})L_4(m_x, m_z, n_0, n_2)$
$- 1020(\boldsymbol{T}_{m_xm_y} \cdot \boldsymbol{T}_{n_1n_3})L_4(m_y, m_z, n_0, n_2) + 424(\boldsymbol{T}_{m_xm_y} \cdot \boldsymbol{T}_{n_1n_3})L_4(m_z, m_z, n_0, n_2)$
$- 934(\boldsymbol{T}_{m_xm_z} \cdot \boldsymbol{T}_{n_0n_2})L_4(m_x, m_y, n_1, n_3) + 934(\boldsymbol{T}_{m_xm_z} \cdot \boldsymbol{T}_{n_0n_2})L_4(m_y, m_z, n_1, n_3)$
$- 934(\boldsymbol{T}_{m_xm_z} \cdot \boldsymbol{T}_{n_0n_3})L_4(m_x, m_y, n_1, n_2) + 934(\boldsymbol{T}_{m_xm_z} \cdot \boldsymbol{T}_{n_0n_3})L_4(m_y, m_z, n_1, n_2)$
$- 934(\boldsymbol{T}_{m_xm_z} \cdot \boldsymbol{T}_{n_1n_2})L_4(m_x, m_y, n_0, n_3) + 934(\boldsymbol{T}_{m_xm_z} \cdot \boldsymbol{T}_{n_1n_2})L_4(m_y, m_z, n_0, n_3)$
$- 934(\boldsymbol{T}_{m_xm_z} \cdot \boldsymbol{T}_{n_1n_3})L_4(m_x, m_y, n_0, n_2) + 934(\boldsymbol{T}_{m_xm_z} \cdot \boldsymbol{T}_{n_1n_3})L_4(m_y, m_z, n_0, n_2)$
$- 424(\boldsymbol{T}_{m_ym_z} \cdot \boldsymbol{T}_{n_0n_2})L_4(m_x, m_x, n_1, n_3) + 1020(\boldsymbol{T}_{m_ym_z} \cdot \boldsymbol{T}_{n_0n_2})L_4(m_x, m_y, n_1, n_3)$
$+ 86(\boldsymbol{T}_{m_ym_z} \cdot \boldsymbol{T}_{n_0n_2})L_4(m_x, m_z, n_1, n_3) - 424(\boldsymbol{T}_{m_ym_z} \cdot \boldsymbol{T}_{n_0n_3})L_4(m_x, m_x, n_1, n_2)$
$+ 1020(\boldsymbol{T}_{m_ym_z} \cdot \boldsymbol{T}_{n_0n_3})L_4(m_x, m_y, n_1, n_2) + 86(\boldsymbol{T}_{m_ym_z} \cdot \boldsymbol{T}_{n_0n_3})L_4(m_x, m_z, n_1, n_2)$
$- 424(\boldsymbol{T}_{m_ym_z} \cdot \boldsymbol{T}_{n_1n_2})L_4(m_x, m_x, n_0, n_3) + 1020(\boldsymbol{T}_{m_ym_z} \cdot \boldsymbol{T}_{n_1n_2})L_4(m_x, m_y, n_0, n_3)$
$+ 86(\boldsymbol{T}_{m_ym_z} \cdot \boldsymbol{T}_{n_1n_2})L_4(m_x, m_z, n_0, n_3) - 424(\boldsymbol{T}_{m_ym_z} \cdot \boldsymbol{T}_{n_1n_3})L_4(m_x, m_x, n_0, n_2)$
$+ 1020(\boldsymbol{T}_{m_ym_z} \cdot \boldsymbol{T}_{n_1n_3})L_4(m_x, m_y, n_0, n_2) + 86(\boldsymbol{T}_{m_ym_z} \cdot \boldsymbol{T}_{n_1n_3})L_4(m_x, m_z, n_0, n_2)),$

$S_{mn} = v544320k02$

$(-131I_{m_xn_0}L_6(m_x, m_y, m_z, n_1, n_2, n_3) - 124I_{m_xn_0}L_6(m_y, m_y, m_z, n_1, n_2, n_3)$
$+ 168I_{m_xn_0}L_6(m_y, m_z, m_z, n_1, n_2, n_3) - 131I_{m_xn_1}L_6(m_x, m_y, m_z, n_0, n_2, n_3)$
$- 124I_{m_xn_1}L_6(m_y, m_y, m_z, n_0, n_2, n_3) + 168I_{m_xn_1}L_6(m_y, m_z, m_z, n_0, n_2, n_3)$
$+ 131I_{m_xn_2}L_6(m_x, m_y, m_z, n_0, n_1, n_3) + 124I_{m_xn_2}L_6(m_y, m_y, m_z, n_0, n_1, n_3)$
$- 168I_{m_xn_2}L_6(m_y, m_z, m_z, n_0, n_1, n_3) + 131I_{m_xn_3}L_6(m_x, m_y, m_z, n_0, n_1, n_2)$
$+ 124I_{m_xn_3}L_6(m_y, m_y, m_z, n_0, n_1, n_2) - 168I_{m_xn_3}L_6(m_y, m_z, m_z, n_0, n_1, n_2)$
$- 44I_{m_yn_0}L_6(m_x, m_x, m_z, n_1, n_2, n_3) + 262I_{m_yn_0}L_6(m_x, m_y, m_z, n_1, n_2, n_3)$
$- 44I_{m_yn_0}L_6(m_x, m_z, m_z, n_1, n_2, n_3) - 44I_{m_yn_1}L_6(m_x, m_x, m_z, n_0, n_2, n_3)$
$+ 262I_{m_yn_1}L_6(m_x, m_y, m_z, n_0, n_2, n_3) - 44I_{m_yn_1}L_6(m_x, m_z, m_z, n_0, n_2, n_3)$
$+ 44I_{m_yn_2}L_6(m_x, m_x, m_z, n_0, n_1, n_3) - 262I_{m_yn_2}L_6(m_x, m_y, m_z, n_0, n_1, n_3)$
$+ 44I_{m_yn_2}L_6(m_x, m_z, m_z, n_0, n_1, n_3) + 44I_{m_yn_3}L_6(m_x, m_x, m_z, n_0, n_1, n_2)$
$- 262I_{m_yn_3}L_6(m_x, m_y, m_z, n_0, n_1, n_2) + 44I_{m_yn_3}L_6(m_x, m_z, m_z, n_0, n_1, n_2)$
$+ 168I_{m_zn_0}L_6(m_x, m_x, m_y, n_1, n_2, n_3) - 124I_{m_zn_0}L_6(m_x, m_y, m_y, n_1, n_2, n_3)$
$- 131I_{m_zn_0}L_6(m_x, m_y, m_z, n_1, n_2, n_3) + 168I_{m_zn_1}L_6(m_x, m_x, m_y, n_0, n_2, n_3)$
$- 124I_{m_zn_1}L_6(m_x, m_y, m_y, n_0, n_2, n_3) - 131I_{m_zn_1}L_6(m_x, m_y, m_z, n_0, n_2, n_3)$
$- 168I_{m_zn_2}L_6(m_x, m_x, m_y, n_0, n_1, n_3) + 124I_{m_zn_2}L_6(m_x, m_y, m_y, n_0, n_1, n_3)$
$+ 131I_{m_zn_2}L_6(m_x, m_y, m_z, n_0, n_1, n_3) - 168I_{m_zn_3}L_6(m_x, m_x, m_y, n_0, n_1, n_2)$
$+ 124I_{m_zn_3}L_6(m_x, m_y, m_y, n_0, n_1, n_2) + 131I_{m_zn_3}L_6(m_x, m_y, m_z, n_0, n_1, n_2)).$

$$
\begin{aligned}
&< i_{3m}, k_{3n} > \\
&\quad R_{mn} = v3\_68040 \\
&\qquad (43(\boldsymbol{T}_{m_x m_y} \cdot \boldsymbol{T}_{n_0 n_2}) L_4(m_x, m_z, n_1, n_3) + 510(\boldsymbol{T}_{m_x m_y} \cdot \boldsymbol{T}_{n_0 n_2}) L_4(m_y, m_z, n_1, n_3) \\
&\qquad - 212(\boldsymbol{T}_{m_x m_y} \cdot \boldsymbol{T}_{n_0 n_2}) L_4(m_z, m_z, n_1, n_3) - 43(\boldsymbol{T}_{m_x m_y} \cdot \boldsymbol{T}_{n_0 n_3}) L_4(m_x, m_z, n_1, n_2) \\
&\qquad - 510(\boldsymbol{T}_{m_x m_y} \cdot \boldsymbol{T}_{n_0 n_3}) L_4(m_y, m_z, n_1, n_2) + 212(\boldsymbol{T}_{m_x m_y} \cdot \boldsymbol{T}_{n_0 n_3}) L_4(m_z, m_z, n_1, n_2) \\
&\qquad + 43(\boldsymbol{T}_{m_x m_y} \cdot \boldsymbol{T}_{n_1 n_2}) L_4(m_x, m_z, n_0, n_3) + 510(\boldsymbol{T}_{m_x m_y} \cdot \boldsymbol{T}_{n_1 n_2}) L_4(m_y, m_z, n_0, n_3) \\
&\qquad - 212(\boldsymbol{T}_{m_x m_y} \cdot \boldsymbol{T}_{n_1 n_2}) L_4(m_z, m_z, n_0, n_3) - 43(\boldsymbol{T}_{m_x m_y} \cdot \boldsymbol{T}_{n_1 n_3}) L_4(m_x, m_z, n_0, n_2) \\
&\qquad - 510(\boldsymbol{T}_{m_x m_y} \cdot \boldsymbol{T}_{n_1 n_3}) L_4(m_y, m_z, n_0, n_2) + 212(\boldsymbol{T}_{m_x m_y} \cdot \boldsymbol{T}_{n_1 n_3}) L_4(m_z, m_z, n_0, n_2) \\
&\qquad - 86(\boldsymbol{T}_{m_x m_y} \cdot \boldsymbol{T}_{n_2 n_3}) L_4(m_x, m_z, n_0, n_1) - 1020(\boldsymbol{T}_{m_x m_y} \cdot \boldsymbol{T}_{n_2 n_3}) L_4(m_y, m_z, n_0, n_1) \\
&\qquad + 424(\boldsymbol{T}_{m_x m_y} \cdot \boldsymbol{T}_{n_2 n_3}) L_4(m_z, m_z, n_0, n_1) + 467(\boldsymbol{T}_{m_x m_z} \cdot \boldsymbol{T}_{n_0 n_2}) L_4(m_x, m_y, n_1, n_3) \\
&\qquad - 467(\boldsymbol{T}_{m_x m_z} \cdot \boldsymbol{T}_{n_0 n_2}) L_4(m_y, m_z, n_1, n_3) - 467(\boldsymbol{T}_{m_x m_z} \cdot \boldsymbol{T}_{n_0 n_3}) L_4(m_x, m_y, n_1, n_2) \\
&\qquad + 467(\boldsymbol{T}_{m_x m_z} \cdot \boldsymbol{T}_{n_0 n_3}) L_4(m_y, m_z, n_1, n_2) + 467(\boldsymbol{T}_{m_x m_z} \cdot \boldsymbol{T}_{n_1 n_2}) L_4(m_x, m_y, n_0, n_3) \\
&\qquad - 467(\boldsymbol{T}_{m_x m_z} \cdot \boldsymbol{T}_{n_1 n_2}) L_4(m_y, m_z, n_0, n_3) - 467(\boldsymbol{T}_{m_x m_z} \cdot \boldsymbol{T}_{n_1 n_3}) L_4(m_x, m_y, n_0, n_2) \\
&\qquad + 467(\boldsymbol{T}_{m_x m_z} \cdot \boldsymbol{T}_{n_1 n_3}) L_4(m_y, m_z, n_0, n_2) - 934(\boldsymbol{T}_{m_x m_z} \cdot \boldsymbol{T}_{n_2 n_3}) L_4(m_x, m_y, n_0, n_1) \\
&\qquad + 934(\boldsymbol{T}_{m_x m_z} \cdot \boldsymbol{T}_{n_2 n_3}) L_4(m_y, m_z, n_0, n_1) + 212(\boldsymbol{T}_{m_y m_z} \cdot \boldsymbol{T}_{n_0 n_2}) L_4(m_x, m_x, n_1, n_3) \\
&\qquad - 510(\boldsymbol{T}_{m_y m_z} \cdot \boldsymbol{T}_{n_0 n_2}) L_4(m_x, m_y, n_1, n_3) - 43(\boldsymbol{T}_{m_y m_z} \cdot \boldsymbol{T}_{n_0 n_2}) L_4(m_x, m_z, n_1, n_3) \\
&\qquad - 212(\boldsymbol{T}_{m_y m_z} \cdot \boldsymbol{T}_{n_0 n_3}) L_4(m_x, m_x, n_1, n_2) + 510(\boldsymbol{T}_{m_y m_z} \cdot \boldsymbol{T}_{n_0 n_3}) L_4(m_x, m_y, n_1, n_2) \\
&\qquad + 43(\boldsymbol{T}_{m_y m_z} \cdot \boldsymbol{T}_{n_0 n_3}) L_4(m_x, m_z, n_1, n_2) + 212(\boldsymbol{T}_{m_y m_z} \cdot \boldsymbol{T}_{n_1 n_2}) L_4(m_x, m_x, n_0, n_3) \\
&\qquad - 510(\boldsymbol{T}_{m_y m_z} \cdot \boldsymbol{T}_{n_1 n_2}) L_4(m_x, m_y, n_0, n_3) - 43(\boldsymbol{T}_{m_y m_z} \cdot \boldsymbol{T}_{n_1 n_2}) L_4(m_x, m_z, n_0, n_3) \\
&\qquad - 212(\boldsymbol{T}_{m_y m_z} \cdot \boldsymbol{T}_{n_1 n_3}) L_4(m_x, m_x, n_0, n_2) + 510(\boldsymbol{T}_{m_y m_z} \cdot \boldsymbol{T}_{n_1 n_3}) L_4(m_x, m_y, n_0, n_2) \\
&\qquad + 43(\boldsymbol{T}_{m_y m_z} \cdot \boldsymbol{T}_{n_1 n_3}) L_4(m_x, m_z, n_0, n_2) - 424(\boldsymbol{T}_{m_y m_z} \cdot \boldsymbol{T}_{n_2 n_3}) L_4(m_x, m_x, n_0, n_1) \\
&\qquad + 1020(\boldsymbol{T}_{m_y m_z} \cdot \boldsymbol{T}_{n_2 n_3}) L_4(m_x, m_y, n_0, n_1) + 86(\boldsymbol{T}_{m_y m_z} \cdot \boldsymbol{T}_{n_2 n_3}) L_4(m_x, m_z, n_0, n_1)), \\
&\quad S_{mn} = v544320k02 \\
&\qquad (-131 I_{m_x n_2} L_6(m_x, m_y, m_z, n_0, n_1, n_3) - 124 I_{m_x n_2} L_6(m_y, m_y, m_z, n_0, n_1, n_3) \\
&\qquad + 168 I_{m_x n_2} L_6(m_y, m_z, m_z, n_0, n_1, n_3) + 131 I_{m_x n_3} L_6(m_x, m_y, m_z, n_0, n_1, n_2) \\
&\qquad + 124 I_{m_x n_3} L_6(m_y, m_y, m_z, n_0, n_1, n_2) - 168 I_{m_x n_3} L_6(m_y, m_z, m_z, n_0, n_1, n_2) \\
&\qquad - 44 I_{m_y n_2} L_6(m_x, m_x, m_z, n_0, n_1, n_3) + 262 I_{m_y n_2} L_6(m_x, m_y, m_z, n_0, n_1, n_3) \\
&\qquad - 44 I_{m_y n_2} L_6(m_x, m_z, m_z, n_0, n_1, n_3) + 44 I_{m_y n_3} L_6(m_x, m_x, m_z, n_0, n_1, n_2) \\
&\qquad - 262 I_{m_y n_3} L_6(m_x, m_y, m_z, n_0, n_1, n_2) + 44 I_{m_y n_3} L_6(m_x, m_z, m_z, n_0, n_1, n_2) \\
&\qquad + 168 I_{m_z n_2} L_6(m_x, m_x, m_y, n_0, n_1, n_3) - 124 I_{m_z n_2} L_6(m_x, m_y, m_y, n_0, n_1, n_3) \\
&\qquad - 131 I_{m_z n_2} L_6(m_x, m_y, m_z, n_0, n_1, n_3) - 168 I_{m_z n_3} L_6(m_x, m_x, m_y, n_0, n_1, n_2) \\
&\qquad + 124 I_{m_z n_3} L_6(m_x, m_y, m_y, n_0, n_1, n_2) + 131 I_{m_z n_3} L_6(m_x, m_y, m_z, n_0, n_1, n_2)).
\end{aligned}
$$

$< i_{3m}, l_{3n} >$

$$
\begin{aligned}
R_{mn} =& v3\_68040 \\
& (-86(\boldsymbol{T}_{m_x m_y} \cdot \boldsymbol{T}_{n_0 n_1}) L_4(m_x, m_z, n_2, n_3) - 1020(\boldsymbol{T}_{m_x m_y} \cdot \boldsymbol{T}_{n_0 n_1}) L_4(m_y, m_z, n_2, n_3) \\
& + 424(\boldsymbol{T}_{m_x m_y} \cdot \boldsymbol{T}_{n_0 n_1}) L_4(m_z, m_z, n_2, n_3) - 43(\boldsymbol{T}_{m_x m_y} \cdot \boldsymbol{T}_{n_0 n_2}) L_4(m_x, m_z, n_1, n_3) \\
& - 510(\boldsymbol{T}_{m_x m_y} \cdot \boldsymbol{T}_{n_0 n_2}) L_4(m_y, m_z, n_1, n_3) + 212(\boldsymbol{T}_{m_x m_y} \cdot \boldsymbol{T}_{n_0 n_2}) L_4(m_z, m_z, n_1, n_3) \\
& - 43(\boldsymbol{T}_{m_x m_y} \cdot \boldsymbol{T}_{n_0 n_3}) L_4(m_x, m_z, n_1, n_2) - 510(\boldsymbol{T}_{m_x m_y} \cdot \boldsymbol{T}_{n_0 n_3}) L_4(m_y, m_z, n_1, n_2) \\
& + 212(\boldsymbol{T}_{m_x m_y} \cdot \boldsymbol{T}_{n_0 n_3}) L_4(m_z, m_z, n_1, n_2) + 43(\boldsymbol{T}_{m_x m_y} \cdot \boldsymbol{T}_{n_1 n_2}) L_4(m_x, m_z, n_0, n_3) \\
& + 510(\boldsymbol{T}_{m_x m_y} \cdot \boldsymbol{T}_{n_1 n_2}) L_4(m_y, m_z, n_0, n_3) - 212(\boldsymbol{T}_{m_x m_y} \cdot \boldsymbol{T}_{n_1 n_2}) L_4(m_z, m_z, n_0, n_3) \\
& + 43(\boldsymbol{T}_{m_x m_y} \cdot \boldsymbol{T}_{n_1 n_3}) L_4(m_x, m_z, n_0, n_2) + 510(\boldsymbol{T}_{m_x m_y} \cdot \boldsymbol{T}_{n_1 n_3}) L_4(m_y, m_z, n_0, n_2) \\
& - 212(\boldsymbol{T}_{m_x m_y} \cdot \boldsymbol{T}_{n_1 n_3}) L_4(m_z, m_z, n_0, n_2) - 934(\boldsymbol{T}_{m_x m_z} \cdot \boldsymbol{T}_{n_0 n_1}) L_4(m_x, m_y, n_2, n_3) \\
& + 934(\boldsymbol{T}_{m_x m_z} \cdot \boldsymbol{T}_{n_0 n_1}) L_4(m_y, m_z, n_2, n_3) - 467(\boldsymbol{T}_{m_x m_z} \cdot \boldsymbol{T}_{n_0 n_2}) L_4(m_x, m_y, n_1, n_3) \\
& + 467(\boldsymbol{T}_{m_x m_z} \cdot \boldsymbol{T}_{n_0 n_2}) L_4(m_y, m_z, n_1, n_3) - 467(\boldsymbol{T}_{m_x m_z} \cdot \boldsymbol{T}_{n_0 n_3}) L_4(m_x, m_y, n_1, n_2) \\
& + 467(\boldsymbol{T}_{m_x m_z} \cdot \boldsymbol{T}_{n_0 n_3}) L_4(m_y, m_z, n_1, n_2) + 467(\boldsymbol{T}_{m_x m_z} \cdot \boldsymbol{T}_{n_1 n_2}) L_4(m_x, m_y, n_0, n_3) \\
& - 467(\boldsymbol{T}_{m_x m_z} \cdot \boldsymbol{T}_{n_1 n_2}) L_4(m_y, m_z, n_0, n_3) + 467(\boldsymbol{T}_{m_x m_z} \cdot \boldsymbol{T}_{n_1 n_3}) L_4(m_x, m_y, n_0, n_2) \\
& - 467(\boldsymbol{T}_{m_x m_z} \cdot \boldsymbol{T}_{n_1 n_3}) L_4(m_y, m_z, n_0, n_2) - 424(\boldsymbol{T}_{m_y m_z} \cdot \boldsymbol{T}_{n_0 n_1}) L_4(m_x, m_x, n_2, n_3) \\
& + 1020(\boldsymbol{T}_{m_y m_z} \cdot \boldsymbol{T}_{n_0 n_1}) L_4(m_x, m_y, n_2, n_3) + 86(\boldsymbol{T}_{m_y m_z} \cdot \boldsymbol{T}_{n_0 n_1}) L_4(m_x, m_z, n_2, n_3) \\
& - 212(\boldsymbol{T}_{m_y m_z} \cdot \boldsymbol{T}_{n_0 n_2}) L_4(m_x, m_x, n_1, n_3) + 510(\boldsymbol{T}_{m_y m_z} \cdot \boldsymbol{T}_{n_0 n_2}) L_4(m_x, m_y, n_1, n_3) \\
& + 43(\boldsymbol{T}_{m_y m_z} \cdot \boldsymbol{T}_{n_0 n_2}) L_4(m_x, m_z, n_1, n_3) - 212(\boldsymbol{T}_{m_y m_z} \cdot \boldsymbol{T}_{n_0 n_3}) L_4(m_x, m_x, n_1, n_2) \\
& + 510(\boldsymbol{T}_{m_y m_z} \cdot \boldsymbol{T}_{n_0 n_3}) L_4(m_x, m_y, n_1, n_2) + 43(\boldsymbol{T}_{m_y m_z} \cdot \boldsymbol{T}_{n_0 n_3}) L_4(m_x, m_z, n_1, n_2) \\
& + 212(\boldsymbol{T}_{m_y m_z} \cdot \boldsymbol{T}_{n_1 n_2}) L_4(m_x, m_x, n_0, n_3) - 510(\boldsymbol{T}_{m_y m_z} \cdot \boldsymbol{T}_{n_1 n_2}) L_4(m_x, m_y, n_0, n_3) \\
& - 43(\boldsymbol{T}_{m_y m_z} \cdot \boldsymbol{T}_{n_1 n_2}) L_4(m_x, m_z, n_0, n_3) + 212(\boldsymbol{T}_{m_y m_z} \cdot \boldsymbol{T}_{n_1 n_3}) L_4(m_x, m_x, n_0, n_2) \\
& - 510(\boldsymbol{T}_{m_y m_z} \cdot \boldsymbol{T}_{n_1 n_3}) L_4(m_x, m_y, n_0, n_2) - 43(\boldsymbol{T}_{m_y m_z} \cdot \boldsymbol{T}_{n_1 n_3}) L_4(m_x, m_z, n_0, n_2)), \\
S_{mn} =& v544320k02 \\
& (-131 I_{m_x n_0} L_6(m_x, m_y, m_z, n_1, n_2, n_3) - 124 I_{m_x n_0} L_6(m_y, m_y, m_z, n_1, n_2, n_3) \\
& + 168 I_{m_x n_0} L_6(m_y, m_z, m_z, n_1, n_2, n_3) + 131 I_{m_x n_1} L_6(m_x, m_y, m_z, n_0, n_2, n_3) \\
& + 124 I_{m_x n_1} L_6(m_y, m_y, m_z, n_0, n_2, n_3) - 168 I_{m_x n_1} L_6(m_y, m_z, m_z, n_0, n_2, n_3) \\
& - 44 I_{m_y n_0} L_6(m_x, m_x, m_z, n_1, n_2, n_3) + 262 I_{m_y n_0} L_6(m_x, m_y, m_z, n_1, n_2, n_3) \\
& - 44 I_{m_y n_0} L_6(m_x, m_z, m_z, n_1, n_2, n_3) + 44 I_{m_y n_1} L_6(m_x, m_x, m_z, n_0, n_2, n_3) \\
& - 262 I_{m_y n_1} L_6(m_x, m_y, m_z, n_0, n_2, n_3) + 44 I_{m_y n_1} L_6(m_x, m_z, m_z, n_0, n_2, n_3) \\
& + 168 I_{m_z n_0} L_6(m_x, m_x, m_y, n_1, n_2, n_3) - 124 I_{m_z n_0} L_6(m_x, m_y, m_y, n_1, n_2, n_3) \\
& - 131 I_{m_z n_0} L_6(m_x, m_y, m_z, n_1, n_2, n_3) - 168 I_{m_z n_1} L_6(m_x, m_x, m_y, n_0, n_2, n_3) \\
& + 124 I_{m_z n_1} L_6(m_x, m_y, m_y, n_0, n_2, n_3) + 131 I_{m_z n_1} L_6(m_x, m_y, m_z, n_0, n_2, n_3)).
\end{aligned}
$$

$< j_{3m}, j_{3n} >$

$$
\begin{aligned}
R_{mn} =& v3\_68040 \\
& (4(\boldsymbol{T}_{m_0m_2} \cdot \boldsymbol{T}_{n_0n_2})L_4(m_1, m_3, n_1, n_3) + 4(\boldsymbol{T}_{m_0m_2} \cdot \boldsymbol{T}_{n_0n_3})L_4(m_1, m_3, n_1, n_2) \\
& + 4(\boldsymbol{T}_{m_0m_2} \cdot \boldsymbol{T}_{n_1n_2})L_4(m_1, m_3, n_0, n_3) + 4(\boldsymbol{T}_{m_0m_2} \cdot \boldsymbol{T}_{n_1n_3})L_4(m_1, m_3, n_0, n_2) \\
& + 4(\boldsymbol{T}_{m_0m_3} \cdot \boldsymbol{T}_{n_0n_2})L_4(m_1, m_2, n_1, n_3) + 4(\boldsymbol{T}_{m_0m_3} \cdot \boldsymbol{T}_{n_0n_3})L_4(m_1, m_2, n_1, n_2) \\
& + 4(\boldsymbol{T}_{m_0m_3} \cdot \boldsymbol{T}_{n_1n_2})L_4(m_1, m_2, n_0, n_3) + 4(\boldsymbol{T}_{m_0m_3} \cdot \boldsymbol{T}_{n_1n_3})L_4(m_1, m_2, n_0, n_2) \\
& + 4(\boldsymbol{T}_{m_1m_2} \cdot \boldsymbol{T}_{n_0n_2})L_4(m_0, m_3, n_1, n_3) + 4(\boldsymbol{T}_{m_1m_2} \cdot \boldsymbol{T}_{n_0n_3})L_4(m_0, m_3, n_1, n_2) \\
& + 4(\boldsymbol{T}_{m_1m_2} \cdot \boldsymbol{T}_{n_1n_2})L_4(m_0, m_3, n_0, n_3) + 4(\boldsymbol{T}_{m_1m_2} \cdot \boldsymbol{T}_{n_1n_3})L_4(m_0, m_3, n_0, n_2) \\
& + 4(\boldsymbol{T}_{m_1m_3} \cdot \boldsymbol{T}_{n_0n_2})L_4(m_0, m_2, n_1, n_3) + 4(\boldsymbol{T}_{m_1m_3} \cdot \boldsymbol{T}_{n_0n_3})L_4(m_0, m_2, n_1, n_2) \\
& + 4(\boldsymbol{T}_{m_1m_3} \cdot \boldsymbol{T}_{n_1n_2})L_4(m_0, m_2, n_0, n_3) + 4(\boldsymbol{T}_{m_1m_3} \cdot \boldsymbol{T}_{n_1n_3})L_4(m_0, m_2, n_0, n_2)), \\
S_{mn} =& v544320k02 \\
& (I_{m_3n_3}L_6(m_0, m_1, m_2, n_0, n_1, n_2) + I_{m_3n_2}L_6(m_0, m_1, m_2, n_0, n_1, n_3) \\
& - I_{m_3n_1}L_6(m_0, m_1, m_2, n_0, n_2, n_3) - I_{m_3n_0}L_6(m_0, m_1, m_2, n_1, n_2, n_3) \\
& + I_{m_2n_3}L_6(m_0, m_1, m_3, n_0, n_1, n_2) + I_{m_2n_2}L_6(m_0, m_1, m_3, n_0, n_1, n_3) \\
& - I_{m_2n_1}L_6(m_0, m_1, m_3, n_0, n_2, n_3) - I_{m_2n_0}L_6(m_0, m_1, m_3, n_1, n_2, n_3) \\
& - I_{m_1n_3}L_6(m_0, m_2, m_3, n_0, n_1, n_2) - I_{m_1n_2}L_6(m_0, m_2, m_3, n_0, n_1, n_3) \\
& + I_{m_1n_1}L_6(m_0, m_2, m_3, n_0, n_2, n_3) + I_{m_1n_0}L_6(m_0, m_2, m_3, n_1, n_2, n_3) \\
& - I_{m_0n_3}L_6(m_1, m_2, m_3, n_0, n_1, n_2) - I_{m_0n_2}L_6(m_1, m_2, m_3, n_0, n_1, n_3) \\
& + I_{m_0n_1}L_6(m_1, m_2, m_3, n_0, n_2, n_3) + I_{m_0n_0}L_6(m_1, m_2, m_3, n_1, n_2, n_3)).
\end{aligned}
$$

$< j_{3m}, k_{3n} >$

$$
\begin{aligned}
R_{mn} =& v3\_68040 \\
& (-2(\boldsymbol{T}_{m_0m_2} \cdot \boldsymbol{T}_{n_0n_2})L_4(m_1, m_3, n_1, n_3) + 2(\boldsymbol{T}_{m_0m_2} \cdot \boldsymbol{T}_{n_0n_3})L_4(m_1, m_3, n_1, n_2) \\
& - 2(\boldsymbol{T}_{m_0m_2} \cdot \boldsymbol{T}_{n_1n_2})L_4(m_1, m_3, n_0, n_3) + 2(\boldsymbol{T}_{m_0m_2} \cdot \boldsymbol{T}_{n_1n_3})L_4(m_1, m_3, n_0, n_2) \\
& + 4(\boldsymbol{T}_{m_0m_2} \cdot \boldsymbol{T}_{n_2n_3})L_4(m_1, m_3, n_0, n_1) - 2(\boldsymbol{T}_{m_0m_3} \cdot \boldsymbol{T}_{n_0n_2})L_4(m_1, m_2, n_1, n_3) \\
& + 2(\boldsymbol{T}_{m_0m_3} \cdot \boldsymbol{T}_{n_0n_3})L_4(m_1, m_2, n_1, n_2) - 2(\boldsymbol{T}_{m_0m_3} \cdot \boldsymbol{T}_{n_1n_2})L_4(m_1, m_2, n_0, n_3) \\
& + 2(\boldsymbol{T}_{m_0m_3} \cdot \boldsymbol{T}_{n_1n_3})L_4(m_1, m_2, n_0, n_2) + 4(\boldsymbol{T}_{m_0m_3} \cdot \boldsymbol{T}_{n_2n_3})L_4(m_1, m_2, n_0, n_1) \\
& - 2(\boldsymbol{T}_{m_1m_2} \cdot \boldsymbol{T}_{n_0n_2})L_4(m_0, m_3, n_1, n_3) + 2(\boldsymbol{T}_{m_1m_2} \cdot \boldsymbol{T}_{n_0n_3})L_4(m_0, m_3, n_1, n_2) \\
& - 2(\boldsymbol{T}_{m_1m_2} \cdot \boldsymbol{T}_{n_1n_2})L_4(m_0, m_3, n_0, n_3) + 2(\boldsymbol{T}_{m_1m_2} \cdot \boldsymbol{T}_{n_1n_3})L_4(m_0, m_3, n_0, n_2) \\
& + 4(\boldsymbol{T}_{m_1m_2} \cdot \boldsymbol{T}_{n_2n_3})L_4(m_0, m_3, n_0, n_1) - 2(\boldsymbol{T}_{m_1m_3} \cdot \boldsymbol{T}_{n_0n_2})L_4(m_0, m_2, n_1, n_3) \\
& + 2(\boldsymbol{T}_{m_1m_3} \cdot \boldsymbol{T}_{n_0n_3})L_4(m_0, m_2, n_1, n_2) - 2(\boldsymbol{T}_{m_1m_3} \cdot \boldsymbol{T}_{n_1n_2})L_4(m_0, m_2, n_0, n_3) \\
& + 2(\boldsymbol{T}_{m_1m_3} \cdot \boldsymbol{T}_{n_1n_3})L_4(m_0, m_2, n_0, n_2) + 4(\boldsymbol{T}_{m_1m_3} \cdot \boldsymbol{T}_{n_2n_3})L_4(m_0, m_2, n_0, n_1)), \\
S_{mn} =& v544320k02 \\
& (I_{m_0n_2}L_6(m_1, m_2, m_3, n_0, n_1, n_3) - I_{m_0n_3}L_6(m_1, m_2, m_3, n_0, n_1, n_2) \\
& + I_{m_1n_2}L_6(m_0, m_2, m_3, n_0, n_1, n_3) - I_{m_1n_3}L_6(m_0, m_2, m_3, n_0, n_1, n_2) \\
& - I_{m_2n_2}L_6(m_0, m_1, m_3, n_0, n_1, n_3) + I_{m_2n_3}L_6(m_0, m_1, m_3, n_0, n_1, n_2) \\
& - I_{m_3n_2}L_6(m_0, m_1, m_2, n_0, n_1, n_3) + I_{m_3n_3}L_6(m_0, m_1, m_2, n_0, n_1, n_2)).
\end{aligned}
$$

$< j_{3m}, l_{3n} >$

$$
\begin{aligned}
R_{mn} =& v3\_68040 \\
& (4(\boldsymbol{T}_{m_0m_2} \cdot \boldsymbol{T}_{n_0n_1})L_4(m_1, m_3, n_2, n_3) + 2(\boldsymbol{T}_{m_0m_2} \cdot \boldsymbol{T}_{n_0n_2})L_4(m_1, m_3, n_1, n_3) \\
& + 2(\boldsymbol{T}_{m_0m_2} \cdot \boldsymbol{T}_{n_0n_3})L_4(m_1, m_3, n_1, n_2) - 2(\boldsymbol{T}_{m_0m_2} \cdot \boldsymbol{T}_{n_1n_2})L_4(m_1, m_3, n_0, n_3) \\
& - 2(\boldsymbol{T}_{m_0m_2} \cdot \boldsymbol{T}_{n_1n_3})L_4(m_1, m_3, n_0, n_2) + 4(\boldsymbol{T}_{m_0m_3} \cdot \boldsymbol{T}_{n_0n_1})L_4(m_1, m_2, n_2, n_3) \\
& + 2(\boldsymbol{T}_{m_0m_3} \cdot \boldsymbol{T}_{n_0n_2})L_4(m_1, m_2, n_1, n_3) + 2(\boldsymbol{T}_{m_0m_3} \cdot \boldsymbol{T}_{n_0n_3})L_4(m_1, m_2, n_1, n_2) \\
& - 2(\boldsymbol{T}_{m_0m_3} \cdot \boldsymbol{T}_{n_1n_2})L_4(m_1, m_2, n_0, n_3) - 2(\boldsymbol{T}_{m_0m_3} \cdot \boldsymbol{T}_{n_1n_3})L_4(m_1, m_2, n_0, n_2) \\
& + 4(\boldsymbol{T}_{m_1m_2} \cdot \boldsymbol{T}_{n_0n_1})L_4(m_0, m_3, n_2, n_3) + 2(\boldsymbol{T}_{m_1m_2} \cdot \boldsymbol{T}_{n_0n_2})L_4(m_0, m_3, n_1, n_3) \\
& + 2(\boldsymbol{T}_{m_1m_2} \cdot \boldsymbol{T}_{n_0n_3})L_4(m_0, m_3, n_1, n_2) - 2(\boldsymbol{T}_{m_1m_2} \cdot \boldsymbol{T}_{n_1n_2})L_4(m_0, m_3, n_0, n_3) \\
& - 2(\boldsymbol{T}_{m_1m_2} \cdot \boldsymbol{T}_{n_1n_3})L_4(m_0, m_3, n_0, n_2) + 4(\boldsymbol{T}_{m_1m_3} \cdot \boldsymbol{T}_{n_0n_1})L_4(m_0, m_2, n_2, n_3) \\
& + 2(\boldsymbol{T}_{m_1m_3} \cdot \boldsymbol{T}_{n_0n_2})L_4(m_0, m_2, n_1, n_3) + 2(\boldsymbol{T}_{m_1m_3} \cdot \boldsymbol{T}_{n_0n_3})L_4(m_0, m_2, n_1, n_2) \\
& - 2(\boldsymbol{T}_{m_1m_3} \cdot \boldsymbol{T}_{n_1n_2})L_4(m_0, m_2, n_0, n_3) - 2(\boldsymbol{T}_{m_1m_3} \cdot \boldsymbol{T}_{n_1n_3})L_4(m_0, m_2, n_0, n_2)), \\
S_{mn} =& v544320k02 \\
& (I_{m_0n_0}L_6(m_1, m_2, m_3, n_1, n_2, n_3) - I_{m_0n_1}L_6(m_1, m_2, m_3, n_0, n_2, n_3) \\
& + I_{m_1n_0}L_6(m_0, m_2, m_3, n_1, n_2, n_3) - I_{m_1n_1}L_6(m_0, m_2, m_3, n_0, n_2, n_3) \\
& - I_{m_2n_0}L_6(m_0, m_1, m_3, n_1, n_2, n_3) + I_{m_2n_1}L_6(m_0, m_1, m_3, n_0, n_2, n_3) \\
& - I_{m_3n_0}L_6(m_0, m_1, m_2, n_1, n_2, n_3) + I_{m_3n_1}L_6(m_0, m_1, m_2, n_0, n_2, n_3)).
\end{aligned}
$$

$< k_{3m}, k_{3n} >$

$$
\begin{aligned}
R_{mn} =& v3\_68040 \\
& ((\boldsymbol{T}_{m_0m_2} \cdot \boldsymbol{T}_{n_0n_2})L_4(m_1, m_3, n_1, n_3) - (\boldsymbol{T}_{m_0m_2} \cdot \boldsymbol{T}_{n_0n_3})L_4(m_1, m_3, n_1, n_2) \\
& + (\boldsymbol{T}_{m_0m_2} \cdot \boldsymbol{T}_{n_1n_2})L_4(m_1, m_3, n_0, n_3) - (\boldsymbol{T}_{m_0m_2} \cdot \boldsymbol{T}_{n_1n_3})L_4(m_1, m_3, n_0, n_2) \\
& - 2(\boldsymbol{T}_{m_0m_2} \cdot \boldsymbol{T}_{n_2n_3})L_4(m_1, m_3, n_0, n_1) - (\boldsymbol{T}_{m_0m_3} \cdot \boldsymbol{T}_{n_0n_2})L_4(m_1, m_2, n_1, n_3) \\
& + (\boldsymbol{T}_{m_0m_3} \cdot \boldsymbol{T}_{n_0n_3})L_4(m_1, m_2, n_1, n_2) - (\boldsymbol{T}_{m_0m_3} \cdot \boldsymbol{T}_{n_1n_2})L_4(m_1, m_2, n_0, n_3) \\
& + (\boldsymbol{T}_{m_0m_3} \cdot \boldsymbol{T}_{n_1n_3})L_4(m_1, m_2, n_0, n_2) + 2(\boldsymbol{T}_{m_0m_3} \cdot \boldsymbol{T}_{n_2n_3})L_4(m_1, m_2, n_0, n_1) \\
& + (\boldsymbol{T}_{m_1m_2} \cdot \boldsymbol{T}_{n_0n_2})L_4(m_0, m_3, n_1, n_3) - (\boldsymbol{T}_{m_1m_2} \cdot \boldsymbol{T}_{n_0n_3})L_4(m_0, m_3, n_1, n_2) \\
& + (\boldsymbol{T}_{m_1m_2} \cdot \boldsymbol{T}_{n_1n_2})L_4(m_0, m_3, n_0, n_3) - (\boldsymbol{T}_{m_1m_2} \cdot \boldsymbol{T}_{n_1n_3})L_4(m_0, m_3, n_0, n_2) \\
& - 2(\boldsymbol{T}_{m_1m_2} \cdot \boldsymbol{T}_{n_2n_3})L_4(m_0, m_3, n_0, n_1) - (\boldsymbol{T}_{m_1m_3} \cdot \boldsymbol{T}_{n_0n_2})L_4(m_0, m_2, n_1, n_3) \\
& + (\boldsymbol{T}_{m_1m_3} \cdot \boldsymbol{T}_{n_0n_3})L_4(m_0, m_2, n_1, n_2) - (\boldsymbol{T}_{m_1m_3} \cdot \boldsymbol{T}_{n_1n_2})L_4(m_0, m_2, n_0, n_3) \\
& + (\boldsymbol{T}_{m_1m_3} \cdot \boldsymbol{T}_{n_1n_3})L_4(m_0, m_2, n_0, n_2) + 2(\boldsymbol{T}_{m_1m_3} \cdot \boldsymbol{T}_{n_2n_3})L_4(m_0, m_2, n_0, n_1) \\
& - 2(\boldsymbol{T}_{m_2m_3} \cdot \boldsymbol{T}_{n_0n_2})L_4(m_0, m_1, n_1, n_3) + 2(\boldsymbol{T}_{m_2m_3} \cdot \boldsymbol{T}_{n_0n_3})L_4(m_0, m_1, n_1, n_2) \\
& - 2(\boldsymbol{T}_{m_2m_3} \cdot \boldsymbol{T}_{n_1n_2})L_4(m_0, m_1, n_0, n_3) + 2(\boldsymbol{T}_{m_2m_3} \cdot \boldsymbol{T}_{n_1n_3})L_4(m_0, m_1, n_0, n_2) \\
& + 4(\boldsymbol{T}_{m_2m_3} \cdot \boldsymbol{T}_{n_2n_3})L_4(m_0, m_1, n_0, n_1)), \\
S_{mn} =& v544320k02 \\
& (I_{m_2n_2}L_6(m_0, m_1, m_3, n_0, n_1, n_3) - I_{m_2n_3}L_6(m_0, m_1, m_3, n_0, n_1, n_2) \\
& - I_{m_3n_2}L_6(m_0, m_1, m_2, n_0, n_1, n_3) + I_{m_3n_3}L_6(m_0, m_1, m_2, n_0, n_1, n_2)).
\end{aligned}
$$

$< k_{3m}, l_{3n} >$

$$
\begin{aligned}
R_{mn} =& v3\_68040 \\
& (-2(\boldsymbol{T}_{m_0m_2} \cdot \boldsymbol{T}_{n_0n_1})L_4(m_1, m_3, n_2, n_3) - (\boldsymbol{T}_{m_0m_2} \cdot \boldsymbol{T}_{n_0n_2})L_4(m_1, m_3, n_1, n_3) \\
& - (\boldsymbol{T}_{m_0m_2} \cdot \boldsymbol{T}_{n_0n_3})L_4(m_1, m_3, n_1, n_2) + (\boldsymbol{T}_{m_0m_2} \cdot \boldsymbol{T}_{n_1n_2})L_4(m_1, m_3, n_0, n_3) \\
& + (\boldsymbol{T}_{m_0m_2} \cdot \boldsymbol{T}_{n_1n_3})L_4(m_1, m_3, n_0, n_2) + 2(\boldsymbol{T}_{m_0m_3} \cdot \boldsymbol{T}_{n_0n_1})L_4(m_1, m_2, n_2, n_3) \\
& + (\boldsymbol{T}_{m_0m_3} \cdot \boldsymbol{T}_{n_0n_2})L_4(m_1, m_2, n_1, n_3) + (\boldsymbol{T}_{m_0m_3} \cdot \boldsymbol{T}_{n_0n_3})L_4(m_1, m_2, n_1, n_2) \\
& - (\boldsymbol{T}_{m_0m_3} \cdot \boldsymbol{T}_{n_1n_2})L_4(m_1, m_2, n_0, n_3) - (\boldsymbol{T}_{m_0m_3} \cdot \boldsymbol{T}_{n_1n_3})L_4(m_1, m_2, n_0, n_2) \\
& - 2(\boldsymbol{T}_{m_1m_2} \cdot \boldsymbol{T}_{n_0n_1})L_4(m_0, m_3, n_2, n_3) - (\boldsymbol{T}_{m_1m_2} \cdot \boldsymbol{T}_{n_0n_2})L_4(m_0, m_3, n_1, n_3) \\
& - (\boldsymbol{T}_{m_1m_2} \cdot \boldsymbol{T}_{n_0n_3})L_4(m_0, m_3, n_1, n_2) + (\boldsymbol{T}_{m_1m_2} \cdot \boldsymbol{T}_{n_1n_2})L_4(m_0, m_3, n_0, n_3) \\
& + (\boldsymbol{T}_{m_1m_2} \cdot \boldsymbol{T}_{n_1n_3})L_4(m_0, m_3, n_0, n_2) + 2(\boldsymbol{T}_{m_1m_3} \cdot \boldsymbol{T}_{n_0n_1})L_4(m_0, m_2, n_2, n_3) \\
& + (\boldsymbol{T}_{m_1m_3} \cdot \boldsymbol{T}_{n_0n_2})L_4(m_0, m_2, n_1, n_3) + (\boldsymbol{T}_{m_1m_3} \cdot \boldsymbol{T}_{n_0n_3})L_4(m_0, m_2, n_1, n_2) \\
& - (\boldsymbol{T}_{m_1m_3} \cdot \boldsymbol{T}_{n_1n_2})L_4(m_0, m_2, n_0, n_3) - (\boldsymbol{T}_{m_1m_3} \cdot \boldsymbol{T}_{n_1n_3})L_4(m_0, m_2, n_0, n_2) \\
& + 4(\boldsymbol{T}_{m_2m_3} \cdot \boldsymbol{T}_{n_0n_1})L_4(m_0, m_1, n_2, n_3) + 2(\boldsymbol{T}_{m_2m_3} \cdot \boldsymbol{T}_{n_0n_2})L_4(m_0, m_1, n_1, n_3) \\
& + 2(\boldsymbol{T}_{m_2m_3} \cdot \boldsymbol{T}_{n_0n_3})L_4(m_0, m_1, n_1, n_2) - 2(\boldsymbol{T}_{m_2m_3} \cdot \boldsymbol{T}_{n_1n_2})L_4(m_0, m_1, n_0, n_3) \\
& - 2(\boldsymbol{T}_{m_2m_3} \cdot \boldsymbol{T}_{n_1n_3})L_4(m_0, m_1, n_0, n_2)), \\
S_{mn} =& v544320k02 \\
& (I_{m_2n_0}L_6(m_0, m_1, m_3, n_1, n_2, n_3) - I_{m_2n_1}L_6(m_0, m_1, m_3, n_0, n_2, n_3) \\
& - I_{m_3n_0}L_6(m_0, m_1, m_2, n_1, n_2, n_3) + I_{m_3n_1}L_6(m_0, m_1, m_2, n_0, n_2, n_3)).
\end{aligned}
$$

$< l_{3m}, l_{3n} >$

$$
\begin{aligned}
R_{mn} =& v3\_68040 \\
& (4(\boldsymbol{T}_{m_0m_1} \cdot \boldsymbol{T}_{n_0n_1})L_4(m_2, m_3, n_2, n_3) + 2(\boldsymbol{T}_{m_0m_1} \cdot \boldsymbol{T}_{n_0n_2})L_4(m_2, m_3, n_1, n_3) \\
& + 2(\boldsymbol{T}_{m_0m_1} \cdot \boldsymbol{T}_{n_0n_3})L_4(m_2, m_3, n_1, n_2) - 2(\boldsymbol{T}_{m_0m_1} \cdot \boldsymbol{T}_{n_1n_2})L_4(m_2, m_3, n_0, n_3) \\
& - 2(\boldsymbol{T}_{m_0m_1} \cdot \boldsymbol{T}_{n_1n_3})L_4(m_2, m_3, n_0, n_2) + 2(\boldsymbol{T}_{m_0m_2} \cdot \boldsymbol{T}_{n_0n_1})L_4(m_1, m_3, n_2, n_3) \\
& + (\boldsymbol{T}_{m_0m_2} \cdot \boldsymbol{T}_{n_0n_2})L_4(m_1, m_3, n_1, n_3) + (\boldsymbol{T}_{m_0m_2} \cdot \boldsymbol{T}_{n_0n_3})L_4(m_1, m_3, n_1, n_2) \\
& - (\boldsymbol{T}_{m_0m_2} \cdot \boldsymbol{T}_{n_1n_2})L_4(m_1, m_3, n_0, n_3) - (\boldsymbol{T}_{m_0m_2} \cdot \boldsymbol{T}_{n_1n_3})L_4(m_1, m_3, n_0, n_2) \\
& + 2(\boldsymbol{T}_{m_0m_3} \cdot \boldsymbol{T}_{n_0n_1})L_4(m_1, m_2, n_2, n_3) + (\boldsymbol{T}_{m_0m_3} \cdot \boldsymbol{T}_{n_0n_2})L_4(m_1, m_2, n_1, n_3) \\
& + (\boldsymbol{T}_{m_0m_3} \cdot \boldsymbol{T}_{n_0n_3})L_4(m_1, m_2, n_1, n_2) - (\boldsymbol{T}_{m_0m_3} \cdot \boldsymbol{T}_{n_1n_2})L_4(m_1, m_2, n_0, n_3) \\
& - (\boldsymbol{T}_{m_0m_3} \cdot \boldsymbol{T}_{n_1n_3})L_4(m_1, m_2, n_0, n_2) - 2(\boldsymbol{T}_{m_1m_2} \cdot \boldsymbol{T}_{n_0n_1})L_4(m_0, m_3, n_2, n_3) \\
& - (\boldsymbol{T}_{m_1m_2} \cdot \boldsymbol{T}_{n_0n_2})L_4(m_0, m_3, n_1, n_3) - (\boldsymbol{T}_{m_1m_2} \cdot \boldsymbol{T}_{n_0n_3})L_4(m_0, m_3, n_1, n_2) \\
& + (\boldsymbol{T}_{m_1m_2} \cdot \boldsymbol{T}_{n_1n_2})L_4(m_0, m_3, n_0, n_3) + (\boldsymbol{T}_{m_1m_2} \cdot \boldsymbol{T}_{n_1n_3})L_4(m_0, m_3, n_0, n_2) \\
& - 2(\boldsymbol{T}_{m_1m_3} \cdot \boldsymbol{T}_{n_0n_1})L_4(m_0, m_2, n_2, n_3) - (\boldsymbol{T}_{m_1m_3} \cdot \boldsymbol{T}_{n_0n_2})L_4(m_0, m_2, n_1, n_3) \\
& - (\boldsymbol{T}_{m_1m_3} \cdot \boldsymbol{T}_{n_0n_3})L_4(m_0, m_2, n_1, n_2) + (\boldsymbol{T}_{m_1m_3} \cdot \boldsymbol{T}_{n_1n_2})L_4(m_0, m_2, n_0, n_3) \\
& + (\boldsymbol{T}_{m_1m_3} \cdot \boldsymbol{T}_{n_1n_3})L_4(m_0, m_2, n_0, n_2)) \\
S_{mn} =& v544320k02 \\
& (I_{m_0n_0}L_6(m_1, m_2, m_3, n_1, n_2, n_3) - I_{m_0n_1}L_6(m_1, m_2, m_3, n_0, n_2, n_3) \\
& - I_{m_1n_0}L_6(m_0, m_2, m_3, n_1, n_2, n_3) + I_{m_1n_1}L_6(m_0, m_2, m_3, n_0, n_2, n_3)).
\end{aligned}
$$

References

Abramowitz, M. and Stegun, I. A. (1972). Handbook of mathematical functions. *New York: National Bureau of Standards*.

Aiello, G., Alfonzetti, S., Borzi, G., Dilettoso, E., and Salerno, N. (2013). GMRES solution of FEM-BEM global systems for electrostatic problems without voltaged conductors. *IEEE Transactions on Magnetics*, 49(5):1701–1704.

Ascher, U. M. and Petzold, L. R. (1998). Computer methods for ordinary differential equations and differential-algebraic equations. *Society for Industrial and Applied Mathematics, New York: John Wiley and Sons*.

Balanis, C. A. (1989). Advanced engineering electromagnetics. *New York: John Wiley and Sons*.

Bladel, J. V. (2007). Electromagnetic fields. *New York: John Wiley and Sons*.

Botha, M. M. (2013). A family of augmented duffy transformations for near-singularity cancellation quadrature. *IEEE Transactions on Antennas and Propogation*, 61(6):3123–3134.

Botha, M. M. (2014). Progress with numerical integration of the near-singular green function gradient on general triangle domains. *International Conference on Electromagnetics in Advanced Applications (ICEAA), Torino, Italy*.

Butler, C. M. (1975). Evaluation of potential integral at singularity of exact kernel in thin-wire calculations. *IEEE Transactions on Antennas and Propogation*, 23(2):293–295.

Chakraborty, S. and Jandhyala, V. (2006). Surface-based broadband electromagnetic-circuit simulation of lossy conductors. *IEE Proceedings - Microwaves, Antennas and Propagation*, 153(2):191–198.

Chen, J. S., Wang, L., Hu, H. Y., and Chi, S. W. (2009). Subdomain radial basis collocation method for heterogeneous media. *International Journal for Numerical Methods in Engineering*, 80(2):163–190.

Chew, W., Michielssen, E., Song, J. M., and Jin, J. M. (2001). Fast and efficient algorithms in computational electromagnetics. *Norwood, MA: Artech House*.

Chew, W. C., Tong, M. S., and Hu, B. (2008). Integral equation methods for electromagnetic and elastic waves. *Morgan and Claypool Publishers*, 3(1):1–241.

Chiang, I. T. and Chew, W. C. (2006a). A coupled PEC-TDS surface integral equation approach for electromagnetic scattering and radiation from composite metallic and thin dielectric objects. *IEEE Transactions on Antennas and Propogation*, 54(11):3511–3516.

Chiang, I. T. and Chew, W. C. (2006b). Thin dielectric sheet simulation by surface integral equation using modified rwg and pulse bases. *IEEE Transactions on Antennas and Propogation*, 54(7):1927–1934.

Cloux, R. D., Maas, G. P., and Wachters, A. J. (1994). Quasi-static boundary element method for electromagnetic simulation of pcbs. *Philips Journal of Research*, 48.

Coifman, R., Rokhlin, V., and Wandzura, S. (1993). The fast multipole method for the wave equation: a pedestrian prescription. *IEEE Transactions on Antennas and Propogation*, 35(3):7–12.

Collins, J. D., Jin, J. M., and Volakis, J. L. (1992). Eliminating interior resonances in finite element boundary integral methods for scattering. *IEEE Transactions on Antennas and Propogation*, 40(12):1583–1585.

Correia, D. M. and Singer, H. (1999). A MoM solution for the EFIE applicable to any combination of thin-wire and surface scatterers down to low frequencies. *International Zurich Symposium and Technical Exhibition on Electromagnetic Compatibility, Zurich, Switzerland.*

Dembart, B. and Yip, E. (1998). The accuracy of fast multipole methods for Maxwell's equations. *IEEE Computational Science and Engineering*, 5(3):48–56.

Djordjevic, M. and Notaros, B. M. (2004). Double higher order method of moments for surface integral equation modeling of metallic and dielectric antennas and scatterers. *IEEE Antennas and Propogation Magazine*, 52(8):2118–2129.

Donepudi, K., Song, J., Jin, J. M., Kang, G., and Chew, W. C. (2000). A novel implementation of multilevel fast multipole algorithm for higher order Galerkin's method. *IEEE Transactions on Antennas and Propogation*, 48(8):1192–1197.

Duffy, M. G. (1982). Quadrature over a pyramid or cube of integrands with a singularity at a vertex. *SIAM Journal on Numerical Analysis*, 19(6):12601262.

Eastwood, J. and Morgan, J. (2008). Higher-order basis functions for MoM calculations. *IET Science, Measurement and Technology*, 2(6):379–386.

Eibert, T. F. (1997). Verknüpfung der Methode der finiten Elemente mit einem Integralgleichungsverfahren für ebene geschichtete Strukturen. *Doctoral Dissertation, Fachbereich Elektrotechnik der Bergischen Universität Wuppertal.*

Eibert, T. F. (2003). Iterative near-zone preconditioning of iterative method of moments electric field integral equation solutions. *IEEE Antennas and Wireless Propagation Letters*, 2(1):101–102.

Eibert, T. F. (2005). A diagonalized multilevel fast multipole method with spherical harmonics expansion of the k-space integrals. *IEEE Transactions on Antennas and Propogation*, 53(2):814–817.

Eibert, T. F. (2007). Some scattering results computed by surface-integral-equations and hybrid finite-element-boundary-integral techniques and accelerated by the multilevel fast multipole method. *IEEE Antennas and Propogation Magazine*, 49(2):61–69.

Eibert, T. F. and Hansen, V. (1995a). On the calculation of potential integrals for linear souce distributions on triangular domains. *IEEE Transactions on Antennas and Propogation*, 43(12):1499–1502.

Eibert, T. F. and Hansen, V. (1995b). On the calculation of potential integrals for linear source distributions on triangular domains. *IEEE Transactions on Antennas and Propogation*, 43(12):1499–1502.

Eibert, T. F. and Hansen, V. (1996a). Calculation of unbounded field problems in free space by a 3-D FEM/BEM hybrid approach. *Journal of Electromagnetic Waves and Applications*, 10(1):61–78.

Eibert, T. F. and Hansen, V. (1996b). On the interior resonance problem of FEM/BEM hybrid and BEM approaches. *IEEE Antennas and Propagation Society International Symposium, Baltimore, Maryland*, 1:154–157.

Eibert, T. F. and Hansen, V. (1997). 3-D FEM/BEM hybrid approach based on a general formulation of huygens principle for planar layered media. *IEEE Transactions on Antennas and Propogation*, 45(7):1105–1112.

Engheta, N., Murphy, W. D., Rohklin, V., and Vassiliou, M. S. (1992). The fast multipole method (FMM) for electromagnetic scattering problems. *IEEE Transactions on Antennas and Propogation*, 40(6):634–641.

Ergül, O. and Gürel, L. (2004). Improving the accuracy of the MFIE with the choice of basis functions. *IEEE Antennas and Propagation Society International Symposium, Monterey, Canada*, 3:3389–3392.

Ergül, O. and Gürel, L. (2008). Efficient solution of the electric-field integral equation using the iterative LSQR algorithm. *IEEE Antennas and Wireless Propagation Letters*, 7:36–39.

Ewe, W., Li, L. W., and Leong, M. (2004). Fast solution of mixed dielectric/conducting scattering problem using volume-surface adaptive integral method. *IEEE Transactions on Antennas and Propogation*, 52(11):3071–3077.

Fink, P. W., Wilton, D. R., and Khayat, M. A. (2005). Issues and methods concerning the evaluation of hypersingular and near-hypersingular integrals in BEM formulations. *Presented at the International Conference on Electromagnetics in Advanced Applications (ICEAA'05), Torino, Italy.*

Fink, P. W., Wilton, D. R., and Khayat, M. A. (2008). Simple and efficient numerical evaluation of near-hypersingular integrals. *IEEE Antennas and Wireless Propagation Letters*, 7:469–472.

Gibson, W. C. (2008). The method of moments in electromagnetics. *New York: Chapman and Hall/CRC.*

Graglia, R., Wilton, D., and Peterson, A. (1997). Higher order interpolatory vector bases for computational electromagnetics. *IEEE Transactions on Antennas and Propogation*, 45(3):329–342.

Graglia, R. D. (1993). On the numerical integration of the linear shape functions times the 3-d greens function or its gradient on a plane triangle. *IEEE Transactions on Antennas and Propogation*, 41(10):1448–1455.

Hairer, E., Norsett, S. P., and Wanner, G. (1993). Solving ordinary differential equations I: Nonstiff Problems. *New York: Springer-Verlag*.

Harman, P. M. (1995). The scientific letters and papers of James Clerk Maxwell. *Cambridge, U.K.:Cambridge University Press*, II.

Harmuth, H. F. and Hussain, G. M. (1994). Propagation of electromagnetic signals. *New York: World Scientific*.

Harrington, R. F. (1961). Time harmonic electromagnetic fields. *New York: McGraw-Hill*.

Harrington, R. F. (1990). Origin and development of the method of moments for field computation. *IEEE Antennas Propagation Magzine*, 32(3):31–35.

Harrington, R. F. (1993). Field computation by moment methods. *New York: Wiley-IEEE Press*.

Harrington, R. F. (2001). Time-harmonic electromagnetic fields. *New York: Wiley Interscience*.

Hodges, R. E. and Samii, Y. R. (1997). The evaluation of MFIE integrals with the use of vector triangle basis functions. *Microwave and Optical Technology Letters*, 14(1):914.

Huber, C., Rucker, W., Hoschek, R., and Richter, K. (1997a). A new method for the numerical calculation of cauchy principal value integrals in BEM applied to electromagnetics. *IEEE Transactions on Magnetics*, 33(2):1386–1389.

Huber, C. J., Rieger, W., Haas, M., and Rucker, W. M. (1997b). The numerical treatment of singular integrals in boundary element calculations. *The Applied Computational Electromagnetics Society*, 12(2).

Huygens, C. (1912). Traite de la lumiere. *Chicago: University of Chicago Press*.

Ilic, M. M. and Notaros, B. M. (2003). Higher order hierarchical curved hexahedral vector finite elements for electromagnetic modeling. *IEEE Transactions on Microwave Theory and Techniques*, 51(3):1026–1033.

Ingber, M. S. and Ott, R. H. (1991). An application of the boundary element method to the magnetic field integral equation. *IEEE Transactions on Microwave Theory and Techniques*, 39(5):606–611.

Iserles, A. (1996). A first course in the numerical analysis of differential equations. *Cambridge: Cambridge University Press*.

Ismatullah and Eibert, T. F. (2008). Adaptive singularity cancellation technique for efficient treatment of near-singular and near-hypersingular integrals in surface integral equation formulations. *IEEE Transactions on Antennas and Propogation*, 56(1):274–278.

Ismatullah and Eibert, T. F. (2009). Surface integral equation solutions by hierarchical vector basis functions and spherical harmanics based multilevel fast multiple method. *IEEE Transactions on Antennas and Propogation*, 57(7):2084–2093.

Jandhyala, V., Wang, Y., Gope, D., and Shi, C. J. (2002). A surface-based integral-equation formulation for coupled electromagnetic and circuit simulation. *Microwave and Optical Technology Letters*, 34(2):103106.

Järvenpää, S., Taskinen, M., and Ylä-Oijala, P. (2003). Singularity extraction technique for integral equation methods with higher order basis functions on plane triangles and tetrahedra. *International Journal for Numerical Methods in Engineering*, 58(8):11491165.

Järvenpää, S., Taskinen, M., and Ylä-Oijala, P. (2006a). Singularity subtraction technique for high-order polynomial vector basis functions on planar triangles. *IEEE Transactions on Antennas and Propogation*, 54(1):42–49.

Järvenpää, S., Taskinen, M., and Ylä-Oijala, P. P. (2006b). Singularity subtraction technique for high-order polynomial vector basis functions on planar triangles. *IEEE Transactions on Antennas and Propogation*, 54(1):42–49.

Jin, J. (2002). The finite element method in electromagnetics. *New York: John Wiley and Sons*.

Jin, J. M. and Riley, D. J. (2008). Finite element analysis of antennas and arrays. *New York: Wiley-IEEE Press*.

Jin, J. M. and Volakis, J. (1991). A finite-element-boundary integral formulation for scattering by three-dimensional cavity-backed apertures. *IEEE Transactions on Antennas and Propogation*, 39(1):97–104.

Jorgensen, E., Kim, O., Meincke, P., and Breinbjerg, O. (2005). Higher order hierarchical legendre basis functions in integral equation formulations applied to complex electromagnetic problems. *IEEE Antennas and Propagation Society International Symposium, Washington. D.C., U.S.A.*, 3A:64–67.

Jung, B. H. and Sarkar, T. K. (2004a). Analysis of scattering from arbitrarily shaped 3-D conducting/dielectric composite objects using a combined field integral equation. *Journal of Electromagnetic Waves and Applications*, 18(6):729743.

Jung, B. H. and Sarkar, T. K. (2004b). Combined field integral equation for the analysis of scattering from three- dimensional conducting bodies coated with a dielectric material. *Microwave and Optical Technology Letters*, 40(6):511516.

Kalbasi, K. and Demarest, K. R. (1993). A multilevel formulation of the method of moments. *IEEE Transactions on Antennas and Propogation*, 41(5):589–599.

Kapur, S. and Long, D. E. (1998). IES3: efficient electrostatic and electromagnetic simulation. *IEEE Computional Science and Engineering*, 5(4):60–67.

Khayat, M. A. and Wilton, D. R. (2005). Numerical evaluation of singular and near-singular potential integrals. *IEEE Transactions on Antennas and Propogation*, 53(10):3180–3190.

Khayat, M. A., Wilton, D. R., and Fink, P. W. (2008). An improved transformation and optimized sampling scheme for the numerical evaluation of singular and near-singular potentials. *IEEE Antennas and Wireless Propagation Letters*, 7:377–380.

Klopf, E. M., Sekeljic, N. J., Ilic, M. M., and Notaros, B. M. (2012). Optimal modeling parameters for higher order MoM-SIE and FEM-MoM electromagnetic simulations. *IEEE Transactions on Microwave Theory and Techniques*, 60(6):2790–2801.

Knockaert, L. (1991). A general Gauss theorem for evaluating singular integrals over polyhedral domains. *Electromagnetics*, 11(2):269–280.

Koc, S., Song, J., and Chew, W. C. (1999). Error analysis for the numerical evaluation of the diagonal forms of the scalar spherical addition theorem. *SIAM Journal on Numerical Analysis*, 36(3):906921.

Kong, J. A. (1986). Electromagnetic wave theory. *New York: John Wiley and Sons*.

Lapidus, L. and Pinder, G. F. (1982). Numerical solutions of partial differential equations in science and engineering. *New York: John Wiley and Sons*.

Li, L. and Eibert, T. F. (2016). Radial angular singularity cancellation transformations derived by variable separation. *IEEE Transactions on Antennas and Propogation*, 64(1):189–200.

Li, L., Wang, K., and Eibert, T. F. (2014a). A projection height independent adaptive radial-angular-R2 transformation for singular integrals. *IEEE Transactions on Antennas and Propogation*, 62(10):5381–5386.

Li, L., Wang, K., Li, H., and Eibert, T. F. (2014b). Analytical finite element matrix elements and global matrix assembly for hierarchical 3-D vector basis functions within the hybrid finite element boundary integral method. *Advances in Radio Science*, 12:1–11.

Lindell, I. V. (1996). Huygens' principle in electromagnetics. *IEE Proceedings - Science, Measurement and Technology*, 143(2):103–105.

Liu, Q. H. and Chew, W. C. (1990). Surface integral equation method for the analysis of an obliquely stratified half-space. *IEEE Transactions on Antennas and Propogation*, 38(5):653–663.

Liu, Q. H., Lin, Y., Liu, J., Lee, J. H., and Sesek, E. (2009a). A 3-D spectral integral method (SIM) for surface integral equations. *IEEE Microwave and Wireless Components Letters*, 19(2):62–64.

Liu, Z. H., Chua, E. K., and See, K. Y. (2009b). Accurate and efficient evaluation of method of moments matrix based on a generalized analytical approach. *Progress In Electromagnetics Research*, 94:367–382.

Lu, C. C. and Chew, W. C. (1995). The use of Huygens' equivalence principle for solving 3-D volume integral equation of scattering. *IEEE Transactions on Antennas and Propogation*, 43(5):500–507.

Martini, E., Carli, G., and Maci, S. (2008). An equivalence theorem based on the use of electric currents radiating in free space. *IEEE Antennas and Wireless Propagation Letters*, 7:421–424.

Mautz, J. and Harrington, R. (1984). An E-field solution for a conducting surface small or comparable to the wavelength. *IEEE Transactions on Antennas and Propogation*, 32(4):330–339.

Mautz, J. and Harrington, R. F. (1978a). Calculation of CFIE impedance matrix elements with RWG and $\hat{n} \times$ RWG functions. *Archiv für Elektronik und Übertragungstechnik*, 32.

Mautz, J. R. and Harrington, R. F. (1978b). H-field and E-field and combined-field solutions for conducting bodies of revolution. *Archiv der elektrischen Übertragung.*, 32.

Mautz, J. R. and Harrington, R. F. (1979). A combined source solution for radiation and scattering from a perfectly conducting body. *IEEE Transactions on Antennas and Propogation*, 27(4):445–454.

Maxwell, J. C. (1873). A treatise on electricity and magnetism. *Oxford, U.K.: Oxford University Press*.

Menshov, A. and Okhmatovski, V. I. (2014). Surface volume surface electric field integral equation for magneto quasi static analysis of complex 3-D interconnects. *IEEE Transactions on Antennas and Propogation*, 62(11):2563–2573.

Mittra, A. and Klein, C. A. (1975). Stability and convergence of moment method solutions. *Numerical and Asymptotic Techniques in Electromagnetics*.

Monzon, J. C. (1993). On surface integral representations: Validity of Huygens' principle and the equivalence principle in inhomogeneous bianisotropic media. *IEEE Transactions on Microwave Theory Technology*, 41(11):1995–2001.

Monzon, J. C. and Damaskos, N. J. (1994). A scheme for eliminating internal resonances: The parasitic body technique. *IEEE Transactions on Antennas and Propogation*, 42(8):1089–1096.

Murphy, W. D., Rokhlin, V., and Vassiliou, M. S. (1990). Solving electromagnetic scattering problems at resonance frequencies. *Journal of Applied Physics*, 67(10).

Nabors, K. and White, J. (1991). Fastcap: a multipole accelerated 3-D capacitance extraction program. *IEEE Transactions on Computer-Aided Design*, 10(11):1447–1459.

Nedelec, J. C. (1980). Mixed finite elements in R3. *Numerische Mathematik*, 35.

Nie, X. C., Yuan, N., Li, L. W., Gan, Y. B., and Yeo, T. S. (2005). A fast volume-surface integral equation solver for scattering from composite conducting-dielectric objects. *IEEE Transactions on Antennas and Propogation*, 53(2):818–824.

Notaros, B. M. (2008). Higher order frequency-domain computational electromagnetics. *IEEE Transactions on Antennas and Propogation*, 56(8):2251–2276.

Oijala, P. Y. (2008). Numerical analysis of combined field integral equation formulations for electromagnetic scattering by dielectric and composite objects. *Progress In Electromagnetics Research*, 3:19–43.

Paige, C. C. and Saunders, M. A. (1982a). Algorithm 583 LSQR: sparse linear equations and least squares problems. *ACM Transactions on Mathematical Software*, 8(2):195–209.

Paige, C. C. and Saunders, M. A. (1982b). LSQR: an algorithm for sparse linear equations and sparse least squares. *ACM Transactions on Mathematical Software*, 8(1):43–71.

Peterson, A. F. (1990). The "interior resonance problem" associated with surface integral equations of electromagnetics: numerical consequences and a survey of remedies. *Electromagnetics 10*.

Peterson, A. F., Wilton, D. R., and Jorgenson, R. E. (1996). Variational nature of Galerkin and nonGalerkin moment method solution. *IEEE Transactions on Antennas and Propogation*, 44(4):500–503.

Polimeridis, A. G., Vipiana, F., Mosig, J. R., and Wilton, D. R. (2013). DIRECTFN: fully numerical algorithms for high precision computation of singular integrals in Galerkin SIE methods. *IEEE Transactions on Antennas and Propogation*, 61(6):3112–3122.

Ramahi, O. M. and Mittra, R. (1991). A surface integral equation method for the finite element solution of waveguide discontinuity problems. *IEEE Transactions on Microwave Theory and Techniques*, 39(3):604–608.

Rao, S. M. and Wilton, D. R. (1990). E-field and H-field and and combined field solution for arbitrarily shaped three-dimensional dielectric bodies. *Electromagnetics*, 10(4):407–421.

Rao, S. M., Wilton, D. R., and Glisson, A. W. (1982). Electromagnetic scattering by surfaces of arbitrary shape. *IEEE Transactions on Antennas and Propogation*, 30(3):409–418.

Razi, A. R. and Kasper, M. (2008). Orthogonal hierarchical nedelec elements. *IEEE Transactions on Microwave Theory and Techniques*, 44(6):1210–1213.

Raziman, T. V., Somerville, W. R. C., Martin, O. J. F., and Ru, E. C. L. (2015). Accuracy of surface integral equation matrix elements in plasmonic calculations. *Journal of the Optical Society of America*, 32(3).

Saad, Y. and Schultz, M. H. (1986). GMRES: a generalized minimal residual algorithm for solving nonsymmetric linear systems. *SIAM Journal on Numerical Analysis*, 7(3):856869.

Shi, W., Liu, J., Kakani, N., and Yu, T. (2002). A fast hierarchical algorithm for three-dimensional capacitance extraction. *IEEE Transactions on Computer-Aided Design Integrated Circuits System*, 21(3):330–336.

Shore, R. and Yaghjian, A. (2005). Dual-surface integral equations in electromagnetic scattering. *IEEE Transactions on Antennas and Propogation*, 53(5):1706–1709.

Shore, R. A. and Yaghjian, A. D. (2002). Dual-surface integral equations in electromagnetic scattering. *in XXVIIth General Assembly of the International Union of Radio Science and Maastricht and Netherlands*.

Sleijpen, G. L. G. and Fokkema, D. R. (1993). BICGSTAB(L) for linear equations involving unsymmetric matrices with complex spectrum. *Electronic Transactions on Numerical Analysis*, 1(9):11–32.

Sommerfeld, A. (1949). Partial differential equations in physics. *New York: Academic Press*.

Song, J., Lu, C. C., and Chew, W. C. (1997). Multilevel fast multipole algorithm for electromagnetic scattering by large complex objects. *IEEE Transactions on Antennas and Propogation*, 45(10):1488–1493.

Song, J. M. and Chew, W. C. (1995). Multilevel fast multipole algorithm for solving combined field integral equations of electromagnetic scattering. *Microwave and Optical Technology Letters*, 10(1):1419.

Srivastava, N., Suaya, R., and Banerjee, K. (2008). High-frequency mutual impedance extraction of VLSI interconnects in the presence of a multi-layer conducting substrate. *Design and Automation and Test in Europe (DATE) Conference*.

Stone, M. and Goldbart, P. (2009). Mathematics for physics. *New York: Pimander-Casaubon*.

Stratton, J. A. (1941). Electromagnetic theory. *New York: McGrawHill Book Company*.

Sun, D. K., Lee, J. F., and Cendes, Z. (2001). Construction of nearly orthogonal nedelec bases for rapid convergence with multilevel preconditioned solvers. *SIAM Journal on Numerical Analysis*, 23(4):10531076.

Tong, M. S. and Chew, W. C. (2012). A novel meshless scheme for solving surface integral equations with flat integral domains. *IEEE Transactions on Antennas and Propogation*, 60(7):3285–3293.

Tzoulis, A. and Eibert, T. F. (2005a). Combining the multilevel fast multipole method with the uniform geometrical theory of diffraction. *Advances in Radio Science*, 3:183–188.

Tzoulis, A. and Eibert, T. F. (2005b). A hybrid FEBI-MLFMM-UTD method for numerical solutions of electromagnetic problems including arbitrarily shaped and electrically large objects. *IEEE Transactions on Antennas and Propogation*, 53(10):3358–3366.

Usner, B. C., Sertel, K., Carr, M. A., and Volakis, J. L. (2006). Generalized volume-surface integral equation for modeling inhomogeneities within high contrast composite structures. *IEEE Transactions on Antennas and Propogation*, 54(1):68–75.

Varmazyar, S. H., Moghadasi, M. N., and Masouri, Z. (2008). A moment method simulation of electromagnetic scattering from conducting bodies. *Progress In Electromagnetics Research*, 81:99–119.

Velamparambil, S., Chew, W. C., and Song, J. (2003). 10 million unknowns: is it that big. *IEEE Antennas Propagation Magzine*, 45(2):43–58.

Vipiana, F., Polemi, A., Maci, S., and Vecchi, G. (2008). A mesh-adapted closed-form regular kernel for 3D singular integral equations. *IEEE Transactions on Antennas and Propogation*, 56(6):1687–1698.

Vipiana, F. and Wilton, D. R. (2011). Optimized numerical evaluation of singular and near-singular potential integrals involving junction basis functions. *IEEE Transactions on Antennas and Propogation*, 59(1):162–171.

Volakis, J. L., Chatterjee, A., and Kempel, L. C. (1998). Finite element method for electromagnetics: antennas and microwave circuits and and scattering applications. *New York: Wiley-IEEE Press*.

Wang, Y., Gope, D., Jandhyala, V., and Shi, C. J. (2004). Generalized kirchoffs current and voltage law formulation for coupled circuit-electromagnetic simulation with surface integral equations. *IEEE Transactions on Microwave Theory Technology*, 52(7):1673–1682.

Webb, J. (1999). Hierarchal vector basis functions of arbitrary order for triangular and tetrahedral finite elements. *IEEE Transactions on Antennas and Propogation*, 47(8):1244–1253.

Wilton, D. R. and Glisson, A. W. (1981). On improving the electric field integral equation at low frequencies. *URSI Radio Science Meeting Digest, Washington. D.C., U.S.A.*

Wilton, D. R., Rao, S. M., Glisson, A. W., Schaubert, D. H., Al-Bundak, O. M., and Butler, C. M. (1984). Potential integrals for uniform and linear source distributions on polygonal and polyhedral domains. *IEEE Transactions on Antennas and Propogation*, 32(3):276–281.

Yaghjian, A. D. (1981). Augmented electric and magneticfield integral equations. *Radio Science*, 16(6).

YlÄ-Oijala, P. and Taskinen, M. (2003). Calculation of CFIE impedance matrix elements with RWG and $\hat{n} \times$ RWG functions. *IEEE Transactions on Antennas and Propogation*, 51(8):1837–1846.

Ylä-Oijala, P. and Taskinen, M. (2005). Application of combined field integral equation for electromagnetic scattering by composite metallic and dielectric objects. *IEEE Transactions on Antennas and Propogation*, 53(3):1168–1173.

Ylä-Oijala, P., Taskinen, M., and Sarvas, J. (2005). Surface integral equation method for general composite metallic and dielectric structures with junctions. *Progress In Electromagnetics Research*, 52:81–108.

Zhang, Y., Cui, T. J., Chew, W. C., and Zhao, J. S. (2003). Magnetic field integral equation at very low frequencies. *IEEE Transactions on Antennas and Propogation*, 51(8):1864–1871.

Zhu, Y. and Cangellaris, A. (2006). Multigrid finite element methods for electromagnetic field modeling. *Hoboken, New Jersey: John Wiley and Sons*.

Zhu, Z., Song, B., and White, J. (2003). Algorithms in FASTIMP: a fast and wideband impedance extraction program for complicated 3-D geometries. *IEEE Transactions on Computer-Aided Design of Integrated Circuits and Systems*, 24(7):981–998.

List of Supervised Student Projects

Bachelor Thesis

- Jianing Han, Singularity Cancellation Transformation, Technische Universität München, 2015.

List of Publications of the Author

Francavilla, M. A., Vipiana, F., Li, L., and Vecchi, G. (2011). An automatic dual-surface approach for the solution of the electric field boundary integral equation in presence of interior resonances. *International Symposium on Antennas and Propagation, Spokane, U.S.A.*

Li, L. and Eibert, T. F. (2016). Radial angular singularity cancellation transformations derived by variable separation. *IEEE Transactions on Antennas and Propogation*, 64(1):189–200.

Li, L., Wang, K., and Eibert, T. F. (2014a). A new radial-angular-R2 transformation for singular integrals on triangular meshes. *European Conference on Antennas and Propagaton, Den Hague, Netherlands.*

Li, L., Wang, K., and Eibert, T. F. (2014b). A projection height independent adaptive radial-angular-R2 transformation for singular integrals. *IEEE Transactions on Antennas and Propogation*, 62(10):5381–5386.

Li, L., Wang, K., and Eibert, T. F. (2015a). Derivation of radial-angular singularity cancellation transformations by the variable separation method. *International Conference on Electromagnetics in Advanced Applications (ICEAA), Torino, Italy.*

Li, L., Wang, K., and Eibert, T. F. (2015b). A new family of radial angular transformations for the near-singularity cancellation technique. *International Symposium on Antennas and Propagation, Vancouver, Canada.*

Li, L., Wang, K., Li, H., and Eibert, T. F. (2014c). Analytical finite element matrix elements and global matrix assembly for hierarchical 3-D vector basis functions within the hybrid finite element boundary integral method. *Advances in Radio Science*, 12:1–11.

Quijano, J. L. A., Vecchi, G., Li, L., Sabbadini, M., Scialacqua, L., Bencivenga, B., Mioc, F., and Foged, L. J. (2010). 3D spatial filtering applications in spherical near field antenna measurements. *Antenna Measurement Techiniques Association (AMTA) 2010 Symposium, October, Atlanta, Georgia, U.S.A.*

Wang, K., Li, L., and Eibert, T. F. (2013a). Comparison of compact monopole antenna arrays with eigenmode excitation and multiport conjugate matching. *IEEE Transactions on Antennas and Propogation*, 61(8):4054–4062.

Wang, K., Li, L., and Eibert, T. F. (2013b). A highly compact four-element monopole array with one-layer decoupling and matching network. *International Symposium on Antennas and Propagation, Orlando, U.S.A.*

Wang, K., Li, L., and Eibert, T. F. (2014a). Compact three-port printed diversity array with combined antenna types. *International Symposium on Antennas and Propagation, Memphis, U.S.A.*

Wang, K., Li, L., and Eibert, T. F. (2014b). A decoupling technique based on partially extended ground plane for compact two-port printed monopole antenna arrays. *German Microwave Conference (GeMiC), Aachen, Germany.*

Wang, K., Li, L., Eibert, T. F., and Tooni, S. (2013c). Equivalent circuits of compact monopole arrays based on scattering parameters. *European Conference on Antennas and Propagaton, Gothenburg, Sweden.*

Wiedenmann, O., Li, L., and Eibert, T. F. (2014). A direct hierarchical multilevel preconditioner for the solution of finite element-boundary integral equations. *European Conference on Antennas and Propagaton, Den Hague, Netherlands.*